Dynamic Modelling and Robust Control

of a

Wind Energy Conversion System

Maarten Steinbuch

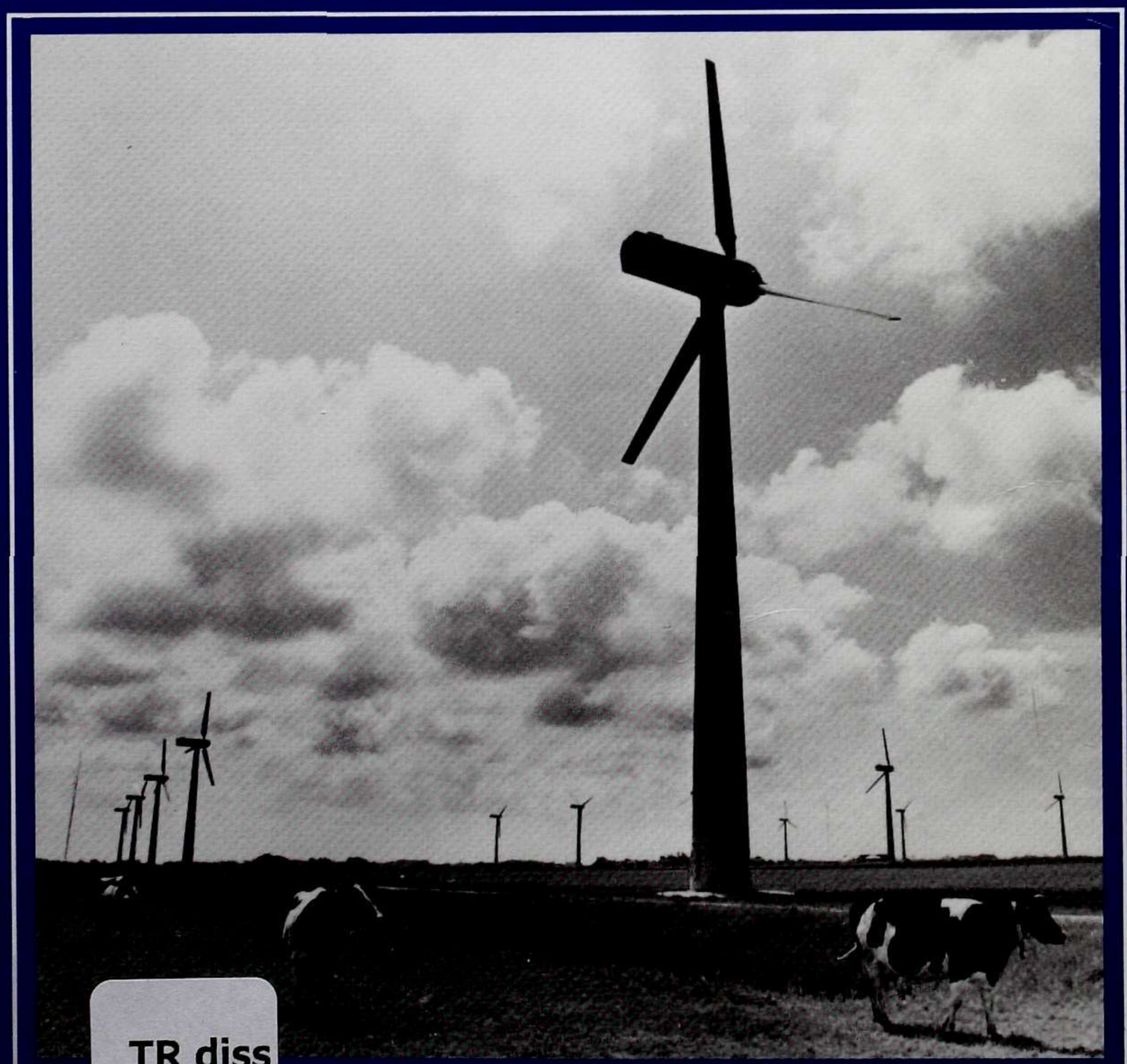

TR diss
1772

4J 2772
>17g24J
TR diss 1772

Dynamic Modelling and Robust Control of a Wind Energy Conversion System

TR diss
1772

On the cover: Wind Energy Park of the Dutch Electricity Generating Board (N.V.Sep), near Oosterbierum (Province of Friesland, The Netherlands).

Part of the work as described in this thesis has been carried out at the Philips Research Laboratories Eindhoven as part of the Philips Research programme.

Dynamic Modelling and Robust Control of a Wind Energy Conversion System

BIBLIOTHEEK TECHNISCHE UNIVERSITEIT
Prometheusplein 1
2628 ZC
DELFT

PROEFSCHRIFT

ter verkrijging van de graad van doctor aan de Technische Universiteit Delft, op gezag van de Rector Magnificus, prof. drs. P.A. Schenck, in het openbaar te verdedigen ten overstaan van een commissie aangewezen door het College van Dekanen op maandag 27 november 1989 te 16.00 uur

door

Maarten Steinbuch

geboren te Zeist,
Werktuigkundig Ingenieur.

druk: wibro dissertatiedrukkerij, helmond

Dit proefschrift is goedgekeurd door de promotor

Prof. ir. O.H. Bosgra

CIP–DATA KONINKLIJKE BIBLIOTHEEK, DEN HAAG

Steinbuch, Maarten

Dynamic modelling and robust control of a wind energy conversion system / Maarten Steinbuch. – [S.l. : s.n.]. – Ill., fig.
Thesis Delft. – With ref.
ISBN 90–9003143–X
SISO 644.9 UDC 621.548(043.3)
Subject headings: wind energy conversion system ; modelling / wind energy conversion system ; robust control.

PREFACE

In 1982 the Dutch Electricity Generating Board (N.V.Sep) decided to build an Experimental Wind Power Plant in co–operation with the Ministry of Economic Affairs. The main objective was to investigate the generation of wind energy in cluster formation and to further develop wind turbine technology. Also Sep wants to study the possibilities of the integration of wind energy with the conventional large–scale power generation. Sep contracted KEMA, Arnhem, to carry out the construction and related research program. As part of the research program in 1983 the study on the control system design for the experimental Wind Farm was initiated and carried out by the Automation Engineering Department of KEMA in close co–operation with Delft University of Technology (DUT), Measurement and Control Group, Department of Mechanical Engineering.

First of all I would like to express my gratitude to the Dutch Electricity Generating Board (N.V.Sep) for their financial support during my years at KEMA ('83–'87), and to Holec Projects for supplying numerical data. Also the opportunity to work at the Automation Engineering Department of KEMA is gratefully acknowledged.
With the initiator of the research on the control system design, dr.ir. F. Meiring, I have had a lot of interesting and fruitful discussions, for which I thank him very much. I want to thank Prof.ir. O.H. Bosgra for all his stimulating thoughts and for the many talks we had and still have. My visits to Delft University were always enjoyable due to the discussions with my fellow control researchers in Delft, for which I owe them gratitude.
Several students have actively participated in the research project, for which I thank them: ir. M.M. Kneepkens (Wageningen University of Agriculture), ir. W.W. de Boer (DUT), ir. S.A.W.M Peters (DUT), ing. H. Koster (Enschede Technical School) and ir. J. Ploeg (DUT).
In the last two years the stimulating research atmosphere at Philips Research Laboratories (Nat.Lab.) Eindhoven has helped me to deepen my results on some necessary points. In addition I want to thank the Department Head of the Mechanical Research Group ir. B. Sastra for giving me the opportunity to combine parts of my wind turbine work with my current work at Philips' Nat.Lab.
Finally my gratitude goes out to Prof.ir. J.A. Schot and dr.ir. M.J. Hoeymakers, both from Eindhoven University of Technology, for pointing out a shortcoming in the model of the electrical conversion system, which has been corrected.

SUMMARY

The application of wind energy conversion systems for the production of electrical energy requires a cheap and reliable operation. Especially at high wind velocities fluctuations from the wind field result in large mechanical loads of the wind turbine. Also fluctuations in the grid voltage may yield large dynamic excitations. In order to realize a long lifetime and a reliable operation active control systems are necessary.
The main goal of the study described in this thesis is to develop an approach for the design of a high performance control system for a wind turbine with variable speed.

The wind turbine system under investigation has a three–bladed rotor which is connected to the generator by a transmission. The electrical conversion system consists of a synchronous generator with a rectifier, direct current transmission and an inverter. The manipulable inputs are the pitch angle of the turbine blades, the field voltage of the generator and the delay angle of the rectifier. Both the generator speed and the direct current are being measured.
The control design problem at full load is to minimize fluctuations in speed and current while reducing the mechanical (fatigue) loads. The feedback system should realize this without excessive use of the input variables and must also be simple to implement.

In order to be able to design a high performance control system a high quality dynamic model is required. Much attention has been given to the modelling of the electrical conversion system. The switching of the thyristors of the rectifier bridge results in periodic behaviour at a high frequency. In order to design a control system an averaged model has been derived through the application of Floquet theory for periodic systems.
The properties of the aerodynamic transfer and of the drive train only have been approximately modelled. Deviations of these nominal models from the real system are accounted for using norm–bounded uncertainty models. Using the nominal model and the uncertainty models the control system design has been carried out.

The control design problem can suitably be handled by the Linear Quadratic design method. However, instead of using the standard solution with observers, in this study the optimization theory has been applied with respect to a predefined structure of the feedback law. In this approach the order and structure of the controller can be selected as part of the problem formulation. The application to the wind turbine system shows that a high performance control system can be obtained using a relatively simple, low order multivariable feedback law. The use of frequency weighting effectively reduces the role of mechanical parasitic dynamics. Application of the multi–model principle in combination with LQ optimization theory provides a way to synthesize controllers which are robust for large (aerodynamic) changes in operating conditions. A quantitative robustness analysis shows how the design parameters of the feedback law can be adapted in order to enhance the robustness of the controller.

The approach taken, involving extensive modelling combined with uncertainty models and with the use of optimization theory and robustness analysis, has been shown to result in a high performance control system. Its main characteristic is the integrated approach of the control problem, with combined control action via the mechanics and the electrical conversion system. It is recommended to apply this integrated approach also to other types of wind turbine systems.

CONTENTS

1. INTRODUCTION 1

2. PROBLEM FORMULATION 5
2.1 The control design problem 5
2.2 System properties and modelling assumptions 7
2.3 Outline of the modelling and control design approach 12

3. DYNAMIC MODELLING OF A SYNCHRONOUS GENERATOR LOADED WITH A RECTIFIER 15
3.1 Introduction and problem statement 15
3.2 General theory on linearization and periodic systems 19
3.2.1 Definitions and preliminaries on differential equations 19
3.2.2 Linearization of two time–interconnected nonlinear differential equations 22
3.2.3 Periodic systems 25
3.2.4 Averaging of two time–interconnected periodic differential equations 30
3.3 Dynamic model of the synchronous generator 32
3.4 Coupling with the DC link 35
3.5 Calculation of the nominal periodic solution 43
3.6 The approximating linear model 45
3.6.1 Linearization 45
3.6.2 The averaged model 48
3.7 Numerical results 50
3.7.1 Nonlinear simulations 51
3.7.2 Linear models 53
3.8 Summary 60

4. WIND TURBINE SYSTEM MODELLING AND ANALYSIS 61
4.1 Description of the complete system 61
4.2 Nominal modelling 62
4.2.1 Aerodynamic transfer at the rotor 62
4.2.2 Drive train dynamics 64
4.2.3 Electrical subsystems 66
4.2.4 Combination of the models 67

4.3 Uncertainty modelling 69
4.3.1 Introduction 69
4.3.2 Norm–bounded uncertainty modelling 71
4.3.3 Uncertainties in the inputs 76
4.3.4 Internal uncertainties 84
4.3.5 Uncertainties in the outputs 89
4.3.6 Combination of the uncertainties 89
4.4 Simulation and system analysis 93
4.4.1 Operating conditions 93
4.4.2 Time and frequency responses 95
4.4.3 System properties 103
4.5 Statement of the control problem 107

5. ROBUST LINEAR QUADRATIC OUTPUT FEEDBACK DESIGN METHOD
5.1 Introduction 111
5.2 Linear Quadratic Output Feedback 112
5.2.1 Proportional feedback 112
5.2.2 Dynamic feedback 115
5.3 Extensions of Linear Quadratic Output Feedback 118
5.3.1 The optimal servo problem 119
5.3.2 Cross–product weighting 123
5.3.3 Frequency weighted Linear Quadratic Output Feedback 124
5.3.4 Selection of decentralized control structure 127
5.3.5 Optimal multi–model robustness 130
5.4 Perturbation robustness analysis 133

6. ROBUST CONTROL DESIGN FOR THE WIND ENERGY CONVERSION SYSTEM 139
6.1 Introduction 139
6.2 Nominal design 140
6.2.1 LQ state feedback 140
6.2.2 LQ output feedback 144
6.2.3 Dynamic LQ output feedback 151
6.3 Multi–model robustification 158
6.4 Robustness analysis of the controlled wind turbine system 162

7 CONCLUSIONS 173

REFERENCES 175

APPENDICES 182
A.1 Numerical data 182
A.2 Mean steady–state model of the generator with DC link 182
A.3 Linearization of the aero–mechanical model 185
A.4 Linear model of the wind turbine system 187
A.5 Linear models in three operating points 189
A.6 LQ state feedback parameters 191
A.7 LQOF parameters 192
A.8 Stepresponses for $LQOF_9$ 194

LIST OF SYMBOLS 196

SAMENVATTING 201

CURRICULUM VITEA 203

1. INTRODUCTION

The application of wind energy conversion systems for the production of electrical energy initially was expected to be one of the major non–conventional energy production sources. Not only due to the lowered oil prices, but also because of operational difficulties, a large increase of wind energy has not occurred in the past few years. Still it is one of the most promising new energy sources.
In order to arrive at cost–effective wind turbine systems, these are placed at locations with high wind velocities, increasingly in large clusters (wind farms). Moreover, the development is towards larger systems (rotor diameter of 30–100 m, power 300–3000 kW), in order to increase the energy production more than the construction and maintenance costs.
In the past years a number of wind turbine installations failed to be reliable, especially at large excitations during storms. Also fatigue loads appeared to be much larger than expected, due to the turbulence of the wind speed affecting a wind turbine rotor. As a result mechanical parts such as blades, hub, gear box etc., more or less often had to be repaired. This forced the development of very reliable systems. Together with the need for low cost systems this resulted in the design of properly non over–dimensioned systems. These designs did put more emphasis on dynamic mechanical load calculations (fatigue loads, structural dynamics) during the design phase. For the same reason variable speed systems were introduced, with which it is possible to lower the mechanical load of the turbine. Recently, developments are directed towards the design of mechanically flexible wind energy conversion systems.

Much research and development efforts have been directed towards construction issues, electrical conversion systems and aerodynamics. Although the attention has moved to industrial development, many questions are left open. For instance, how should a large wind turbine system with a variable speed be operated such that low mechanical loads occur during life–time? A related question is to what extent the dynamics of a wind turbine system affect the overall performance. Performance indicators are for instance the amount of energy production, life time, costs/kWh.
In the design phase of the construction much can be done to obtain wind turbine systems which are guaranteed to withstand a predefined spectrum of wind excitations during their life–time. However, the way wind excitations lead to mechanical loads in the various parts of a wind turbine system depends heavily on the dynamic properties of the construction and on the control system applied.

Wind excitations can be rejected completely, for instance by adjusting the pitch angle of the blades. However, this might give a low energy production and/or high mechanical loads of the blades. On the other hand, once mechanical forces have come into the system, the load flow should be made such that both low mechanical loads and a high energy production occur. In other words the question arises how energy can be transported in some optimal way from the rotor to the generator and electrical grid. For both cases the control system plays a central role.

The main issue of this thesis is to investigate the design of active controllers for variable speed wind energy conversion systems. To be able to address this design question, a detailed model of the dynamic behaviour of the wind turbine system is needed. With this knowledge the design problem of a high performance controller will be approached. The main goal is to obtain an operational mode of a variable speed wind turbine system such that all dynamics are properly taken into account and that the mechanical loads are low.

The study described has been carried out on behalf of the construction, development and operation of the Wind Energy Park of the Dutch Electricity Generating Board (N.V.Sep), near Oosterbierum, the Netherlands. This experimental wind power plant consists of 18 wind turbines of 300 kW nominal electrical power each. The main purpose of the wind farm is to investigate the use of wind power on a large scale. Especially, the wake effects, load control and impact on the local power grid are studied. The study reported here has been carried out during the preparational phase of the Wind Farm project.

The wind energy conversion system considered in this study is a variable speed, three–bladed horizontal axis wind turbine with a synchronous generator and direct current transmission. Its rated power is 300 kW. In figure 1.1 the components are drawn schematically.

The blades are made of steel and do result in a relatively heavy construction. The wind turbine is equipped with variable pitch using an electro–mechanical servo–mechanism. At high wind speeds a reduction of the mechanical loads can therefore be achieved. The gear box is a three–step planetary gear. This gear box is connected with the generator through a rubber coupling.

The synchronous generator is loaded with a controlled bridge–rectifier. With a dc–reactor the system is connected to a bridge–inverter and to the grid. Due to the direct current link, the generator speed is variable. Storage of kinetic energy in the rotor may be utilized to obtain a controlled mechanical load flow through the system.

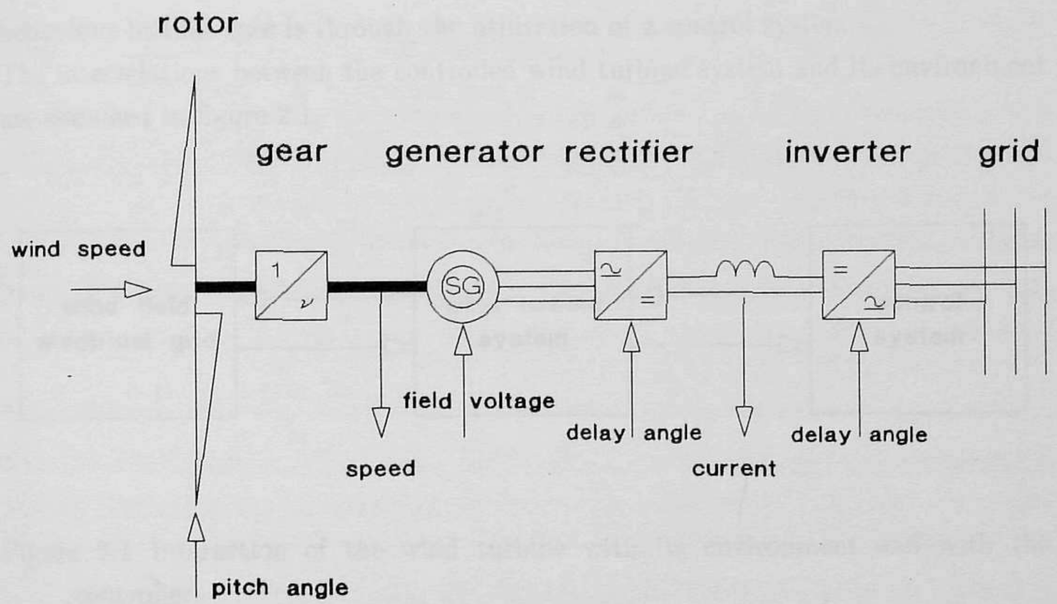

Figure 1.1 Wind turbine with synchronous generator and direct current transmission.

The wind turbine system has multiple control inputs: the delay angle of the rectifier, the field voltage of the synchronous generator and the pitch angle of the blades. The practical installation in the wind farm is such that there are three clusters of six wind turbines each. Within these clusters the wind turbines are interconnected with their dc–current circuits. In each cluster only one inverter is used. The delay angle of the inverter is used to control the direct voltage for each cluster of wind turbines.

2. PROBLEM FORMULATION

2.1 THE CONTROL DESIGN PROBLEM

The coupling of the wind turbine with its environment causes large dynamic loads and (un)desirable behaviour. In this study the design of a given wind turbine system is assumed to be the starting point. The only way to modify the dynamic behaviour in that case is through the utilization of a control system.
The interrelations between the controlled wind turbine system and its environment are sketched in figure 2.1.

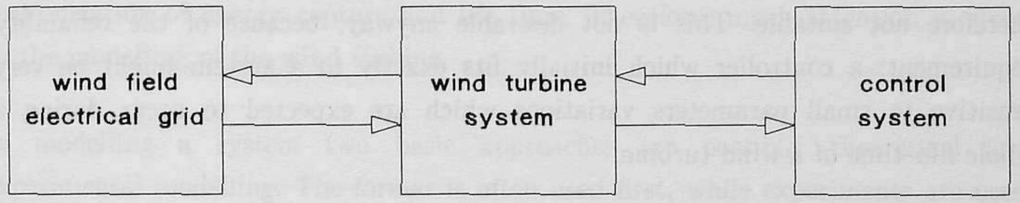

Figure 2.1 Interaction of the wind turbine with its environment and with the controller.

The main goal of a controller is to shape the closed–loop system behaviour in order to enhance the system performance. Before a controller can be designed, the performance requirements must be stated. For the wind turbine the following general requirements must be met:

1) maximum energy production,
2) maximum life–time, with low maintenance costs,
3) reliable operation,
4) good power quality,
5) acceptable impact on its environment (for instance noise).

The most important requirements are 1,2 and 3. The maximum life–time and reliability requirements are strongly related to mechanical loads. The good electrical power quality is of importance especially when the power grid is weak. Also, a good power quality makes load control of wind farms easier.
Although the last requirement (5) may be very important in certain situations, it is not very well known how control systems can attribute to this.

On the other hand, the controller should possess the following properties:

1) maximum closed–loop performance (stability, disturbance attenuation, tracking...), at an acceptable level of control effort,
2) low dynamic order, because of hardware constraints,
3) robust.

We restrict our attention to controllers which are implementable in a low cost hardware setup. There is a trade–off between complexity and performance. In this study no experimental validation of the results has been possible yet. This must be done in a supplementary study.

The robustness requirement comes from the observation that unknown effects are likely to occur, especially from the aerodynamics. Moreover, in our case small scale experiments are not possible. Exact fitting of the controller to the system is therefore not suitable. This is not desirable anyway, because of the reliability requirement: a controller which initially fits exactly to a system might be very sensitive to small parameters variations which are expected to occur during a whole life–time of a wind turbine.

Statement of the problem.

The **main problem** is how to design a **high performance robust controller for the wind turbine system**, satisfying the requirements on the system and on the controller stated above. To this end, the following subproblems are posed:

1. the modelling problem:

– in which way does the control design problem impose requirements on the dynamic modelling of the system, and how can these requirements be met?
– is it possible to model the knowledge we have on uncertainties in the behaviour of our system, such that this knowledge can be used to obtain a better controller?

2. the control problem:

– how could the wind turbine problem statement be transcribed into performance specifications which can be used by a control design method?
– how to design a high performance low order controller for the wind turbine?
– in what way can the robustness requirement be met?

In the next sections an outline is given of the approach taken in this thesis, to solve the above mentioned problems.

2.2 SYSTEM PROPERTIES AND MODELLING ASSUMPTIONS

For any control system to be designed it is necessary to have a methodology for *the control design as well as for the modelling of the system to be controlled.* The description of the system can be simple load curves. However, to be able to design a controller with which the plant is to be operated in several conditions properly it is necessary to have a more detailed model. Such a model should contain at least the most important dynamics. If the performance specifications are strong the task for the controller becomes more important. In that case the modelling should be done with care because the accuracy of the model of the system bounds the achievable closed–loop performance. For the wind turbine under investigation the controller is used to realize the (strong) performance requirements such as maximization of energy capture and life time. Therefore, much attention is given to the modelling of the wind turbine.

In modelling a system two basic approaches are possible: theoretical and experimental modelling. The former is often used first, while experiments are used for verification and validation. Obviously, for control system design an experimental model obtained by identification techniques is finally preferred. However, identification of wind energy systems has only recently received attention [Mattsson, 1984; v.Engelen, 1986] and is still in a premature phase of application. Moreover, without having a theoretical model we do not know what is relevant in the behaviour and what is not. Also, uncertainty modelling and the design of robust controllers is not (yet) possible with purely experimental based models.
In our situation experiments were not yet possible as the actual wind turbine system was still in its construction phase and so did not yet exist physically. Therefore, in this study a theoretical model is build. Based on a general description of the wind turbine and its environment, assumptions are made to arrive at a solvable modelling problem.

Consider the wind energy conversion system as part of the whole wind energy farm (figure 2.2), with couplings to both the other wind turbines as well as to the environment.

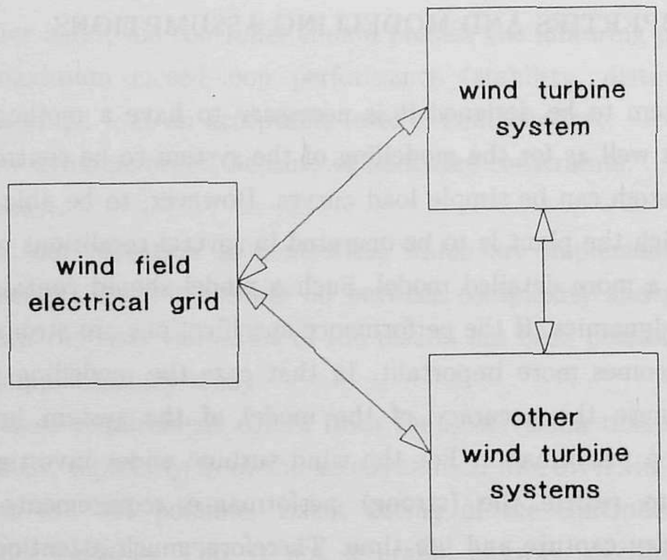

Figure 2.2 Coupling of the wind turbine system with other wind turbine systems and with the environment.

Properties 2.1

Several interaction mechanisms couple the **wind turbine to its two surroundings**:

1. aerodynamic couplings between the wind turbines (wake effects),
2. electrical couplings with the other wind turbines through the common DC grid,
3. bilateral relation of the wind field with the wind turbine,
4. interaction with the large utility grid,
5. the drive train (rotor, gear, generator) is mechanically supported by the hub and tower construction.

Assumptions 2.1

Because we look at solutions for the control problem implemented at the individual wind turbine systems in this study, we restrict the modelling to the wind turbine itself. The interactions with the other wind turbines and with the environment are assumed to be unilateral:

1. wake effects caused by other turbines are neglected because the distance between the turbines is relatively large. Otherwise all wind turbines should be taken into the model. See for preliminary results on such a large model [Steinbuch et al., 1988],
2. because the inverter is controlled, both the electrical coupling with the other wind turbines (property 2.1.2) and the impedance of the large utility grid (property 2.1.4) are neglected,

3. the wind field upstream is assumed not to be affected by the wind turbine (property 2.1.3). This would need elaborated aerodynamic models,
4. because the wind turbine under investigation has been designed to be a non–flexible system, the mechanical supports are relatively rigid. Because of this the (dynamical) interactions between the drive train and support are assumed to be described by rigid elements.

Subsequently the aerodynamic, mechanical and electrical properties and assumptions are stated, see also figure 2.3.

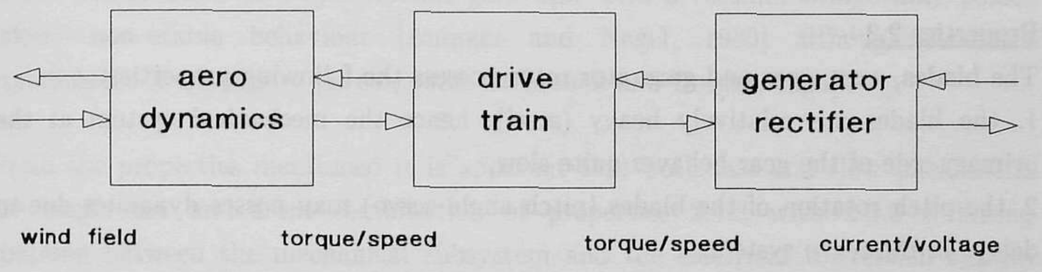

Figure 2.3 Blockdiagram of the wind turbine system.

Properties 2.2

The most important **aerodynamic properties** of the system are:

1. the wind field is stochastic and spatially distributed and will give local effects: the wind speed at some point on the blades gives local values for the lift coefficient (i.e. local forces),
2. the rotation of the blades in combination with the possible non–uniform wind speed results in periodic forces ('sampling effect'),
3. variations of the pitch angle and the rotor speed may be such that it leads locally to non steady–state aerodynamics.

Assumptions 2.2

Because the rotor blades are extremely stiff they are modelled as rigid (see properties and assumptions 2.3). Due to this we assume that:

1. the local aerodynamic forces are averaged over the blade length. The wind speed input is taken as one single signal representing the mean wind speed over the rotor surface,

2. sampling effects are assumed to be independent periodic disturbances of a single wind speed,
3. because the blades are quite heavy (properties 2.3) the rotor acts like a low pass filter. Therefore it is assumed that local non steady–state aerodynamics are not relevant.

In summary, the aerodynamic transfer is modelled as steady–state (nonlinear) process–characteristics (so–called C_p curves). These relate variations of the pitch angle, the rotor speed and the wind speed instantaneously to variations in the rotor torque.

Properties 2.3

The **blades, axes, gear and generator rotor** possess the following properties:
1. the blades are relatively heavy (steel), hence the mechanical system at the primary side of the gear behaves quite slow,
2. the pitch rotation of the blades (pitch angle servo) may posses dynamics due to delays in the servo system,
3. the gear has a large reduction (22), and torques in the secondary shaft are amplified to the primary shaft,
4. in the secondary shaft a flexible element is mounted.
Note that because of property 2.3.3 it is very important to model the variation in the electro–mechanical torque accurately.

Assumptions 2.3

1. the blades are assumed to be rigid so pitch angle variations imposed by the servo actuator are assumed to hold for the whole blade length. In order to investigate this assumption a parasitic phenomenon is modelled as uncertainty (chapter 4),
2. all structural modes are assumed to be concentrated in the flexible element in the secondary shaft and are represented by one single flexible mechanism.

With these assumptions the mechanical dynamics are largely underestimated. A separate study should be devoted to the dynamic modelling of all mechanics involved. This might be done by lumped parameter models, or by a finite elements approach. Both cases however, need more information of the actual parameters than currently available.

Properties 2.4

For the combination of a **synchronous generator loaded with a rectifier bridge** the following properties are known:
1. the system possesses fast as well as slow dynamics [Steinbuch and Meiring, 1986] also due to high frequent periodic behaviour of the switching thyristors of the rectifier,
2. the field voltage exciter system is a relatively slow device,
3. variation of the delay angle of the rectifier results almost immediately in variations of the current and torque. This is also the case for disturbances from the grid voltage,
4. the combination of a synchronous generator with a rectifier bridge may posses (slow) non–stable behaviour [Auinger and Nagel, 1980] although feedback stabilization is quite easy [Ernst, 1986; Steinbuch and Bosgra, 1988].

From the properties mentioned it is apparent that both fast and slow phenomena are important and from combination of properties 2.4.3 with 2.3.3 a strong coupling between the mechanical subsystem and the electrical conversion system seems to exists. Hence, much modelling effort is put into the modelling of the electrical system.

Assumptions 2.4

1. the inverter voltage is taken as independent disturbance input to the system (see also assumption 2.1.2),
2. the electronic equipment with which the firing angles of the thyristors in the rectifier bridge are generated is not modelled. The delay angle of the rectifier is assumed to be an instantaneously manipulable input,
3. because the field voltage exciter system is relatively slow, it can be modelled rather approximately.

2.3 OUTLINE OF THE MODELLING AND CONTROL DESIGN APPROACH

Modelling

The properties of the system can be summarized as follows: stochastic, nonlinear aerodynamics are coupled to the mechanics in an averaging way. The mechanical part is slow, but possesses also some parasitic dynamics. The coupling with the electrical conversion system is strong. The synchronous generator with rectifier has both slow and fast dynamics.

Based on these properties it might be argued to make a very large nonlinear model to describe the behaviour of the wind turbine system in its environment. However, the controller should be designed such that it does not need all this information. The reason is that otherwise the feedback system might become too complicated and even more important the closed–loop performance will be too sensitive for variations in the system. A more feasible approach is to make a **nominal model** which is a simplification of reality to a certain extend (part one of the modelling problem of section 2.1). Next, the possible differences between the nominal model and the real system must be described in an **uncertainty model** (part two of the modelling problem of section 2.1). To obtain the necessary information reduction the uncertainty model must be of a different kind than the nominal model. Depending on the modelling assumptions this uncertainty model can have very different forms. However, the use of these models for robust control design imposes strong requirements on the form of the uncertainty models. The main modelling problem is to find a proper balance between the nominal model and the uncertainty model given the restrictions on the form of the latter. The more accurate the nominal model is, the higher the achievable performance but the lower the robustness. This is the essential coupling between modelling and control design.

Based on the assumptions given in the previous section for each subsystem the following models are needed:

1. A relatively simple nominal model of the aerodynamics. Variations and uncertainties of such a model are quite large and must be taken into an uncertainty model.
2. A nominal model of the drive train, possessing the most important dynamic characteristics. Unknown parasitics and parameter variations must be modelled as uncertainties.
3. A model of the average behaviour of the synchronous generator with rectifier, which still contains the most important slow and fast phenomena but not the high

frequent thyristor–switching behaviour. The difference between the accurate and the averaged model must be treated as model uncertainty.

The modelling of the synchronous generator with rectifier involves a detailed description of its behaviour. This will be the subject of chapter 3, in which also the average model is derived.

In chapter 4 both the aerodynamic and mechanical models will be derived as well as some additional actuator and sensor models. In addition to the obtained nominal models, full account is given to the derivation of uncertainty models for all subsystems. The representation of these uncertainty models is chosen such that it can be used within the control design procedure.

Control system design

After the nominal and uncertainty modelling, the behaviour and system properties of the uncontrolled wind turbine are investigated (chapter 4). Based on these observations a precise statement of the control problem will be given. In this study we restrict our attention to the full load case (wind speed above rated). Especially at high wind speeds low mechanical loads and a high performance control are needed. Here we give already some general remarks on the control design procedure followed.

Recall that we want a maximum performance with a small control effort and that a low order robust controller must realize this (control problem statement of section 2.1). The number of methods known in literature which can solve such a problem is very limited. One of the well–known methods developed in the last decades is the Linear Quadratic control method utilizing a quadratic performance criterion [Anderson and Moore, 1971]. The question to be answered first is if and how the performance requirements on the closed–loop wind turbine system can be put into the quadratic performance index (sections 4.5 and 6.1).

The requirements of low order and robustness must also be met. Instead of using standard LQ theory we will use controller parameter optimization in a predetermined structure with respect to a modified quadratic performance index (chapter 5). It will be shown how the output feedback formulation gives the possibility to design low order, decentralized, multi–model robust controllers.

The robustness problem is further evaluated in section 5.4 with the question how the behaviour of the closed–loop system under perturbations can be analysed.

In chapter 6 the design methods are applied to the wind turbine system under investigation. It will be shown how the control problem can be solved.

Finally, the main results and conclusions are summarized in chapter 7.

3. DYNAMIC MODELLING OF A SYNCHRONOUS GENERATOR LOADED WITH A RECTIFIER

3.1 INTRODUCTION AND PROBLEM STATEMENT

Description of the configuration

The electrical conversion system used in the wind turbine consists of a synchronous generator with a rectifier bridge. The rectifier is connected to a direct current (DC) line, together with 5 other wind turbines in the wind farm. The DC power is fed into the large utility grid by an inverter, see figure 3.1.

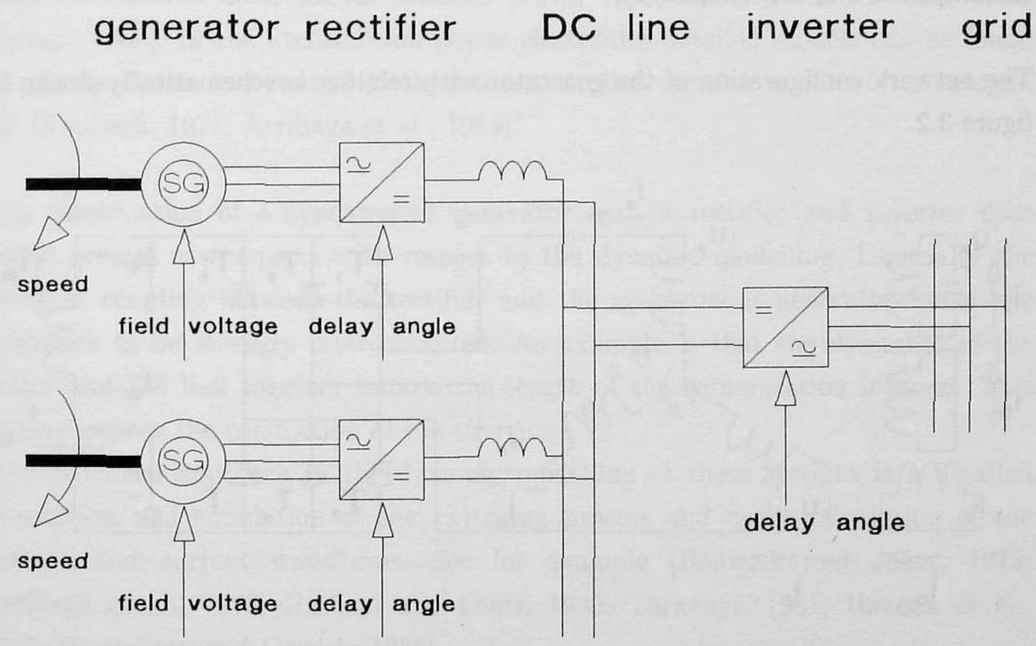

Figure 3.1 Coupling of the generators with the direct current link and with the grid.

The synchronous generator with DC link has the following properties (see also *properties 2.4, chapter 2*):

- the generator speed is imposed by the drive train and hence will only vary slowly,
- the field voltage u_F is realized by an exciter system with a large time constant,
- both the rectifier and inverter consists of thyristors in bridge connection. In both devices the thyristors are controllable through their delay angles,

- the delay angle α_r of the rectifier is a fast input without any significant dynamics,
- *the cyclic operation of the inverter is assumed to be decoupled from the rectifier* by the presence of the DC reactor. Because of this assumption high frequency interference problems between rectifier and inverter are not taken into account,
- important outputs are the electro–mechanical torque T_e and the DC current i_{dc}.

In order to restrict our attention to the modelling problem of the generator with rectifier, the model of the exciter system (u_F) is given in the next chapter. The *DC voltage u_i at the inverter side is taken as input. Any dynamic bilateral* coupling with the other wind turbines and with the grid is therefore neglected (assumptions 2.1, 2.4, chapter 2).

The network configuration of the generator with rectifier is schematically drawn in figure 3.2.

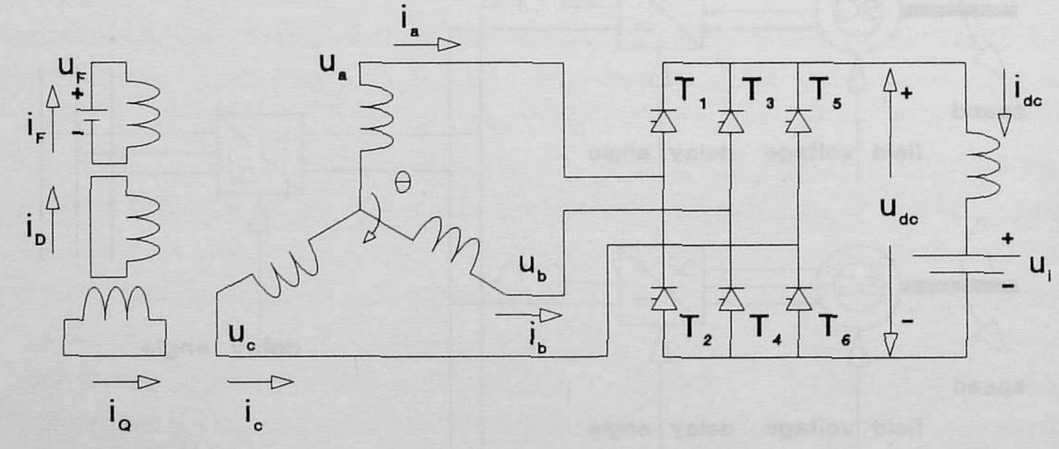

Figure 3.2 Coupling of the synchronous generator with the rectifier.

The following observations are made:

- the generator has three rotor windings,
- the three–phase stator windings are coupled to six thyristors of the rectifier,
- the operation is such that depending on the electrical angle θ, two or three thyristors are conducting. If the angle is such that the current must go from one branch to another, this takes some time. This is called commutation. During this time all three branches have non–zero currents,

- after commutation only two phases have an (equal) current. This topology is called the non–commutation stage,
- *the switching process is cyclic with respect to the thyristors and stator phases.*

From these observations it may be concluded that the synchronous generator loaded with the rectifier possesses a periodic character with cyclic switching between topologies.

<u>*Modelling problem*</u>

Dynamic modelling of synchronous machines has a long history and is a fully explored research area, see for instance [Park, 1928; Anderson and Fouad, 1982; Kovacs, 1984]. In the literature on power electronics detailed models can be found on the operation and control of thyristor–controlled rectifier and inverter bridges, see [Kimbark, 1971; Arrillaga et al., 1983].

The combination of a synchronous generator with a rectifier and inverter does reveal several new aspects with respect to the dynamic modelling. Especially the bilateral coupling between the rectifier and the synchronous generator forces the dynamics to be strongly interconnected. An example is that the dynamics of the stator and DC link together impose the length of the commutation interval. This in turn defines the conduction of the thyristors.

A well–known approach in the dynamic modelling of these systems is a detailed description and simulation of the switching process and exact calculation of the voltage and current waveforms. See for example [Bonwick and Jones, 1973; Arrillaga et al., 1978; Hashem and Louis, 1980; Tarkanyi, 1981; Haneda et al., 1982; Harrington and Gawish, 1985].

These models are nonlinear and describe the cyclic behaviour (in our case 400 Hz). A major drawback is that the computational burden is very high. In this study we are interested in the control system design with a moderate frequency content of the feedback, as stated in chapter 2. Hence, the knowledge of the exact cyclic behaviour of the system will not be used by the controller. We have to separate the two time–scales involved: the cyclic and the average behaviour. Therefore the *main modelling problem* is to approximate the periodic behaviour by averaged models.

To obtain such models several methods can be found in literature. These approximations are based mostly on the combination of the 'standard' Park synchronous generator model with an average description of the voltage and current waveforms at the rectifier side, see e.g. [El–Serafi and Khalil, 1976; Harashima and Naitoh, 1977; Tarkanyi, 1981; Badawy, 1984; Steinbuch, 1986]. However, this neglects the important bilateral dynamic coupling between the synchronous generator and rectifier. Other approaches include all kinds of physical assumptions to arrive at simplified models, for instance assuming a constant current or neglecting the resistance. Examples are given in [Clade and Persoz, 1968; Hashem and Louis, 1980; Buyse et al., 1985; Mostafa and Iung, 1985; Ernst, 1986]. A simplified model based on equivalent circuits is given by [Hoeijmakers, 1988].
We conclude that in the literature on electrical machines no rigorous treatment can be found on the average dynamic modelling of a synchronous generator with rectifier, in the sense of accounting for the switching nature of the system.

On the other hand in the power electronics literature more work has been done on modelling of switching devices (such as resonant converters) using averaged linearized models. See for instance the work of [Grötzbach, 1981; Vorperian and Cuk, 1983; Verghese, Elbuluk and Kassakian, 1986; Elbuluk et al.,1988; Grötzbach and von Lutz, 1986]. In most cases the approach followed is to describe the dynamics within one period with linear models which are time–interconnected, i.e. for each switching mode one linear model is used following one another in the next mode. The average model is then obtained by calculation of the transition from the beginning to the end of the period or to apply state–space averaging [Dirkman, 1983; Verghese, Ilic–Spong and Lang, 1986].
One of the complicating properties of the synchronous generator with rectifier, is that the switching moment itself is a function of the state–variables. This issue is only addressed in a few references [Louis, 1983; Grotzbach, 1981; Elbuluk, 1986]. The other complicating fact is that the system is time–varying within each stage of a period.

In this study the dynamic model is based on the idealized Park equations for the synchronous generator which are coupled through a time–dependent switching matrix to the DC–link dynamic equation. This model is the 'standard' nonlinear detailed description of the behaviour of the commutating and non–commutating phases. The next step is to obtain an approximate linear model from one period to the following.

The approach taken in this thesis is to extend the ideas suggested in the power electronics literature to the synchronous generator with rectifier. First a derivation is given of the linearization of two nonlinear time–interconnected sets of differential equations. Secondly, well–known theory on averaging of differential equations with periodic coefficients will be applied to the system. The so–called Floquet theory is in fact the underlying averaging principle applied.

This chapter is organised as follows. In section 3.2 general theory on linearization and periodic differential equations is given. In section 3.3 the dynamic model for the synchronous generator is described. In section 3.4 the coupling with the rectifier bridge is established resulting in a cyclic nonlinear model. To be able to linearise this model the nominal periodic solution is calculated in section 3.5, whereas the procedure to find the approximate linear model is described in section 3.6. In section 3.7 numerical results will be presented. Finally a summary is given (§3.8).

3.2 GENERAL THEORY ON LINEARIZATION AND PERIODIC SYSTEMS

3.2.1 Definitions and preliminaries on differential equations

Definition 3.1. A function f(x) is said to be Lipschitz if it satisfies the Lipschitz condition over an interval [a,b]:

$$\|f(x)-f(\tilde{x})\| \leq k(x)\|x-\tilde{x}\| \qquad a \leq x,\tilde{x} \leq b$$

where k is a piecewise continuous function on [a,b] and ||.|| denotes the norm.

Definition 3.2. A function f(x) is said to be sufficiently smooth if the partial derivatives $\partial f_i / \partial x_i$ are continuous over [a,b]. Then f(.) is Lipschitz.

Consider the vector differential equation:

$$\dot{x}(t) = f(x(t),t), \qquad t \epsilon [a,b] \tag{3.1}$$

with the initial condition

$$x(t_0) = x_0 \qquad t \epsilon [a,b]$$

A solution x(t) is unique if f(.) satisfies a Lipschitz condition over its domain [a,b] [Kailath, 1980, p.596–597].
Moreover, if the function f(.) is sufficiently smooth a solution x(t) always exists.

Definition 3.3. A nonlinear function f(.) is said to be linearizable if f(.) is sufficiently smooth over its domain [a,b].

The vector differential equation

$$\dot{x}(t) = f(x(t),u(t),t) \tag{3.2}$$

can be linearized around a nominal solution $(\bar{x}(t),\bar{u}(t))$, with

$$x(t) = \bar{x}(t) + \Delta x(t)$$

$$u(t) = \bar{u}(t) + \Delta u(t)$$

by defining a Taylor expansion of f(.) from (3.2):

$$f(x(t),u(t)) = f(\bar{x}(t),\bar{u}(t),t) + \frac{\partial f}{\partial x}\Big|_{\bar{x},\bar{u}} \Delta x(t) + \frac{\partial f}{\partial u}\Big|_{\bar{x},\bar{u}} \Delta u(t) + O(\Delta x^2,\Delta u^2)$$

where $O(\Delta x^2,\Delta u^2)$ represents quadratic and higher order terms.

Neglecting in the Taylor expansion the higher order terms $O(\Delta x^2,\Delta u^2)$ and substitution into (3.2) yields:

$$\Delta\dot{x}(t) = \frac{\partial f}{\partial x}\Big|_{\bar{x},\bar{u}} \Delta x(t) + \frac{\partial f}{\partial u}\Big|_{\bar{x},\bar{u}} \Delta u(t) \tag{3.3}$$

Lemma 3.1.
For every linear differential equation

$$\dot{x}(t) = A(t)x(t) \qquad x(t_0)=x_0, \quad t\epsilon[a,b] \tag{3.4}$$

with A(t) piecewise continuous, A(t)x(t) satisfies the Lipschitz condition over every finite interval [a,b]. Hence a unique solution for (3.4) exists.
Proof: see [Kailath, 1980, p.598]. □

Definition 3.4. The state transition matrix $\phi(.)$ [Zadeh and Desoer, 1963, p.168–169; Kailath, 1980, p.598–599] of a linear differential equation of the form (3.4) is defined as the unique solution to:

1. $d\phi(t,t_0)/dt = A(t)\phi(t,t_0)$, $\quad \phi(t_0,t_0)=I$ $\quad t\epsilon[a,b]$
2. $\phi(t,t)=I$ $\quad t\epsilon[a,b]$

Then the following holds:

1. $x(t) = \phi(t,t_0)x(t_0)$ $\quad t,t_0\epsilon[a,b]$
2. $\phi(t_1,t_2)=\phi(t_1,t_3)\phi(t_3,t_2)$ $\quad t_1,t_2,t_3\epsilon[a,b]$
3. $\phi(.)$ is invertible: $\phi^{-1}(t_1,t_0)=\phi(t_0,t_1)$ $\quad t,t_0\epsilon[a,b]$

Definition 3.5. The linear differential equation

$$\dot{x}(t) = Ax(t) \qquad x(t_0)=x_0, \quad t\epsilon[a,b] \tag{3.5}$$

is said to be time–invariant if A is constant. In all other cases the set of equations is said to be time–varying.

For a time–invariant system, the state transition matrix can be written as

$$\phi(t,t_0) = \exp\{A(t-t_0)\} \tag{3.6}$$

Lemma 3.2.
In the inhomogeneous differential equation

$$\dot{x}(t) = f(x(t),u(t),t) \qquad x(t_0)=x_0, \quad t\epsilon[a,b] \tag{3.7}$$

with

$$f(x(t),u(t),t) = A(t)x(t)+B(t)u(t)$$

where B(t) and u(t) are continuous functions, the function f(.) satisfies a Lipschitz condition if the homogeneous part A(t)x(t) does. Then the solution of (3.7) can be written as

$$x(t) = \phi(t,t_0)x(t_0) + \int_{t_0}^{t} \phi(t,\tau)B(\tau)u(\tau)d\tau \tag{3.8}$$

with $\phi(t,t_0)$ the state transition matrix related to $\dot{x}(t) = A(t)x(t)$.
Proof: see [Kailath, 1980, p.600]. □

The solution (3.8) is often not analytically calculable. It is well known that numerical approximation is possible by discretization of (3.8) into small subintervals $\Delta T=(t-t_0)/N$. The choice of N is subject to the time–scales involved (eigenvalues of A(t) at each t, gradients of A(t), B(t) and u(t) with respect to the time variable t). Assume that N>>1 such that $\|A(t_{i-1})-A(t_i)\|$, $\|B(t_{i-1})-B(t_i)\|$ and $\|u(t_{i-1})-u(t_i)\|$ are sufficiently small. Define $A(t_i)=A(i)$, $B(t_i)=B(i)$ and $u(t_i)=u(i)$, i=1,..,N, as piecewise constant and denote $x(t_i)=x(i)$. Then using (3.6) the solution at each time $t_0+i\Delta T$ is approximated by [Chen, 1984, pp.166–167; Kailath, 1980, pp.117–118]:

$$x(i) = \phi(i,0)x(0) + \sum_{j=0}^{i-1} \phi(i,j+1)B_d(j)u(j) \qquad \text{for } 0\leq i\leq N \tag{3.9}$$

with

$$\phi(i,j) = A_d(i)A_d(i-1)...A_d(j) \qquad \phi(i,i) = I, \tag{3.10}$$

$$A_d(i) = \exp\{A(i)\Delta T\}, \tag{3.11}$$

$$B_d(i) = [\exp\{A(i)\Delta T\}-I]A(i)^{-1}B(i). \tag{3.12}$$

for A(i) invertible.

3.2.2 Linearization of two time–interconnected nonlinear differential equations

Consider the following set of nonlinear time–invariant differential equations:

$$\dot{x}_1(t) = f_1(x_1(t),u_1(t)) \qquad x_1(t_0)=x_{10} \qquad t_0 \leq t \leq t_1 \tag{3.13}$$

$$\dot{x}_2(t) = f_2(x_2(t),u_2(t)) \qquad x_2(t_1)=x_{21} \qquad t_1 \leq t \leq t_2 \tag{3.14}$$

with the interconnection relation:

$$x_2(t_1) = Hx_1(t_1), \qquad H \text{ a constant matrix} \tag{3.15}$$

Assume that the time t_1 at which (3.15) holds, depends on the solution to equation (3.13) in the following way:

$$t_1: \quad Q_1x_1(t_1) = 0, \qquad Q_1 \text{ a constant matrix} \tag{3.16}$$

Both functions $f_1(.)$ and $f_2(.)$ are assumed to be sufficiently smooth on their domain (definition 3.2).

Graphically the solution to (3.13)–(3.16) may be shown as in figure 3.3.

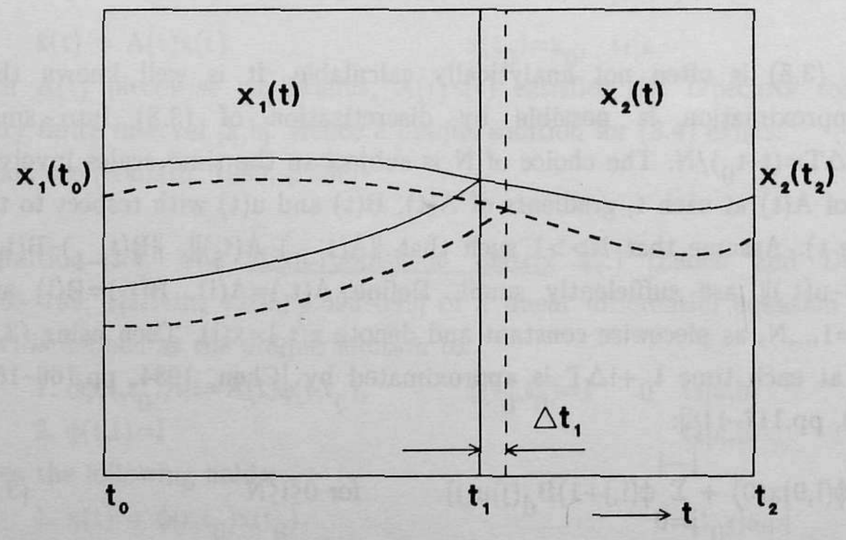

Figure 3.3 Solution of two time–interconnected nonlinear differential equations.

Because of the connectivity equation (3.15) the solution $x_2(t)$ is related to $x_1(t)$. The time t_1 is such that (3.16) holds.

In the sequel we are interested to obtain a description of the variations of the state variables at t_2 as a function of small perturbation of the initial condition $x_1(t_0)$ and of the inputs.

Define a nominal solution as $(\bar{x}_1(t),\bar{u}_1(t),\bar{x}_2(t),\bar{u}_2(t),\bar{t}_1)$, such that (3.13)–(3.16) are satisfied for these values.
Define all other possible solutions as perturbations around the nominal ones:

$$\begin{aligned} x_i(t) &= \bar{x}_i(t) + \Delta x_i(t) && i=1,2 \\ u_i(t) &= \bar{u}_i(t) + \Delta u_i(t) && i=1,2 \\ t_1 &= \bar{t}_1 + \Delta t_1 \end{aligned} \tag{3.17}$$

Because f_1 and f_2 are sufficiently smooth (definition 3.2), (3.13) and (3.14) are linearizable (definition 3.3), with the result:

$$\Delta\dot{x}_1(t) = \left.\frac{\partial f_1}{\partial x_1}\right|_{\bar{x}_1,\bar{u}_1} \Delta x_1(t) + \left.\frac{\partial f_1}{\partial u_1}\right|_{\bar{x}_1,\bar{u}_1} \Delta u_1(t) \qquad t_0 \leq t \leq t_1 \tag{3.18}$$

$$\Delta\dot{x}_2(t) = \left.\frac{\partial f_2}{\partial x_2}\right|_{\bar{x}_2,\bar{u}_2} \Delta x_2(t) + \left.\frac{\partial f_2}{\partial u_2}\right|_{\bar{x}_2,\bar{u}_2} \Delta u_2(t) \qquad t_1 \leq t \leq t_2 \tag{3.19}$$

Relation (3.16) must be satisfied in the perturbed situation also:

$$Q_1\left\{\bar{x}_1(t_1)+\Delta x_1(t_1)\right\} = 0$$

or

$$Q_1\left\{\bar{x}_1(\bar{t}_1+\Delta t_1)+\Delta x_1(\bar{t}_1+\Delta t_1)\right\} = 0$$

Linearization gives:

$$Q_1\bar{x}_1(\bar{t}_1) + Q_1\frac{\partial x_1}{\partial t_1}\Delta t_1 + Q_1\Delta x_1(\bar{t}_1) = 0$$

Because the first term equals zero (nominal solution) we obtain:

$$\Delta t_1 = -\left[Q_1\frac{\partial x_1}{\partial t_1}\right]^{-1}Q_1\Delta x_1(\bar{t}_1) \tag{3.20}$$

For equation (3.15) we get with (3.17):

$$\bar{x}_2(\bar{t}_1+\Delta t_1)+\Delta x_2(\bar{t}_1+\Delta t_1) = H\left[\bar{x}_1(\bar{t}_1+\Delta t_1)+\Delta x_1(\bar{t}_1+\Delta t_1)\right]$$

Linearization gives:

$$\frac{\partial x_2}{\partial t_1}\Delta t_1+\Delta x_2(\bar{t}_1) = H\left[\frac{\partial x_1}{\partial t_1}\Delta t_1+\Delta x_1(\bar{t}_1)\right]$$

or

$$\Delta x_2(\bar{t}_1) = \left[H\frac{\partial x_1}{\partial t_1} - \frac{\partial x_2}{\partial t_1}\right]\Delta t_1+H\Delta x_1(\bar{t}_1)$$

With (3.20):

$$\Delta x_2(\bar{t}_1) = \left\{\left[\frac{\partial x_2}{\partial t_1} - H\frac{\partial x_1}{\partial t_1}\right]\left[Q_1\frac{\partial x_1}{\partial t_1}\right]^{-1}Q_1+H\right\}\Delta x_1(\bar{t}_1) \qquad (3.21)$$

or

$$\Delta x_2(\bar{t}_1) = \hat{H}\Delta x_1(\bar{t}_1) \qquad (3.22)$$

Clearly, the difference between H and $\hat{H}$ is equal to

$$\hat{H}\text{–}H = \left[\frac{\partial x_2}{\partial t_1} - H\frac{\partial x_1}{\partial t_1}\right]\left[Q_1\frac{\partial x_1}{\partial t_1}\right]^{-1}Q_1 \qquad (3.23)$$

which is due to the interdependence of t_1 and x_1,x_2.
In (3.21) the partial derivatives are equal to the nonlinear functions $f_1(.)$ and $f_2(.)$ from (3.13),(3.14), evaluated at $\bar{t}_1$.

Solution of the equations.
The solution to the original set of nonlinear equations (3.13)–(3.16) can now be approximated by the solution of the linear time–varying differential equations:

$$\begin{aligned}\Delta\dot{x}_1(t) &= A_1(t)\Delta x_1(t)+B_1(t)\Delta u_1(t) \qquad \Delta x_1(t_0)=\Delta x_{10},\ t_0\le t\le t_1\\ \Delta\dot{x}_2(t) &= A_2(t)\Delta x_2(t)+B_2(t)\Delta u_2(t) \qquad \Delta x_2(t_2)=\hat{H}\Delta x_1(t_1),\ t_1\le t\le t_2\end{aligned} \qquad (3.24)$$

with

$$A_1(t) = \left.\frac{\partial f_1}{\partial x_1}\right|_{\bar{x}_1,\bar{u}_1} \qquad B_1(t) = \left.\frac{\partial f_1}{\partial u_1}\right|_{\bar{x}_1,\bar{u}_1}$$

$$A_2(t) = \left.\frac{\partial f_2}{\partial x_2}\right|_{\bar{x}_2,\bar{u}_2} \qquad B_2(t) = \left.\frac{\partial f_2}{\partial u_2}\right|_{\bar{x}_2,\bar{u}_2}$$

and

$$\hat{H} = H+\left\{f_2\left[\bar{x}_2(\bar{t}_1),\bar{u}_2(\bar{t}_1)\right]-Hf_1\left[\bar{x}_1(\bar{t}_1),\bar{u}_1(\bar{t}_1)\right]\right\}\left\{Q_1f_1\left[\bar{x}_1(\bar{t}_1),\bar{u}_1(\bar{t}_1)\right]\right\}^{-1}Q_1$$

The solution is obtained by application of lemma 3.2:

$$\Delta x_1(t) = \phi_1(t,t_0)\Delta x_{10} + \int_{t_0}^{t}\phi_1(t,\tau)B_1(\tau)\Delta u_1(\tau)d\tau \qquad t_0\le t\le t_1$$

$$\Delta x_2(t) = \phi_2(t,t_1)\Delta x_2(t_1) + \int_{t_1}^{t}\phi_2(t,\tau)B_2(\tau)\Delta u_2(\tau)d\tau \qquad t_1\le t\le t_2$$

and with (3.22) we obtain:

$$\Delta x_2(t) = \phi_2(t,t_0)\hat{H}\phi_1(t_1,t_0)\Delta x_{10} + \phi_2(t,t_1)\hat{H}\int_{t_0}^{t_1}\phi_1(t_1,\tau)B_1(\tau)\Delta u_1(\tau)d\tau + \int_{t_1}^{t}\phi_2(t,\tau)B_2(\tau)\Delta u_2(\tau)d\tau \qquad t_1\le t\le t_2 \qquad (3.25)$$

This completes the derivation of the solution to the two coupled equations (3.13)–(3.16).

3.2.3 Periodic systems

In this section some definitions and theories are given on periodic linear differential equations. Most important result is the Floquet theorem with which periodic systems can be transformed into systems with constant coefficients.
General theory of periodic linear dynamical systems is given e.g. in the book of [Yakubovich and Starzhinskii, 1975]. We will also refer to [Brockett, 1970; Richards, 1983; D'Angelo, 1970].

Definition 3.6. A function f(.) is said to be periodic of period T if f(t+T)=f(t) for all admissible t. [Brockett, 1970, p.46–49].

Consider the nonlinear time–varying differential equation

$$\dot{x}(t) = f(x(t),t) \qquad (3.26)$$

and assume that the function is periodic of period T, independent of its argument x(t):

$$f(.,t+T) = f(.,t)$$

Definition 3.7. The nominal periodic solution of (3.26) is defined as the time function $(\bar{x}(t),\bar{u}(t))$ with the property that it satisfies equation (3.26) for all t, and that both $\bar{x}(t)$ and $\bar{u}(t)$ are periodic of period T: $\bar{x}(t+T)=\bar{x}(t)$, $\bar{u}(t+T)=\bar{u}(t)$.

Consider the linear time–varying differential equation

$$\dot{x}(t) = A(t)x(t), \qquad x(t_0)=x_0 \tag{3.27}$$

and assume that the coefficients are periodic of period T:

$$A(t+T) = A(t)$$

Lemma 3.3.

The state transition matrix (definition 3.4) of (3.27) has the following properties:

1) all properties given in definition 3.4, and

2) $$\phi(t+T,t_0) = \phi(t,t_0)\phi(t_0+T,t_0) \tag{3.28}$$

Proof: see [Yakubovich and Starzhinskii, 1975, p.88]. □

Lemma 3.4.

For the transition matrix of (3.27) the following holds:

$$\phi(t_0+T,t_0) = C\phi(T,0)C^{-1}$$

with $C=\phi(t_0,0)$.

Proof: $\phi(t_0+T,t_0)=\phi(t_0+T,t_0)\phi(t_0,0)\phi^{-1}(t_0,0)=\phi(t_0+T,0)\phi^{-1}(t_0,0)$ by definition 3.4. With lemma 3.3 we obtain by substitution of $t=t_0$, $t_0=0$:

$\phi(t_0+T,t_0)=\phi(t_0,0)\phi(T,0)\phi^{-1}(t_0,0)$ □

By definition 3.4 of state transition matrices we have

$$x(t+T) = \phi(t+T,t_0)x(t_0)$$

and with lemma 3.3 we obtain

$$x(t+T) = \phi(t,t_0)\phi(t_0+T,t_0)x(t_0) \quad \Leftrightarrow$$

$$x(t+T) = \phi(t,t_0)x(t_0+T)$$

From this it may be concluded that all we need to calculate a solution x(t), is an initial condition $x(t_0)$ and the value of the state transition matrix $\phi(t,t_0)$ for $t_0 \leq t \leq t_0+T$.

Moreover, the transition over a time–interval with length T is given by

$$x(t_0+T) = \phi(t_0+T,t_0)x(t_0)$$

Definition 3.8. The state transition matrix $\phi(t_0+T,t_0)$ of a system (3.27) with coefficients periodic of period T is called the monodromy matrix [Yakubovich and Starzhinskii, 1975, p.89].

Definition 3.9. The eigenvalues of the monodromy matrix $\phi(t_0+T,t_0)$ are called the multipliers of system (3.27). The set of all multipliers is called the spectrum of equation (3.27). [Yakubovich and Starzhinskii, 1975, p.94]. The multipliers are denoted as ρ_i, i=1,...,n.

Note by lemma 3.4 and the property $\rho(X)=\rho(CXC^{-1})$ of eigenvalues that the multipliers are shift–invariant with respect to time and independent of t_0.

Theorem 3.1. Floquet theory

The state transition matrix of a system given by the equations (3.27) may be expressed in the form

$$\phi(t,t_0) = P(t,t_0)\exp\{R(t_0)[t-t_0]\} \tag{3.30}$$

where the nxn matrix function P(.) is periodic of period T, nonsingular for all t, continuous, with an integrable piecewise continuous derivative and such that $P(t_0,t_0)=I_n$. Matrix $R(t_0)$ is a constant nxn matrix. In the case that A(.) of (3.27) is real, all matrices in (3.30) are also real.

Proof: follows immediately by applying all properties of state transition matrices to (3.30). See also [Yakubovich and Starzhinskii, 1975, p.90]. □

Due to definition 3.4 the matrix $R(t_0)$ can be calculated from the monodromy matrix as follows:

$$R(t_0) = \frac{1}{T}\ln\phi(t_0+T,t_0) \tag{3.31}$$

See for exceptional cases where the ln(.) function does not exist [Brockett, 1970, p.22].

Corollary 3.1. Lyapunov reducibility result.
Given the system (3.27), and the relation (3.30) then the substitution of

$$x(t) = P(t,t_0)y(t)$$

transforms (3.27) into

$$\dot{y}(t) = R(t_0)y(t), \qquad y(t_0)=x(t_0) \tag{3.32}$$

which is a linear time–invariant set of equations.

Lemma 3.5.
Define as in lemma 3.4 the nxn matrix $C=\phi(t_0,0)$ then

$$R(t_0)=CR(0)C^{-1}$$

Proof: by definition according to (3.30) we have with $t=t_0+T$

$$\phi(t_0+T,t_0) = P(t_0+T,t_0)\exp\{R(t_0)T\} = P(t_0,t_0)\exp\{R(t_0)T\} = \exp\{R(t_0)T\}$$

which is equal to $C\phi(T,0)C^{-1}$ by lemma 3.4. So

$$\exp\{R(t_0)T\} = CP(T,0)\exp\{R(0)T\}C^{-1}$$

$$= CF(0,0)\exp\{R(0)T\}C^{-1} = C\exp\{R(0)T\}C^{-1}$$

As $Ce^{A}C^{-1}=\exp(CAC^{-1})$ then

$$\exp\{R(t_0)T\} = C\exp\{R(0)T\}C^{-1} = \exp\{CR(0)C^{-1}T\}$$

which gives the result. □

Lemma 3.5 indicates that matrix R(.) is unique up to a certain nonsingular similarity transformation.

Definition 3.10. The eigenvalues of the matrix R(.) of theorem 3.1 are called the characteristic exponents λ_i, i=1,...,n of system (3.27), [Richards, 1983, p.21].

Lemma 3.6.
The characteristic exponents λ_i, i=1,...,n, of a system (3.27), are unique modulo an additive term $2\pi jm/T$, m integer. The relation between the characteristic exponents and the multipliers is given by

$$e^{\lambda_i T} = \rho_i, \qquad i=1,...,n \tag{3.33}$$

Both parameters are independent of the initial time t_0.

Proof: see [Yakubovich and Starzhinskii, 1975, p.95]. The independence follows from lemma's 3.4 and 3.5. □

Lemma 3.7.
The solution of (3.27) is asymptotically orbitally stable [Willems, 1970, definition 2.14] if and only if

$$|\rho_i| < 1 \qquad \forall\ i=1,...,n$$

or

$$Re(\lambda_i) < 0 \qquad \forall\ i=1,...,n$$

where Re(.) denotes real part of a complex valued argument.
For orbitally stability [Willems, 1970, definition 2.13] equality is also admissible.
Proof: follows by inspection of eq. (3.32) and (3.33), and the properties of $P(t,t_0)$ (theorem 3.1). □

Definition 3.11. Given the solution to (3.27) we define the averaged solution as $\tilde{x}(t)=y(t)$ with y(t) the solution to (3.32). This means that the function $P(t,t_0)$ is approximated with $\tilde{P}(t,t_0)=I$. Model (3.32) is called the averaged model of (3.27).

Note that other solutions may be defined as averaged. For example the mean signal content:

$$\tilde{P}(t,t_0) = \int_{t_0}^{t} P(\tau,t_0)d\tau.$$

Another possibility is to use $\min_{\tilde{P}}\|\tilde{P}-P\|$, penalizing deviations of y(t) from the real solution x(t) over the period. This might be combined with uncertainty minimization (chapter 4). A very important benefit of using definition 3.11 is that at the 'sample instants' t_0+mT, m integer, the averaged solution is exact: $y(t_0+mT)=x(t_0+mT)$. A large similarity is therefore present with the discretization involved with digital control of continuous time systems. In chapter 4 we will use this property to address the uncertainty modelling associated.

3.2.4 Averaging of two time–interconnected periodic differential equations

In the previous sections the linearization of two time–interconnected differential equations has been treated as well as general theory on linear differential equations with coefficients which are periodic.
In the case of the synchronous generator with rectifier both situations occur simultaneously. However, for this system an additional difficulty occurs namely that the switching time t_2 between the second (3.14) and the first topology (3.13) *is not a constant, as was also the case with the time* t_1. *The variations of this* point of time depend on the states and inputs in the following way. Define a time moment t_u with $t_1 \leq t_u \leq t_2$ such that

$$Q_2(t_u)x_2(t_u)+Q_3(t_u)u_2(t_u)=0 \tag{3.34}$$

with $Q_2(.)$ and $Q_3(.)$ functions sufficiently smooth at t_u. The time t_2 of the end of the period is defined by

$$t_2 = t_u + \alpha \tag{3.35}$$

with α some delay.
Finally, at t_2 the following interconnection relation holds:

$$x_1(t_2) = H^T x_2(t_2) \tag{3.36}$$

thus defining the initial state for the next period.

The combination of the model (3.13)–(3.16) with (3.34)–(3.36) defines a nonlinear set of equations with a solution which is only periodic in steady–state: for dynamic variations the period t_2–t_0 is not a constant.
In order to be able to derive a linear model we approximate the true behaviour as small variations around a nominal periodic solution. Perturbations of the time moments (t_1 and t_2) will be represented by variations of state variables at constant points of time. This is a necessary step to obtain a linearized description of the system.
In addition to the linearization of (3.13)–(3.16) the equations (3.34)–(3.36) will be linearized. Defining $t_u=\bar{t}_u+\Delta t_u$ with $\bar{t}_u$ given by the nominal solution, linearization of (3.34) results in (compare with (3.16),(3.20)):

$$\Delta t_u = - Q_u^{-1}(\bar{t}_u)Q_2(\bar{t}_u)\Delta x_2(\bar{t}_u) - Q_u^{-1}(\bar{t}_u)Q_3(\bar{t}_u)\Delta u_2(\bar{t}_u) \tag{3.37}$$

with

$$Q_u(\bar{t}_u) = Q_2(\bar{t}_u)\frac{\partial x_2(\bar{t}_u)}{\partial t} + Q_3(\bar{t}_u)\frac{\partial u_2(\bar{t}_u)}{\partial t} + \frac{\partial Q_2(\bar{t}_u)}{\partial t}\bar{x}_2(\bar{t}_u) + \frac{\partial Q_3(\bar{t}_u)}{\partial t}\bar{u}_2(\bar{t}_u)$$

Linearization of (3.36) with $t_2=\bar{t}_2+\Delta t_2$ gives (compare with the result for (3.15)):

$$\Delta x_1(\bar{t}_2) = H^T \Delta x_2(\bar{t}_2) + \left\{H^T \frac{\partial x_2(\bar{t}_2)}{\partial t} - \frac{\partial x_1(\bar{t}_2)}{\partial t}\right\}\Delta t_2 \tag{3.38}$$

Again the second term reflects the transition of variations of time–moments into equivalent (linearized) variations of state variables.
Combining (3.37) and (3.38) with the perturbed version of (3.35) yields:

$$\Delta x_1(\bar{t}_2) = H^T \Delta x_2(\bar{t}_2) + \hat{H}_2 \Delta x_2(\bar{t}_u) + \hat{H}_3 \Delta u_2(\bar{t}_u) + \hat{H}_4 \Delta\alpha \tag{3.39}$$

with

$$\hat{H}_2 = - \left\{H^T \frac{\partial x_2(\bar{t}_2)}{\partial t} - \frac{\partial x_1(\bar{t}_2)}{\partial t}\right\} Q_u^{-1}(\bar{t}_u)Q_2(\bar{t}_u)$$

$$\hat{H}_3 = - \left\{H^T \frac{\partial x_2(\bar{t}_2)}{\partial t} - \frac{\partial x_1(\bar{t}_2)}{\partial t}\right\} Q_u^{-1}(\bar{t}_u)Q_3(\bar{t}_u)$$

$$\hat{H}_4 = - \left\{H^T \frac{\partial x_2(\bar{t}_2)}{\partial t} - \frac{\partial x_1(\bar{t}_2)}{\partial t}\right\}$$

In (3.39) $\Delta x_2(t_2)$ follows from (3.25) for $t=t_2$ giving the transition from $\Delta x_1(t_0)$ to $\Delta x_2(t_2)$ and similarly $\Delta x_2(t_u)$ follows from (3.25) with $t=t_u$. Then the transition is known from variations at t_0 to variations at the beginning of the next period. This is the monodromy matrix (definition 3.8) of the linearized model.

Summarizing the following procedure can be applied:
1) *given the differential equations* (3.13),(3.14) *with the related conditions* (3.15),(3.16), where the functions f(.) are both periodic of period T, calculate the nominal periodic solution (definition 3.7),
2) calculate the linearized model (3.24) according to the results of §3.2.2,
3) calculate the monodromy matrix (definition 3.8) using the formulae (3.9) – (3.12), see also [Lee, 1963; D'Angelo, 1970, p.197] applied to (3.25) and (3.39),
4) derive the averaged (definition 3.11) model (3.32) by calculation of (3.31).

Note that using the resulting averaged model an **exact asymptotic stability analysis** is possible, because with respect to stability no approximations are involved other than linearization.
In the remaining part of this chapter the theory presented will be applied to the synchronous generator with rectifier and DC link.

3.3 DYNAMIC MODEL OF THE SYNCHRONOUS GENERATOR

The generator has a rotor with two damper windings and one field winding and a stator with three–phase windings, see figure 3.4.
The **inputs** of the model are the field voltage u_F and terminal voltages u_a,u_b,u_c with a,b,c the three phases and the speed ω_g of the generator shaft which is converted to the (normalized) electrical speed $\omega=\omega_g p/\omega_{nom}$ with p the number of pole pairs.
The **outputs** are the electro–mechanical torque and the terminal currents i_a,i_b,i_c.
The **internal variables** are the damper currents i_D and i_Q and the field current i_F as well as the rotor angle θ.

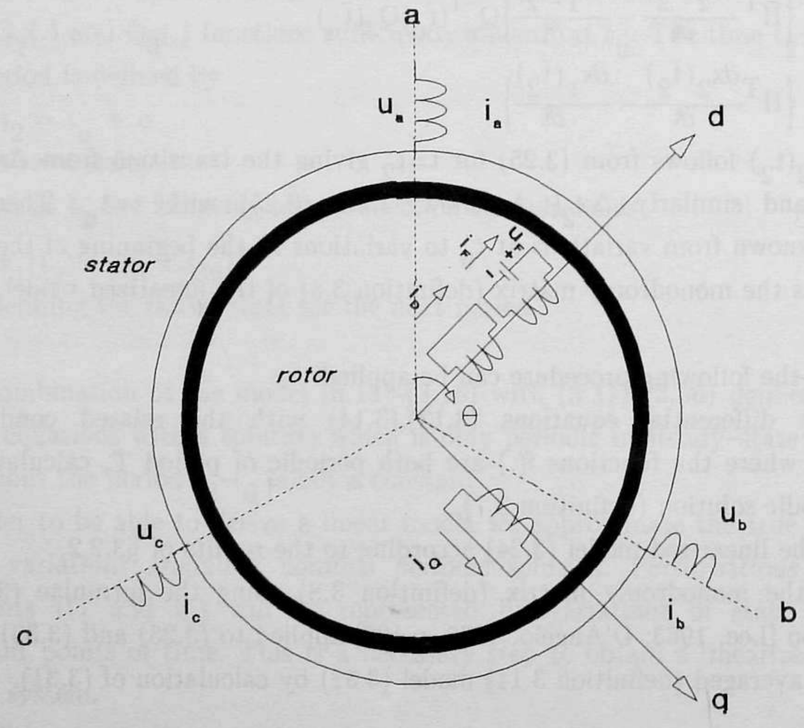

Figure 3.4 Synchronous generator with two damper windings.

For the description of the synchronous machine the following *assumptions* are made:

–magnetic saturation and hysteresis are neglected,
–eddy currents are neglected,
–no temperature dependence,
–symmetrical geometry.

With these assumptions the model of the idealized synchronous machine is obtained, as described by [Park, 1928]. The set of differential equations for the windings of the generator are given by the equation

$$L(\theta)di'/dt = R(\omega,\theta)i' + Bu' \tag{3.40}$$

where i' and u' are the stator and rotor currents and voltages.
The coefficients in this equation are periodic of period $2\pi/3$ *with respect to the* angle θ (i.e. $L(\theta+2\pi/3)=L(\theta)$, definition 3.6) where θ is the rotor angle. This is the angle between the direction of the a–phase of the stator and the d–axis of the rotating rotor (figure 3.4). This rotor angle results from the differential equation

$$d\theta/dt = \omega \tag{3.41}$$

with the speed ω assumed to be dictated by the mechanical model.

By applying the well–known Park transformation [Park, 1928; Anderson and Fouad, 1982] an orthogonal similarity transformation of (3.40) is performed. The Park transformation is defined as:

$$P(\theta) = \sqrt{2/3}\begin{bmatrix} 1/2\sqrt{2} & 1/2\sqrt{2} & 1/2\sqrt{2} \\ \cos\theta & \cos(\theta-2\pi/3) & \cos(\theta+2\pi/3) \\ \sin\theta & \sin(\theta-2\pi/3) & \sin(\theta+2\pi/3) \end{bmatrix} \tag{3.42}$$

This transformation can be interpreted as a projection of the rotating stator variables on the rotor axes. In fact the Park transformation is a nice application of the Floquet theory as stated in section 3.2 (theorem 3.1). The matrix P(.) in this theorem is equal to $P(\theta)$.
The state and input variables belonging to the stator windings are transformed by $P(\theta)$ (corollary 3.1):

$$\begin{bmatrix} i_0 \\ i_d \\ i_q \end{bmatrix} = P(\theta)\begin{bmatrix} i_a \\ i_b \\ i_c \end{bmatrix}, \qquad \begin{bmatrix} u_0 \\ u_d \\ u_q \end{bmatrix} = P(\theta)\begin{bmatrix} u_a \\ u_b \\ u_c \end{bmatrix} \tag{3.43}$$

with $[i_0\ i_d\ i_q]^T$ the new state variables (projected stator currents), $[i_a\ i_b\ i_c]^T$ the terminal stator currents in the three phases a, b and c, $[u_0\ u_d\ u_q]^T$ the projected *stator voltages and finally with* $[u_a\ u_b\ u_c]^T$ *the terminal voltages.*
In this way the periodically changing flux linkage parameters are becoming constants because of the projection of the variables on the rotating d and q axes on the shaft. This is completely in accordance with the Lyapunov reducibility result (§3.2.3, Corollary 3.1). This fact seems not to have found much appreciation in the literature on electrical machines.

Using the voltage equation for the three phases of the stator windings and for the three rotor windings and by transformation of the set of equations using the Park matrix (3.42) the following state–space model is obtained [Anderson and Fouad, 1982]:

$$L\dot{i} = R(\omega)i + Bu \tag{3.44}$$

with state vector $i=(i_d,i_q,i_F,i_D,i_Q)^T$ and input vector $u=(u_d,u_q,u_F)^T$. Currents i_d and i_q and voltages u_d and u_q are projections of the terminal currents and voltages on the rotor axes d and q [Anderson and Fouad, 1982], as explained above. Variables i_F and u_F are the field current and voltage respectively, and states i_D and i_Q are the currents in both damper windings.
The transformed inductance matrix L is:

$$L = \begin{bmatrix} L_s & M \\ M^T & L_r \end{bmatrix} \tag{3.45}$$

with

$$L_s = \begin{bmatrix} L_d & 0 \\ 0 & L_q \end{bmatrix}, \quad M = \begin{bmatrix} L_{md} & L_{md} & 0 \\ 0 & 0 & L_{mq} \end{bmatrix}, \quad L_r = \begin{bmatrix} L_F & L_{md} & 0 \\ L_{md} & L_D & 0 \\ 0 & 0 & L_Q \end{bmatrix}$$

and the resistance matrix is:

$$R(\omega) = \begin{bmatrix} -R_s - \omega\mathscr{L}_s & -\omega\mathscr{M} \\ 0 & -R_r \end{bmatrix} \tag{3.46}$$

with

$$\mathscr{L}_s = \begin{bmatrix} 0 & L_q \\ -L_d & 0 \end{bmatrix}, \quad \mathscr{M} = \begin{bmatrix} 0 & 0 & L_{mq} \\ -L_{md} & -L_{md} & 0 \end{bmatrix}, \quad R_s = \begin{bmatrix} R_d & 0 \\ 0 & R_q \end{bmatrix} \quad R_r = \begin{bmatrix} R_F & 0 & 0 \\ 0 & R_D & 0 \\ 0 & 0 & R_Q \end{bmatrix}$$

finally the input matrix of (3.44) is:

$$B = \begin{bmatrix} -1 & 0 & 0 \\ 0 & -1 & 0 \\ 0 & 0 & 1 \\ 0 & 0 & 0 \\ 0 & 0 & 0 \end{bmatrix} \tag{3.47}$$

Some entries of matrix R depend on generator frequency ω introducing nonlinearities in (3.44).

The output of this model to the drive train of the wind turbine system is the electro–mechanical torque T_e:

$$T_e = \{(L_d - L_q)i_d i_q + L_{md}(i_F + i_D)i_q - L_{mq} i_d i_Q\}/3 \tag{3.48}$$

which is a nonlinear function of states i; the coefficients are elements of matrix L.
The input variables of the state space model (3.44) are ω, u_F as a controllable input, and voltages u_d and u_q. These voltages are related to generator terminal voltage and to the load angle of the machine [Steinbuch, 1986].

3.4 COUPLING WITH THE DC LINK

For the time being it is assumed that the thyristors in the rectifier themselves are *infinitely fast (chapter 2, assumption 2.4.2). It is always possible to add some* dynamics later on or to describe this as model uncertainty (chapter 4).
The structure of the coupling between the synchronous generator and the DC link has already been sketched in figure 3.2.
The voltage differential equation of the DC link is:

$$L_{dc}\dot{i}_{dc} = -R_{dc} i_{dc} - u_i + u_{dc} \tag{3.49}$$

with i_{dc} the current in the direct current link, u_{dc} the voltage on the rectifier side and u_i *the voltage on the inverter side.* L_{dc} *is the inductance of the DC ripple* reactor in the circuit, with a resistance R_{dc}.

The switching of the thyristors T_1 to T_6 depend on the delay angle α_r and on the voltage waveforms of the synchronous generator (see figure 3.5). In the figure the *three voltages* u_a, u_b *and* u_c *are the three–phase terminal voltage of the* synchronous machine idealized as sinoids. For an explanation we start at the situation where T_4 and T_5 are conducting and where $i_a=0$, $i_b=-i_{dc}$, $i_c=i_{dc}$. If $u_a \geq u_c$ then T_1 is going to conduct (see also figures 3.2 and 3.5). The angle over which this is delayed is equal to α_r. Thyristor T_5 can not immediately close: current i_c has to go to zero in a finite time. The angle in which thyristor T_5 and T_1 and T_4 are open is equal to the commutation angle μ_r. At the end of this commutation interval T_5 is closed, i_c is zero, and T_1 and T_4 are conducting. This process is cyclic with respect to all three phases and all thyristors.
The selective opening and closing of the thyristors result in a cyclic situation with two basic topologies. The first is directly after the switching moment and is the commutation phase. In this phase an equalising current runs from one branch

to another. As explained above in this case three branches are coupled. The second situation is the non–commutating topology in which only two branches are coupled.

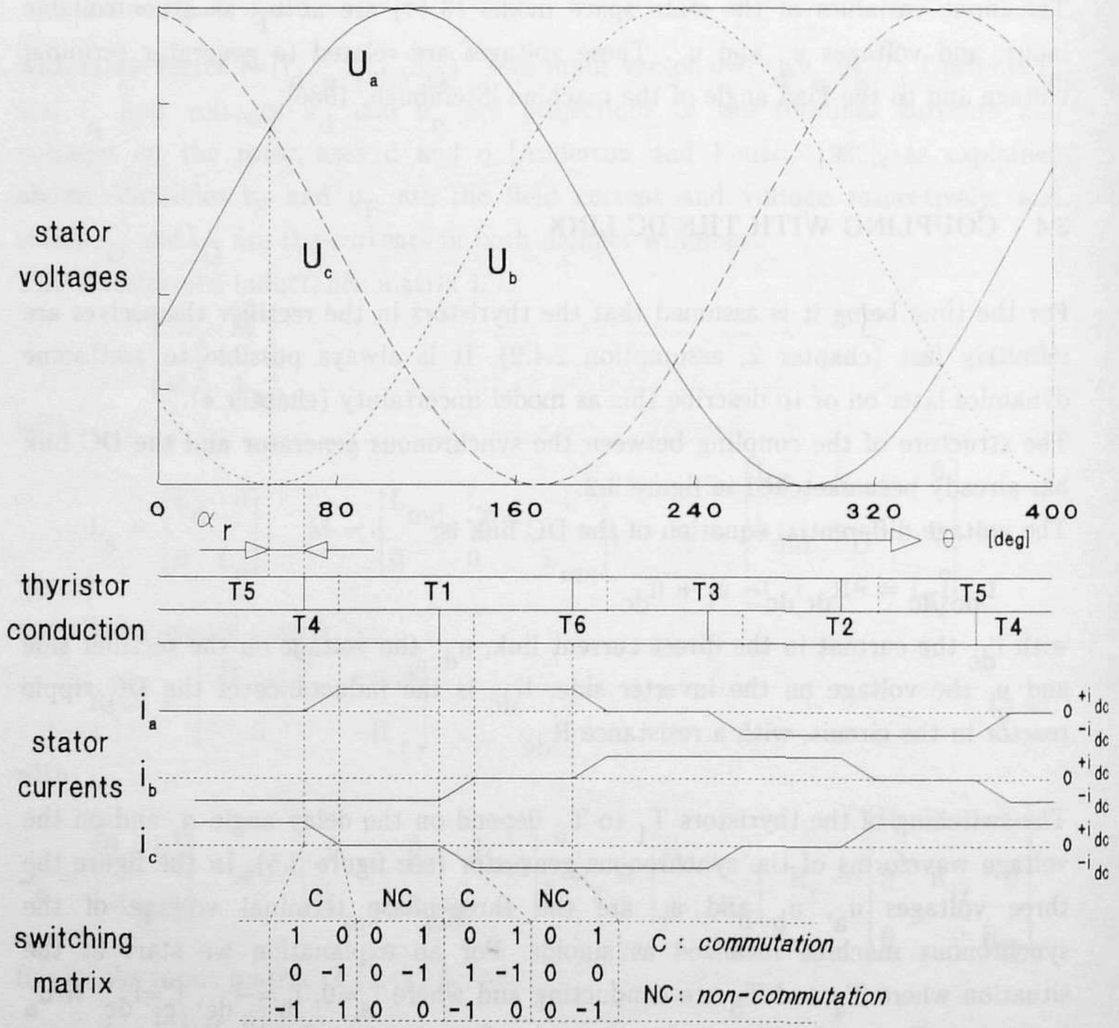

Figure 3.5 Switching of the thyristors as a function of terminal voltage.

The coupling of the stator windings of the synchronous generator with the rectifier can be described with a switching matrix as follows.

Define T as the switching matrix such that:

$$\begin{bmatrix} i_a \\ i_b \\ i_c \end{bmatrix} = T \begin{bmatrix} i_\epsilon \\ i_{dc} \end{bmatrix} \tag{3.50}$$

with i_ϵ a new state variable which is a linear combination of the equalising current and the direct current, defined such that at the switching moment $i_\epsilon=0$ and at the end of commutation $i_\epsilon=i_{dc}$. See for another definition of the state variables [Hashem and Louis, 1980]. The condition $i_\epsilon=i_{dc}$ can be written down in the relation

$$Q_1 \begin{bmatrix} i_\epsilon \\ i_{dc} \end{bmatrix} = 0, \qquad \text{with } Q_1=[-1\ 1] \tag{3.51}$$

Similarly, it can be proven that for the voltages the following holds:

$$T^T \begin{bmatrix} u_a \\ u_b \\ u_c \end{bmatrix} = \begin{bmatrix} 0 \\ u_{dc} \end{bmatrix} \tag{3.52}$$

From the switching table of figure 3.5 *the entries of* T *can be deduced. Suppose* that at a certain rotor angle θ the switching matrix is

$$T = \begin{bmatrix} 1 & 0 \\ 0 & -1 \\ -1 & 1 \end{bmatrix} \tag{3.53}$$

then with (3.50) and (3.52) it follows directly that

$$\begin{aligned} i_a &= i_\epsilon & u_a - u_c &= 0 \\ i_b &= -i_{dc} & u_c - u_b &= u_{dc} \\ i_c &= i_{dc} - i_\epsilon \end{aligned}$$

Combining this with figures 3.2 and 3.5 gives the conclusion that thyristors T_1, T_4 and T_5 are conducting, while T_2, T_3 and T_6 are closed. This situation represents the commutation topology. At the end of this phase $i_\epsilon=i_{dc}$.
The following stage is the non–commutating situation with:

$$T = \begin{bmatrix} 0 & 1 \\ 0 & -1 \\ 0 & 0 \end{bmatrix} \tag{3.54}$$

then with (3.50) and (3.52) it follows that

$$\begin{aligned} i_a &= i_{dc} & u_a - u_b &= u_{dc} \\ i_b &= -i_{dc} \\ i_c &= 0 \end{aligned}$$

In this case only thyristors T_1 and T_4 are open.

From the above conditions it can be derived that in between both topologies $i_\epsilon = i_{dc}$ so that (3.51) holds.
During the non–commutation topology the difference between two of the three stator voltages becomes smaller, in the case of the example $u_c - u_b$. At some time (angular measure θ_u) the difference equals zero: $u_c = u_b$. Exactly after the delay α_r the next cycle begins (at $\theta = \theta_u + \alpha_r$). The condition for θ_u is:

$$Q_2 \begin{bmatrix} u_a \\ u_b \\ u_c \end{bmatrix} = 0 \tag{3.55}$$

In the case of the example above $Q_2 = [0\ -1\ 1]$.
With the variable θ the phenomena are shifting through the three branches a,b and c.
From this example a very important remark can be made. In the commutating phase there are two state variables (currents) at the stator side, while in the non–commutating situation only one variable (i_{dc}) is present. In the following sections the importance of this will become clear.

Coupling with the Park model

Using equations (3.50) and (3.52) the dynamic equation (3.44) of the synchronous generator can be transformed to the new state variables. With the Park transformation according to (3.42) we obtain:

$$\begin{bmatrix} i_0 \\ i_d \\ i_q \end{bmatrix} = P(\theta) \begin{bmatrix} i_a \\ i_b \\ i_c \end{bmatrix} = P(\theta) T \begin{bmatrix} i_\epsilon \\ i_{dc} \end{bmatrix} \quad \text{and} \quad T^T \begin{bmatrix} u_a \\ u_b \\ u_c \end{bmatrix} = T^T P^{-1}(\theta) \begin{bmatrix} u_0 \\ u_d \\ u_q \end{bmatrix} = \begin{bmatrix} 0 \\ u_{dc} \end{bmatrix} \tag{3.56}$$

Because the Park transformation is orthogonal ($P^{-1} = P^T$) the second part of (3.56) is equivalent to:

$$T^T P^T(\theta) \begin{bmatrix} u_0 \\ u_d \\ u_q \end{bmatrix} = \begin{bmatrix} 0 \\ u_{dc} \end{bmatrix} \tag{3.57}$$

Because of continuity the zero variables i_0 and u_0 are zero and can be omitted. Define the reduced Park matrix:

$$\overline{P}(\theta) = \sqrt{2/3} \begin{bmatrix} \cos\theta & \cos(\theta - 2\pi/3) & \cos(\theta + 2\pi/3) \\ \sin\theta & \sin(\theta - 2\pi/3) & \sin(\theta + 2\pi/3) \end{bmatrix} \tag{3.58}$$

and define

$$S(\theta) = \overline{P}(\theta) T(\theta) \tag{3.59}$$

Applying trigonometric formulas gives the result.
With (3.59):

$$\begin{bmatrix} i_d \\ i_q \end{bmatrix} = S(\theta) \begin{bmatrix} i_\epsilon \\ i_{dc} \end{bmatrix} \tag{3.60}$$

and with deletion of the zero variables form the inverse Park matrix P^{-1} ($\overline{P^{-1}} = (\overline{P})^T$):

$$S^T(\theta) \begin{bmatrix} u_d \\ u_q \end{bmatrix} = \begin{bmatrix} 0 \\ u_{dc} \end{bmatrix} \tag{3.61}$$

To be able to transform the dynamic model of the synchronous generator to the new state variables it is necessary to have an expression for the derivatives $\dot{i}_{d,q}$. Using (3.60) we obtain:

$$\dot{i}_{d,q} = \frac{d}{dt}\left\{ S(\theta) \begin{bmatrix} i_\epsilon \\ i_{dc} \end{bmatrix} \right\} = \frac{d\overline{P}(\theta)}{d\theta} \cdot \frac{d\theta}{dt} \cdot T \begin{bmatrix} i_\epsilon \\ i_{dc} \end{bmatrix} + S(\theta) \begin{bmatrix} \dot{i}_\epsilon \\ \dot{i}_{dc} \end{bmatrix} + \cdot\cdot \frac{dT}{dt}$$

In this equation the last term on the right hand side is zero in every subinterval and hence can be deleted. Because $d\theta/dt = \omega$ (3.41) we obtain:

$$\dot{i}_{d,q} = \omega \mathscr{A}(\theta) \begin{bmatrix} i_\epsilon \\ i_{dc} \end{bmatrix} + S(\theta) \begin{bmatrix} \dot{i}_\epsilon \\ \dot{i}_{dc} \end{bmatrix}$$

with

$$\mathscr{A}(\theta) = \frac{d\overline{P}(\theta)}{d\theta} T \tag{3.62}$$

From (3.58) the derivative $d\overline{P}(\theta)/d\theta$ follows:

$$\frac{d\overline{P}(\theta)}{d\theta} = \sqrt{2/3} \begin{bmatrix} -\sin\theta & -\sin(\theta - 2\pi/3) & -\sin(\theta + 2\pi/3) \\ \cos\theta & \cos(\theta - 2\pi/3) & \cos(\theta + 2\pi/3) \end{bmatrix} \tag{3.63}$$

If these equations are substituted in the dynamic model (3.44) and using (3.45)–(3.47) the result is:

$$\begin{bmatrix} L_s S(\theta) & M \\ M^T S(\theta) & L_r \end{bmatrix} \begin{bmatrix} \dot{i}_\epsilon \\ \dot{i}_{dc} \\ \dot{i}_r \end{bmatrix} = -\begin{bmatrix} (R_s + \omega \mathscr{L}_s) S(\theta) + \omega L_s \mathscr{A}(\theta) & \omega \mathscr{M} \\ \omega M^T \mathscr{A}(\theta) & R_r \end{bmatrix} \begin{bmatrix} i_\epsilon \\ i_{dc} \\ i_r \end{bmatrix} - \begin{bmatrix} I \\ 0 \end{bmatrix} \begin{bmatrix} u_d \\ u_q \end{bmatrix} + \begin{bmatrix} 0 \\ u_F \\ 0 \end{bmatrix} \tag{3.64}$$

with $i_r = [i_F\ i_D\ i_Q]^T$.

Premultiplying this with $\begin{bmatrix} S^T(\theta) & 0 \\ 0 & I \end{bmatrix}$ and using eq.(3.61), yields:

$$\begin{bmatrix} S^T(\theta)L_s S(\theta) & S^T(\theta)M \\ M^T S(\theta) & L_r \end{bmatrix} \begin{bmatrix} \dot{i}_\epsilon \\ \dot{i}_{dc} \\ \dot{i}_r \end{bmatrix} =$$

$$\begin{bmatrix} S^T(\theta)[(-R_s-\omega\mathscr{L}_s)S(\theta)-\omega L_s\mathscr{A}(\theta)] & -\omega S^T(\theta)\mathscr{M} \\ -\omega M^T\mathscr{A}(\theta) & -R_r \end{bmatrix} \begin{bmatrix} i_\epsilon \\ i_{dc} \\ i_r \end{bmatrix} +$$

$$\begin{bmatrix} 0 \\ -1 \\ 0 \end{bmatrix} u_{dc} + \begin{bmatrix} 0 \\ 0 \\ [1\ 0\ 0]^T \end{bmatrix} u_F$$

Elimination of the internal variable u_{dc} is possible using the state equation for the direct current link (3.49) which yields the final complete nonlinear model of the synchronous generator with DC link in the *generalized state space* notation [Rosenbrock, 1974; Verghese et al., 1981]:

$$E(\theta)\dot{x} = A(\theta,\omega)x + Bu \tag{3.65}$$

with

$$x = [i_\epsilon\ i_{dc}\ i_F\ i_D\ i_Q]^T$$

$$u = [u_i\ u_F]^T$$

$$E(\theta) = \begin{bmatrix} S^T(\theta)L_s S(\theta)+\begin{bmatrix} 0 & 0 \\ 0 & L_{dc} \end{bmatrix} & S^T(\theta)M \\ M^T S(\theta) & L_r \end{bmatrix}$$

$$A(\theta,\omega) = \begin{bmatrix} S^T(\theta)[(-R_s-\omega\mathscr{L}_s)S(\theta)-\omega L_s\mathscr{A}(\theta)]+\begin{bmatrix} 0 & 0 \\ 0 & -R_{dc} \end{bmatrix} & -\omega S^T(\theta)\mathscr{M} \\ -\omega M^T\mathscr{A}(\theta) & -R_r \end{bmatrix}$$

$$B = \begin{bmatrix} 0 & 0 \\ -1 & 0 \\ 0 & 1 \\ 0 & 0 \\ 0 & 0 \end{bmatrix},$$

with $S(\theta)$ from (3.59), $\mathscr{A}(\theta)$ form (3.63), and L_s, L_r, M, R_s, R_r, $\mathscr{L}_s$ and $\mathscr{M}$ from (3.45)–(3.47). Note that $E(\theta)=E(\theta)^T$.

Model (3.65) can be used for nonlinear simulations with (3.51) and (3.55) defining the switching moments. However, to use (3.55) we have to obtain an output equation for the voltages. From the Park transformation we have

$$\begin{bmatrix} u_a \\ u_b \\ u_c \end{bmatrix} = \bar{P}^T(\theta)\begin{bmatrix} u_d \\ u_q \end{bmatrix}$$

and the voltages u_d and u_q can be extracted from (3.64):

$$\begin{bmatrix} u_d \\ u_q \end{bmatrix} = E_1(\theta)\dot{x} + E_2(\theta,\omega)x$$

with

$$E_1(\theta) = [-L_s S(\theta) \quad -M]$$

$$E_2(\theta,\omega) = [-(R_s+\omega\mathscr{L}_s)S(\theta)-\omega L_s\mathscr{A}(\theta) \quad -\omega\mathscr{M}]$$

Substitution of (3.65) gives:

$$\begin{bmatrix} u_d \\ u_q \end{bmatrix} = \left\{E_1(\theta)E^{-1}(\theta)A(\theta,\omega) + E_2(\theta,\omega)\right\}x + E_1(\theta)E^{-1}(\theta)Bu \tag{3.66}$$

Combining this with (3.55) gives the condition for the time θ_u, which is α_r before the end of the period:

$$Q_2'(\theta,\omega)x + Q_3(\theta)u = 0 \tag{3.67}$$

with

$$Q_2'(\theta,\omega) = Q_2 P^T(\theta)\left\{E_1(\theta)E^{-1}(\theta)A(\theta,\omega) + E_2(\theta,\omega)\right\}$$

$$Q_3(\theta) = Q_2 P^T(\theta)E_1(\theta)E^{-1}(\theta)B$$

Finally, the output equation for the torque is

$$T_e = \left\{(L_d-L_q)S_1(\theta)\begin{bmatrix} i_\epsilon \\ i_{dc} \end{bmatrix}[i_\epsilon\ i_{dc}]S_2^T(\theta) + \right.$$

$$\left. L_{md}(i_F+i_D)S_2(\theta)\begin{bmatrix} i_\epsilon \\ i_{dc} \end{bmatrix} - L_{mq}S_1(\theta)\begin{bmatrix} i_\epsilon \\ i_{dc} \end{bmatrix} i_Q\right\}/3 \tag{3.68}$$

with $S_1(\theta)$ and $S_2(\theta)$ such that $S(\theta)=\begin{bmatrix} S_1(\theta) \\ S_2(\theta) \end{bmatrix}$.

Suppose θ is such that the commutation phase is active and that the switching matrix T is equal to (3.53). From (3.58) and (3.59) and some trigonometric relations we get:

$$S(\theta) = \sqrt{2}\begin{bmatrix} \sin(\theta+\pi/3) & -\sin(\theta) \\ -\cos(\theta+\pi/3) & \cos(\theta) \end{bmatrix}$$

whereas for the non–commutation phase with T according to (3.54) the matrix $S(\theta)$ becomes

$$S(\theta) = \sqrt{2}\begin{bmatrix} 0 & -\sin(\theta-\pi/3) \\ 0 & \cos(\theta-\pi/3) \end{bmatrix}$$

Using these expressions it is easily verified that the generalized state space model (3.65) has five states at commutation. During the non–commutating topology the extra current i_ϵ is not present (both in $E(\theta)$ and in $A(\theta)$ the first row and column are zero vectors).
This means we have a periodically switching generalized state space model with a variable model order.

Analysis of the model

Rewriting the model (3.65) into its two intervals of interest and scaling the time variable from t to θ: $dx/dt=dx/d\theta \cdot d\theta/dt=dx/d\theta \cdot \omega$, the final model can be described as follows:

$$\begin{aligned}
&\omega E_1(\theta)\frac{dx_1}{d\theta} = A_1(\theta,\omega)x_1 + B_1u_1,\ x(\theta_0) = x_0 && \text{for } \theta_0 \le \theta < \theta_1\\
&0 = Q_1x_1 && \text{for } \theta=\theta_1\\
&\omega E_2(\theta)\frac{dx_2}{d\theta} = A_2(\theta,\omega)x_2 + B_2u_2, && \text{for } \theta_1 < \theta \le \theta_2\\
&0 = Q_2'(\theta,\omega)x + Q_3(\theta)u && \text{for } \theta=\theta_u,\ \theta_2=\theta_u+\alpha_r
\end{aligned}$$

The equations satisfy a Lipschitz condition (definition 3.1) because in each subinterval (for each $S(\theta)$) the coefficients are piecewise continuous, differentiable functions (definition 3.2).

At θ_0 the commutation period begins with five internal states. At a moment θ, $i_\epsilon=i_{dc}$, such that relation (3.51) is satisfied. This moment is called $\theta=\theta_1$. After this switching event the non–commutation model (2) is valid up to the next cycle, with $T=\theta_2-\theta_0=\pi/3$, where $\theta_2=\theta_u+\alpha_r$ with θ_u defined by (3.67) and α_r the delay angle of the rectifier. Continuity of the state variables is guaranteed if the following interconnection relations hold:

$$\begin{aligned}
&x_2(\theta_1) = Hx_1(\theta_1),\\
&x_1(\theta_2) = H^Tx_2(\theta_2),
\end{aligned} \tag{3.69}$$

with $H=[0\ I_4]$, of which the latter assures that $i_\epsilon=0$ at $\theta=\theta_0(\theta_2)$.
It is possible to use this model for numerical simulations (section 3.7), but while the model is in the first interval at every simulation step condition (3.51) must be checked. If i_ϵ approaches i_{dc} the simulation time–step is decreased to assure sufficiently small errors at $\theta=\theta_1$. The same holds for the calculation of time $\theta_2(\theta_u)$. The resulting model is not suited for control system design. For that reason an averaged model will be derived in section 3.6 after the nominal periodic solution has been modelled.

3.5 CALCULATION OF THE NOMINAL PERIODIC SOLUTION

One important problem to solve before we can do numerical analyses with the dynamic model (3.65) is to obtain the nominal periodic solution (definition 3.7). As explained in the preceding section the complete behaviour of the system is described by two stages.

The input variables $u=[u_F\ u_i]^T$ and ω are constant in the nominal case. Because of (3.41) $\theta\equiv\omega t$. The other input parameter is $\theta_0(\alpha_r)$ which is assumed to be given (see also below). According to definition 3.7 we have to solve (3.65) for a solution for which $x(\theta+T)=x(\theta)$. For a numerical simulation all we need to know is the initial condition $x(\theta_0)$, such that the solution is the nominal periodic one belonging to the given ω, u and θ_0. As a result $x(\theta_0)$ and the switching moment θ_1 are found.
Because the problem is not analytically solvable, we use a numerical iterative calculation. First take a θ_1: $\theta_0 \le \theta_1 \le \theta_0+T$ and calculate with the formula's (3.9)–(3.12) applied to (3.65):

$$x_1(\theta_1) = A_1x_1(\theta_0) + B_1u_1 \tag{3.70}$$
$$x_2(\theta_0+T) = A_2x_2(\theta_1) + B_2u_2 \tag{3.71}$$

with $u_1=u$, $u_2=u$ are constant.
At the time θ_1 the interconnection relation (3.69) must be satisfied:

$$x_2(\theta_1) = Hx_1(\theta_1), \qquad \text{with } H=[0\ I_4]$$

as well as

$$Q_1x_1(\theta_1) = 0 \qquad \text{with } Q_1=[-1\ 1\ 0\ 0\ 0] \tag{3.72}$$

The necessary condition for the solution x(t) to be periodic of period T is that:

$$x_2(\theta_0+T) = Hx_1(\theta_0)$$

and from (3.69):

$$x_1(\theta_0) = H^Tx_2(\theta_0+T) \tag{3.73}$$

which assures that the current $i_\epsilon(\theta_0)=0$.
From these relations the following result is obtained:

Lemma 3.8.
The nominal periodic solution $(x_1(\theta_0),\theta_1)$ for the system (3.70),(3.71) under the conditions given by (3.93),(3.72),(3.73) is

$$x_1(\theta_0) = V^{-1}(\theta_0,\theta_1)W(\theta_0,\theta_1) \tag{3.74}$$

with

$$V(\theta_0,\theta_1) = I - H^T A_2(\theta_0,\theta_1)HA_1(\theta_0,\theta_1)$$
$$W(\theta_0,\theta_1) = H^T(A_2(\theta_0,\theta_1)HB_1(\theta_0,\theta_1)u_1 + B_2(\theta_0,\theta_1)u_2)$$

The matrices $V(\theta_0,\theta_1)$ and $W(\theta_0,\theta_1)$ are functions of the variable θ_1 due to the time–varying nature of (3.65). The value θ_1 is the solution to

$$Q_1\left\{A_1(\theta_0,\theta_1)V^{-1}(\theta_0,\theta_1)W(\theta_0,\theta_1) + B_1(\theta_0,\theta_1)u_1\right\} = 0 \qquad (3.75)$$

Proof: Substitution of (3.70) in (3.71) using (3.69) gives (omitting the arguments):

$$x_2(\theta_0+T) = A_2HA_1x_1(\theta_0) + A_2HB_1u_1 + B_2u_2$$

premultiplying with H^T, and using the boundary conditions (3.73) yields

$$x_1(\theta_0) = H^T x_2(\theta_0+T) = H^T A_2HA_1x_1(\theta_0) + H^T(A_2HB_1u_1+B_2u_2)$$

or

$$(I- H^T A_2HA_1)x_1(\theta_0) = H^T(A_2HB_1u_1+B_2u_2)$$

which gives the first result.

Equation (3.72) can be elaborated as follows:

$$Q_1x_1(\theta_1) = 0 \qquad \Rightarrow \qquad Q_1\{A_1x_1(\theta_0) + B_1u_1\} = 0$$

and substitution of (3.74) gives (3.75). This completes the proof. □

The variable θ_1 can be found using an iterative optimization scheme (see below). Using this value, with eq.(3.74) the periodic solution $x_1(\theta_0)$ can be calculated. The formula's (3.74–75) have also been derived by Padiyar and Kalra [1986] for a six–pulse converter.

The following procedure is used:

1) determine models A_1,A_2,B_1,B_2 (3.70),(3.71) for given θ_1,u_i,ω,θ_0
2) solve (3.75) and find a new θ_1,
3) use this new θ_1 and go to step 1 until (3.75) is exactly matched, then go to 4:
4) using the calculated θ_1 and the related A_1,A_2,B_1,B_2, calculate V and W and finally calculate the nominal periodic solution $x_1(\theta_0)$ (definition 3.7) with (3.74).
5) calculate the time θ_u for which (3.67) holds. Then adjust θ_0 and go to step 1 until $\theta_0-\theta_u+\pi/3=\alpha_r$.

Remark: if the inputs are constant over the interval of interest, the most convenient way to calculate a first guess for the nominal periodic solution is to calculate the commutation delay ($\mu_r=\theta_1-\theta_0$) using a steady state model of the synchronous machine, see e.g.[Steinbuch, 1986], see also Appendix A.2.

3.6 THE APPROXIMATING LINEAR MODEL

Using the model (3.65) it is possible to perform nonlinear simulations with some initial condition. However, every dynamic nonlinear simulation needs a variable step size due to the fact that the switching moments θ_1 and θ_2 are functions of the trajectories. For this problem several algorithms are worked out in literature, see the references in the beginning of this chapter.
Because we are not primarily interested in the high–frequent (400Hz) behaviour of the system and we are not able to design periodic controls, an averaged model will be derived.

Given the nominal periodic solution we are able to derive a model which describes small perturbations around the nominal solution. The problem statement as well as the solution for the linearization of two time–interconnected nonlinear differential equations, has already been presented in section 3.2. The central result of §3.2 is the set of equations (3.24),(3.25) and (3.39). In section 3.6.1 the required partial derivatives will be calculated for the system (3.65) under investigation. The resulting set of equations is periodic of period $T=\pi/3$.
The next step is to derive a simplified sampled data model as described in section 3.2.4. This is obtained through application of the Floquet theory (theorem 3.1) and corollary 3.1. The averaged model is then defined as in definition 3.11, see section 3.6.2 for the application to the system.

3.6.1 Linearization

Because it is very important for the coupling with the other subsystems in the process we need ω as well as α_r as inputs of the model.
The angular velocity ω has two major nonlinear effects. First, it appears directly into matrix $A(\theta,\omega)$ of eq.(3.65), due to the induced voltages. Secondly, because $\omega=d\theta/dt$ the angle θ is a function of ω. In the sequel we will use (3.65) with the derivative scaled to the rotor angle θ, because this is the most convenient way to apply the averaging approach. Using $dt=d\theta/\omega$ (3.65) becomes:

$$\omega E(\theta)\frac{dx}{d\theta} = A(\theta,\omega)x + Bu$$

or

$$\frac{dx}{d\theta} = \frac{1}{\omega}E^{-1}(\theta)A(\theta,\omega)x + \frac{1}{\omega}E^{-1}(\theta)Bu \qquad (3.76)$$

Note that because all matrix functions are Lipschitz (definition 3.1) the equations are linearizable (definition 3.3). Using expression (3.3) and using a bar to indicate the nominal solution, we obtain with $x=\bar{x}+\Delta x$, $\omega=\bar{\omega}+\Delta\omega$ (for the time being $\Delta u=0$):

$$E(\theta)d\Delta x/d\bar{\theta} = \frac{1}{\bar{\omega}}A(\bar{\theta},\bar{\omega})\Delta x + \left[\frac{\partial\{A(\bar{\theta},\bar{\omega})/\omega\}}{\partial\omega}\bar{x}(\bar{\theta}) - \frac{1}{\bar{\omega}^2}B\bar{u}\right]\Delta\omega \tag{3.77}$$

and from the formula for $A(\theta,\omega)$ (3.65) the partial derivative follows:

$$\frac{\partial\{A(\bar{\theta},\bar{\omega})/\bar{\omega}\}}{\partial\omega} = \begin{bmatrix} S^T(\bar{\theta})R_sS(\bar{\theta})+\begin{bmatrix}0 & 0\\ 0 & R_{dc}\end{bmatrix} & 0 \\ 0 & R_r\end{bmatrix}\cdot\frac{1}{\bar{\omega}^2} \tag{3.78}$$

Once the nominal periodic solution $\bar{x}(\bar{\theta}),\bar{u}(\bar{\theta})$ is known, the input vector with respect to $\Delta\omega$ can be calculated. Combining (3.77) with linearization with respect to the input $u=\bar{u}+\Delta u$ the linear model becomes:

$$\frac{dx}{d\theta} = \frac{1}{\bar{\omega}}E(\bar{\theta})^{-1}A(\bar{\theta},\bar{\omega})\Delta x + \frac{1}{\bar{\omega}}E(\bar{\theta})^{-1}B\Delta u + \frac{1}{\bar{\omega}^2}E(\bar{\theta})^{-1}\left[\begin{bmatrix} S^T(\bar{\theta})R_sS(\bar{\theta})+\begin{bmatrix}0 & 0\\ 0 & R_{dc}\end{bmatrix} & 0 \\ 0 & R_r\end{bmatrix}\bar{x}(\bar{\theta})-B\bar{u}\right]\Delta\omega \tag{3.79}$$

In order to obtain the correction term in (3.39) we have to linearize the switching condition (3.67). Assume that $\theta=\bar{\theta}+\Delta\theta$, $\omega=\bar{\omega}+\Delta\omega$, $x_2=\bar{x}_2+\Delta x_2$, $u_2=\bar{u}_2+\Delta u_2$ (second interval) then linearization of (3.67) gives (see also (3.37)):

$$\Delta\theta_2 = -Q_u^{-1}(\bar{\theta}_u,\bar{\omega})Q_2'(\bar{\theta}_u,\bar{\omega})\Delta x_2(\bar{\theta}_u) - Q_u^{-1}(\bar{\theta}_u,\bar{\omega})Q_3(\bar{\theta}_u)\Delta u_2(\bar{\theta}_u) - Q_u^{-1}(\bar{\theta}_u,\bar{\omega})\frac{\partial Q_2'(\bar{\theta}_u,\bar{\omega})}{\partial\omega}\bar{x}_2(\bar{\theta}_u)\Delta\omega(\bar{\theta}_u) + \Delta\alpha_r \tag{3.80}$$

with

$$Q_u(\bar{\theta}_u,\bar{\omega}) = Q_2'(\bar{\theta}_u,\bar{\omega})\frac{\partial\bar{x}_2(\bar{\theta}_u)}{\partial\theta} + \frac{\partial Q_2'(\bar{\theta}_u,\bar{\omega})}{\partial\theta}\overline{\omega x}_2(\bar{\theta}_u) + \frac{\partial Q_3'(\bar{\theta}_u,\bar{\omega})}{\partial\omega}\overline{\omega u}_2(\bar{\theta}_u)$$

and where it is assumed that the input is constant within each interval ($\partial\bar{u}/\partial\theta=0$) The partial derivatives are:

$$\frac{\partial\bar{x}_2(\bar{\theta}_u)}{\partial\theta} = \frac{1}{\bar{\omega}}E^{-1}(\bar{\theta}_u)A(\bar{\theta}_u,\bar{\omega})\bar{x}(\bar{\theta}_u) + \frac{1}{\bar{\omega}}E^{-1}(\bar{\theta}_u)B\bar{u}$$

$$\frac{\partial Q_2'(\theta,\omega)}{\partial\theta} = \frac{\partial}{\partial\theta}\left[Q_2P^T(\theta)\left\{E_1(\theta)E^{-1}(\theta)A(\theta,\omega) + E_2(\theta,\omega)\right\}\right]$$

$$= Q_2\frac{\partial P^T}{\partial\theta}(E_1E^{-1}A+E_2) + Q_2P^T\left\{\frac{\partial E_1}{\partial\theta}E^{-1}A - E_1E^{-1}\frac{\partial E}{\partial\theta}E^{-1}A + E_1E^{-1}\frac{\partial A}{\partial\theta} + \frac{\partial E_2}{\partial\theta}\right\}$$

(leaving the argument (θ,ω) out for notational convenience), with

$$\frac{\partial E(\theta)}{\partial\theta} = \begin{bmatrix} \mathscr{S}^T(\theta)L_sS(\theta)+S^T(\theta)L_s\mathscr{A}(\theta) & \mathscr{S}^TM \\ M^T\mathscr{A}(\theta) & \end{bmatrix}$$

and (note that $\partial S/\partial\theta=\mathscr{S}$ and $\partial\mathscr{S}/\partial\theta=-S$):

$$\frac{\partial A(\theta,\omega)}{\partial\theta} = -\begin{bmatrix} \mathscr{S}^T(\theta)\left\{(R_s+\omega\mathscr{L}_s)S(\theta)+\omega L_s\mathscr{A}(\theta)\right\}+S^T(\theta)\left\{(R_s+\omega\mathscr{L}_s)\mathscr{A}(\theta)-\omega L_sS(\theta)\right\} & \omega\mathscr{S}^T(\theta)\mathscr{M} \\ -\omega M^TS(\theta) & 0\end{bmatrix}$$

$$\frac{\partial E_1(\theta)}{\partial\theta} = [-L_s\mathscr{A}(\theta) \quad 0]$$

$$\frac{\partial E_2(\theta,\omega)}{\partial\theta} = [-(R_s+\omega\mathscr{L}_s)\mathscr{A}(\theta)+\omega L_sS(\theta) \quad 0]$$

For the other derivatives we find:

$$\frac{\partial Q_3(\theta,\omega)}{\partial\theta} = \frac{\partial}{\partial\theta}\left\{Q_2P^T(\theta)E_1(\theta)E^{-1}(\theta)B\right\} = Q_2\frac{\partial P^T}{\partial\theta}E_1E^{-1}B + Q_2P^T\left\{\frac{\partial E_1}{\partial\theta}E^{-1}B - E_1E^{-1}\frac{\partial E}{\partial\theta}E^{-1}B\right\}$$

and finally

$$\frac{\partial Q_2'(\theta,\omega)}{\partial\omega} = Q_2P^T\left\{E_1E^{-1}\frac{\partial A}{\partial\omega}+\frac{\partial E_2}{\partial\omega}\right\}$$

with

$$\frac{\partial A(\theta,\omega)}{\theta\omega} = \begin{bmatrix} -S^T(\theta)\mathscr{L}_sS(\theta)-S^T(\theta)L_s\mathscr{A}(\theta) & -S^T\mathscr{M} \\ -M^T\mathscr{S}(\theta) & 0\end{bmatrix}$$

$$\frac{\partial E_2(\theta,\omega)}{\partial\omega} = [-\mathscr{L}_sS(\theta)-\omega L_s\mathscr{A}(\theta) \quad -\mathscr{M}]$$

Finally, the output equation (3.68) for the torque T_e is in its linearized form with respect to the state variables:

$$\Delta T_e = C(\bar{\theta},\bar{x})\Delta x \tag{3.81}$$

with (leaving the argument (θ,x) out for notational convenience):

$$C^T = \frac{1}{3}\begin{bmatrix} (L_d-L_q)[2S_{11}S_{21}i_\epsilon+(S_{11}S_{22}+S_{12}S_{21})i_{dc}]+L_{md}(i_F+i_D)S_{21}-L_{mq}i_Q S_{11} \\ (L_d-L_q)[2S_{12}S_{22}i_{dc}+(S_{11}S_{22}+S_{12}S_{21})i_\epsilon]+L_{md}(i_F+i_D)S_{22}-L_{mq}i_Q S_{12} \\ L_{md}(S_{21}i_\epsilon+S_{22}i_{dc}) \\ L_{md}(S_{21}i_\epsilon+S_{22}i_{dc}) \\ -L_{mq}(S_{11}i_\epsilon+S_{12}i_{dc}) \end{bmatrix}$$

with S_{ij} element of $S(\theta)$.

3.6.2 The averaged model

Recall that the set of differential equations (3.65) and the output equations (3.67),(3.68) are both periodic of period $T=\pi/3$ in steady–state. This property holds also for the linearized model obtained in the preceding section. This enables us to average (definition 3.11) the solution, such that with a linear time–invariant model the behaviour is approximated. The procedure (section 3.2.4) is as follows.

1) The linearized differential equation (3.79) can be used to calculate the transition from a deviation at θ_0 to a deviation at θ_1 (first interval): $\Delta x_1(\theta_0),\Delta u_1(\theta_0) \rightarrow \Delta x_1(\theta_1)$.
2) The transition from $\Delta x_1(\theta_1)$ to $\Delta x_2(\theta_1)$ is defined by (3.21):
$$\Delta x_2(\theta_1) = \left\{\left[\frac{\partial x_2}{\partial\theta_1} - H\frac{\partial x_1}{\partial\theta_1}\right]\left[Q_1\frac{\partial x_1}{\partial\theta_1}\right]^{-1}Q_1+H\right\}\Delta x_1(\theta_1)$$
The derivatives follow from (3.76) for $\theta=\theta_1$.
3) The transition from $\Delta x_2(\theta_1)$ to $\Delta x_2(\theta_2)$ can be calculated with (3.79).
4) The transition from $\Delta x_2(\theta_2)$ to $\Delta x_1(\theta_2)$ can be calculated with (3.38):
$$\Delta x_1(\theta_2) = H^T\Delta x_2(\theta_2) + \left\{H^T\frac{\partial x_2}{\partial\theta} - \frac{\partial x_1}{\partial\theta}\right\}\Delta\theta_2$$
with the derivatives from (3.76) for $\theta=\theta_2$ and with $\Delta\theta_2$ from (3.80). In equation (3.80) the value $\Delta x_2(\theta_u)$ can be calculated with (3.79) using $\Delta x_2(\theta_1)$.

Summarizing (and leaving input variations out for simplicity):

$$\Delta x_1(\theta_0) \xrightarrow{(3.79)} \Delta x_1(\theta_1)) \xrightarrow{(3.21)} \Delta x_2(\theta_1) \xrightarrow{(3.79)} \Delta x_2(\theta_2) \xrightarrow{(3.38)} \Delta x_1(\theta_2)$$

$$\Delta x_2(\theta_1) \xrightarrow{(3.79)} \Delta x_2(\theta_u) \xrightarrow{(3.80)} \Delta\theta_2$$

The result is a sampled data (discrete time) model describing small perturbations from one period to the next. If we want to have a continuous time equivalent, this model can be transformed to continuous time by application of equation (3.31).
The output equation (3.81) becomes simpler because C is periodic of period T and we only want to know the value at θ_0 and θ_0+T (definition 3.11). For example choose θ_0 as the calculation moment. Then $S_{11}(\theta_0)=0$, $S_{21}(\theta_0)=0$ and $i_\epsilon=0$, which gives:

$$C^T = \frac{1}{3}\begin{bmatrix} (L_d-L_q)2S_{12}S_{22}i_{dc}+L_{md}(i_F+i_D)S_{22}-L_{mq}i_Q S_{12} \\ L_{md}S_{22}i_{dc} \\ L_{md}S_{22}i_{dc} \\ -L_{mq}S_{12}i_{dc} \end{bmatrix} \qquad (3.82)$$

One question is left open and deals with the choice of state variables. By theorem 3.1 and corollary 3.1 it follows that the real variables x(t) depend on the transformed ones (y(t), eq.(3.31)) by a time–varying matrix $P(t,\theta_0)$, periodic of period T. At the sample instances θ_0, θ_0+T, θ_0+2T,..θ_0+mT, we have from theorem 3.1 that $x(\theta_0+mT)=y(\theta_0+mT)$. So at the sampling instances there is no additional approximation error. The approximation involved here is $P(\theta,\theta_0)=I_n$ (averaged solution, definition 3.11). As already mentioned in section 3.2.3 the approximation error $\|\tilde{P}-P\|$ (or any other measure) can be quantified, and may be used in an uncertainty modelling (chapter 4).
Note that the characteristic exponents of the system do not depend on P nor on θ_0. With respect to stability analysis of the model the solution obtained is exact.

In the next section numerical results will be presented of the approach described.

3.7 NUMERICAL RESULTS

With the nonlinear and linearized model derived in the preceding sections it is possible to simulate and analyse the system. Numerical data used for the parameters of the synchronous machine and DC link are given in Appendix A.1. Using the *mean* steady–state model for the generator and DC link (Appendix A.2), it is possible to calculate some initial values. For instance, assume we know ω, T_e(mean), α_r and u_i then we can calculate the values u_F and θ_0. Using the value θ_0 the nominal periodic solution $(x_1(\theta_0),\theta_1)$ according to section 3.5, eq.(3.74), can be found.
The analysis is restricted to one full load and one partial load operating point:

		full load	partial load	
ω		1.00	0.75	[pu]
T_e		1.00	0.50	[pu]
α_r		0.30	0.30	[rad]
u_i		1.8123	2.2179	[pu]
P_e		300	100	[kW]

which results in

$\theta_0(\theta)$		1.4135	1.1547	[rad]
$\mu_r(=\theta_1-\theta_0)$		0.6127	0.1808	[rad]
	i_ϵ	0.0	0.0	[pu]
	i_{dc}	1.7526	0.5162	[pu]
$x_1(\theta_0) =$	i_F	2.8437	1.4767	[pu]
	i_D	0.1454	0.0925	[pu]
	i_Q	0.3321	0.2174	[pu]
	u_i	1.9557	2.1736	[pu]
$u =$				
	u_F	1.01e–2	5.14e–3	[pu]

Remark: the value for u_i has been adjusted such that the nominal periodic solution is exact (section 3.5). From the values above the initial value is very close to the ultimate voltage. All variables are given in per units.

Nonlinear simulations are carried out with $x_1(\theta_0)$, $u(=u_F,\alpha_r,u_i)$ and ω as inputs for the algorithm. These simulations provide an insight into the topology switch (section 3.7.1). Application of the linearization approach from section 3.6 gives a

low–frequent approximation of the dynamics (section 3.7.2) and offers the possibility to apply system theoretic tools.

3.7.1 Nonlinear simulations

Full load condition

In figure 3.6 the nonlinear responses are given at full load (P_e=300 kW), started in the calculated nominal periodic solution. The duration of the simulation is 3 cycles which is $3^*\pi/3$ rad ($=\pi/419$ s). From the figure we see a periodic behaviour with two different stages within one cycle. In the first (commutation) stage, the current i_ϵ increases from zero to i_{dc}. When $i_\epsilon=i_{dc}$ (constraint relation (3.51)) the next (non–commutation) stage begins. The current i_ϵ is then again zero (actually i_ϵ is not present at all in the model for the non–commutation topology). After $\pi/3$ rad from the beginning (nominal periodic solution) the next cycle occurs. At this full load condition the ratio between commutation and non–commutation time is

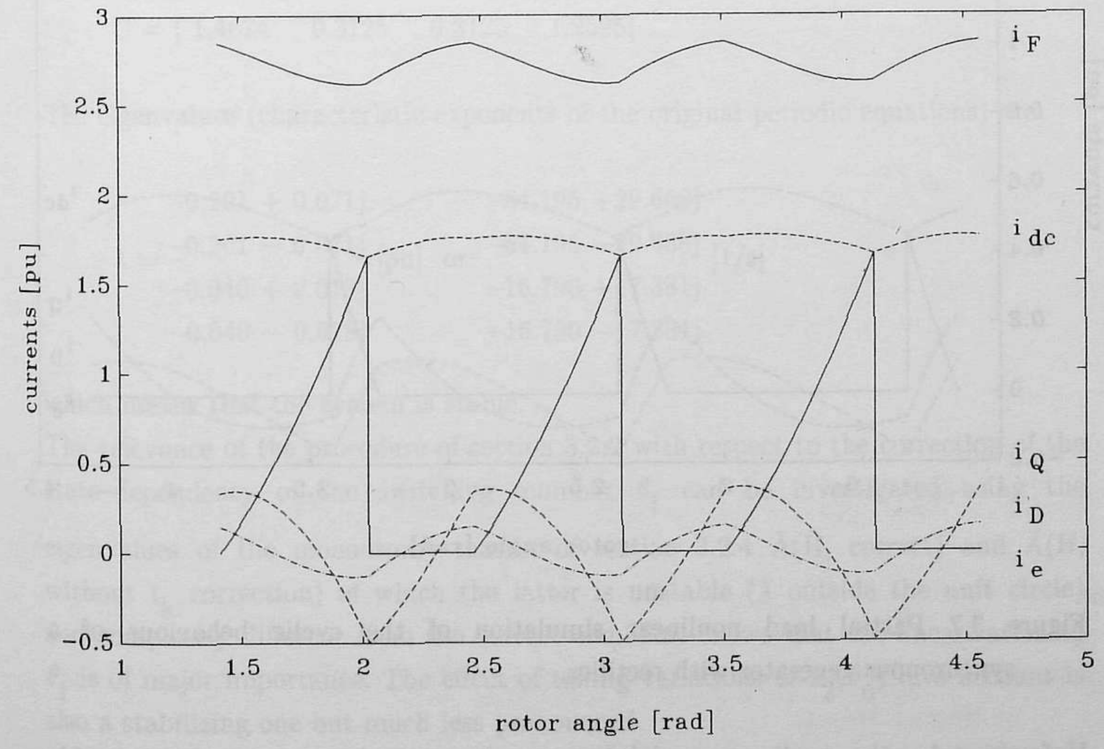

Figure 3.6 Full–load nonlinear simulation of the cyclic behaviour of a synchronous generator with rectifier.

almost one (see also the value of μ_r in the table above). We shall see later that at partial load this ratio is entirely different. In figure 3.6 the damper currents i_D and i_Q cycle around zero which is in accordance with their zero *mean* steady–state value (Appendix A.2). The currents i_{dc} and i_F contain a ripple due to the switching nature of the process.

Partial load

At partial load (P_e=100 kW) all values are decreased in magnitude (i_{dc}(mean)=0.5 pu), see figure 3.7. The duration of the commutation period has been reduced significantly. The ripple in the currents i_{dc} and i_F have been increased relatively. Note that also θ_0 has changed.

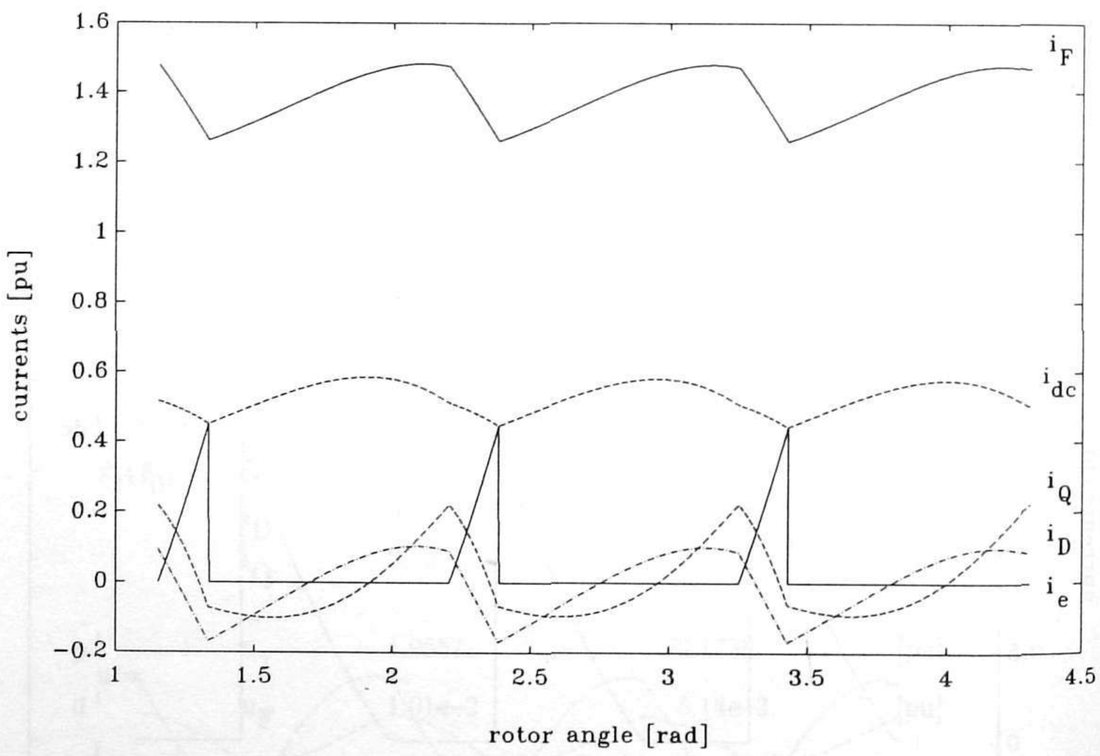

Figure 3.7 Partial load nonlinear simulation of the cyclic behaviour of a synchronous generator with rectifier.

Unfortunately, the nonlinear model is very computer–time consuming. For this reason long simulation runs have not been carried out.

3.7.2 Linear models

Full load condition

With the results of section 3.6 a linear continuous–time model has been calculated with the following results:

$$\dot{x} = Ax + Bu \qquad y = Cx$$

with $x^T=[i_{dc}\ i_F\ i_D\ i_Q]^T$, $u^T=[u_i\ u_F\ \omega\ \alpha_r]$, $y=T_e$, and with

$$A = \begin{bmatrix} -3.0011 & 2.4235 & 2.4138 & 1.1915 \\ -1.6547 & 1.3353 & 1.5071 & 0.7309 \\ -2.3320 & 1.8824 & 1.6908 & 0.8477 \\ 0.9873 & -0.8196 & -0.8156 & -0.5072 \end{bmatrix}$$

$$B = \begin{bmatrix} -0.9745 & 0.2758 & 1.9604 & -0.7297 \\ -0.5718 & 5.0039 & 1.1511 & -0.3969 \\ -0.7208 & -4.4574 & 1.4492 & -0.5727 \\ 0.3559 & -0.1143 & -0.7166 & 0.2292 \end{bmatrix}$$

$$C = [\ 1.4674 \quad 0.3125 \quad 0.3125 \quad 1.2525]$$

The eigenvalues (characteristic exponents of the original periodic equations) are:

$$\lambda = \begin{matrix} -0.201 + 0.071j \\ -0.201 - 0.071j \\ -0.040 + 0.018j \\ -0.040 - 0.018j \end{matrix} \text{ [pu] or } \begin{matrix} -84.195 + 29.668j \\ -84.195 - 29.668j \\ -16.790 + 7.381j \\ -16.790 - 7.381j \end{matrix} \text{ [1/s]}$$

which means that the system is stable.

The relevance of the procedure of section 3.2.2 with respect to the correction of the state–dependency of the switching moment θ_1 can be investigated using the eigenvalues of the monodromy matrix of section 3.2.4 $\bar{A}(\hat{H}$, correct) and $\bar{A}(H$, without t_k correction) of which the latter is unstable (λ outside the unit circle) and completely different from the correct one. This shows that the linearization to θ_1 is of major importance. The effect of taking variations of $\theta_2(\theta_u)$ into account is also a stabilizing one but much less pronounced.

The step responses of the states x and output y are given in figures 3.8–3.11. The most interesting observations are:

–the voltage u_i of the inverter (grid) excites especially the dynamics (figure 3.8) with a low static gain,

–current i_{dc}, i_F and torque T_e have similar responses,

–excitation of u_F (figure 3.9) gives a large static gain. The responses are significantly slower than with the inverter voltage,

–excitation of the speed ω (figure 3.10) gives a behaviour very similar to excitation of u_i with large dynamic responses,

–finally, with α_r (figure 3.11) responses are found similar to both the voltage u_i and ω excitation but with a larger steady–state gain.

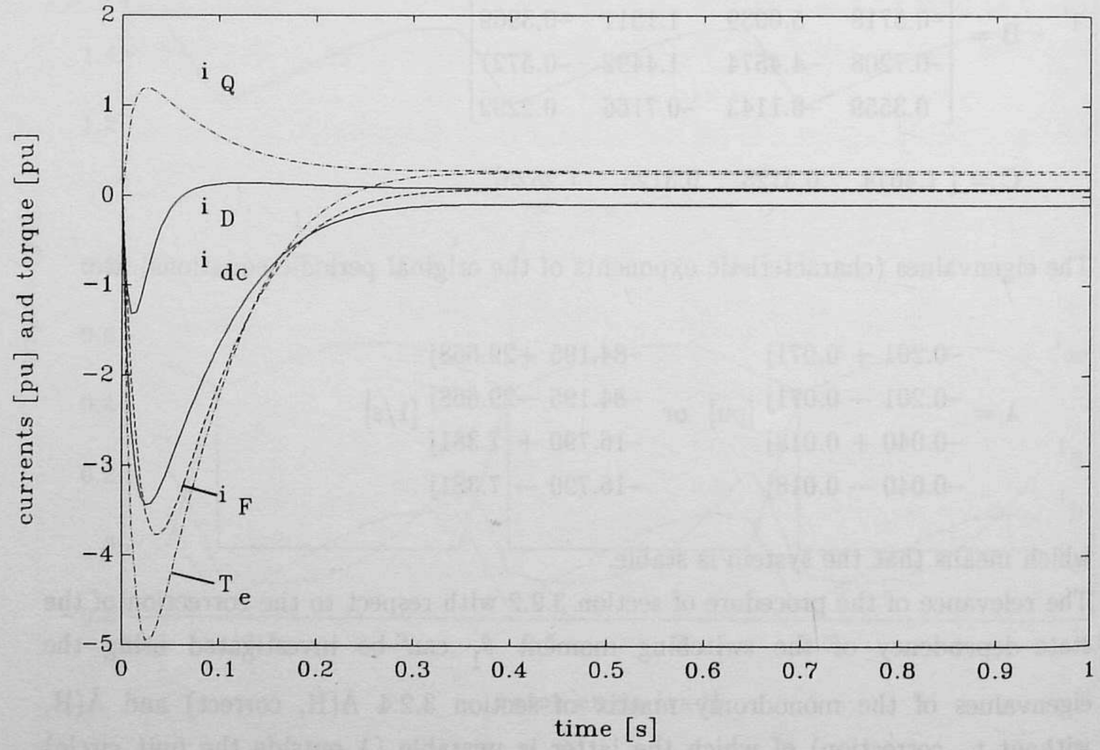

Figure 3.8 Step responses of the averaged linear model at full load to an increase in inverter voltage

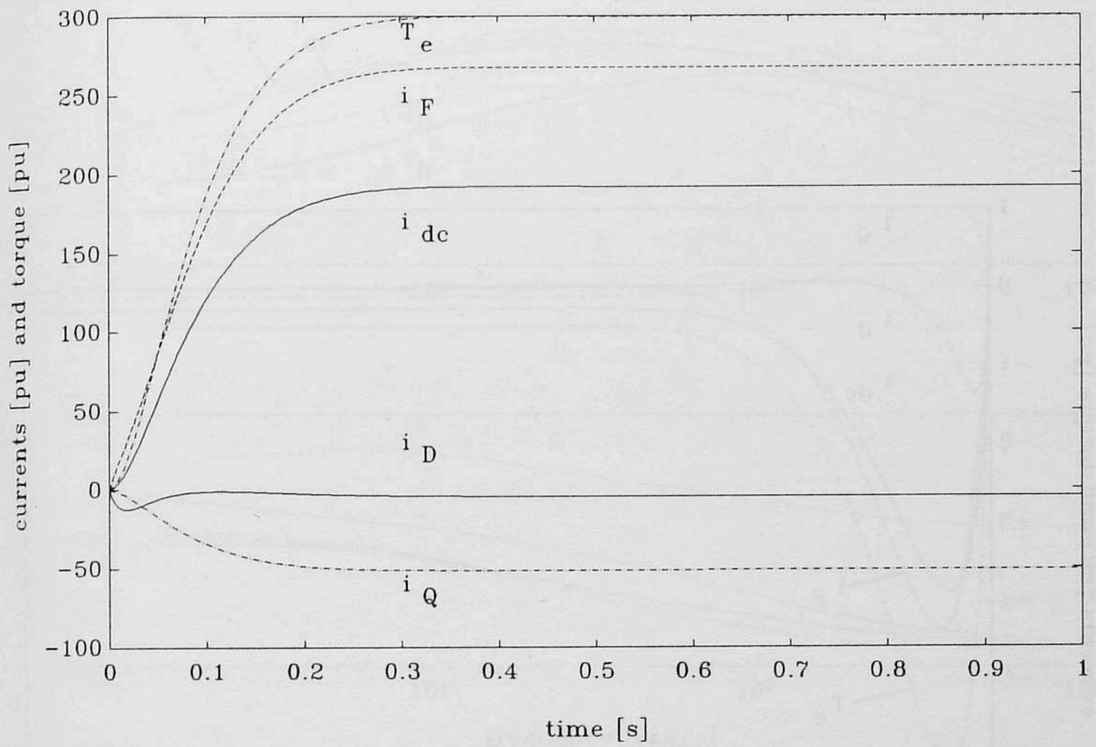

Figure 3.9 Step responses of the averaged linear model at full load to an increase in field voltage

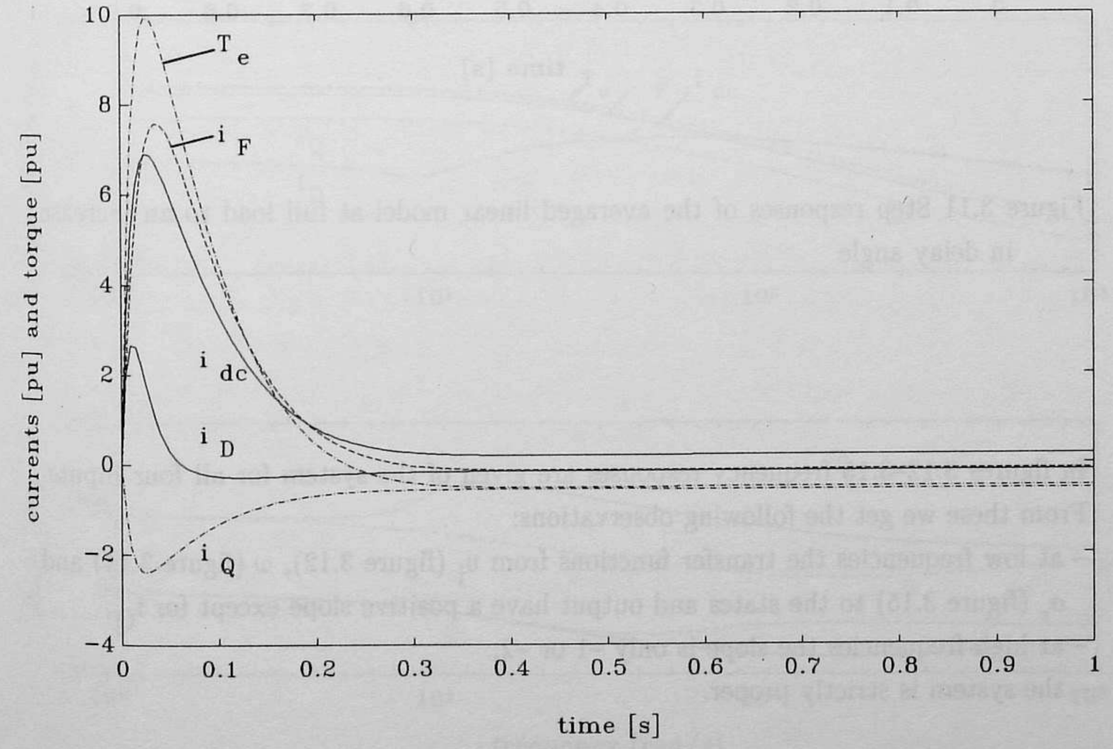

Figure 3.10 Step responses of the averaged linear model at full load to an increase in generator speed

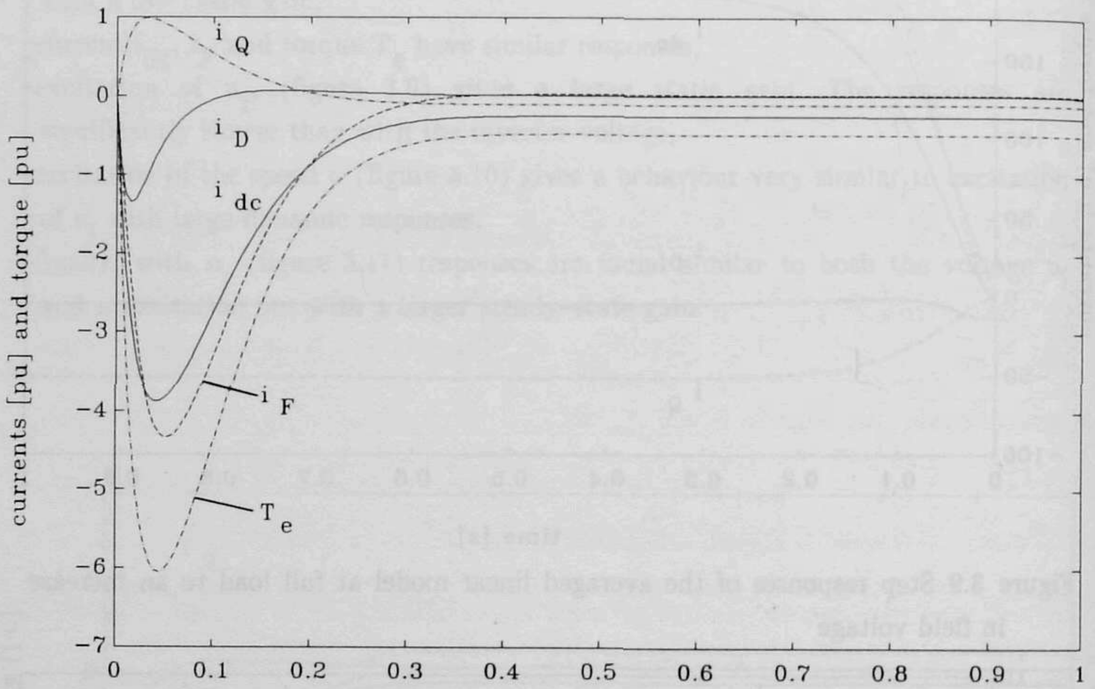

Figure 3.11 Step responses of the averaged linear model at full load to an increase in delay angle

In figures 3.12–3.15 frequency responses are given of the system for all four inputs. From these we get the following observations:

- at low frequencies the transfer functions from u_i (figure 3.12), ω (figure 3.14) and α_r (figure 3.15) to the states and output have a positive slope except for i_Q,
- at high frequencies the slope is only –1 or –2,
- the system is strictly proper.

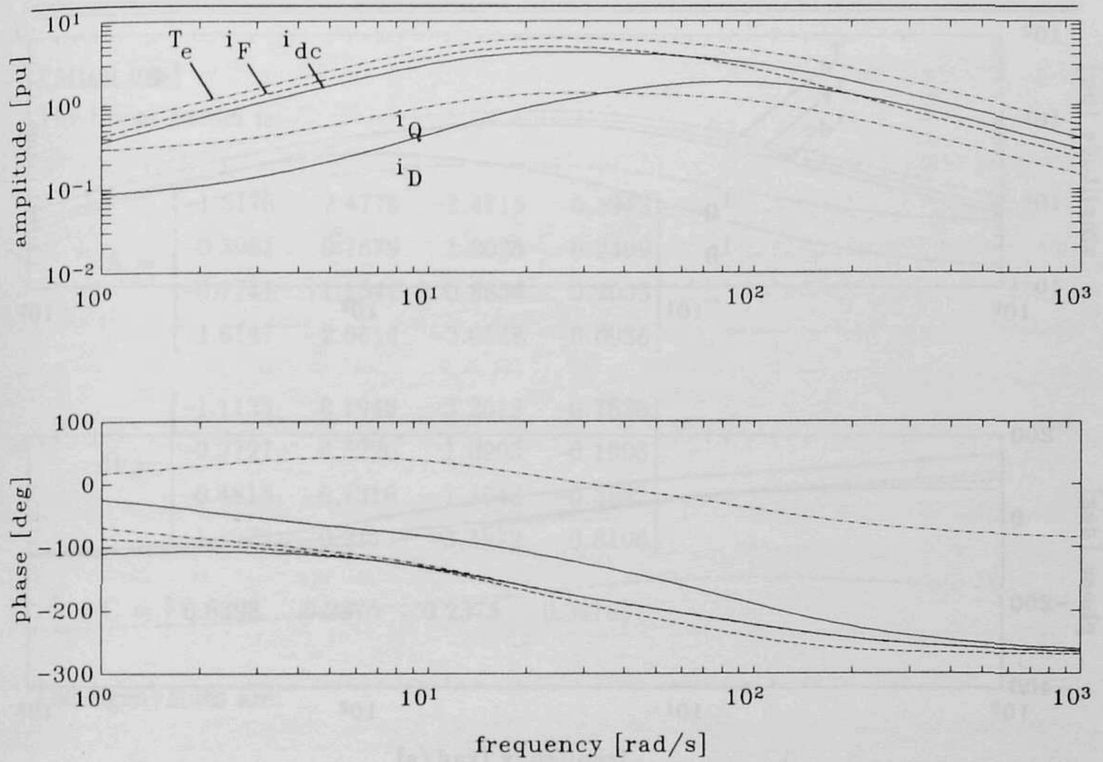

Figure 3.12 Bode diagram of the averaged linear model at full load with as input the inverter voltage

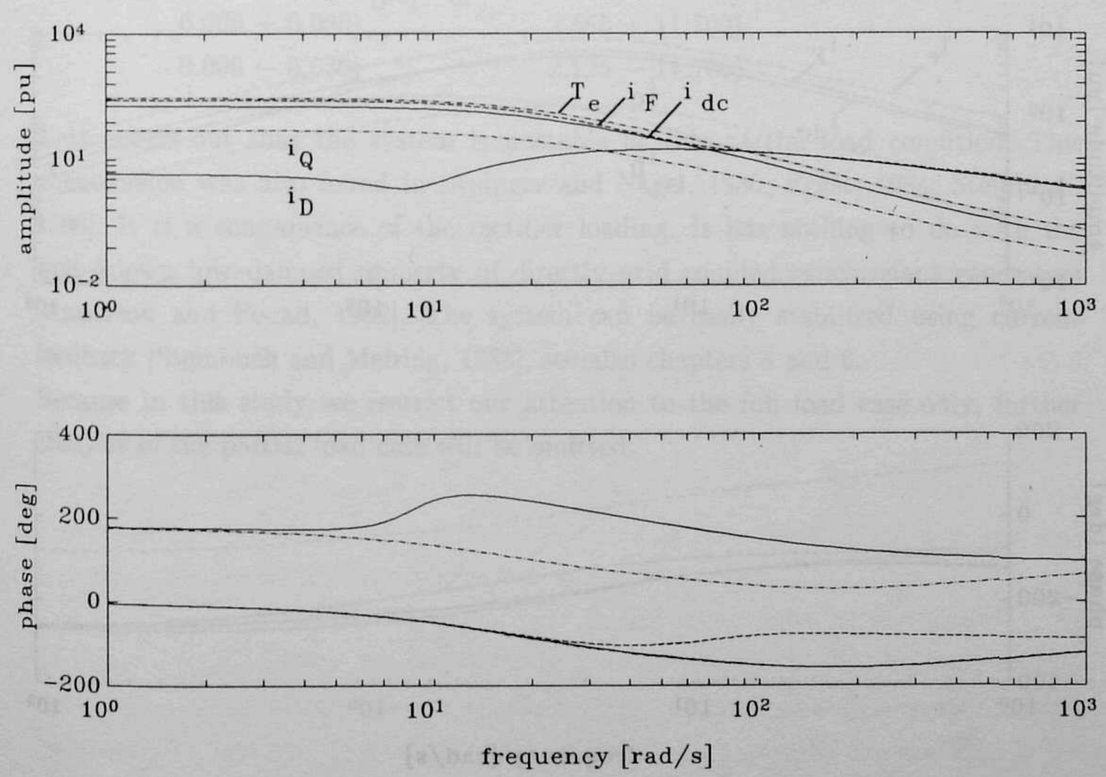

Figure 3.13 Bode diagram of the averaged linear model at full load with as input the field voltage

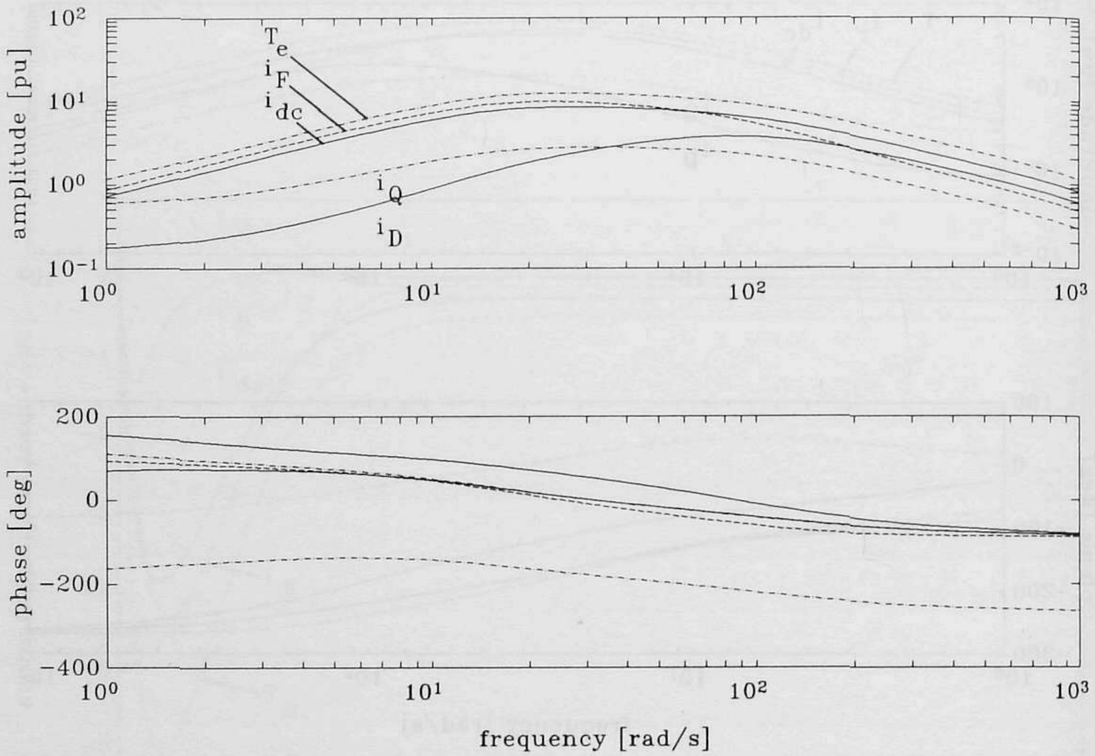

Figure 3.14 Bode diagram of the averaged linear model at full load with as input the generator speed

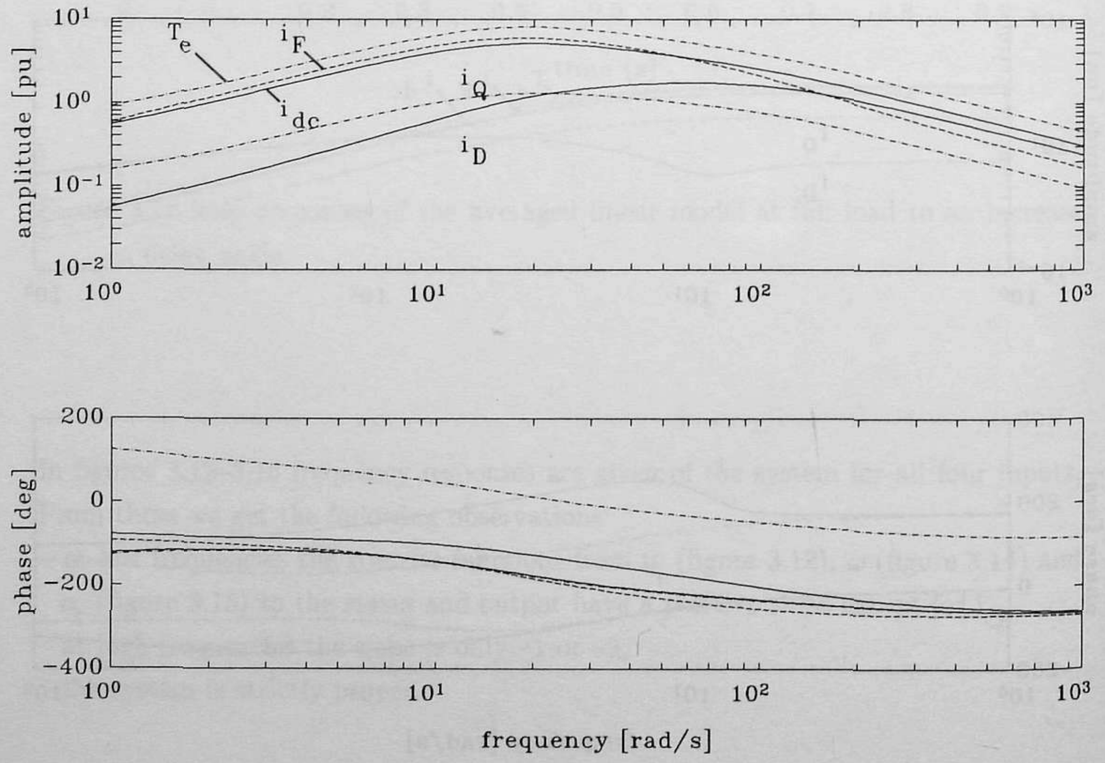

Figure 3.15 Bode diagram of the averaged linear model at full load with as input the delay angle

Partial load

The linear model is:

$$A = \begin{bmatrix} -1.5176 & 2.4776 & 2.4715 & 0.5943 \\ -0.3961 & 0.7679 & 1.0025 & 0.2499 \\ -0.7741 & 1.1341 & 0.8856 & 0.2035 \\ 1.6147 & -2.6614 & -2.6548 & -0.6936 \end{bmatrix}$$

$$B = \begin{bmatrix} -1.1133 & 0.1946 & 3.2519 & -0.7626 \\ -0.3727 & 6.5220 & 1.0903 & -0.1995 \\ -0.4815 & -6.1316 & 1.4048 & -0.3882 \\ 1.1972 & -0.2113 & -3.4972 & 0.8106 \end{bmatrix}$$

$$C = [\ 0.8398 \quad 0.2375 \quad 0.2375 \quad 0.3416]$$

The eigenvalues are:

$$\lambda = \begin{matrix} -0.285 + 0.071j \\ -0.285 - 0.071j \\ 0.006 + 0.030j \\ 0.006 - 0.030j \end{matrix} \text{ [pu] or } \begin{matrix} -119.360 + 29.737j \\ -119.360 - 29.737j \\ 2.565 + 11.700j \\ 2.125 - 11.700j \end{matrix} \text{ [1/s]}$$

This points out that the system is unstable at this partial load condition. This phenomenon was also found in [Auinger and Nagel, 1980; Ernst, 1984; Steinbuch, 1986]. It is a consequence of the rectifier loading. It has nothing to do with the well–known low–damped property of directly–grid coupled synchronous generators [Anderson and Fouad, 1982]. The system can be easily stabilized using current feedback [Steinbuch and Meiring, 1986], see also chapters 4 and 6.
Because in this study we restrict our attention to the full load case only, further analysis of the partial load case will be omitted.

3.8 SUMMARY

In this chapter a dynamic model has been derived for a synchronous generator loaded with a rectifier bridge. The model is based on the description of two topologies: the commutation and non–commutation stages. The switching of the thyristors is modelled in detail while the switching moments depend on the state–variables of the system.
Because simulation of this nonlinear model is extremely time–consuming and also for control system design purposes an approximating linear model has been derived. This linear model is based on an averaged description of the dynamics of the generator and rectifier in which the switching–time state–dependency is of major importance. The results are based on the application of the Floquet theory. Due to this exact, asymptotic stability analysis is possible with the model.
With a numerical example the cyclic behaviour has been shown, both at partial and at full load. Using the averaged model, linear models have been calculated. The most important properties are that at partial load an instability occurs, while at full load both fast and slow phenomena are present.
In the next chapters the linear model will be used for control system design of the complete wind turbine system.

4 WIND TURBINE MODELLING AND ANALYSIS

4.1 DESCRIPTION OF THE COMPLETE SYSTEM

As described in chapter 1 the wind energy conversion system investigated in this study is a variable speed wind turbine. A blockdiagram of the system is given below.

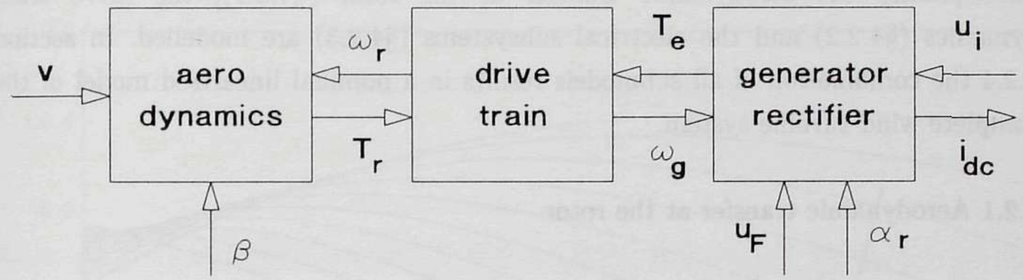

Figure 4.1 Blockdiagram of the energy conversion system

The aerodynamic part has as inputs the wind speed v, the pitch angle β of the blades and the rotor speed ω_r and creates a rotor torque T_r. The pitch angle can be actively controlled using a servo actuator. The torque acts on the drive train which exhibits some dynamic properties. The generator speed and rotor speed result. The former is an input for the electrical conversion system. This system has as inputs the field voltage u_F generated by the exciter, the speed ω_g of the *secondary shaft, the delay angle* α_r *of the rectifier and the grid or inverter voltage* u_i. The outputs are the direct current i_{dc} and the electrical torque T_e which in turn acts on the drive train.

The synchronous generator with rectifier has been modelled in the previous chapter. Here we will discuss the modelling of the aerodynamics, the drive train, the coupling with the model of chapter 3 and the model of the exciter. The approach applied will be corresponding to the assumptions of chapter 2. In section 4.2 the nominal model will be derived. Due to linearization errors, unknown parameter values and approximations (assumptions chapter 2) the nominal model differs from the actual system. To account for these differences in the control system design, a model of the uncertainties is necessary. In section 4.3 this

uncertainty modelling will be worked out.

In section 4.4 the models found are used to evaluate the properties of the system. Finally, the requirements on the closed–loop system are stated more precisely (section 4.5).

4.2 NOMINAL MODELLING

Subsequently the aerodynamic transfer at the rotor (§4.2.1), the drive train dynamics (§4.2.2) and the electrical subsystems (§4.2.3) are modelled. In section 4.2.4 the combination of all submodels results in a nominal linearized model of the complete wind turbine system.

4.2.1 Aerodynamic transfer at the rotor

The aerodynamic part is defined as the transfer between the wind speed in front of the rotor to the effective rotor torque. In fact, the blades are rotating through an inhomogeneous (stochastic) wind field meaning that the rotor torque will contain periodic variations. However, because rotor speed changes can be considered as being very slow this periodic character is modelled as originating from the external wind disturbance (chapter 2, assumption 2.2.2).
The local transfer between wind speed and torque can be calculated for all places on the blades using detailed aerodynamic models. However, the wind field is a rather unknown stochastic variable. Moreover, when designing flexible systems the local blade speed and torque relations are very important. In this study the blades are assumed infinitely rigid in the frequency range of interest. Therefore, a very simplified model is used for the aerodynamics with a *mean* (spatial–averaged) wind speed as input (chapter 2, assumptions 2.2.1, 2.2.3). The aerodynamic transfer is modelled as steady–state (nonlinear) process characteristics using the so–called C_p–curves [Le Gouriérès, 1982].
It should be noted that the simplifications will result in relatively large model uncertainties, as will be described in section 4.3.

The rotor power can be calculated with [Le Gouriérès, 1982]:

$$P_r = C_p(\lambda,\beta)\cdot\tfrac{1}{2}\rho\pi R^2\cdot v^3 \qquad [W] \qquad (4.1)$$

with $C_p(\lambda,\beta)$ [–] the power coefficient calculated from aerodynamic design data,

averaged over the blade length. Variable λ is the ratio between the blade–tip speed and the wind speed:

$$\lambda = \frac{\omega_r R}{v} \qquad [-] \qquad (4.2)$$

and ω_r [rad/s] is the rotor speed, R [m] is the radius of the rotor and ρ [kg/m^3] is the air density.
The power coefficient C_p or aerodynamic efficiency, can be calculated or measured. In figure 4.2 an example is given of calculated data on which the turbine design has been based.

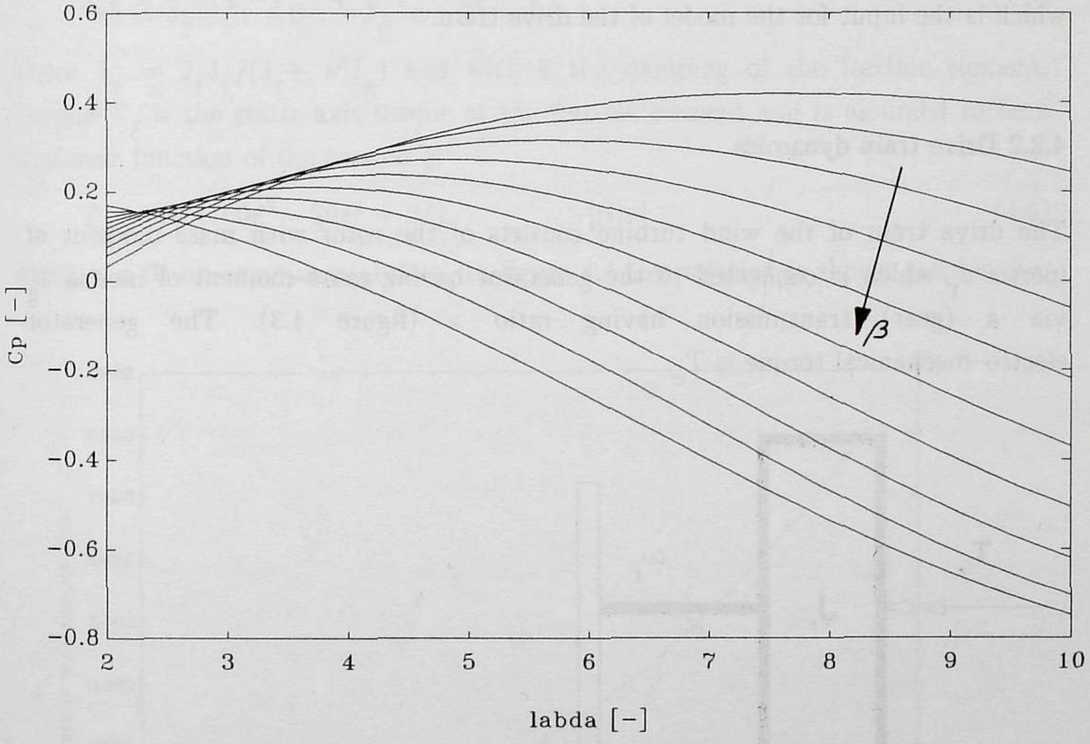

Figure 4.2. Power coefficient as a function of tip/wind speed ratio λ, with pitch angle β as parameter.

From the figure it follows that for a certain pitch angle β there exists an optimal tip/wind speed ratio λ_{opt} such that C_p is maximal. This points out that a variable speed system offers the possibility to maximize the captured energy by tracking wind speed v with rotor speed ω_r such that $\lambda=\lambda_{opt}$. A pitch angle β=0 is best for this situation. However, at full load conditions the incoming energy should be bounded. This is done using the pitch angle, see also section 4.4.

The pitch angle is controlled by an electro–mechanical actuator. This (controlled) actuator is modelled as a first order system with time constant τ_β:

$$\dot{\beta} = \frac{1}{\tau_\beta}\cdot(\beta_r - \beta) \tag{4.3}$$

with β_r the reference input.
Due to limitations of the actuator a bound is active on the rate of change of the pitch angle: $|d\beta/dt| \leq 5^0/s$ (= 0.087 rad/s).

Finally, the output of the model is the rotor torque:

$$T_r = P_r/\omega_r \qquad [Nm] \tag{4.4}$$

which is the input for the model of the drive train.

4.2.2 Drive train dynamics

The drive train of the wind turbine consists of the rotor with mass–moment of inertia J_r which is connected to the generator having mass–moment of inertia J_g via a (gear) transmission having ratio ν (figure 4.3). The generator electro–mechanical torque is T_e.

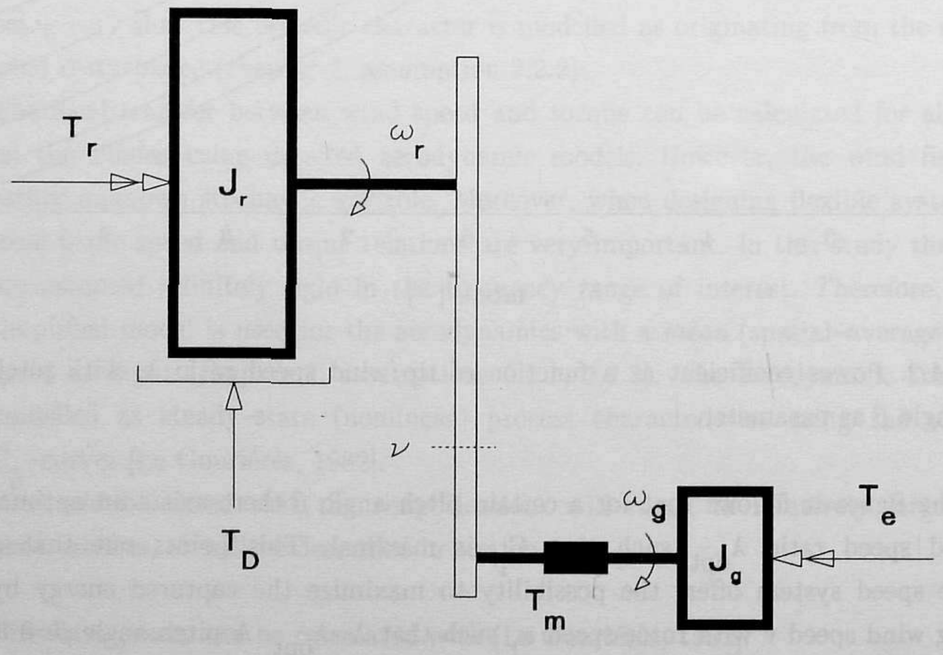

Figure 4.3 Drive train of the wind turbine.

The assumption is made that all the structural modes are concentrated in a flexible element in the secondary shaft and that the primary shaft and gear are infinitely rigid. Structural modes of the (steel) blades are assumed to be in the high frequency range only (chapter 2, assumptions 2.3). The deletion of these parasitic dynamics will be compensated by definition of uncertainties in section 4.3.

Denoting the relative angle of displacement in the secondary shaft by ξ ($d\xi/dt = \nu\int\omega_r - \int\omega_g$) it can be verified that the equation of motion is:

$$J_v\ddot{\xi} = \frac{\nu J_v}{J_r}(T_r - T_D) + \frac{J_v}{J_g}T_e - k\dot{\xi} - T_\xi \ , \tag{4.5}$$

where $J_v = J_r J_g/(J_r + \nu^2 J_g)$ and with k the damping of the flexible element. Torque T_ξ is the static axis torque at the flexible element and is assumed to be a nonlinear function of the torsion ξ:

$$T_\xi = 10^4(100\xi^3 - 20\xi^2 + 2\xi), \qquad [Nm] \tag{4.6}$$

which is a fit on experimental data. In figure 4.4 this relation is shown graphically.

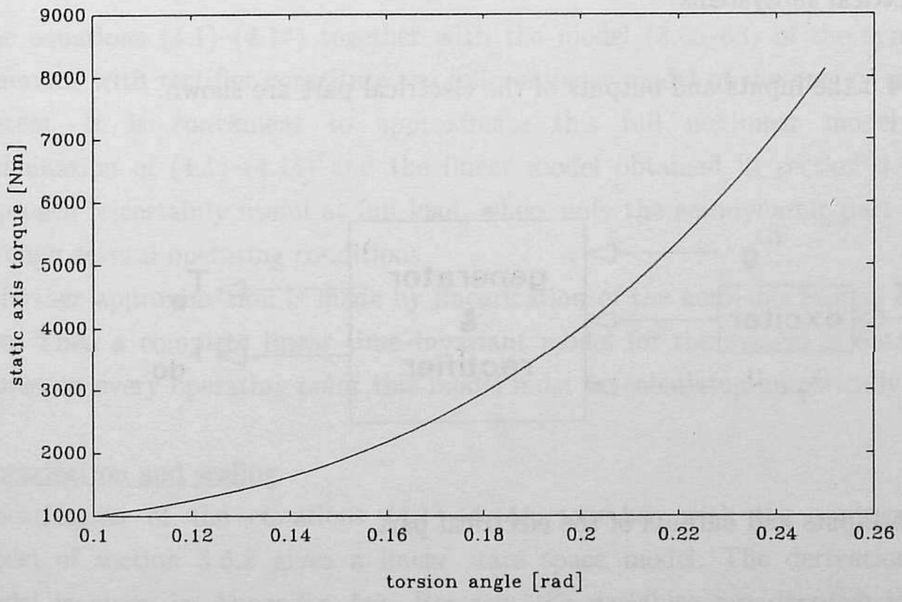

Figure 4.4 Torque as a function of shaft rotational deformation

The total amount of friction of the drive train is supposed to have the form:

$$T_D = C_1 + C_2/\omega_r + C_3\omega_r, \qquad [Nm] \tag{4.7}$$

with C_1, C_2, C_3 appropriate constants (Appendix A.1).

Generator speed ω follows from

$$J_g\dot{\omega}_g = T_\xi + k\dot{\xi} - T_e, \tag{4.8}$$

This speed is measured using a sensor with first order dynamics:

$$\dot{\omega}_{gm} = \frac{1}{\tau_\omega}\cdot(\omega_g - \omega_{gm}) \tag{4.9}$$

Finally the rotor speed can be calculated from

$$\omega_r = (\dot{\xi}+\omega_g)/\nu \qquad [rad/s] \tag{4.10}$$

Mechanical torque in the secondary axis follows from:

$$T_m = k\dot{\xi} + T_\xi \qquad [Nm] \tag{4.11}$$

and is of importance for analyzing the fatigue load. The equations (4.1)–(4.11) provide a model for the aero–mechanical part. This part is bilaterally coupled to the model of the electrical conversion system through ω_g and T_e. Note that the model is nonlinear. For control system design purposes a linearization will be carried out, see section 4.2.4.

4.2.3 Electrical subsystems

In figure 4.5 the inputs and outputs of the electrical part are shown.

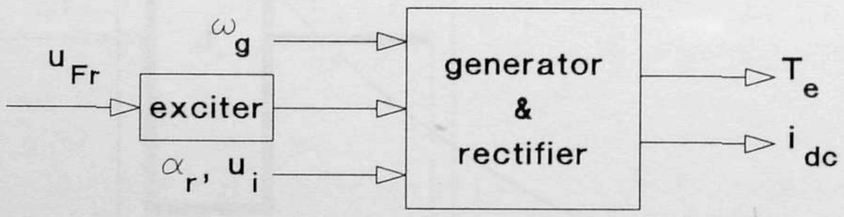

Figure 4.5 Inputs and outputs of the electrical part

The model for the synchronous generator and rectifier has been given in chapter 3. Some additions are necessary.
First, the mechanical speed should be related to the normalized speed ω used in the generator model. This relation is:

$$\omega[pu] = \frac{p\cdot\omega_g[rad/s]}{\omega_{nom}[rad/s]} \tag{4.12}$$

with pu means *per unit*, with p the number of pole pairs in the generator and with ω_{nom} the design speed (see Appendix A.1 for data).
For the output torque T_e we have the following relation:

$$T_e[Nm] = T_e[pu]\cdot T_B[Nm] \tag{4.13}$$

with the basis torque $T_B = pS_{nom}/\omega_{nom}$, with S_{nom} the nominal power (see also Appendix A.1).

Exciter

The generator used has a brushless exciter system with rotating diodes. Because the field voltage input will be used primarily at low frequencies we approximate this system with a rather simple model [Anderson and Fouad, 1982]:

$$\dot{u}_F = \frac{1}{\tau_F}\cdot(u_{Fr} - u_F) \tag{4.14}$$

with τ_F the exciter time constant.

4.2.4 Combination of the models

The equations (4.1)–(4.14) together with the model (3.65–68) of the synchronous generator with rectifier constitute the full nonlinear model of the energy conversion system. It is convenient to approximate this full nonlinear model by the combination of (4.1)–(4.14) and the linear model obtained in section 3.6.2. This approach is certainly useful at full load, where only the aerodynamic part traverses through several operating conditions.
A further approximation is made by linearization of the aero–mechanical equations also. Then a complete linear time–invariant model for the system is obtained. Of course, in every operating point this model must be calculated numerically.

Linearization and scaling

Linearization of the equations (4.1)–(4.14), together with the averaged linear model of section 3.6.2 gives a linear state space model. The derivation of this model is given in Appendix A.3. Remark: the variables are denoted with their original symbols but here have the meaning of variation about their nominal values. The inputs, states and outputs are scaled, see Appendix A.4.
The complete state space model is:

$$\begin{aligned}\dot{x} &= Ax + Bu + Ew\\ y &= Cx\end{aligned} \tag{4.15}$$

with

$$x^T = [\beta\ \xi\ d\xi/dt\ \omega_g\ \omega_{gm}\ u_F\ i_{dc}\ i_F\ i_D\ i_Q]^T$$
$$u^T = [\beta_r\ u_{Fr}\ \alpha_r]^T$$
$$w^T = [v\ u_i]^T$$
$$y^T = [\omega_{gm}\ i_{dc}\ \omega_r\ T_m]$$

and written out:

$$\frac{d}{dt}\begin{bmatrix} \beta \\ \xi \\ d\xi/dt \\ \omega_g \\ \omega_{gm} \\ u_F \\ i_{dc} \\ i_F \\ i_D \\ i_Q \end{bmatrix} = \begin{bmatrix} a_{11} & 0 & 0 & 0 & 0 & 0 & 0 & 0 & 0 & 0 \\ 0 & 0 & 1 & 0 & 0 & 0 & 0 & 0 & 0 & 0 \\ a_{31} & a_{32} & a_{33} & a_{34} & 0 & 0 & a_{37} & a_{38} & a_{39} & a_{30} \\ 0 & a_{42} & a_{43} & 0 & 0 & 0 & a_{47} & a_{48} & a_{49} & a_{40} \\ 0 & 0 & 0 & a_{54} & a_{55} & 0 & 0 & 0 & 0 & 0 \\ 0 & 0 & 0 & 0 & 0 & a_{66} & 0 & 0 & 0 & 0 \\ 0 & 0 & 0 & a_{74} & 0 & a_{76} & a_{77} & a_{78} & a_{79} & a_{70} \\ 0 & 0 & 0 & a_{84} & 0 & a_{86} & a_{87} & a_{88} & a_{89} & a_{80} \\ 0 & 0 & 0 & a_{94} & 0 & a_{96} & a_{97} & a_{98} & a_{99} & a_{90} \\ 0 & 0 & 0 & a_{04} & 0 & a_{06} & a_{07} & a_{08} & a_{09} & a_{00} \end{bmatrix} \begin{bmatrix} \beta \\ \xi \\ d\xi/dt \\ \omega_g \\ \omega_{gm} \\ u_F \\ i_{dc} \\ i_F \\ i_D \\ i_Q \end{bmatrix} +$$

$$\begin{bmatrix} b_{11} & 0 & 0 \\ 0 & 0 & 0 \\ 0 & 0 & 0 \\ 0 & 0 & 0 \\ 0 & 0 & 0 \\ 0 & b_{62} & 0 \\ 0 & 0 & b_{73} \\ 0 & 0 & b_{83} \\ 0 & 0 & b_{93} \\ 0 & 0 & b_{03} \end{bmatrix} \begin{bmatrix} \beta_r \\ u_{Fr} \\ \alpha_r \end{bmatrix} + \begin{bmatrix} 0 & 0 \\ 0 & 0 \\ e_{31} & 0 \\ 0 & 0 \\ 0 & 0 \\ 0 & 0 \\ 0 & e_{72} \\ 0 & e_{82} \\ 0 & e_{92} \\ 0 & e_{02} \end{bmatrix} \begin{bmatrix} v \\ u_i \end{bmatrix}$$

$$\begin{bmatrix} \omega_{gm} \\ i_{dc} \\ \omega_r \\ T_m \end{bmatrix} = \begin{bmatrix} 0 & 0 & 0 & 0 & 1 & 0 & 0 & 0 & 0 & 0 \\ 0 & 0 & 0 & 0 & 0 & 0 & 1 & 0 & 0 & 0 \\ 0 & 0 & c_{33} & c_{34} & 0 & 0 & 0 & 0 & 0 & 0 \\ 0 & c_{42} & c_{43} & 0 & 0 & 0 & 0 & 0 & 0 & 0 \end{bmatrix} \begin{bmatrix} \beta \\ \xi \\ d\xi/dt \\ \omega_g \\ \omega_{gm} \\ u_F \\ i_{dc} \\ i_F \\ i_D \\ i_Q \end{bmatrix}$$

The parameters are given in Appendix A.4.

Remark: only the first two outputs of (4.15) namely ω_{gm} and i_{dc} are the measured variables. The other two outputs are for analysis purposes.

In every operating condition this linear model can be calculated. For numerical data see Appendix A.1. Before we proceed with the analysis of the system, the uncertainties in the derived model are examined.

4.3 UNCERTAINTY MODELLING

4.3.1 Introduction

The nominal model describes the behaviour of the system under all assumptions made (§2.2,§4.2). The true performance of the system might thus be different from the nominal one.

For the wind turbine system most uncertainties in the linear design model are due to:

- –the linearization errors resulting from small deviations from the operating point,
- –the discretization of the model of the electrical subsystem,
- –the neglected high frequency structural modes in the system (tower, blades, drive train),
- –the stochastic nature of the power coefficient [Steinbuch, 1986] and its approximate calculation,
- –the uncertainties in the parameter values of the sensors and actuators,
- –the uncertainties in the values of some internal parameters such as torsional damping and stiffness.

The main problem in uncertainty modelling is to find a description for a set of models such that the behaviour of the true system is guaranteed to be covered. On the other hand the set of models covered should not be larger than necessary in order to obtain non–conservative results. The true behaviour can be approximated by the nominal model in very different ways. For instance, linearization gives a continuous range of models depending on the operating conditions. Also real and complex parameter variations might occur both with a deterministic (bounded) or with a stochastic nature. The structure of a model can also be perturbed, for instance with parasitic dynamics. These (un)certainties can therefore be modelled in very different ways. The question however is how uncertainty models can be used for control system design. The goal in this respect is to design a control system based primarily on the nominal model such that it is robust. This means that the closed–loop system maintains important properties, such as stability, under all admissible perturbations of the nominal model as described by the uncertainty model. The number of ways this robustness property can be analyzed is rather limited.

For single–input single–output (siso) systems the Nyquist plot or the gain and phase–margins are in most cases very appropriate. However, for multi–input multi–output (mimo) systems these indicators can only be used one feedback loop

at a time, so no overall statements are possible. In the last years much research effort has been spend to access the mimo robustness problem. The most important development is based on norm–bounded uncertainty modelling using singular values as indicators [Stein and Doyle, 1978; Doyle and Stein, 1981]. Other possibilities are simulation and state–space oriented matrix perturbations using Lyapunov stability tests [Yedavalli and Liang, 1985; Yedavalli, 1986]. Recently the polynomial parameter variations approach with Hurwitz stability criteria [Barmish, 1988] has emerged.
The singular value analysis method is very appropriate for all situations with little knowledge about the perturbations, due to the use of norms. It's major disadvantage is its conservatism [Doyle, Wall and Stein, 1982] meaning that the uncertainty model set is much larger than necessary. For that reason Doyle [1982] introduced the Structured Singular Value analysis. This method has enlarged the non–conservative applicability tremendously.
The method using simulations is restricted to well–known parameter variations and may be computationally very cumbersome. The method based on Lyapunov stability criteria can be used for real parameter variations in state space models. The recent polynomial parameter variations approach is still rather restrictive with respect to the uncertainties handled, but might become important.

The observations with respect to the physical nature of model perturbations can now be combined with the possible analysis tools. The conjecture is made that the structured singular value based method is the least restrictive with respect to the nature of the uncertainties. This means the uncertainties must fit into a norm–bounded description. For most uncertainties this is possible. Exceptions are stochastic parameter changes and pure phase changes.
An important model variation is the variation of the linear model with an operating point. This is the most structured perturbation because all coefficients of a model change depending on only a small number of parameters (operating conditions). For this kind of perturbations the multi–model synthesis tool will be developed (chapter 5).

In this section the norm–bounded uncertainty modelling is treated in general first (§4.3.2) resulting in a general uncertainty model structure. The other sections (§§4.3.3–4.3.6) are devoted to the application to the wind turbine system, with a distinction between uncertainties at the inputs, internal and at the outputs.

4.3.2 Norm–bounded uncertainty modelling

The modelling of norm–bounded uncertainties can be done in several ways: as additional state space system [Lunze,1984], by transformation to input– or output uncertainties and as additional feedback loops [Doyle, 1984; Tahk and Speyer, 1987]. The method of Lunze is quite general and can be transformed to the additional feedback loop description. Transformation of all uncertainties to input or output perturbations may give rather conservative results and the uncertainty model may depend on the controller transfer function. The additional feedback loop is very useful if (structured) singular value analysis is applied.

Define the nominal model as

$$\begin{aligned} \dot{x} &= Ax + Bu \\ y &= Cx + Du \end{aligned} \tag{4.16}$$

while the perturbed model is:

$$\begin{aligned} \dot{x} &= Ax + Bu + W_1 w \\ y &= Cx + Du + W_2 w \\ v &= V_1 x + V_2 u \end{aligned} \tag{4.17}$$

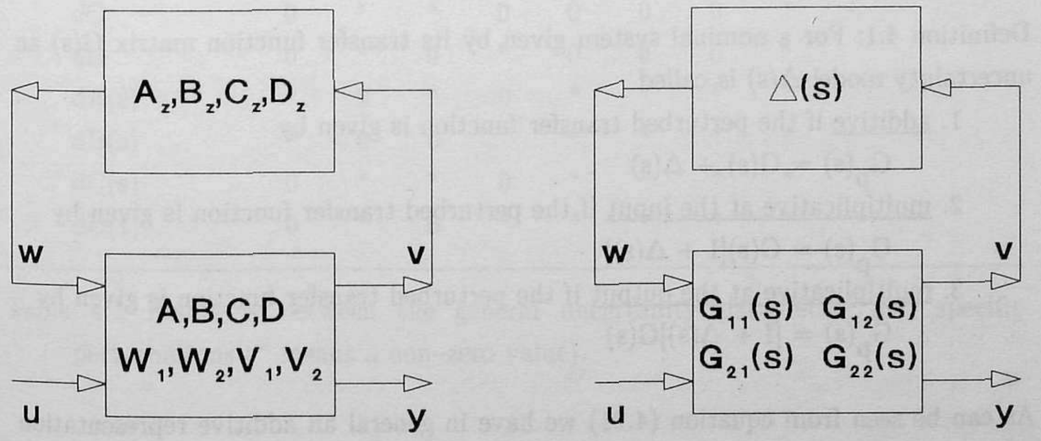

a. state space representation b. transfer function representation

Figure 4.6 General interconnection of uncertainties and system.

with the dynamic uncertainty model as

$$\dot{z} = A_z z + B_z v$$
$$w = C_z z + D_z v \qquad (4.18)$$

In a blockdiagram (4.17),(4.18) is given in figure 4.6a.
If we represent (4.18) as transfer function matrix we obtain:

$$w = \Delta(s)v \qquad (4.19)$$

with (see also figure 4.6b):

$$\Delta(s) = C_z(sI-A_z)^{-1}B_z + D_z$$

For the other transfer functions we get:

$$\begin{bmatrix} v \\ y \end{bmatrix} = \begin{bmatrix} G_{11}(s) & G_{12}(s) \\ G_{21}(s) & G_{22}(s) \end{bmatrix} \begin{bmatrix} w \\ u \end{bmatrix} \qquad (4.20)$$

with

$$G_{11}(s) = V_1(sI-A)^{-1}W_1$$
$$G_{12}(s) = V_1(sI-A)^{-1}B + V_2$$
$$G_{21}(s) = C(sI-A)^{-1}W_1 + W_2$$
$$G_{22}(s) = C(sI-A)^{-1}B + D$$

If (4.19) is substituted into (4.20) we obtain the transfer function from u to y, by elimination of the variables v and w:

$$y=[G_{22}(s)+G_{21}(s)\Delta(s)\{I-G_{11}(s)\Delta(s)\}^{-1}G_{12}(s)]u \qquad (4.21)$$

Definition 4.1: For a nominal system given by its transfer function matrix G(s) an uncertainty model $\Delta(s)$ is called

1. <u>additive</u> if the perturbed transfer function is given by
   $G_p(s) = G(s) + \Delta(s)$
2. <u>multiplicative at the input</u> if the perturbed transfer function is given by
   $G_p(s) = G(s)[I + \Delta(s)]$
3. <u>multiplicative at the output</u> if the perturbed transfer function is given by
   $G_p(s) = [I + \Delta(s)]G(s)$

As can be seen from equation (4.21) we have in general an additive representation but by choosing $G_{21}(s)=G_{22}(s)$ we obtain a multiplicative description of the uncertainties at the input and by choosing $G_{12}(s)=G_{22}(s)$ we obtain a multiplicative description of the uncertainties at the output. In this way the general framework can be converted to the familiar uncertainty models in robustness analyses [Doyle and Stein, 1981].

In the norm–bounded robustness analysis methods the only knowledge which is used consist of the singular values σ (σ(A): det[σI–A'A]=0) of $\Delta(s)$, in most cases even only the maximum singular value $\bar{\sigma}(\Delta(s))$ [Doyle and Stein, 1981]. This in fact defines the information reduction (chapter 2) necessary to obtain a relative simple model for the uncertainties.
In the sequel it will be shown that a very large class of uncertainties can be modelled by the model (4.17),(4.18).

The possible uncertainties which can arise in the model (4.16) are parameter variations in the matrices A,B,C,D which lead to non–dynamic real perturbations. Also, the entries of these matrices can be perturbed with additional dynamics for instance extra sensor dynamics (C), actuator dynamics (B) or parasitic dynamics (A). We denote the constant parameter variations as dA,dB,dC,dD and the dynamic uncertainties as dA(s),dB(s),dC(s),dD(s). For each of these perturbations the corresponding model which fits into (4.17),(4.18) can be found. The result is given in table 4.1.

	W_1	W_2	V_1	V_2	A_z	B_z	C_z	D_z
dA	*	0	*	0	0	0	0	*
dB	*	0	0	*	0	0	0	*
dC	0	*	*	0	0	0	0	*
dD	0	*	0	*	0	0	0	*
dA(s)	*	0	*	0	*	*	*	*
dB(s)	*	0	0	*	*	*	*	*
dC(s)	0	*	*	0	*	*	*	*
dD(s)	0	*	0	*	*	*	*	*

Table 4.1 Relations between the general uncertainty parameters and specific perturbations (* means a non–zero value).

Note that by combining (4.16)–(4.19) we can write:

$$sIx = Ax + Bu + dA(s)x + dB(s)u$$
$$y = Cx + Du + dC(s)x + dD(s)u$$

The perturbations can be written into one matrix:

$$S(s) = \begin{bmatrix} dA(s) & dB(s) \\ dC(s) & dD(s) \end{bmatrix}$$

For each perturbation we define the decomposition [Terlouw, 1989]:

$$S(s) = \begin{bmatrix} W_1 \\ W_2 \end{bmatrix} \Delta(s) [V_1 \; V_2]$$

Hence,

$$dA(s) = W_1 \Delta(s) V_1$$
$$dB(s) = W_1 \Delta(s) V_2$$
$$dC(s) = W_2 \Delta(s) V_1$$
$$dD(s) = W_2 \Delta(s) V_2$$

which follows also from table 4.1.

Suppose A is perturbed to A+dA. From the table it follows that $W_1 \neq 0$, $V_1 \neq 0$, $D_z \neq 0$, all other parameters are zero. In (4.17),(4.18) we get:

$$\dot{x} = Ax + Bu + W_1 w$$
$$y = Cx + Du$$
$$v = V_1 x$$

with the uncertainty model

$$w = D_z v$$

and combined

$$\dot{x} = Ax + Bu + W_1 D_z V_1 x \qquad \Leftrightarrow$$
$$\dot{x} = (A+dA)x + Bu$$

with $dA = W_1 D_z V_1$.

If additional actuator dynamics are present (dB(s)), then $W_1 \neq 0$, $V_2 \neq 0$, $(A_z, B_z, C_z, D_z) \neq 0$, and all other parameters are zero. In (4.17),(4.18) we get:

$$\dot{x} = Ax + Bu + W_1 w$$
$$y = Cx + Du$$
$$v = V_2 u$$

with the dynamic uncertainty model

$$\dot{z} = A_z z + B_z v$$
$$w = C_z z + D_z v$$

and combined

$$\dot{x} = Ax + Bu + W_1 C_z z + W_1 D_z V_2 u$$
$$\dot{z} = A_z z + B_z V_2 u$$

or as transfer functions

$$sIx = Ax + Bu + W_1 [C_z (sI - A_z)^{-1} B_z + D_z] V_2 u \qquad \Leftrightarrow$$
$$sIx = Ax + [B + dB(s)]u$$

with $dB(s) = W_1 [C_z (sI - A_z)^{-1} B_z + D_z] V_2$.
In this case dB(s) is modelled as additive perturbation. If we want to have a multiplicative uncertainty description, we simply set $W_1 = B$ and $B_p = B[I + dB(s)]$, with $dB(s) = [C_z (sI - A_z)^{-1} B_z + D_z] V_2$. Note that by assuming $D_z \neq 0$ the uncertainty model is proper and is in fact a combination of dB and dB(s).

For the general case where additive uncertainty is modelled over the transfer function matrix of the system we only need dD(s). Then $W_2 \neq 0$, $V_2 \neq 0$, $(A_z, B_z, C_z, D_z) \neq 0$. In (4.17),(4.18) we get:

$$\dot{x} = Ax + Bu$$
$$y = Cx + Du + W_2 w$$
$$v = V_2 u$$

with the dynamic uncertainty model

$$\dot{z} = A_z z + B_z v$$
$$w = C_z z + D_z v$$

and combined

$$\dot{x} = Ax + Bu$$
$$\dot{z} = A_z z + B_z V_2 u$$

or as transfer functions

$$sIx = Ax + Bu$$
$$y = Cx + \{D + W_2 [C_z (sI - A_z)^{-1} B_z + D_z] V_2\} u \qquad \Leftrightarrow$$
$$y = Cx + [D + dD(s)]u$$

with $dD(s) = W_2 [C_z (sI - A_z)^{-1} B_z + D_z] V_2$.

The actual size of the vectors w and v is directly related to the number of perturbation types modelled. In the next sections the modelling of the uncertainties will be done based on physical considerations. In section 4.3.6 all uncertainties are combined and rewritten in the general framework presented above.

4.3.3 Uncertainties in the inputs

Pitch angle

First we consider the uncertainties in the pitch angle. These consist of three types: the servo–actuator, the aerodynamics and parasitic flexibilities, see figure 4.7.

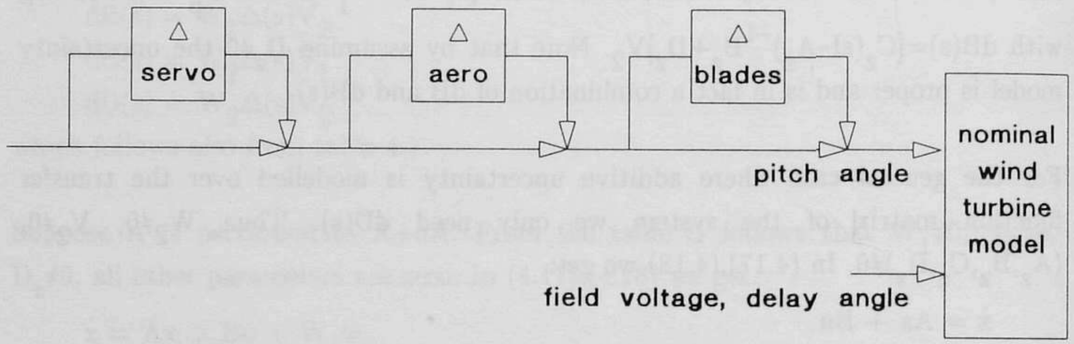

Figure 4.7 Uncertainties in the pitch angle input.

In the figure the multiplicative representation for model uncertainty is used (definition 4.1.2). This is the most convenient one because the uncertainties are exactly located and can be manipulated easier. This is especially the case when more perturbations are modelled in one loop. The servo system is modelled nominally as a first order transfer function:

$$g_\beta(s) = \frac{1}{\tau_\beta s+1} \qquad \text{with } \tau_\beta = 0.2 \text{ s}$$

The time constant τ_β is not exactly known. Assume that the perturbed real time constant indicated by the index p, is bounded by:

$$0.1 \leq \tau_{\beta p} \leq 0.4 \text{ s}$$

then it follows for the multiplicative uncertainty $\Delta_{\beta 1}$:

$$g_{\beta p}(s) = g_\beta(s)\{1+\Delta_{\beta 1}(s)\},$$

or

$$\Delta_{\beta 1}(s) = \frac{(\tau_\beta - \tau_{\beta p})s}{\tau_{\beta p} s+1} \qquad \text{with } \tau_\beta=0.2,\ 0.1\leq\tau_{\beta p}\leq 0.4$$

The Bode plot of this transfer function is shown in figure 4.8.

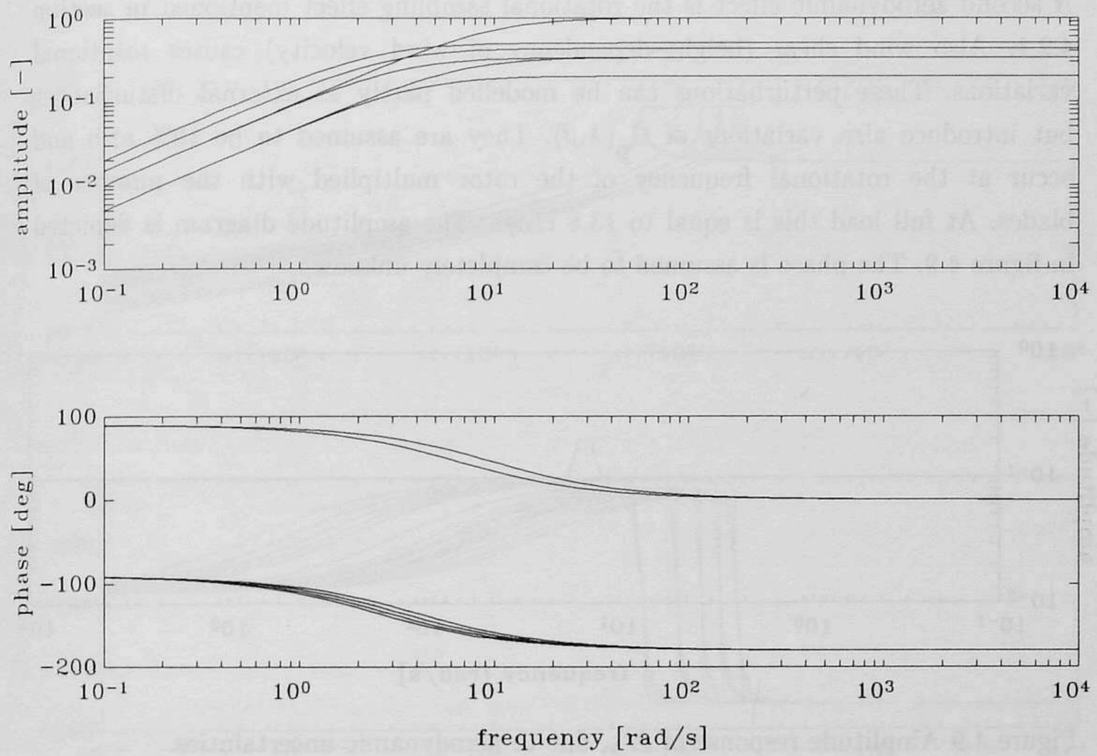

Figure 4.8 Frequency response of the uncertainty $\Delta_{\beta 1}$ due to uncertainty in the pitch servo.

Note that in accordance with the definition, the amplitude of this diagram is precisely the singular value of $\Delta_{\beta 1}(j\omega)$. At low frequencies the worst case is given by a large time constant, while at high frequencies the small $\tau_{\beta p}$ gives the largest uncertainties. The phase differences are quite large, depending on the sign of $(\tau_\beta - \tau_{\beta p})$.

The maximum uncertainty bound is the envelope or $\bar{\sigma}=\max(\Delta_{\beta 1}(j\omega))$ for $\omega\in\mathbb{R}^+$ with $\bar{\sigma}$ the maximum singular value. The phase information is discarded so that a worst case situation is assumed.

The second uncertainty in the pitch angle is a purely aerodynamic. In [Steinbuch and Meiring, 1986] it is shown that the input gain $\partial C_p/\partial\beta$ varies tremendously with wind speed. This variation will be handled using the multi–model approach, see chapter 6. However, the function $C_p(\lambda,\beta)$ itself is not known exactly and has stochastic properties [Steinbuch, 1986]. A variation of 10% is assumed.

A second aerodynamic effect is the rotational sampling effect mentioned in section 4.2.1. Also wind shear (height–dependency of wind velocity) causes rotational variations. These perturbations can be modelled partly as external disturbances but introduce also variations of $C_p(\lambda,\beta)$. They are assumed to be 10% also and occur at the rotational frequency of the rotor multiplied with the number of blades. At full load this is equal to 13.8 rad/s. The amplitude diagram is depicted in figure 4.9. The phase is assumed to be completely unknown.

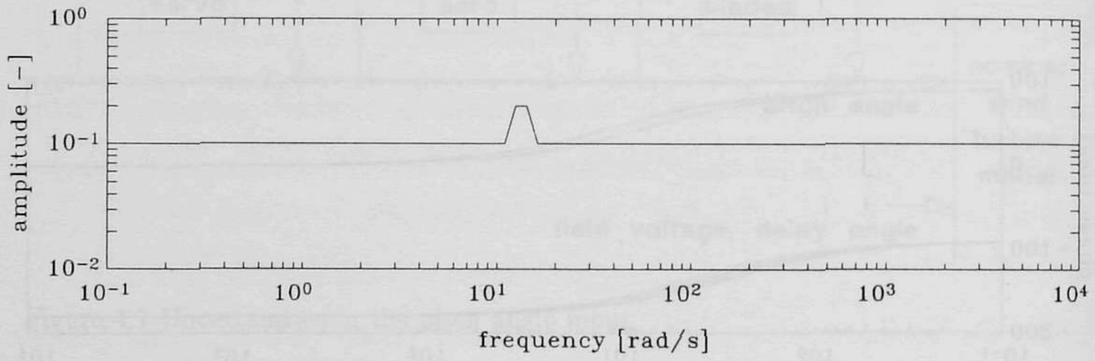

Figure 4.9 Amplitude response of $\Delta_{\beta 2}$ due to aerodynamic uncertainties.

Finally, the blades contain certain parasitic mechanical dynamics. These are not modelled nominally: $g_r(s)=1$. Assume a second order model is sufficient:

$$g_{rp}(s) = \frac{1}{\frac{s^2}{\omega_e^2}+2\frac{\zeta}{\omega_e}s+1}$$

with $0.005 \leq \zeta \leq 0.05$ is the relative damping and with a resonance frequency $60 \leq \omega_e \leq 180$ rad/s. Then with $g_{rp}(s)=g_r(s)\{1+\Delta_{\beta 3}(s)\}$ and $g_r(s)=1$ we obtain as uncertainty:

$$\Delta_{\beta 3}(s) = \frac{-s^2-2\zeta\omega_e s}{s^2+2\zeta\omega_e s+\omega_e^2}$$

The worst case is the singular value of $\Delta_{\beta 3}$, maximized over ζ and ω_e:

$$\bar{\sigma}(\Delta_{\beta 3}(j\omega)) = \max_{\zeta,\omega_e} \left| \frac{-s^2-2\zeta\omega_e s}{s^2+2\zeta\omega_e s+\omega_e^2} \right|_{s=j\omega}, \quad \text{with} \quad \begin{matrix} 0.005 \leq \zeta \leq 0.05 \\ 60 \leq \omega_e \leq 180 \text{ rad/s} \end{matrix}$$

In figure 4.10 for a finite number of frequencies ω_e and the lowest damping (ζ=0.005) the transfer function of $\Delta_{\beta 3}$ is plotted.

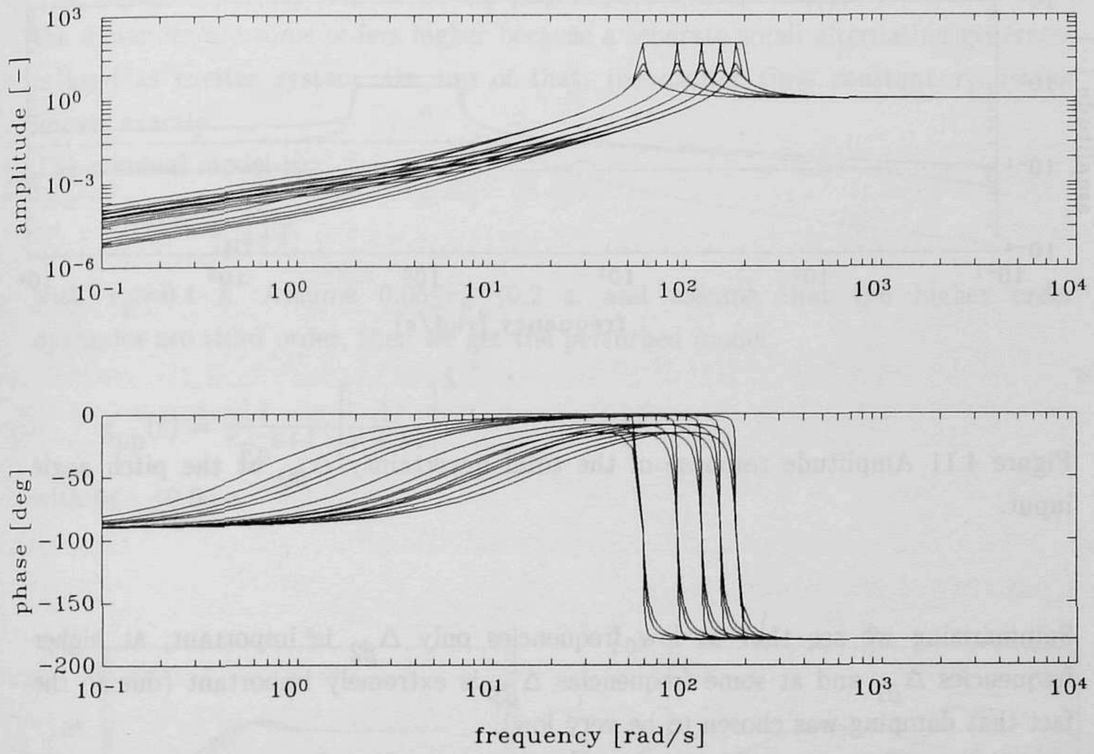

Figure 4.10 Frequency response of the uncertainty $\Delta_{\beta 3}$, due to parasitic dynamics.

The complete uncertainty model of the pitch angle β can be calculated as follows. Because the models are all linear we can combine all uncertainties (figure 4.7). The transfer function becomes (the argument s is omitted here):

$$g_r g_a g_\beta \{1+\Delta_{\beta 3}\}\{1+\Delta_{\beta 2}\}\{1+\Delta_{\beta 1}\} = g_r g_a g_\beta \{1+\Delta_{\beta t}\}$$

If we discard the possibility that phase changes in one uncertainty compensate these of others, we have the worst case situation:

$$\bar{\sigma}(\Delta_{\beta t}) = \{1+\bar{\sigma}(\Delta_{\beta 3})\}\{1+\bar{\sigma}(\Delta_{\beta 2})\}\{1+\bar{\sigma}(\Delta_{\beta 1})\} - 1$$

The result is shown below.

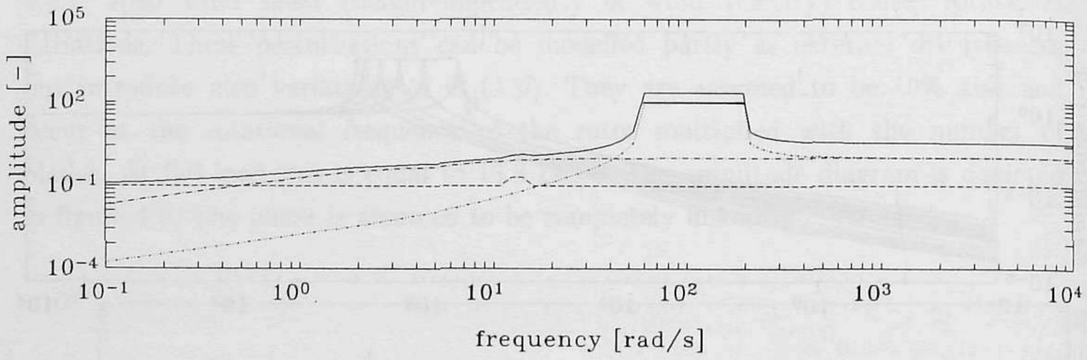

Figure 4.11 Amplitude response of the total uncertainty $\Delta_{\beta t}$, at the pitch angle input.

Summarizing we see that at low frequencies only $\Delta_{\beta 2}$ is important, at higher frequencies $\Delta_{\beta 1}$ and at some frequencies $\Delta_{\beta 3}$ is extremely important (due to the fact that damping was chosen to be very low).
Next the multiplicative description is converted into the general description given earlier. In this case we have from table 4.1 (dB(s)≠0): $W_1 \neq 0$, $V_2 \neq 0$, $(A_z, B_z, C_z, D_z) \neq 0$. Because the perturbations are multiplicative we need to take W_1 equal to the first column of B of (4.15). The bound on $\Delta(s) = C_z(sI - A_z)^{-1}B_z + D_z$ is given by $\bar{\sigma}(\Delta_{\beta t})$. Matrix V_2 can be taken as $V_2 = [1\ 0\ 0]$.

Note that all uncertainties have been taken as multiplicative in the input. Another possibility is to choose the perturbations in the A matrix of (4.15) at the appropriate places (for instance at A(1,1)). Obtaining a single scalar uncertainty $\bar{\sigma}(\Delta_{\beta t})$ would have been possible by combination of the vectors W_1 and V_2 but would take more manipulations.

Field voltage exciter

The model for the exciter has been chosen as a first order transfer function. In fact the dynamics are some orders higher because a separate small alternating generator is used as exciter system. On top of that, the exciter time constant τ_F is not known exactly.
The nominal model is:

$$g_u(s) = \frac{1}{\tau_F s + 1}$$

with $\tau_F = 0.1$ s. Assume $0.05 \leq \tau_{Fp} \leq 0.2$ s. and assume that the higher order dynamics are third order, then we get the perturbed model:

$$g_{up}(s) = \frac{1}{\tau_{Fp} s + 1} \cdot \left[\frac{1}{\tau_q s + 1}\right]^3$$

with $0 \leq \tau_q \leq 0.05$ s.

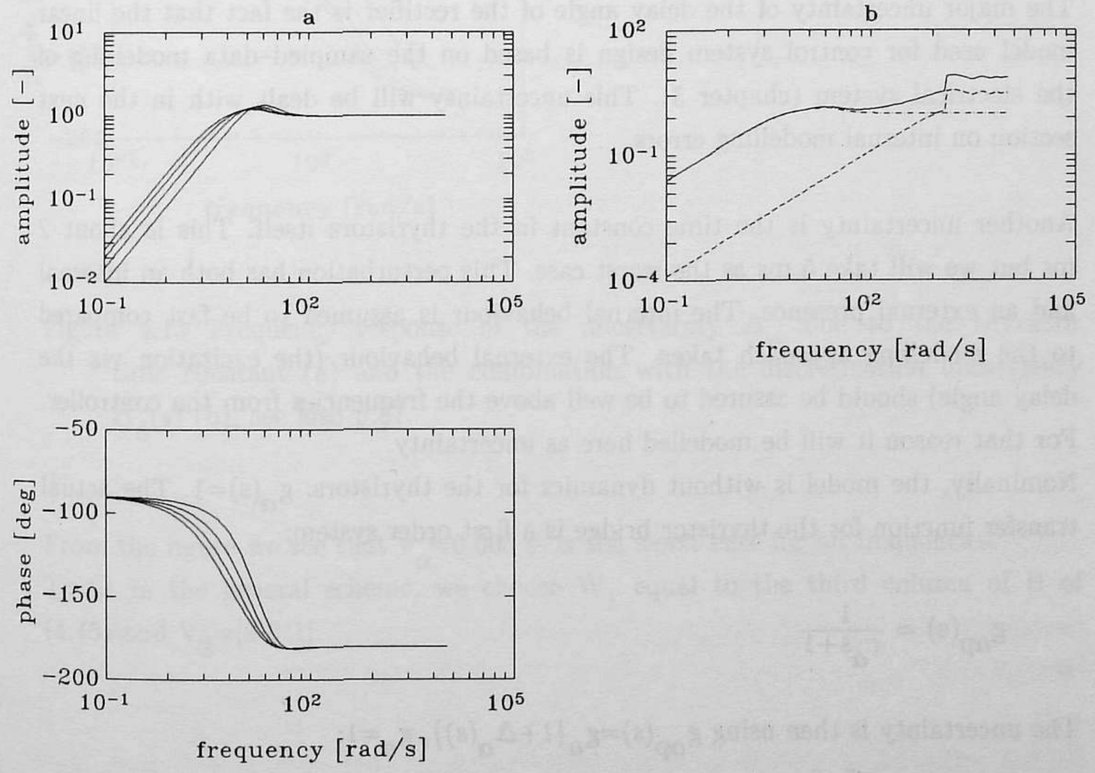

Figure 4.12 Frequency response of the uncertainty Δ_u (a), at the field voltage input and the combination with the discretization uncertainty $\Delta_d(s)$ (b), see also p.87.

Then the uncertainty becomes, with $g_{up}(s)=g_u(s)\{1+\Delta_u(s)\}$:

$$\Delta_u(s) = \frac{g_{up}(s)}{g_u(s)} - 1 = \frac{(\tau_F s+1)-(\tau_{Fp} s+1)(\tau_q s+1)^3}{(\tau_{Fp} s+1)(\tau_q s+1)^3}$$

with τ_F=0.1 s., $0.05 \leq \tau_{Fp} \leq 0.2$ s. and $0 \leq \tau_q \leq 0.05$ s..

In figure 4.12(a) the frequency response of this uncertainty is shown.

Again this uncertainty can be put into the general framework by choosing W_1 equal to the second column of B of (4.15) and V_2=[0 1 0]. Also in this case the choice for a multiplicative input description instead of perturbing A(6,6) of (4.15), is the most convenient here.

Delay angle of the rectifier

The major uncertainty of the delay angle of the rectifier is the fact that the linear model used for control system design is based on the sampled–data modelling of the electrical system (chapter 3). This uncertainty will be dealt with in the next section on internal modelling errors.

Another uncertainty is the time constant in the thyristors itself. This is about 2 ms but we will take 5 ms as the worst case. This perturbation has both an internal and an external presence. The internal behaviour is assumed to be fast compared to the modelling approach taken. The external behaviour (the excitation via the delay angle) should be assured to be well above the frequencies from the controller. For that reason it will be modelled here as uncertainty.
Nominally, the model is without dynamics for the thyristors: $g_\alpha(s)=1$. The actual transfer function for the thyristor bridge is a first order system:

$$g_{\alpha p}(s) = \frac{1}{\tau_\alpha s+1}$$

The uncertainty is then using $g_{\alpha p}(s)=g_\alpha\{1+\Delta_\alpha(s)\}$, g_α=1:

$$\Delta_\alpha(s) = \frac{-\tau_\alpha s}{\tau_\alpha s+1}$$

with $0.001 \leq \tau_\alpha \leq 0.005$ s.

In figure 4.13(a) the frequency response is given.

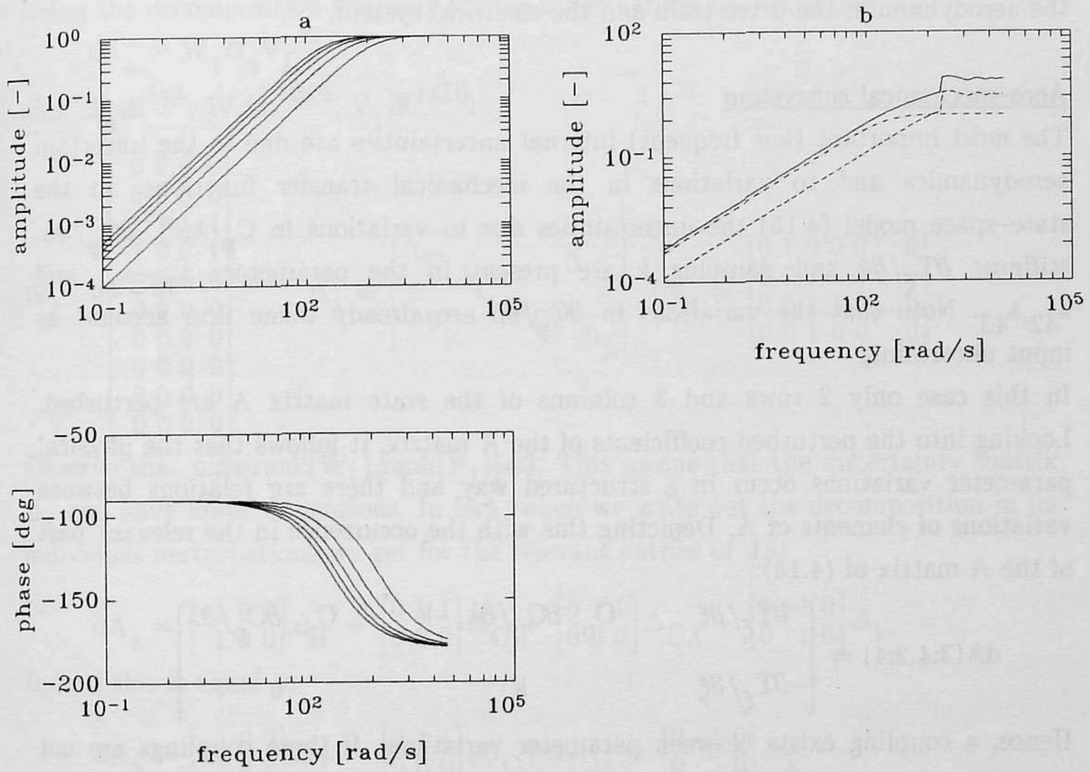

Figure 4.13 Frequency response of the uncertainty Δ_α due to the thyristor time constant (a) and the combination with the discretization uncertainty $\Delta_d(s)$ (b), see also p.87.

From the figure we see that τ_α=0.005 s. is the worst case for all frequencies.
To fit in the general scheme, we choose W_1 equal to the third column of B of (4.15) and V_2=[0 0 1].

4.3.4 Internal uncertainties

In this section a description is given for the internal uncertainties in the model of the aerodynamics, the drive train and the electrical system.

Aero–mechanical subsystem

The most important (low frequent) internal uncertainties are due to the uncertain aerodynamics and to variations in the mechanical transfer functions. In the state–space model (4.15) the uncertainties due to variations in $C_p(\lambda,\beta)$, $\partial C_p/\partial\lambda$, stiffness $\partial T_\xi/\partial\xi$ and damping k are present in the parameters a_{32}–a_{34} and a_{42},a_{43}. Note that the variations in $\partial C_p/\partial\beta$ are already taken into account as input uncertainty.

In this case only 2 rows and 3 columns of the state matrix A are perturbed. Looking into the perturbed coefficients of the A matrix, it follows that the physical parameter variations occur in a structured way and there are relations between variations of elements of A. Depicting this with the occurrence in the relevant part of the A matrix of (4.15):

$$dA(3{:}4,2{:}4) = \begin{bmatrix} \partial T_\xi/\partial\xi & C_p,\ \partial C_p/\partial\lambda,\ -k & C_p,\ \partial C_p/\partial\lambda \\ -\partial T_\xi/\partial\xi & k & 0 \end{bmatrix}$$

Hence, a coupling exists between parameter variations. If these couplings are not taken into account conservative results will be obtained.

The following procedure is used. From the general approach presented earlier we have the situation: $W_1 \neq 0$, $V_1 \neq 0$, $D_z \neq 0$. Denoting D_z by Δ we need to find a decomposition of dA such that:

$$dA = W_1 \Delta V_1 \qquad (4.22)$$

with Δ square, diagonal and of **minimal size**. It follows from (4.22) that (with W_1 and V_1 full rank) the size of Δ equals the rank of dA. So with each physical perturbation a dA is associated with a certain rank.

Definition 4.2: A rank ρ perturbation is a perturbation which results in rank(dA)=ρ.

For all perturbations we have in our case the result that they are all **rank one perturbations**. For instance modelling the variation for $\partial T_\xi/\partial_\xi$ gives:

$$dA_T = W_1 \Delta_T V_1$$

with $\Delta_T = \delta_T \in \mathbb{R}^1$, $W_1 = [0\ 0\ 1\ -1\ 0\ ..\ 0]^T \in \mathbb{R}^{10x1}$, $V_1 = [0\ 1\ 0\ ..\ 0] \in \mathbb{R}^{1x10}$.

Remark: for rank ρ perturbations with $\rho>1$ the uncertainty matrix Δ will have repeated blocks.

Doing the decomposition similarly for the other variations, we obtain

$$dA_a = W_1 \Delta_a V_1$$

with $\Delta_a \in \mathbb{R}^{4x4}$, $W_1 \in \mathbb{R}^{10x4}$, $V_1 \in \mathbb{R}^{4x10}$:

$$W_1 = \begin{bmatrix} 0&0&0&0 \\ 0&0&0&0 \\ 1&1&1&-1 \\ -1&0&0&1 \\ 0&0&0&0 \\ 0&0&0&0 \\ 0&0&0&0 \\ 0&0&0&0 \\ 0&0&0&0 \\ 0&0&0&0 \end{bmatrix} \qquad \Delta_a = \begin{bmatrix} \Delta_T & & & 0 \\ & \Delta_C & & \\ & & \Delta_{C\lambda} & \\ 0 & & & \Delta_k \end{bmatrix} \qquad V_1 = \begin{bmatrix} 0&1&0&0&0&..&0 \\ 0&0&1&1&0&..&0 \\ 0&0&1&1&0&..&0 \\ 0&0&1&0&0&..&0 \end{bmatrix}$$

Observe that max[rank(W_1),rank(V_1)]=3. This means that the uncertainty matrix Δ_a can have lower dimensions. In fact, when we write out the decomposition in its individual perturbations we get for the relevant entries of dA:

$$dA_a = \begin{bmatrix} -1&0&0 \\ 1&0&0 \end{bmatrix}\Delta_T + \begin{bmatrix} 0&1&1 \\ 0&0&0 \end{bmatrix}\Delta_C + \begin{bmatrix} 0&1&1 \\ 0&0&0 \end{bmatrix}\Delta_{C\lambda} + \begin{bmatrix} 0&-1&0 \\ 0&1&0 \end{bmatrix}\Delta_k$$

Indeed this is equal to

$$dA_a = \begin{bmatrix} -1&0&0 \\ 1&0&0 \end{bmatrix}\Delta_T + \begin{bmatrix} 0&1&1 \\ 0&0&0 \end{bmatrix}(\Delta_C+\Delta_{C\lambda}) + \begin{bmatrix} 0&-1&0 \\ 0&1&0 \end{bmatrix}\Delta_k$$

The new decomposition has rank three:

$$W_1 = \begin{bmatrix} 0&0&0 \\ 0&0&0 \\ 1&1&-1 \\ -1&0&1 \\ 0&0&0 \\ 0&0&0 \\ 0&0&0 \\ 0&0&0 \\ 0&0&0 \\ 0&0&0 \end{bmatrix} \qquad \Delta_a = \begin{bmatrix} \Delta_T & & 0 \\ & \Delta_C+\Delta_{C\lambda} & \\ 0 & & \Delta_k \end{bmatrix} \qquad V_1 = \begin{bmatrix} 0&1&0&0&0&..&0 \\ 0&0&1&1&0&..&0 \\ 0&0&1&0&0&..&0 \end{bmatrix}$$

where in Δ_a the element $\Delta_C+\Delta_{C\lambda}$ (in the sequel denoted as Δ_{Cp}) must be taken as $|\Delta_C|+|\Delta_{C\lambda}|$ eventually because perturbations of Δ_C and $\Delta_{C\lambda}$ are assumed independent.

Note that taking both uncertainties together is understandable because C_p and $\partial C_p/\partial\lambda$ affect the state matrix A at exactly the same entries. Moreover, it can be viewed as perturbations in the same direction. This was also the case with the input uncertainties of the pitch angle which were taken together because they were in series of one another.

Summarizing this part, when modelling perturbations in state space models first investigate the rank of each perturbation. Then after collecting them into the matrices W, Δ and V check if max[rank(W),rank(V)]=rank(Δ). If this does not hold a reduction of the dimension of the uncertainty matrix Δ is possible.

In order to investigate the effect of perturbations on closed–loop performance we are interested in the maximum singular value $\bar{\sigma}(\Delta_a)$. The $\bar{\sigma}(\Delta_a)$ is calculated for each entry of Δ_a for the situation where C_p and $\partial C_p/\partial\lambda$ vary with ±20% (in order to account also for the rotational sampling effects but for convenience here frequency independent), stiffness $\partial T_a/\partial\xi$ varies ±20% and damping k varies ±50%. The result is the diagonal gain matrix Δ_a=diag(Δ_T,Δ_{Cp},Δ_k)=diag(365.1, 0.0029, 0.245) for v=16 m/s. The second and third number varies with operating condition. They are (0.0115, 0.184) in v=12 m/s and (0.0528, 0.137) in v=20 m/s. Note that these uncertainties are real and if they are treated as being complex conservative results will be obtained.

Electrical subsystem

The electrical subsystem has been modelled using linearization and averaging of the original periodic nonlinear model. This means that the linear model for the synchronous generator and rectifier is only valid for frequencies much lower than the sampling frequency (1/T). The uncertainty due to this discretization is very similar to the problem of implementation of continuous–time based controllers in a digital control set–up, see for instance [Thompson et al., 1986]. The perturbation model can be quantified as follows.

Note that if a discrete time model had been used for control system design a natural limitation would have been occurred at the sample frequency. Here we use a continuous–time model and we have to answer the question: which uncertainty model is appropriate for the discretization effects?

Two modelling stages can be defined. First, the real system have been discretisized yielding a sampled–data model G(z). Secondly, a zero–order–hold (ZOH) function is assumed to transfer G(z) to its continuous–time equivalent G(s) (this is equivalent to the averaging $P(t,t_0)=I$, definition 3.11). For the sampling stage the model G(z) exactly represents the model G(s) up to half the sampling frequency 1/(2T) (Shannon's theorem for signal recovery). The related uncertainty Δ_s is therefore zero up to $\omega = 2\pi/(2T) = 1257$ rad/s = 200 Hz at full load and undefined (the nominal model G(z) is not defined between the samples) above this

frequency. However, from the nonlinear simulations of chapter 3 small variations of the variables are assumed to be bounded up to 100% variation between the samples. So $\bar{\sigma}(\Delta_s(s))=1$ above 200 Hz.

The second uncertainty is the transfer function of a ZOH:

$$g_{ZOH}(s) = \frac{1-e^{-sT}}{sT}$$

and the uncertainty is defined with $g_{ZOH}(s)=\{1+\Delta_{ZOH}\}$, (because the nominal model is 1):

$$\Delta_{ZOH}(s) = g_{ZOH}(s)-1 = \frac{1-e^{-sT}-sT}{sT}$$

with $T=\pi/(3*\omega[pu]*\omega_{nom}[rad/s])$, which is at full load $\pi/(3*1*418.88)=0.0025$ s. The uncertainties Δ_s and Δ_{ZOH} are plotted in figure 4.14.

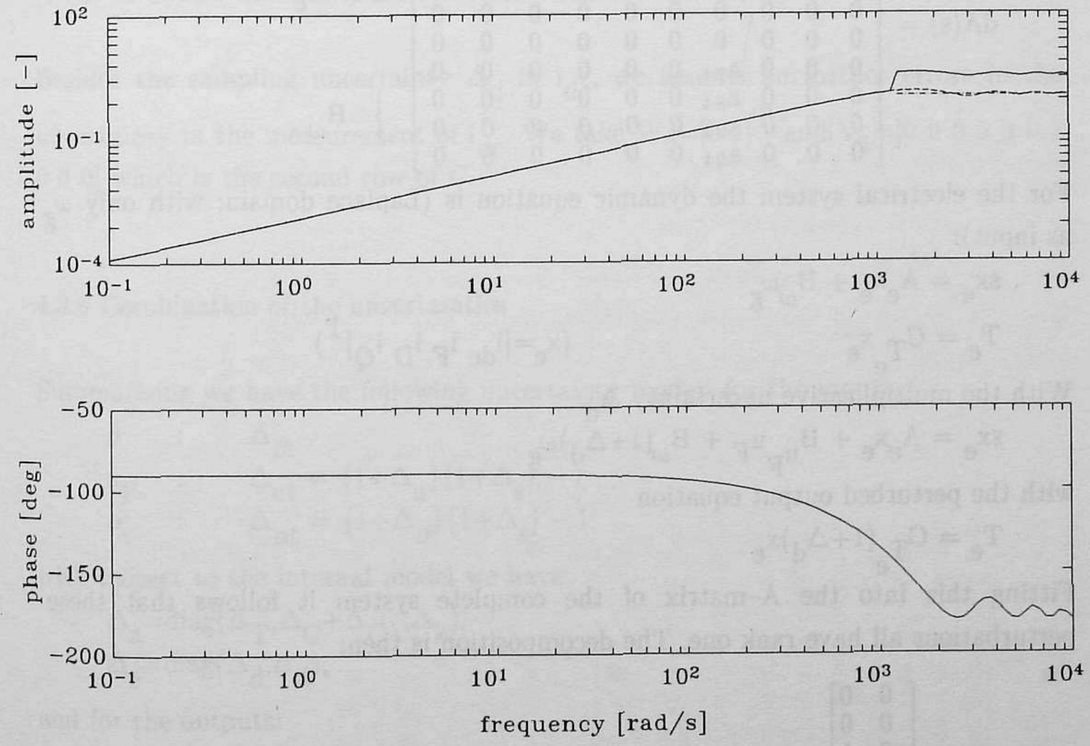

Figure 4.14 Frequency response of the uncertainties Δ_s and Δ_{ZOH} due to the sampled–data modelling of the electrical subsystem, for T=2.5 ms.

The combination of Δ_s and Δ_{ZOH} will be denoted as discretization uncertainty:

$$\Delta_d = (1+\Delta_s)(1+\Delta_{ZOH})-1$$

The model uncertainty due to the sampled data modelling should be added to all inputs u_F (see fig 4.12b), α_r (see figure 4.13b) and ω_g and to all outputs T_e and i_{dc} of the electrical system. Another possibility is to perturb all elements of the state matrix A_e and the matrices B_e, C_e and D_e of the electrical system or to model it as additive to the transfer function of the electrical subsystem. The multiplicative (electrical) input/output description seems to be the most convenient in this case. Here we only take into account the uncertainty in the coupling with the rest of the model. Such couplings are the uncertainties in ω_g and T_e which are purely internal errors of the type dA(s). So $W_1 \neq 0$, $V_1 \neq 0$ and $(A_z,B_z,C_z,D_z) \neq 0$. The A matrix is perturbed with Δ_d with the following structure:

$$dA(s) = \begin{bmatrix} 0 & 0 & 0 & 0 & 0 & 0 & 0 & 0 & 0 & 0 \\ 0 & 0 & 0 & 0 & 0 & 0 & 0 & 0 & 0 & 0 \\ 0 & 0 & 0 & 0 & 0 & 0 & a_{37} & a_{38} & a_{39} & a_{30} \\ 0 & 0 & 0 & 0 & 0 & 0 & a_{47} & a_{48} & a_{49} & a_{40} \\ 0 & 0 & 0 & 0 & 0 & 0 & 0 & 0 & 0 & 0 \\ 0 & 0 & 0 & 0 & 0 & 0 & 0 & 0 & 0 & 0 \\ 0 & 0 & 0 & a_{74} & 0 & 0 & 0 & 0 & 0 & 0 \\ 0 & 0 & 0 & a_{84} & 0 & 0 & 0 & 0 & 0 & 0 \\ 0 & 0 & 0 & a_{94} & 0 & 0 & 0 & 0 & 0 & 0 \\ 0 & 0 & 0 & a_{04} & 0 & 0 & 0 & 0 & 0 & 0 \end{bmatrix} \begin{matrix} \\ \\ \} \\ \\ \} \\ \\ \\ \\ \} \end{matrix} \begin{matrix} \\ \\ CT_e \\ \\ -CT_e \\ \\ \\ \\ B_\omega \end{matrix}$$

For the electrical system the dynamic equation is (Laplace domain; with only ω_g as input):

$$sx_e = A_e x_e + B_\omega \omega_g$$

$$T_e = C_{T_e} x_e \qquad (x_e=[i_{dc}\ i_F\ i_D\ i_Q]^T)$$

With the multiplicative uncertainty Δ_d:

$$sx_e = A_e x_e + B_{u_F} u_F + B_\omega(1+\Delta_d)\omega_g$$

with the perturbed output equation

$$T_e = C_{T_e}(1+\Delta_d)x_e$$

Fitting this into the A–matrix of the complete system it follows that these perturbations all have rank one. The decomposition is then:

$$W_1 = \begin{bmatrix} 0 & 0 \\ 0 & 0 \\ 0 & 1 \\ 0 & -1 \\ 0 & 0 \\ 0 & 0 \\ a_{74} & 0 \\ a_{84} & 0 \\ a_{94} & 0 \\ a_{04} & 0 \end{bmatrix} \quad \Delta_e = \begin{bmatrix} \Delta_d & \\ & \Delta_d \end{bmatrix} \quad V_1 = \begin{bmatrix} 0\,0\,0\,1\,0 & 0 & 0 & 0 & 0 \\ 0\,0\,0\,0\,0 & a_{37} & a_{38} & a_{39} & a_{30} \end{bmatrix}$$

Note that Δ_e does not contain repeated blocks because the perturbations in question have completely uncorrelated phases but happen to have the same amplitude.

4.3.5 Uncertainties in the outputs

The two outputs are the direct current i_{dc} and the speed ω_{gm}. The nominal model for the speed measurement is taken as a first order transfer function $g_\omega(s)=1/(\tau_\omega s+1)$, with $\tau_\omega=0.1$ s. The measurement is done using a zero–crossings counter of the generator voltage. The resolution is such that with $\tau_\omega=0.1$ s. the errors are less than 2%. Therefore $\bar{\sigma}(\Delta_\omega)=0.02$ for all frequencies. Modelling this as dC(s) we find from table 4.1 $W_2 \neq 0$, $V_1 \neq 0$, $(A_z,B_z,C_z,D_z) \neq 0$. The matrix $W_2=[1\ 0]^T$ and $V_1=[0\ 0\ 0\ 0\ 1\ 0\ 0\ 0\ 0\ 0]$ which is the first row of the output matrix C of (4.15) to obtain the multiplicative description of section 4.3.2.

Besides the sampling uncertainty Δ_d in i_{dc}, we assume no further errors in the uncertainty in the measurement of i_{dc}. We take $W_2=[0\ 1]^T$ and $V_1=[0\ 0\ 0\ 0\ 0\ 0\ 1\ 0\ 0\ 0]$ which is the second row of C.

4.3.6 Combination of the uncertainties

Summarizing we have the following uncertainty models for the inputs:

$$\begin{aligned} \beta &: \quad \Delta_{\beta t} \\ u_F &: \quad \Delta_{ut} = \{1+\Delta_u\}\{1+\Delta_s\} - 1 \\ \alpha_r &: \quad \Delta_{\alpha t} = \{1+\Delta_\alpha\}\{1+\Delta_s\} - 1 \end{aligned}$$

with respect to the internal model we have

$$\Delta_a = \mathrm{diag}(\Delta_T, \Delta_C+\Delta_{C\lambda}, \Delta_k),$$
$$\Delta_e = \mathrm{diag}(\Delta_d, \Delta_d),$$

and for the outputs:

$$\begin{aligned} \omega_{gm} &: \quad \Delta_\omega \\ i_{dc} &: \quad \Delta_d \end{aligned}$$

In order to be able to analyze the stability and performance for all uncertainties simultaneously, we combine all the above mentioned perturbations into the general framework (4.17) of section 4.3.1:

$$\dot{x} = Ax + Bu + W_1 w$$
$$y = Cx + Du + W_2 w$$
$$v = V_1 x + V_2 u$$

We then obtain:

$$W_1 = \begin{bmatrix} \Delta_{\beta t} & \Delta_{ut} & \Delta_{\alpha t} & \Delta_T & \Delta_C & \Delta_k & \Delta_d & \Delta_d & \Delta_\omega & \Delta_d \end{bmatrix}$$
$$\begin{bmatrix} b_{11} & 0 & 0 & 0 & 0 & 0 & 0 & 0 & 0 & 0 \\ 0 & 0 & 0 & 0 & 0 & 0 & 0 & 0 & 0 & 0 \\ 0 & 0 & 0 & 1 & 1 & -1 & 0 & 1 & 0 & 0 \\ 0 & 0 & 0 & -1 & 0 & 1 & 0 & -1 & 0 & 0 \\ 0 & 0 & 0 & 0 & 0 & 0 & 0 & 0 & 0 & 0 \\ 0 & b_{62} & 0 & 0 & 0 & 0 & 0 & 0 & 0 & 0 \\ 0 & 0 & b_{73} & 0 & 0 & 0 & a_{74} & 0 & 0 & 0 \\ 0 & 0 & b_{83} & 0 & 0 & 0 & a_{84} & 0 & 0 & 0 \\ 0 & 0 & b_{93} & 0 & 0 & 0 & a_{94} & 0 & 0 & 0 \\ 0 & 0 & b_{03} & 0 & 0 & 0 & a_{04} & 0 & 0 & 0 \end{bmatrix}$$

$$W_2 = \begin{bmatrix} 0 & 0 & 0 & 0 & 0 & 0 & 0 & 0 & 1 & 0 \\ 0 & 0 & 0 & 0 & 0 & 0 & 0 & 0 & 0 & 1 \end{bmatrix}$$

$$\Delta_t = \begin{bmatrix} \Delta_{\beta t} & & & & & & & & & \\ & \Delta_{ut} & & & & & & & & \\ & & \Delta_{\alpha t} & & & & & & & [0] \\ & & & \Delta_T & & & & & & \\ & & & & \Delta_C+\Delta_{C\lambda} & & & & & \\ & & & & & \Delta_k & & & & \\ & & & & & & \Delta_d & & & \\ & & & & & & & \Delta_d & & \\ & & & & & & & & \Delta_\omega & \\ & & [0] & & & & & & & \Delta_d \end{bmatrix}$$

$$V_1 = \begin{bmatrix} 0 & 0 & 0 & 0 & 0 & 0 & 0 & 0 & 0 & 0 \\ 0 & 0 & 0 & 0 & 0 & 0 & 0 & 0 & 0 & 0 \\ 0 & 0 & 0 & 0 & 0 & 0 & 0 & 0 & 0 & 0 \\ 0 & 1 & 0 & 0 & 0 & 0 & 0 & 0 & 0 & 0 \\ 0 & 0 & 1 & 1 & 0 & 0 & 0 & 0 & 0 & 0 \\ 0 & 0 & 1 & 0 & 0 & 0 & 0 & 0 & 0 & 0 \\ 0 & 0 & 0 & 1 & 0 & 0 & 0 & 0 & 0 & 0 \\ 0 & 0 & 0 & 0 & 0 & 0 & a_{37} & a_{38} & a_{39} & a_{30} \\ 0 & 0 & 0 & 0 & 1 & 0 & 0 & 0 & 0 & 0 \\ 0 & 0 & 0 & 0 & 0 & 0 & 1 & 0 & 0 & 0 \end{bmatrix} \qquad V_2 = \begin{bmatrix} 1 & 0 & 0 \\ 0 & 1 & 0 \\ 0 & 0 & 1 \\ 0 & 0 & 0 \\ 0 & 0 & 0 \\ 0 & 0 & 0 \\ 0 & 0 & 0 \\ 0 & 0 & 0 \\ 0 & 0 & 0 \\ 0 & 0 & 0 \end{bmatrix}$$

$$\begin{bmatrix} \Delta_{\beta t} \\ \Delta_{ut} \\ \Delta_{\alpha t} \\ \Delta_T \\ \Delta_C+\Delta_{C\lambda} \\ \Delta_k \\ \Delta_d \\ \Delta_d \\ \Delta_\omega \\ \Delta_d \end{bmatrix}$$

The question can be raised if certain perturbations can be taken together as was the case with the internal errors. Observe that rank(Δ_t)=10, rank(W_1)=6, rank(W_2)=2, rank(V_1)=6, rank(V_2)=3. So max[rank(W_1)+rank(W_2), rank(V_1)+rank(V_2)]=9. This points a possible reduction with one of the uncertainties. Because we can never combine W_1 with W_2 nor V_1 with V_2, we look only to those perturbations which are coupled to both W_1 and V_1. Take max[rank(W_1,column 4–8),rank(V_1,row 1–5)]=max[3,4]=4, with 5 associated uncertainties Δ. Still one Δ may be reducible. If we look into the rows of V_1 which are rank deficient, we find row2=row3+row4. Take the corresponding columns in W_1: 5,6,7. Calculate max[rank(W_1,column 5–7),rank(V_1,row 2–4)]= max[3,2]=3, with 3 associated uncertainties Δ. So there are no reducible Δ's.

Scaling of the uncertainty model

In order to fit in the procedure of the structured singular value analysis and to obtain the least conservative results the uncertainty matrix Δ_t must be scaled [Stein, 1984]. This scaling must be such that all elements of the block–diagonal Δ_t have equal gain, for all frequencies.

The problem is to find the block–diagonal, invertible matrices S_1 and S_2 such that

$$\Delta_{ts} = S_1^{-1}\Delta_t S_2^{-1} = \text{diag}(\delta,\delta,\ldots,\delta) \qquad \text{(kxk)} \qquad (4.23)$$

for some arbitrary $\delta>0$. In our case $k=10$. From this definition it follows that taking the singular value $\bar{\sigma}(\Delta_{ts})=\delta$ covers the same uncertainties as the original set. Otherwise, $\bar{\sigma}(\Delta_t)$ is equal to the maximum over the elements of Δ_t. In this way we have constrained the conservatism to appear only in the system transfer matrix and in the off–diagonal terms in case of normal singular value analysis (see section 5.4).

With (4.23) the uncertainty feedback of figure 4.6 becomes

$$w = \Delta_t v = S_1 \Delta_{ts} S_2 v$$

Defining the new variables $w'=S_1^{-1}w$, $v'=S_2 v$ we get

$$w' = \Delta_{ts} v' \qquad (4.24)$$

with $\Delta_{ts}=\text{diag}(\delta,\delta,\ldots,\delta)\in\mathbb{R}^{kxk}$ and (4.20) becomes

$$\begin{aligned} sx &= Ax + Bu + W_1 S_1 w' \\ y &= Cx + W_2 S_1 w' \\ v' &= S_2 V_1 x + S_2 V_2 u \end{aligned} \qquad (4.25)$$

In the case of the wind energy conversion system the matrices S_1 and S_2 are found as follows. First note that all uncertainties are scalars (rank 1 perturbations) and we have no repeated blocks. Without loss of generality we set S_2=I. We choose

S_1=diag(s_1,s_2,...,s_k). Two approaches are possible to find s_i. First the elements of the uncertainty matrix Δ_t (which depend of frequency jω) are represented by transfer functions. However, because the uncertainty characteristics are not simply given by one transfer function but rather by a collection of transfer functions, the smallest 'upper bounding' transfer function may be hard to find. Nevertheless, because modelling uncertainty involves some reasonably arbitrary choices, an appropriate approximating upper bounding transfer function may be chosen. For instance for the pitch angle uncertainty (figure 4.10) it is unnecessary to take an uncertainty model which has a lower value at very high frequencies than the value at the resonant peaks. A good controller will not move around such 'gains'.

The other approach is to calculate S_1 for each frequency based only on the amplitude of the uncertainty information.
Formalizing this we have, with δ=1:

$$S_1(\omega) = \text{diag}\Big[|\Delta_{\beta t}(j\omega)|,|\Delta_{ut}(j\omega)|,|\Delta_{\alpha t}(j\omega)|,|\Delta_T|, \\ |\Delta_C|+|\Delta_{C\lambda}|,|\Delta_k|,|\Delta_d(j\omega)|,|\Delta_d(j\omega)|,|\Delta_\omega(j\omega)|,|\Delta_d(j\omega)|\Big]$$

so that for each frequency $|S_1^{-1}(\omega)\Delta_t(j\omega)| = I$ (10x10). The diagonal entries of $S_1(\omega)$ are plotted in figure 4.15.

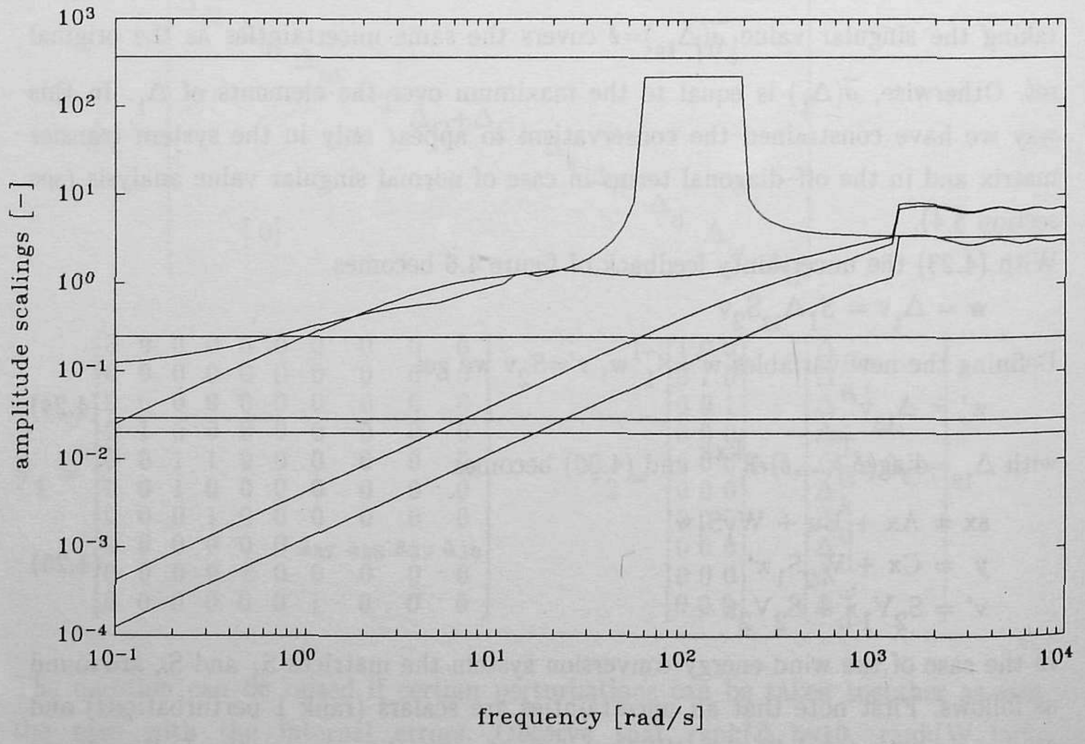

Figure 4.15 Diagonal scaling factors for the uncertainty matrix.

A drawback of this approach is that the matrix $S_1(\omega)$ can only be used for (structured) singular value analysis. It can not be used as part of the transfer function data.
In chapter 6.4 the uncertainty model will be used for analysis of the closed–loop system.

4.4 SIMULATION AND SYSTEM ANALYSIS

Using the model as it is derived in the preceding sections, it is possible to investigate its dynamic properties. We restrict our analysis to the full load case only. In the partial load case a servo–problem exists which is described in detail in [Ploeg, 1988; Bongers and Dijkstra, 1988]. In the full load case the system has three inputs (β_r,u_{Fr},α_r) and two outputs (ω_{gm},i_{dc}). Especially in the full load case low mechanical loads and high performance behaviour are required.
The operating conditions are very important for the aerodynamic model (section 4.4.1). Time and frequency responses are shown in section 4.4.2 and some system properties are investigated in section 4.4.3.

4.4.1 Operating conditions

The full load cases are defined as those operating conditions where the nominal electrical power (300kW) is delivered. For the wind turbine under investigation this is only the case for wind speeds above 12 m/s. In this nominal situation also the rotational speeds are kept constant. At the rotor a constant power is necessary for stationairity (rotor power (4.1) must be constant). This results in an implicit relation between the wind speed v, the power coefficient and the needed pitch angle β following from eq.(4.1)–(4.2). For the data used (see figure 4.2 and Appendix A.1) figure 4.16 is obtained as static characteristics.
From the figure it follows that with increasing wind speed the power coefficient decreases and the pitch angle increases. This is in accordance with the static condition that the rotor power P_r of (4.1) must be constant.

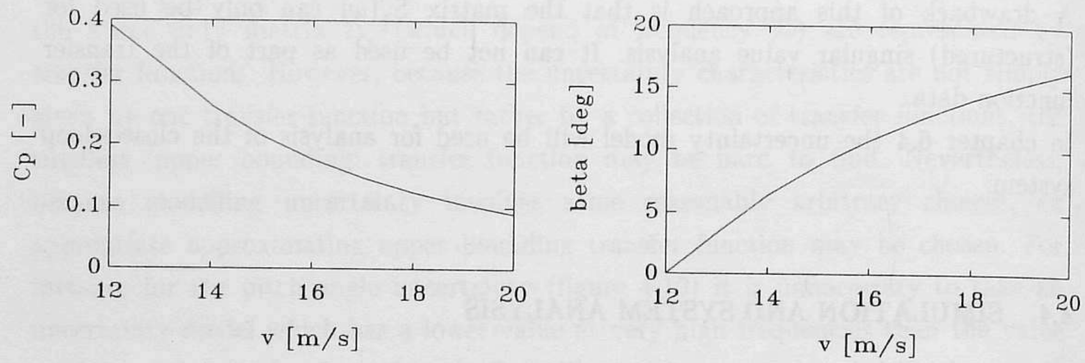

Figure 4.16 Static characteristics in the full load case.

At each wind speed it is possible to calculate the state space model (4.15). Because speed, torque and power are constant most of the model is independent of wind speed v. Only the aerodynamic parameters such as C_p (figure 4.16) and its partial derivatives vary with v. As already has been shown in a previously reported study [Steinbuch and Meiring, 1986] both $\partial C_p/\partial\beta$ and $\partial C_p/\partial\lambda$ are highly nonlinear functions of the wind speed v (figure 4.17).

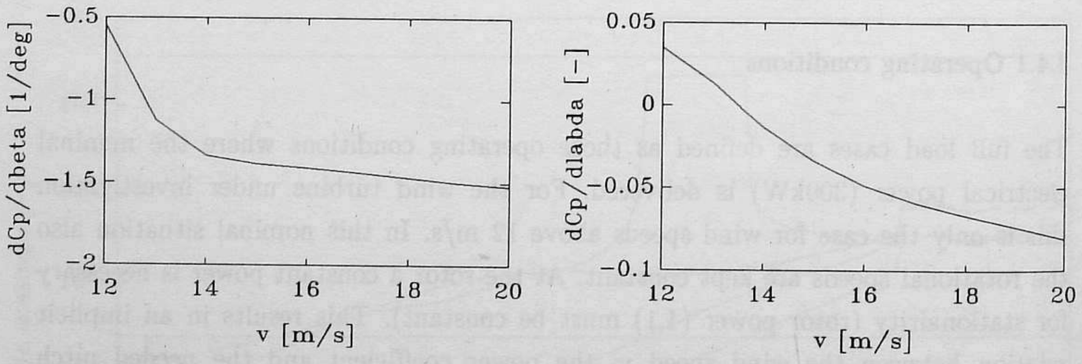

Figure 4.17 Variation of the input sensitivities $\partial C_p/\partial\beta$ and $\partial C_p/\partial\lambda$ with v.

The figure shows that $\partial C_p/\partial\beta$ varies a factor 3 with v. Parameter $\partial C_p/\partial\lambda$ even shows a more drastically variation. However, especially the parameter $\partial C_p/\partial\beta$ is of great importance because large loop gain variations in the pitch angle input are the result.

For the operating points v=12,16 and 20 m/s the state space models (4.15) have been calculated for the data used (Appendix A.1). The resulting (A,B,C,E)

matrices are given in Appendix A.5. As outputs not only the measurable outputs ω_{gm} and i_{dc} are given but also the rotor speed ω_r and the mechanical torque T_m. The torque is used as indicator for mechanical loads whereas the rotor speed is used for gaining insight into the behaviour of the system.

4.4.2 Time and frequency responses

First the responses are shown for the v=16 m/s model. At the end of the section the problem of the nonlinearities in the aerodynamics will be addressed.

Time responses

In figure 4.18 the step responses are given for a unit step (1 rad) of the pitch angle input (β_r). The four responses are the measured generator speed ω_{gm}, direct current i_{dc}, rotor speed ω_r and the mechanical torque T_m in the secondary axis.

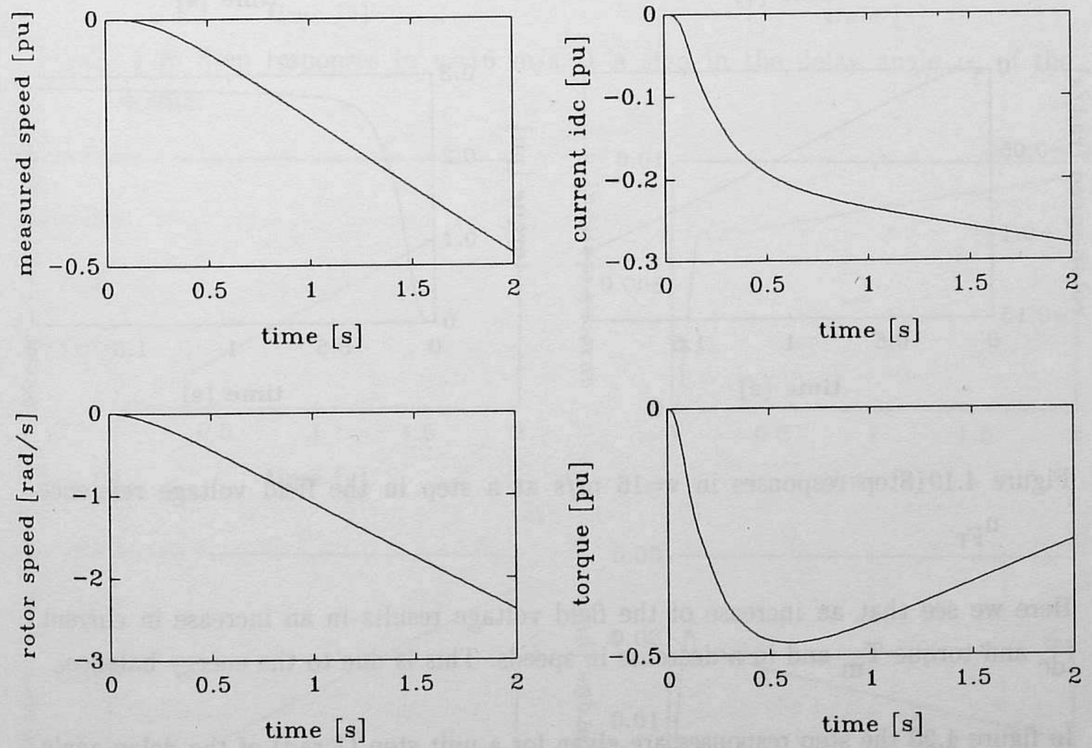

Figure 4.18 Step responses in v=16 m/s at a unit step in the pitch angle input β_r.

Both generator speed and rotor speed respond very slowly. All variables decrease which is accordingly the fact that increasing the pitch angle, yields a decrease in the incoming power.

In figure 4.19 the step responses are given for a unit step of the field voltage reference u_{Fr}.

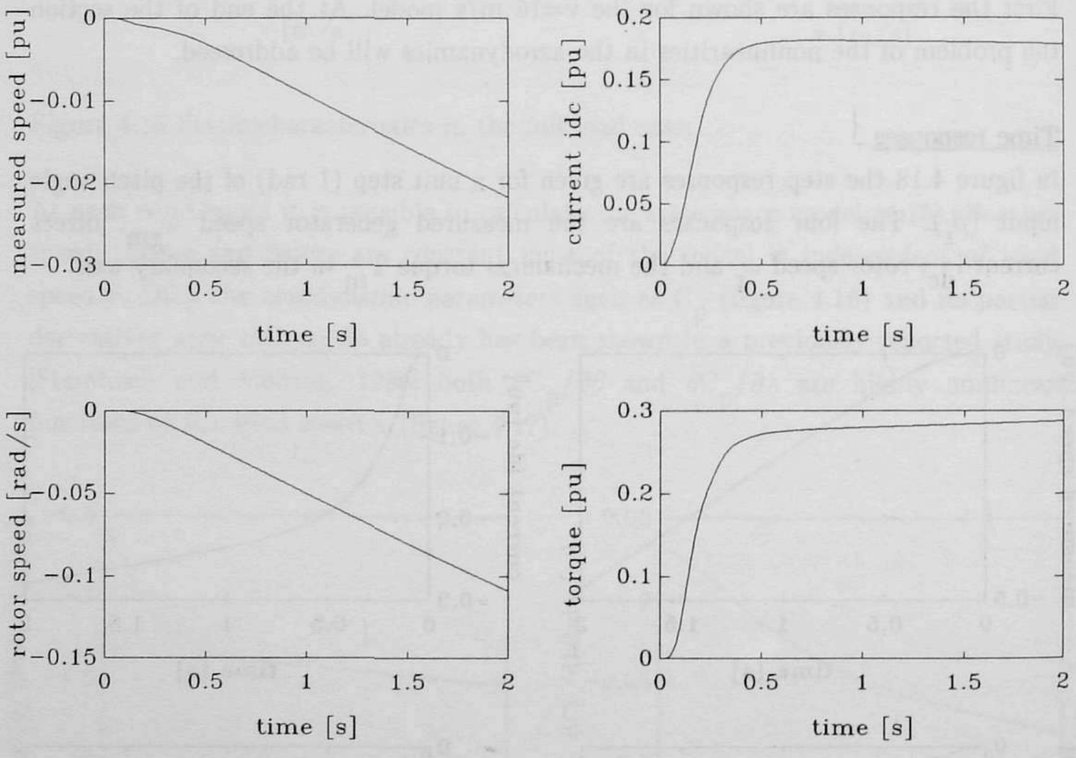

Figure 4.19 Step responses in v=16 m/s at a step in the field voltage reference u_{Fr}.

Here we see that an increase of the field voltage results in an increase in current i_{dc} and torque T_m and in a decrease in speeds. This is due to the energy balance.

In figure 4.20 the step responses are given for a unit step (1 rad) of the delay angle α_r of the rectifier.

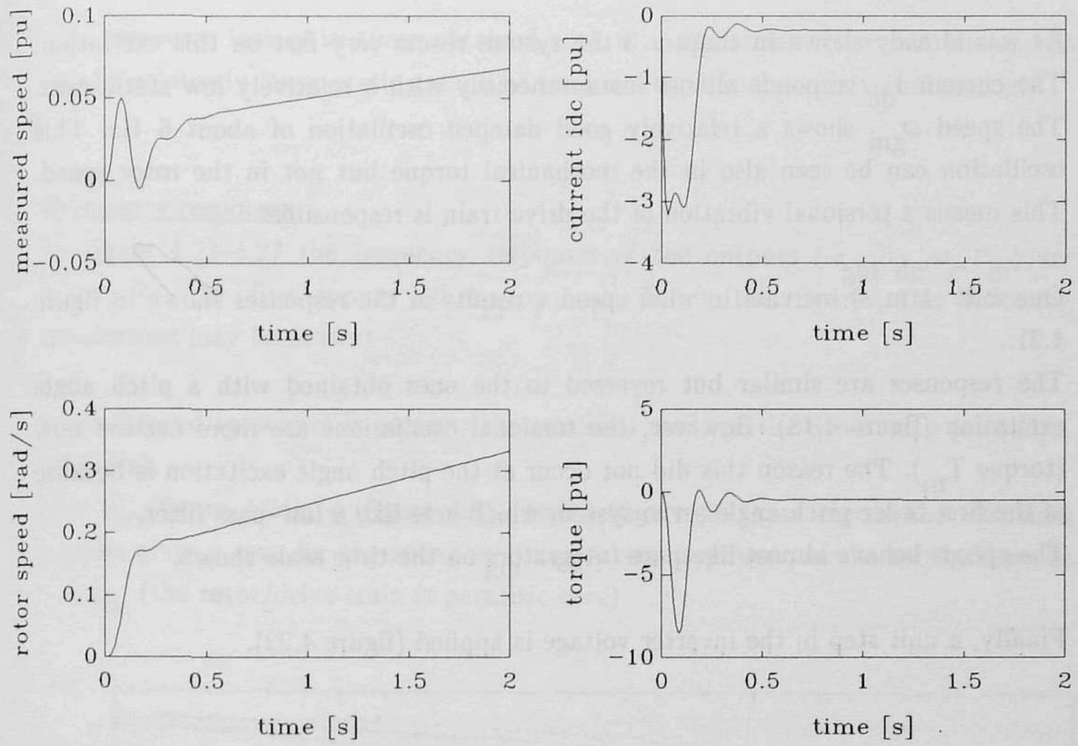

Figure 4.20 Step responses in v=16 m/s at a step in the delay angle α_r of the rectifier.

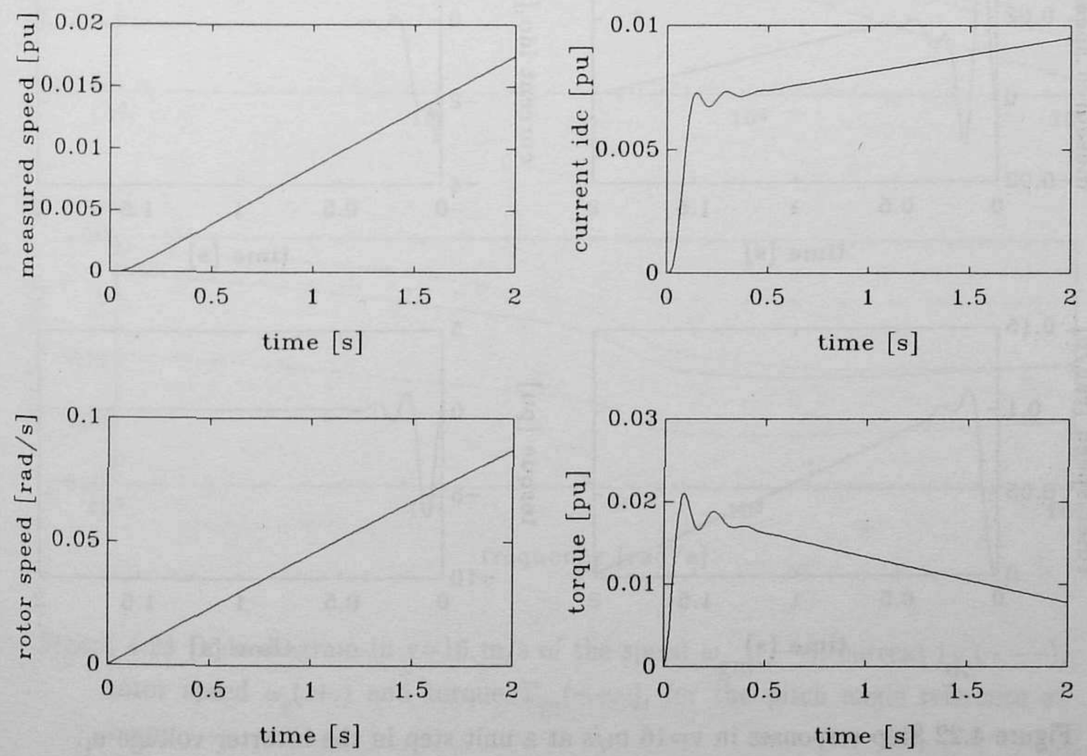

Figure 4.21 Step responses in v=16 m/s at a unit step in the wind speed v.

As was already shown in chapter 3 the system reacts very fast on this excitation. The current i_{dc} responds almost instantaneously with a relatively low static gain. The speed ω_{gm} shows a relatively good damped oscillation of about 6 Hz. This oscillation can be seen also in the mechanical torque but not in the rotor speed. This means a torsional vibration of the drive train is responsible.

One unit (1 m/s) increase in wind speed v results in the responses shown in figure 4.21.
The responses are similar but reversed to the ones obtained with a pitch angle excitation (figure 4.18). However, the torsional oscillations are more excited now (torque T_m). The reason this did not occur at the pitch angle excitation is because of the first order pitch angle servo system which acts like a low–pass filter.
The speeds behave almost like pure integrators on the time scale shown.

Finally, a unit step in the inverter voltage is applied (figure 4.22).

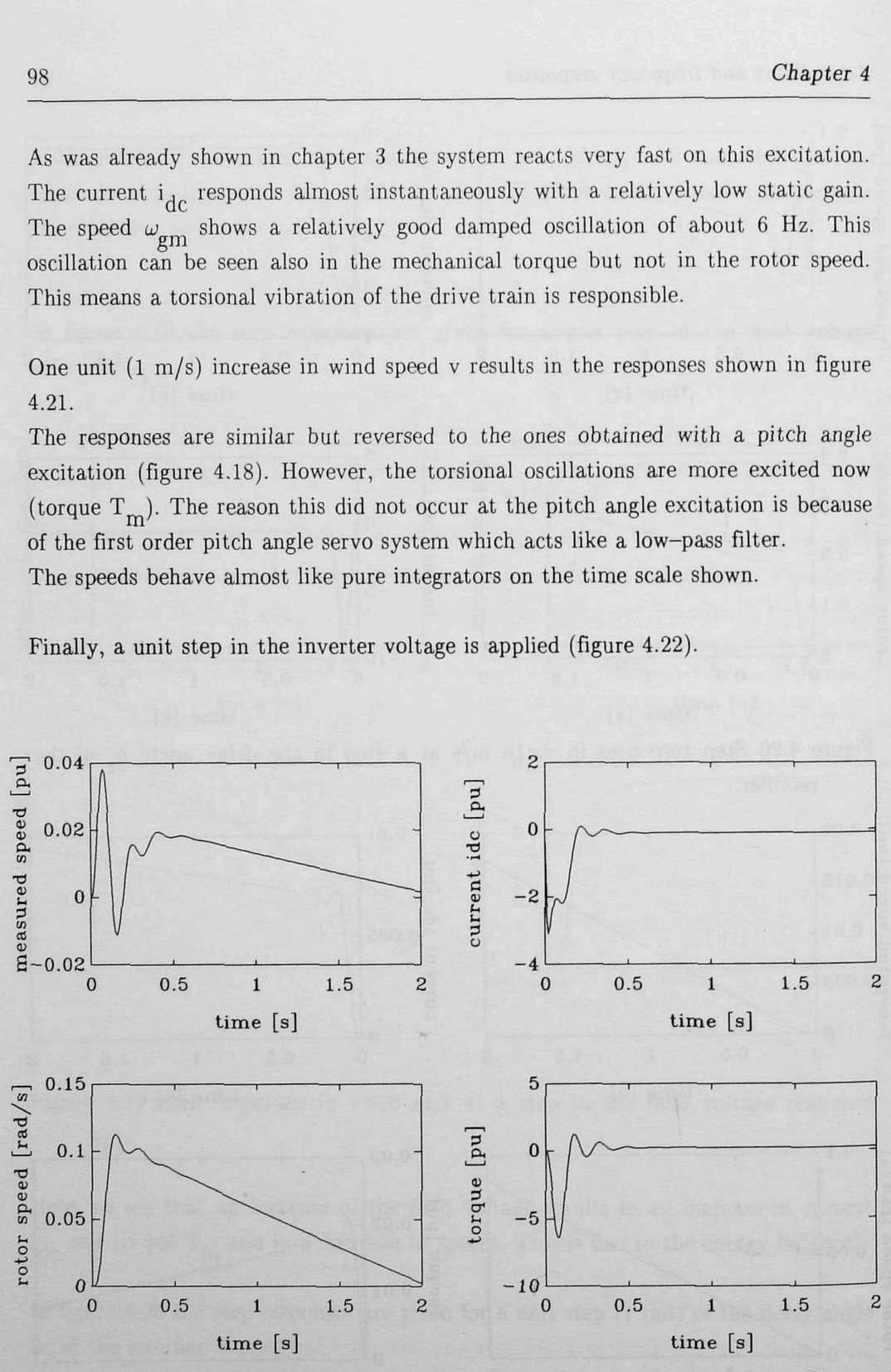

Figure 4.22 Step responses in v=16 m/s at a unit step in the inverter voltage u_i.

The responses look alike those obtained with a α_r excitation. However, the speeds have a relatively lower static gain. The torsional oscillations are excited strongly.

Frequency responses

In figure 4.23–4.27 the frequency responses of the outputs (ω_{gm},i_{dc},ω_r,T_m) are given for the five inputs (β_r,u_{Fr},α_r,v,u_i). From the figures the following conclusions may be drawn:

–one damped resonance is present: the torsional mode of the drive train (40 rad/s, 6.5 Hz),
–for u_{Fr}(figure 4.24), α_r(figure 4.25) and u_i(figure 4.27) as inputs the electrical mode gives a zero for the speed ω_{gm} and a zero is present at the torsional mode in i_{dc} (the rotor/drive train is parasitic here).

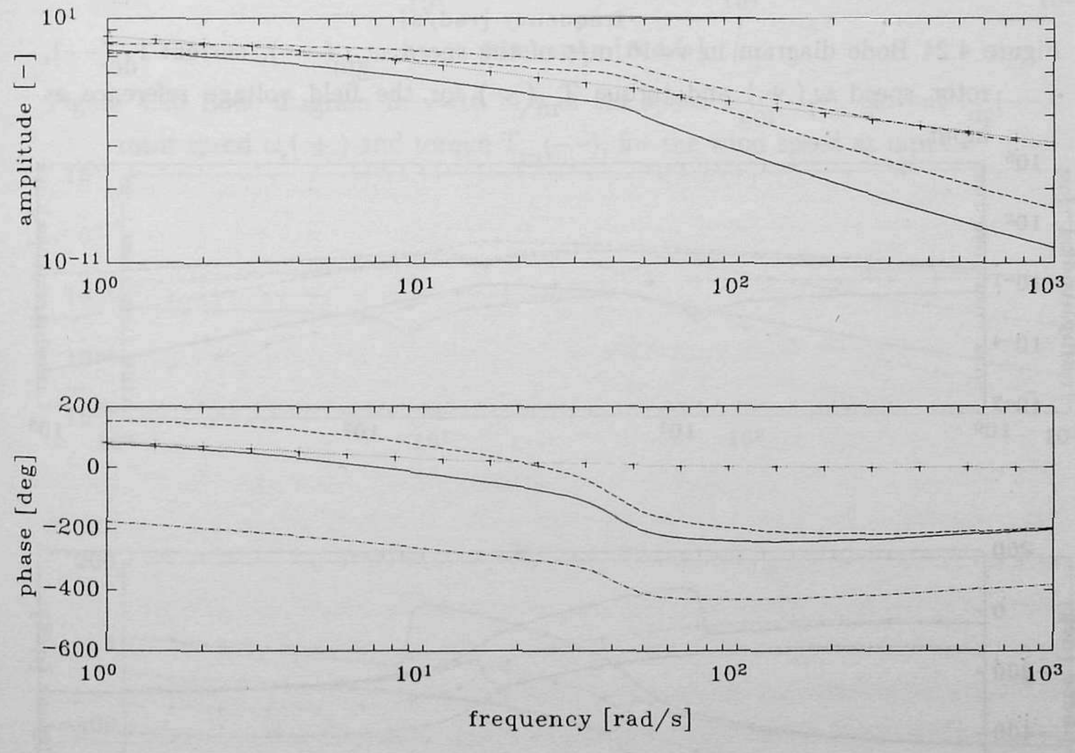

Figure 4.23 Bode diagram in v=16 m/s of the speed ω_{gm}(——), current i_{dc}(– – –), rotor speed ω_r(.+.) and torque T_m(–.–.–), for the pitch angle reference as input.

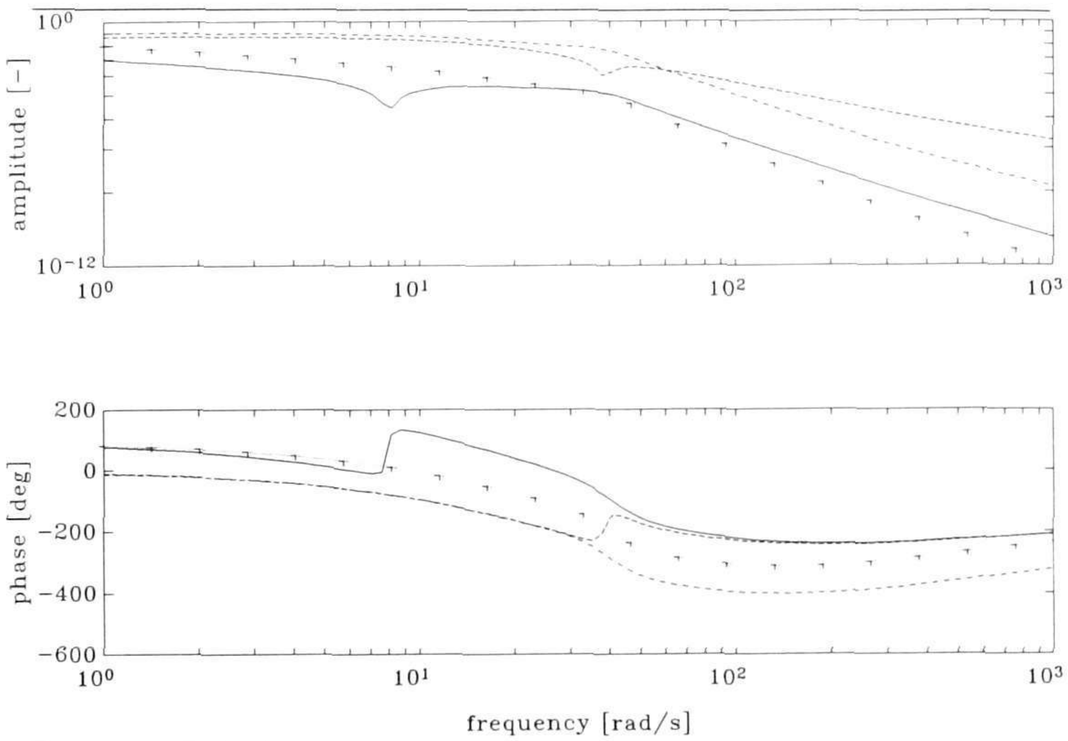

Figure 4.24 Bode diagram in v=16 m/s of the speed ω_{gm}(——), current i_{dc}(– –), rotor speed ω_r(.+.) and torque T_m(–.–) for the field voltage reference as input.

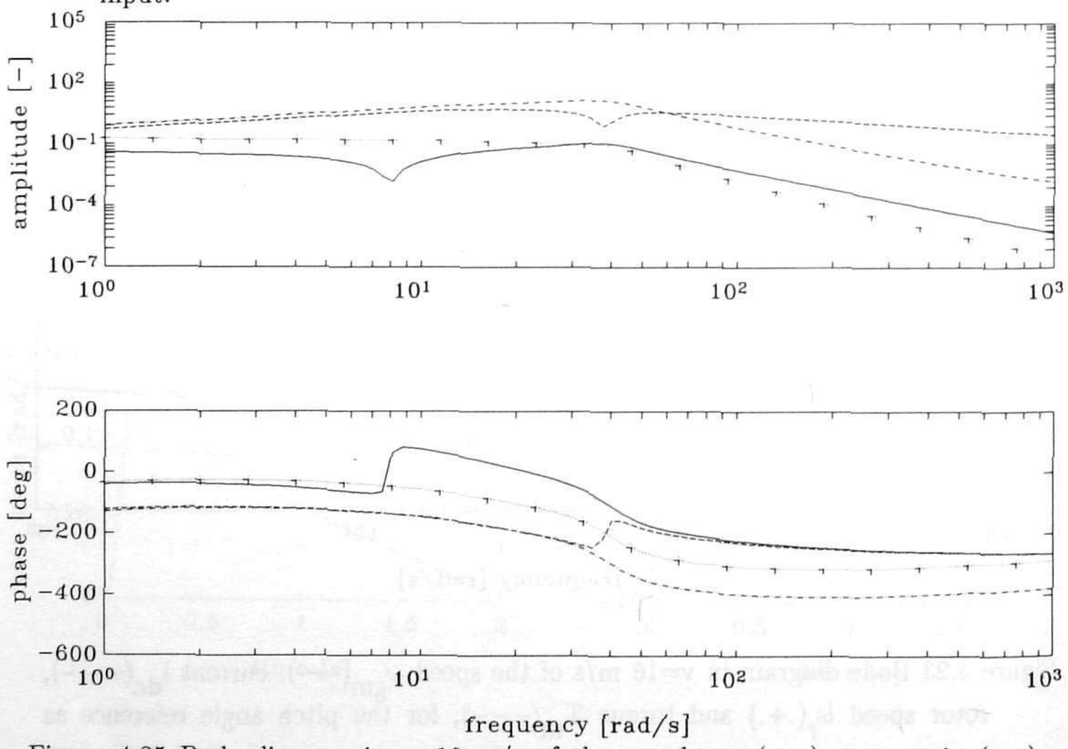

Figure 4.25 Bode diagram in v=16 m/s of the speed ω_{gm}(——), current i_{dc}(– –), rotor speed ω_r(.+.) and torque T_m(–.–) for the rectifier delay angle as input.

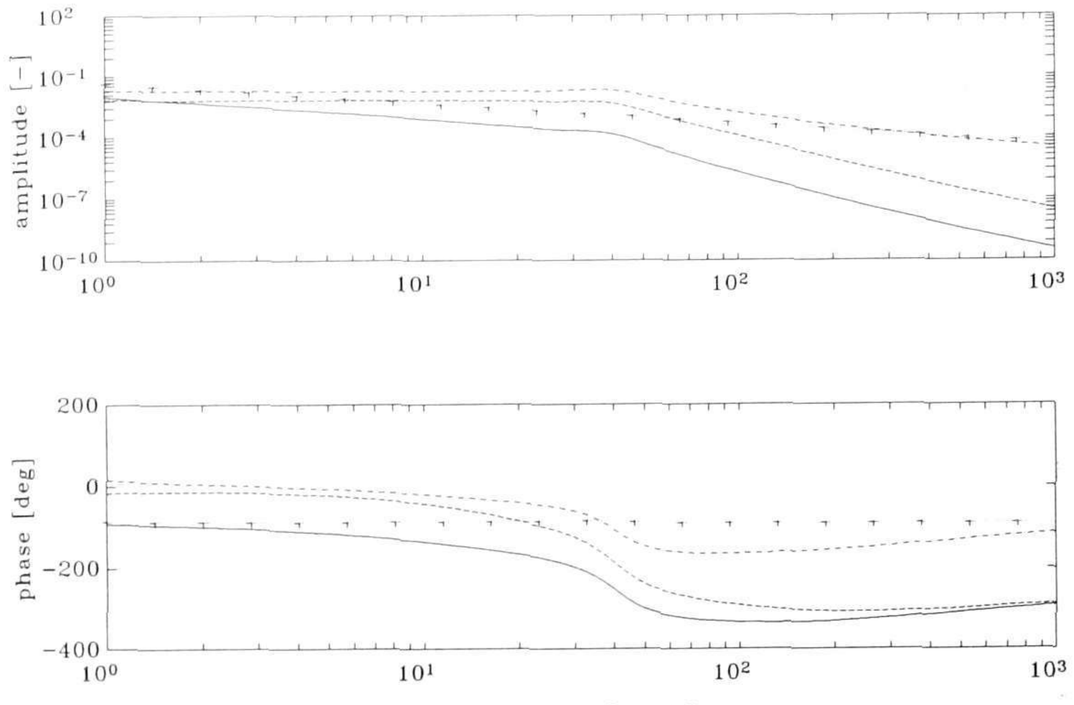

Figure 4.26 Bode diagram in v=16 m/s of the speed ω_{gm}(——), current i_{dc}(– –), rotor speed ω_r(.+.) and torque T_m(–.–), for the wind speed as input.

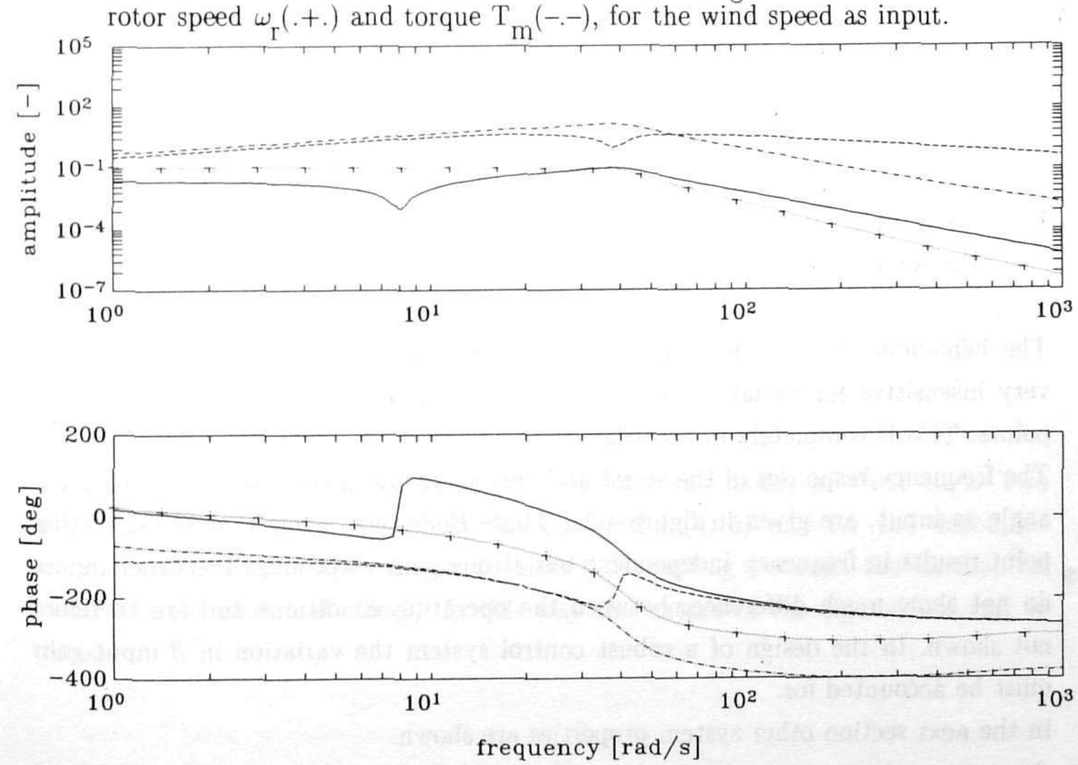

Figure 4.27 Bode diagram in v=16 m/s of the speed ω_{gm}(——), current i_{dc}(– –), rotor speed ω_r(.+.) and torque T_m(–.–), for the inverter voltage as input.

Aerodynamic nonlinearities

The nonlinearities in the aerodynamic model are nicely shown in figure 4.28 in which the step responses are given for three models (v=12,16,20 m/s) at a step change in β_r (1 rad/s).

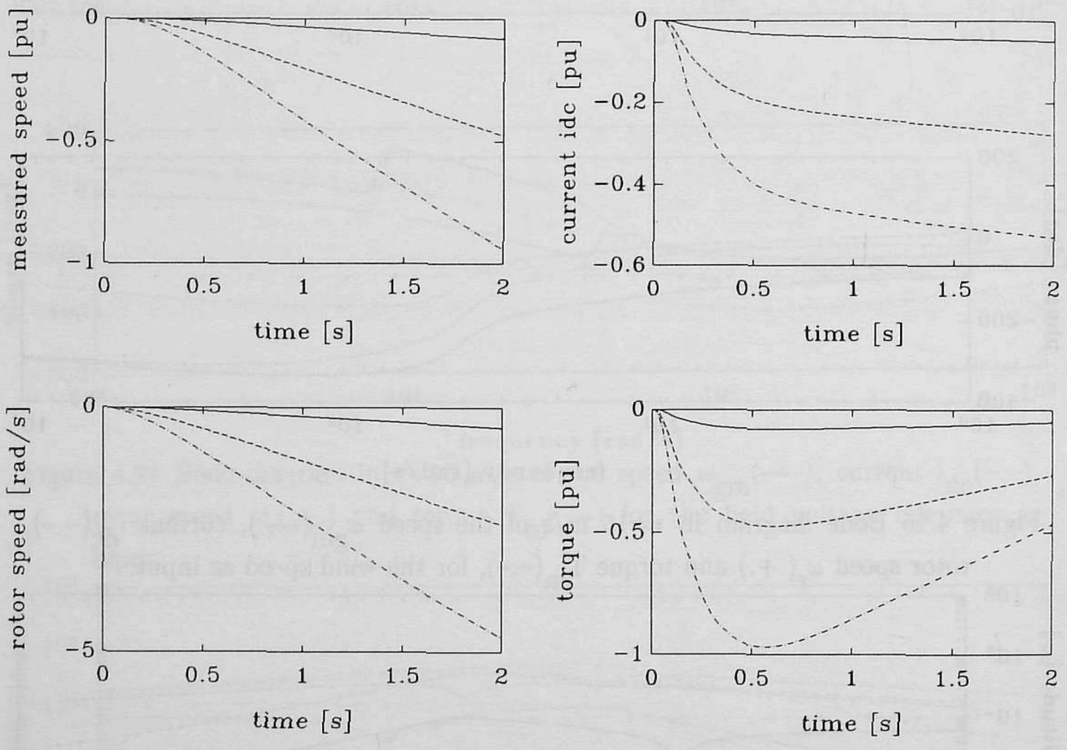

Figure 4.28 Step responses in v=12(——), 16(– – –), 20(–.–.–) m/s at a unit step in the pitch angle.

The behaviour in v=12 m/s differs significantly in the sense that the system is very insensitive for variations in the pitch angle compared to the other operating points. This is completely in accordance with figure 4.17.

The frequency responses of the speed and current in the three cases, with the pitch angle as input, are given in figure 4.29. These Bode plots show that the operating point results in frequency independent but strong gain variations. The other inputs do not show much differences between the operating conditions and are therefore not shown. In the design of a robust control system the variation in β input gain must be accounted for.

In the next section other system properties are shown.

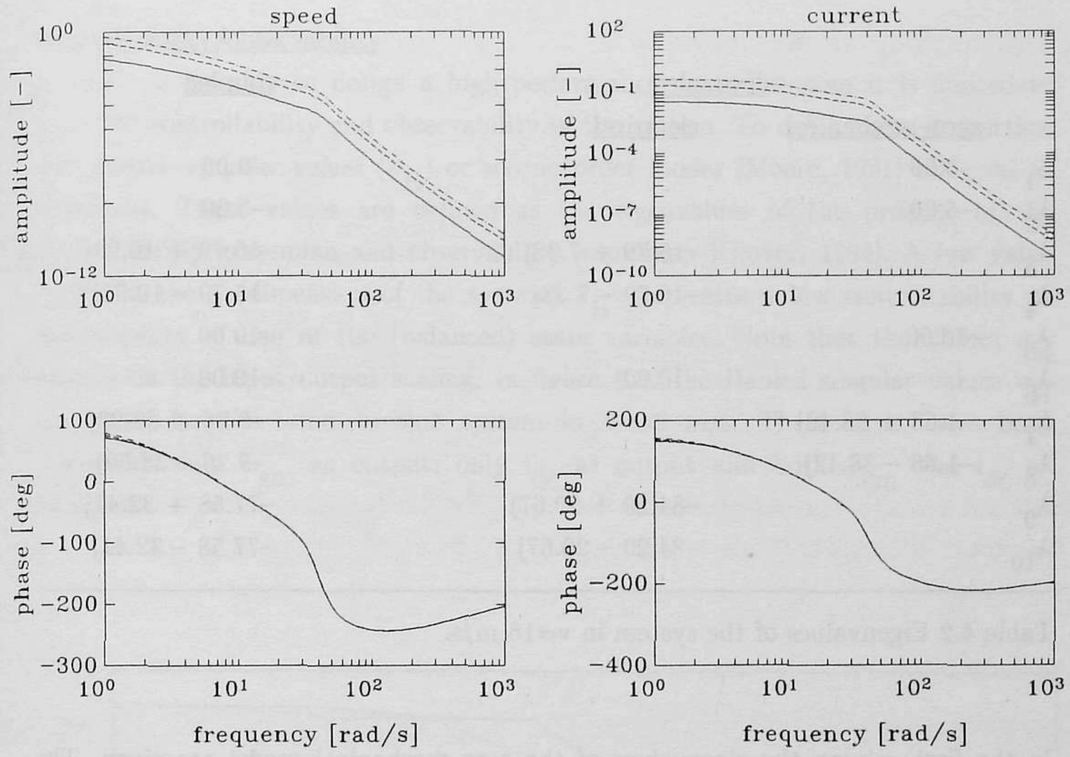

Figure 4.29 Bode diagrams in v=12(——), 16(– – –), 20(–.–.–) m/s, for the pitch angle reference as input.

4.4.3 System properties

In this section we investigate some system properties such as pole locations, controllability/observability and the effects of local feedback.

Poles/Zeros

In table 4.2 the system eigenvalues are given for the model in v=16 m/s. Two cases have been calculated, namely for the model (4.15) and for the decoupled situation where T_e is assumed to be zero (no coupling between the mechanical model and the electrical model). In this way the nature of the eigenvalues can be traced.

	decoupled		coupled
	aero–mechanical	electrical	
λ_1	–0.09		–0.06
λ_2	–5.00		–5.00
λ_3		–16.79 + 7.38j	–15.79 + 10.92j
λ_4		–16.79 – 7.38j	–15.79 – 10.92j
λ_5	–10.00		–10.00
λ_6		–10.00	–10.00
λ_7	–1.63 + 38.42j		–9.26 + 38.90j
λ_8	–1.63 – 38.42j		–9.26 – 38.90j
λ_9		–84.20 + 29.67j	–77.58 + 32.41j
λ_{10}		–84.20 – 29.67j	–77.58 – 32.41j

Table 4.2 Eigenvalues of the system in v=16 m/s.

In the first column the eigenvalues of the aero–mechanical model are given. The first eigenvalue λ_1 indicates a near integrator ($\tau_1=1/\lambda_1=11.1$ s). This is due to the large inertia of the rotor, see also the step responses. The second value λ_2 is the pole of the pitch servo. The eigenvalue λ_5 is from the measurement of the generator speed. The torsional oscillations are $\lambda_{7,8}$ and have a low damping.
The electrical eigenvalues (second column) were already shown in chapter 3. The lowest ones ($\lambda_{3,4}$) are responsible for damped oscillations in the step responses. Value λ_6 is due to the time constant of the field voltage exciter. For more comments see chapter 3.
Combination of both sub–models gives the eigenvalues shown in the third column. First note that λ_2,λ_5 and λ_6 have not changed because they are 'outside' the system. The coupling gives a change in the rotor time constant $\tau_1=1/\lambda_1=16.7$ s. The electrical poles $\lambda_{3,4}$ are a bit less damped. Most important however is the fact that the coupling gives a good damping to the torsional mode. This means that via the electrical subsystem a nice 'impedance' is put on the mechanical system reducing mechanical vibrations. At the end of this section we will see what happens if this electrical system is locally controlled.

The system (three inputs and two outputs) has no transmission zeros. Evaluating the zeros for pairs of inputs and outputs does reveal zeros but none in the right half plane.

Controllability/observability

In order to be able to design a high performance control system it is desired to have full controllability and observability of the system. To check these properties, the *Hankel–singular values* (σ_H) or second order modes [Moore, 1981] are used as indicators. These values are defined as the eigenvalues of the product of the controllability grammian and observability grammian [Glover, 1984]. A low value of one of the n (dimension of the system) σ_H's indicates a low controllability or observability of one of the (balanced) state variables. Note that the values σ_H depend on the input/output scaling. In figure 4.30 the Hankel singular values σ_H are given for the wind turbine system in v=16 m/s. Three cases have been evaluated: only ω_{gm} as output, only i_{dc} as output and both ω_{gm} and i_{dc} as outputs.

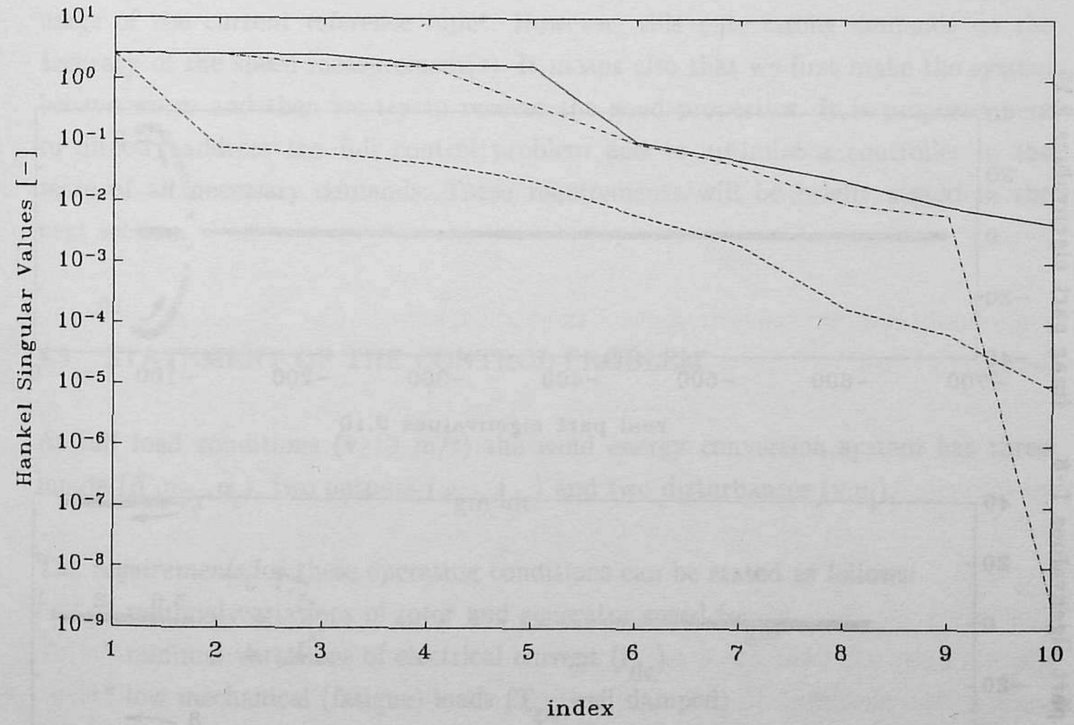

Figure 4.30 Hankel singular values of the system in v=16 m/s, with ω_{gm}(– – –) and i_{dc}(–.–.–) as single outputs and combined (——).

From the figure we see that for the situation with both outputs (——) all σ_H's are nonzero. This means that the system is completely controllable and observable.

However, if i_{dc} is chosen as the only output, one mode is no longer relevant. Obviously, this is the measurement pole of ω_{gm}.

Local feedback

A control system structure very often applied in power electronics and electrical drives is the use of Constant Current Control (CCC). This is a local feedback loop from i_{dc} to α_r (or in general to the supply voltage). Because the influence of α_r is very fast it is possible to control the direct current with a high bandwidth. Then the reference input of this slave–loop is used by a speed controller. This configuration may be well suited for a drive situation but is not necessarily the best solution for wind energy applications. To investigate this a CCC loop is closed using proportional feedback and the root–loci (with the numbering of table 4.2) of the system (v=16 m/s) are calculated with respect to the gain of the CCC loop, see figure 4.31.

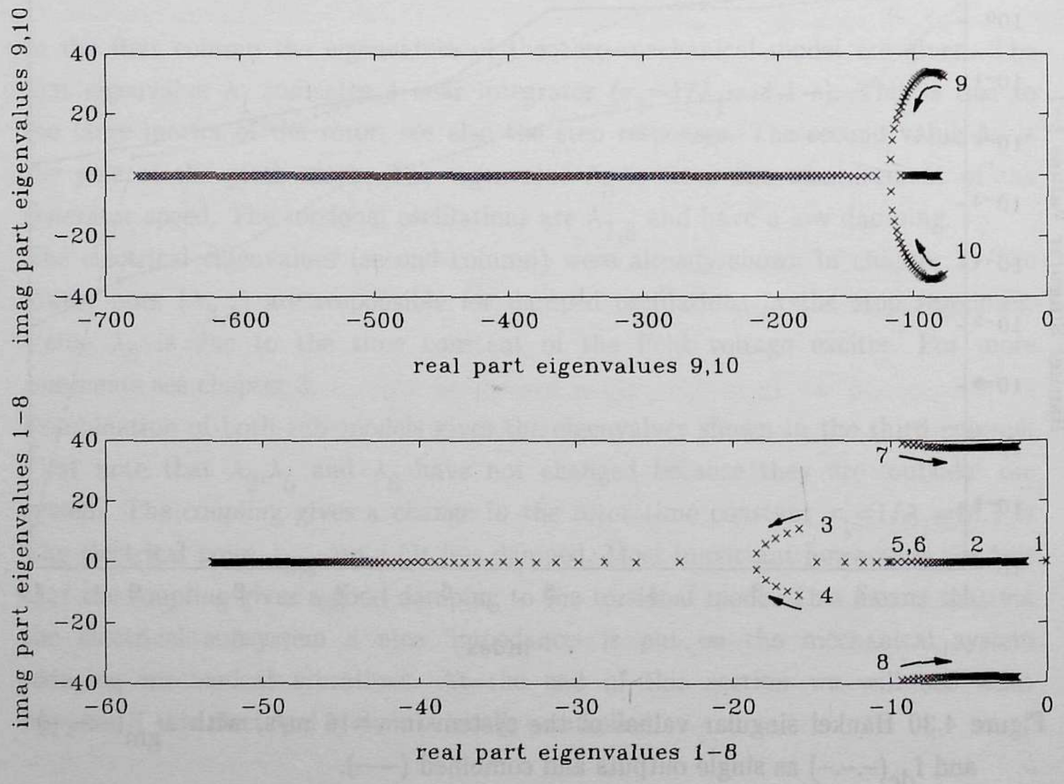

Figure 4.31 Root loci with respect to the direct current control loop.

From the figure we see that the low damped 'electrical' poles ($\lambda_{3,4}$) are damped very efficiently. This is an important result because it means that the known instability of synchronous machines with a rectifier (§3.7, [Auinger and Nagel, 1977; Ernst, 1986]) is easily stabilized. This is also mentioned in [Steinbuch, 1986]. From the root–loci it follows that a high bandwidth is easily obtained for the current loop ($\lambda_{9,10}$). However, the poles ($\lambda_{7,8}$) which result from the torsional oscillations of the drive train are negatively damped and move to values which are even less damped (–1.58±38.50j) than the decoupled system. This is a major disadvantage of using CCC in electro–mechanical systems in general. This phenomenon can be understood by assuming a constant i_{dc} which means a constant power output (because the control input is α_r). This implies that every increase of the speed of the secondary axis results in a decrease of the electrical torque form the electrical machine. This is in fact a negative impedance for the mechanical system.

If a CCC is applied it is possible to stabilize the mechanical modes by proper usage of the current reference input. However, this puts strong demands on the accuracy of the speed measurement(s). It means also that we first make the system behave worse and then we try to recover the good properties. It is proposed here to directly address the full control problem and to optimize a controller in the sense of all necessary demands. These requirements will be briefly stated in the next section.

4.5 STATEMENT OF THE CONTROL PROBLEM

At full load conditions (v≥12 m/s) the wind energy conversion system has three inputs (β_r,u_{Fr},α_r), two outputs (ω_{gm},i_{dc}) and two disturbances (v,u_i).

The ***requirements*** for these operating conditions can be stated as follows:

* minimal variations of rotor and generator speed (ω_{gm})
* minimal variations of electrical current (i_{dc})
* low mechanical (fatigue) loads (T_m well damped)
* low control effort (β_r,u_{Fr},α_r)
* low order robust controller

Remarks:

1. The tolerated speed variations above the nominal value are small (<10%) because of possible excitation of eigenfrequencies of the tower construction.

2. The requirements are conflicting. For instance, the speed and electrical power output variations are coupled due to the energy balance. Only with fast pitch angle excitation both variables can be kept constant during wind speed fluctuations. However, this can only be achieved with large (fast) excitation of the pitch angle (high control effort) and resulting in large mechanical loads in the blades.

3. The requirements with respect to the variations of the inputs are boundedness of the field voltage and delay angle variations. The latter must keep the same value in steady state. In addition, the variations in the pitch angle are bounded ($\beta \geq 0$). Also, an important restriction exists in the pitch angle excitation system, with respect to the rate of change of the pitch angle ($d\beta/dt \leq 5$ o/s).

4. The requirements on the controller complexity originate from implementation aspects. A compromise between complexity (order and structure) and performance must be found. It also means that we first try to find an appropriate constant (nonadaptive) controller.

5. Because experimental tests are not easy to perform in this application a priori statements about robustness are necessary.

6. All requirements must be met for disturbances from the wind speed and from the grid.

Evaluating the literature on the control system design of wind energy conversion systems most solutions are based on an approach where the multivariable control problem is considered in terms of multiple single input single output control problems, see for instance [Hinrichsen, 1984; Barton et al., 1979]. This means that the maximum achievable performance will not be obtained. Several studies have been done on LQG–based designs, see [Liebst, 1983; Murdoch et al., 1983 and Mattsson, 1984]. However, these wind turbines did not have a rectifier loading and/or the resulting controllers were rather complex. In the work of [Mattsson,

1984; Ernst, 1986] pitch and speed control are separated from the control of the electrical system and are designed with relatively simple models.

In contrast to the literature, in this study a full–load control system will be designed using an integrated (multivariable) approach utilizing the model of the complete system. Moreover, the important question of robustness is raised and quantitatively answered which has not been given much attention in the current literature on wind energy conversion systems.

Based on the above mentioned requirements, the control problem is posed as an optimization problem. In the next chapter the theory will be considered and in chapter 6 the method will be applied to the wind turbine system.

5. ROBUST LINEAR QUADRATIC OUTPUT FEEDBACK DESIGN METHOD

5.1 INTRODUCTION

The wind turbine control design problem as stated in section 4.5 puts strong requirements on the closed–loop behaviour. Formulating these requirements in general terms the control system design problem can be characterized with:

1. conflicting requirements: low control effort, high control quality
2. low order, simple control systems
3. robustness with respect to structured norm–bounded model perturbations (as described in §4.3) as well as robustness with respect to model variations due to changing operating conditions (§4.4.1–2).

A well–known design method suitable to address the problem (1) of conflicting requirements is the Linear Quadratic (LQ) design method [Anderson and Moore, 1971; Kwakernaak and Sivan, 1972]. This method uses a quadratic performance criterion with which the weighted sum of deviations of the state and input variables is penalized. Minimization of the performance criterion yields an optimal feedback law compromising control effort and control quality. The standard textbook solution for LQ control is the design of a dynamic controller consisting of a state estimator and a state feedback law [Kwakernaak and Sivan, 1972].
However, in order to meet requirement 2 i.e. low order and with a simple structure, here the minimization of the LQ performance criterion will be considered with respect to a predetermined structure of the feedback law [Levine and Athans, 1970]. This method will be called the Linear Quadratic Output Feedback (LQOF) method. The basic results known for the LQOF design problem of proportional and dynamic feedback will be presented in section 5.2.
Extensions of the LQOF method will be presented in section 5.3. These extensions include the servo control design problem, frequency weighting, structure selection and multi–model optimization. Both frequency weighting and multi–model optimization can be used to meet the third requirement i.e. the robustness of the closed–loop system. In order to quantify this robustness for norm–bounded perturbations the perturbation robustness analysis method based on the use of structured singular values will be presented (§5.4). In chapter 6 the techniques will be applied to the wind turbine system.

5.2 LINEAR QUADRATIC OUTPUT FEEDBACK

5.2.1 Proportional feedback

Consider the continuous–time linear time–invariant system to be controlled:

$$\begin{aligned} \dot{x} &= Ax + Bu \qquad x(0)=x_0 \\ y &= Cx \end{aligned} \tag{5.1}$$

where x is the n–dimensional state vector, u is the m–dimensional input vector, and y is the l–dimensional vector of measured outputs. The matrices A,B,C all have appropriate dimensions. The initial condition is $x(0)=x_0$.

We will first address the control design problem of proportional output feedback:

$$u = Fy \tag{5.2}$$

where F is a real mxl matrix.

Combination of the feedback law (5.2) and the system (5.1) gives the closed–loop system:

$$\dot{x} = \bar{A}x \qquad x(0)=x_0 \tag{5.3}$$

with $\bar{A}=A+BFC$ the closed–loop state matrix.

Definition 5.1. The set $\mathscr{S}_F$ of stabilizing output feedback gains is defined as the set of real mxl matrices F with the property that $Re\lambda(A+BFC)<0$.

If the set $\mathscr{S}_F$ is empty ($\mathscr{S}_F \in \phi$) there exists no feedback law of the form (5.2) such that the closed–loop system (5.3) is stable. If the system has the properties (A,B) stabilizable and (C,A) detectable then there exists a dynamic stabilizing controller for the system [Naeije and Bosgra, 1977]. Dynamic feedback will be considered in section 5.2.2.

Definition 5.2. For the system (5.1) the performance criterion is defined as

$$J = \int_0^\infty (x^T Q x + u^T R u)dt, \tag{5.4}$$

with $Q \geq 0$, $Q=Q^T \in \mathbb{R}^{nxn}$ and $R>0$, $R=R^T \in \mathbb{R}^{mxm}$. The matrices Q and R are called the weighting matrices.

Optimization Problem 5.1

The Linear Quadratic Output Feedback problem for proportional feedback is stated as:

$$\min_{F \in \mathscr{S}_F} J \tag{5.5}$$

with $\mathscr{S}_F$ and J according to definitions 5.1 and 5.2 respectively, under the constraints $\mathscr{S}_F \notin \phi$ and the system (5.1),(5.2).

Necessary conditions for the solution to (5.5) are given by the requirement $\partial J/\partial F=0$. This can be worked out resulting in the following theorem.

Theorem 5.1.

Define the real nxn matrix $X=x_0x_0^T$ and let $F \in \mathscr{S}_F$, $\mathscr{S}_F \notin \phi$, then in order for F to solve (5.5) it is necessary that:

$$F = -R^{-1}B^T P S C^T (CSC^T)^{-1} \tag{5.6}$$

where $P=P^T \geq 0$ is the solution of the Lyapunov equation:

$$P(A+BFC) + (A+BFC)^T P + Q + C^T F^T R F C = 0 \tag{5.7}$$

and where $S=S^T \geq 0$ is the solution of the Lyapunov equation:

$$S(A+BFC)^T + (A+BFC)S + X = 0 \tag{5.8}$$

Proof: [Levine and Athans, 1970; Anderson and Moore, 1971] □

Remarks:

1. The set of equations (5.6)–(5.8) is implicit: the solution F must be found using an iterative algorithm, see [Mäkilä and Toivonen, 1987] for a review on this subject; an initially stabilizing F is necessary.

2. If we assume that C=I (C^{-1} exists) as is the case with state feedback, equation (5.6) reduces to the optimal LQ regulator:

$$F = -R^{-1}B^T P \tag{5.9}$$

with (5.7) the corresponding Ricatti equation, after proper substitutions:

$$PA + A^T P - PBR^{-1}B^T P + Q = 0$$

3. These are necessary conditions only and it is possible that solutions of these conditions do not solve (5.5). Sufficient conditions for the solution of (5.5) are not known.

4. For any feedback law satisfying these necessary conditions, the performance criterion (5.4) can be expressed as [Levine and Athans, 1970]:

$$J = \mathrm{tr}(PX) = x_0 P x_0^T \tag{5.10}$$

with tr(.) the trace operator.

The design of an optimal constant gain output feedback law involves the selection of the weighting matrices Q and R, the choice of the initial condition x_0 and the choice of an initial stabilizing feedback law. An algorithm (remark 1) is used to calculate a minimizing solution F of (5.5).

The feedback law obtained depend on the initial state x_0 via the matrix $X=x_0x_0^T$ as defined in theorem 5.1, see eq.(5.6) and (5.8). In the wind turbine case we do not know one initial state but instead we want to design a feedback law suitable for many initial states and other disturbances (wind speed and grid voltage). In the literature it is suggested to choose a matrix X with the property that rank(X)>1 to obtain a feedback which is optimal in a sense of averaging over several initial states [Levine and Athans, 1970]. In chapter 6 it will be shown for the wind turbine system how the matrix X can be used as a design parameter, in addition to the weighting matrices Q and R.

As mentioned in section 4.5 (remark 4) the requirement on the controller is that it should be as simple as possible. In the Optimization Problem 5.1 with the feedback law (5.2), every input u of the system is a function of every output y. One way to obtain a reduction of complexity of the feedback is to impose some special (decentralized) structure on F, for instance by choosing entries of F zero. For such situations the optimization problem will be formulated.

Definition 5.3. *The set $\mathscr{S}_0$ is defined as the set of zero entries of real mxl matrices, the set $\mathscr{S}_{Fc}$ is defined as the set of matrices $F\in\mathscr{S}_F$ (definition 5.1), satisfying*

$$F(i,j)=0, \qquad \text{for all } (i,j)\in\mathscr{S}_0$$

So for a two–input two–output system (m=2,l=2) a decentralized controller could be defined as $\mathscr{S}_0=\{(1,2),(2,1)\}$, with $F\in\mathscr{S}_{Fc}$ resulting in $F=\begin{bmatrix} f & 0 \\ 0 & g \end{bmatrix}$ with f and g to be designed.

Optimization Problem 5.2

The Linear Quadratic Output Feedback problem for proportional feedback subject to constraints on the structure of the feedback law in the sense of definition 5.3, is given by:

$$\min_{F\in\mathscr{S}_{Fc}} J \tag{5.11}$$

with $\mathscr{S}_{Fc}$ and J according to definitions 5.3 and 5.2 respectively, under the constraints $\mathscr{S}_{Fc}\neq\phi$ and the system (5.1),(5.2).

Necessary conditions for the solution to (5.11) are $\partial J/\partial F(i,j)=0$ for each nonzero element of F. This can be worked out as follows. Define e_i as the identity vector with all elements zero except entry i, which is equal to one. The necessary conditions for a solution $F\in\mathscr{S}_{Fc}$ to solve (5.11) are that $\mathscr{S}_{Fc}\neq\phi$ and

$$\frac{\partial J}{\partial F(i,j)} = 2e_i^T[B^TP+RFC]SC^Te_j = 0, \text{ for all } (i,j)\notin\mathscr{S}_0 \tag{5.12}$$

where P and S are the solutions to equations (5.7) and (5.8).

The number of equations defined by (5.12) is equal to the number of free parameters in F. This set of equations must be solved in combination with the P– and S–equation (5.7) and (5.8) from theorem 5.1. The algorithm mentioned in remark 1 of theorem 5.1 can be modified such that it also solves Optimization Problem 5.2.

The optimization problems stated above are suited to design proportional feedback laws. In order to realize the high performance requirements for the wind turbine system (section 4.5) it might be also necessary to include dynamic compensation of the system. In the next section the optimization problem will be formulated for that case.

5.2.2 Dynamic feedback

In this section it will be shown that the LQOF method for proportional feedback can easily be extended to cover the design of dynamic feedback. Using an extended state vector the dynamic LQOF problem is reducible to the proportional LQOF problem described in the preceding section.

Suppose a controller is to be designed with a predefined order q. A state space model for a general dynamic controller is:

$$\begin{aligned} \dot{p} &= Hp + Gy \qquad p(0)=p_0 \\ u &= Kp + Fy \end{aligned} \tag{5.13}$$

with inputs equal to the outputs y of system (5.1) and with the outputs u as inputs to system (5.1). A blockdiagram of system (5.1) controlled with the dynamic feedback law (5.13) is given below.

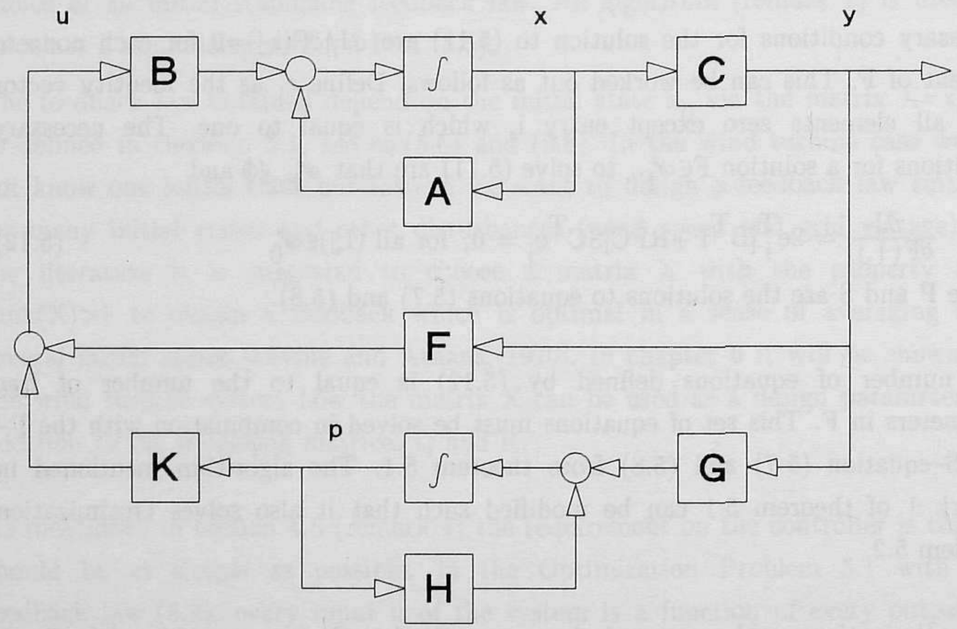

Figure 5.1 Blockdiagram of the system with a general dynamic feedback.

The control design problem is to find the feedback parameters (H,G,K,F) such that a performance criterion of the form (5.4) is minimized under the constraints (5.1) and (5.13).

For a solution we first write down the resulting closed–loop state–space model:

$$\begin{bmatrix} \dot{x} \\ \dot{p} \end{bmatrix} = \begin{bmatrix} A+BFC & BK \\ GC & H \end{bmatrix} \begin{bmatrix} x \\ p \end{bmatrix} \qquad \begin{bmatrix} x(0) \\ p(0) \end{bmatrix} = \begin{bmatrix} x_0 \\ p_0 \end{bmatrix} \tag{5.14}$$

which follows directly by combination of (5.1) and (5.13).

Now define the following matrices:

$$\tilde{A} = \begin{bmatrix} A & 0 \\ 0 & 0 \end{bmatrix} \qquad \tilde{B} = \begin{bmatrix} B & 0 \\ 0 & I \end{bmatrix} \qquad \tilde{C} = \begin{bmatrix} C & 0 \\ 0 & I \end{bmatrix} \qquad \tilde{F} = \begin{bmatrix} F & K \\ G & H \end{bmatrix}$$

then using simple matrix manipulations it can be shown that (5.14) is equal to:

$$\begin{bmatrix} \dot{x} \\ \dot{p} \end{bmatrix} = (\tilde{A}+\tilde{B}\tilde{F}\tilde{C}) \begin{bmatrix} x \\ p \end{bmatrix} \qquad \begin{bmatrix} x(0) \\ p(0) \end{bmatrix} = \begin{bmatrix} x_0 \\ p_0 \end{bmatrix} \tag{5.15}$$

This means that the matrix $\tilde{F}$ can be interpreted as a proportional feedback law of the system $(\tilde{A},\tilde{B},\tilde{C})$. Indeed if we define the new open–loop system

$$\begin{bmatrix} \dot{x} \\ \dot{p} \end{bmatrix} = \begin{bmatrix} A & 0 \\ 0 & 0 \end{bmatrix} \begin{bmatrix} x \\ p \end{bmatrix} + \begin{bmatrix} B & 0 \\ 0 & I \end{bmatrix} \begin{bmatrix} u \\ u_p \end{bmatrix} \qquad \begin{bmatrix} x(0) \\ p(0) \end{bmatrix} = \begin{bmatrix} x_0 \\ p_0 \end{bmatrix}$$
$$\begin{bmatrix} y \\ p \end{bmatrix} = \begin{bmatrix} C & 0 \\ 0 & I \end{bmatrix} \begin{bmatrix} x \\ p \end{bmatrix} \tag{5.16}$$

or $\dot{\tilde{x}} = \tilde{A}\tilde{x} + \tilde{B}\tilde{u}$,

$\tilde{y} = \tilde{C}\tilde{x}$

then application of the proportional feedback law

$$\begin{bmatrix} u \\ u_p \end{bmatrix} = \begin{bmatrix} F & K \\ G & H \end{bmatrix} \begin{bmatrix} y \\ p \end{bmatrix} \tag{5.17}$$

or $\tilde{u}=\tilde{F}\tilde{y}$

results in the closed–loop system (5.14).

Equations (5.16),(5.17) define a system similar to (5.1),(5.2). If we also define the extended matrices $\tilde{Q},\tilde{R},\tilde{X}$:

$$\tilde{Q} = \begin{bmatrix} Q_1 & 0 \\ 0 & Q_2 \end{bmatrix} \quad \tilde{R} = \begin{bmatrix} R_1 & 0 \\ 0 & R_2 \end{bmatrix} \quad \tilde{X} = \begin{bmatrix} X_1 & 0 \\ 0 & X_2 \end{bmatrix} = \begin{bmatrix} x_0 x_0^T & 0 \\ 0 & p_0 p_0^T \end{bmatrix} \tag{5.18}$$

the following problem can be stated.

Define $\mathscr{F}_{\tilde{F}}$ as the set of real (m+q)x(l+q) matrices $\tilde{F}$ such that $\tilde{A}+\tilde{B}\tilde{F}\tilde{C}$ is stable, and define the **performance criterion for dynamic compensation** as

$$\tilde{J} = \int_0^\infty \left\{ [x^T\ p^T]\tilde{Q} \begin{bmatrix} x \\ p \end{bmatrix} + [u^T\ u_p^T]\tilde{R} \begin{bmatrix} u \\ u_p \end{bmatrix} \right\} dt, \quad \tilde{Q}\geq 0,\ \tilde{R}>0 \tag{5.19}$$

Note that by using $\tilde{Q},\tilde{R},\tilde{X}$ according to (5.18) it is possible not only to weight deviations in x and u but also in the regulator states p and inputs u_p.

Optimization Problem 5.3

The Linear Quadratic Output Feedback problem for dynamic compensation is stated as:

$$\min_{\tilde{F}\in\mathscr{S}_{\tilde{F}}} \tilde{J} \tag{5.20}$$

under the constraints $\mathscr{S}_{\tilde{F}}\neq\phi$ and the system (5.16),(5.17) and with $\tilde{J}$ according to (5.19).

Necessary conditions for the solution to (5.20) are given by $\partial\tilde{J}/\partial\tilde{F}=0$, i.e. $\partial J/\partial F=0$, $\partial J/\partial K=0$, $\partial J/\partial G=0$, $\partial J/\partial H=0$. This again results in theorem 5.1 applied to the extended matrices $(\tilde{A},\tilde{B},\tilde{C},\tilde{F},\tilde{Q},\tilde{R},\tilde{X})$.
In this way the dynamic LQOF problem has been reduced to the proportional Optimization Problem 5.1. Application of Optimization Problem 5.2 (5.11) gives the opportunity to select elements of $\tilde{F}$ zero a priori. An example is to take H=0: the resulting controller (5.13) then has the structure of an *optimal multivariable PI controller*. In the case of the wind turbine system this is very important in order to obtain zero steady–state errors at constant disturbances from the wind speed and/or grid voltage. In the following section this problem will be worked out.

5.3 EXTENSIONS OF LINEAR QUADRATIC OUTPUT FEEDBACK

The Optimization Problems 5.1–5.3 for the design of proportional and dynamic Linear Quadratic Output Feedback laws are the basic tools. Several extensions are possible some of which will be described in this section.
In order to design closed–loop systems with prescribed asymptotic behaviour i.e. steady–state requirements, the servo control design problem with LQOF will be stated first. In section 5.3.2 the quadratic performance criterion will be extended with a weighting term of products of states and inputs. This is of importance for instance for LQOF with frequency weighting, which will be described in section 5.3.3. In section 5.3.4 a procedure will be developed to select decentralized control structures, in order to arrive at simple feedback laws. Finally, the multi–model robust LQOF method will be presented with which the feedback parameters are optimized for multiple models.

5.3.1 The optimal servo problem

Recall from chapter 4 that the nominal model for the wind turbine system is given by (4.15):

$$\begin{aligned}\dot{x} &= Ax + Bu + Ew \qquad x(0)=x_0\\ y &= Cx\end{aligned} \tag{5.21}$$

where w is the vector of external disturbances (wind speed and grid voltage). These disturbances have both stochastic and deterministic properties in the case of the wind turbine system. For instance the wind speed has a fluctuating nature and its mean value over some time of interest may vary from time to time. In all cases the requirements demand a constant speed, current and delay angle of the rectifier at steady–state.
In the linear model (5.21) the stochastic nature of w can be treated similarly to the deterministic optimal control problem as stated in section 5.2.1, see [Naeye, 1979]. Because all solutions to (5.5) or (5.11) give a stable closed–loop system all variables tend to zero if $t\to\infty$, which means that all steady–state requirements are met. However, for the case where w is allowed to have a nonzero deterministic part the servo control problem must be stated explicitly.
Here we restrict our attention to the case where w represents constant disturbances. More general formulations are possible for other disturbances as well as for reference signals, see [Davison, 1972, 1976, 1981].

Suppose that the requirements on the closed–loop behaviour define a subset y_i of l_i elements out of the outputs y of system (5.21) which should meet the steady–state requirement:

$$\lim_{t\to\infty} y_i(t)=0 \tag{5.22}$$

with $y_i=M_y y$, M_y a real $l_i$xl matrix. In the case of the wind turbine system M_y is a 2x2 identity matrix because both speed and current should solve (5.22).
Similarly for the inputs we select m_i inputs u_i out of the m inputs u:

$$\lim_{t\to\infty} u_i(t)=0 \tag{5.23}$$

with $u_i=M_u u$, M_u a real $m_i$xm matrix. In the case of the wind turbine system the only input required to have a constant steady–state value is the delay angle of the rectifier, so $M_u=[0\ 0\ 1]$.

The servo control design problem is stated as follows:

> For the system (5.21) with w constant, the servo control design problem is to find a feedback law relating y and u, such that the requirements (5.22),(5.23) are met and that a good (in a sense to be defined) closed–loop transient behaviour occurs.

Davison [1972] has given a solution to the servo control design problem using a special controller structure consisting of a *servo–compensator* and a *stabilizing compensator*, see figure 5.2.

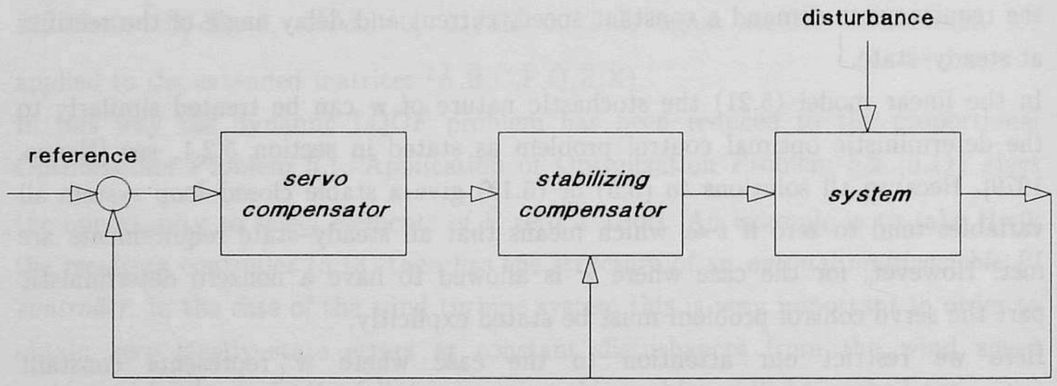

Figure 5.2 Controller structure for the servo control problem for constant disturbances.

The *servo–compensator* is chosen [Davison, 1972] such that it contains a representation of the dynamics of the disturbances. In our case we have only constant disturbances yielding a servo–compensator with pure integrators:

$$\dot{p}_y = M_y y \qquad p_y(0)=p_{y0} \tag{5.24}$$
$$\dot{p}_u = M_u u \qquad p_u(0)=p_{u0}$$

The outputs of the servo–compensator are the integrator states p_y and p_u.

Lemma 5.1

Consider the system (5.21). A necessary and sufficient condition for the existence of a linear time–invariant controller for (5.21) such that (5.22) and (5.23) hold for all constant disturbances w and such that the closed–loop system is stable, is that the following conditions are met:

1) (A,B) stabilizable
2) (C,A) detectable
3) $m \geq m_i+l_i$
4) $\text{rank}\begin{bmatrix} A & B \\ M_y C & D \\ 0 & M_u D \end{bmatrix} = n+l_i+m_i$

Moreover, assume that conditions 1)–4) are satisfied, then a controller with the structure as depicted in figure 5.2 with the servo–compensator (5.24) solves the servo control design problem.

Proof: see [Davison, 1976] for the original proof; add $M_u u$ to the output vector defined in [Davison, 1976] to obtain condition 4. □

For the design of the *stabilizing compensator* augment the system (5.21) with the servo–compensator equations (5.24):

$$\begin{bmatrix} \dot{x} \\ \dot{p}_y \\ \dot{p}_u \end{bmatrix} = \begin{bmatrix} A & 0 & 0 \\ M_y C & 0 & 0 \\ 0 & 0 & 0 \end{bmatrix} \begin{bmatrix} x \\ p_y \\ p_u \end{bmatrix} + \begin{bmatrix} B \\ 0 \\ M_u \end{bmatrix} u \qquad \begin{bmatrix} x(0) \\ p_y(0) \\ p_u(0) \end{bmatrix} = \begin{bmatrix} x_0 \\ p_{y0} \\ p_{u0} \end{bmatrix} \tag{5.25}$$
$$\begin{bmatrix} y \\ p_y \\ p_u \end{bmatrix} = \begin{bmatrix} C & 0 & 0 \\ 0 & I & 0 \\ 0 & 0 & I \end{bmatrix} \begin{bmatrix} x \\ p_y \\ p_u \end{bmatrix}$$

Because the asymptotic behaviour is already satisfied by (5.24), the (constant) disturbance w is not necessary for the design of the stabilizing compensator [Davison, 1976]. For system (5.25) any control design method can be used. Here we will use the LQOF method, of which all results obtained so far (§5.2) are applicable. For the most general case of the design of a dynamic feedback law we extend the system (5.25) according to (5.16):

$$\dot{\tilde{x}} = \tilde{A}\tilde{x} + \tilde{B}\tilde{u},$$
$$\tilde{y} = \tilde{C}\tilde{x}$$

with

$$\tilde{x} = \begin{bmatrix} x \\ p_y \\ p_u \\ p \end{bmatrix}, \quad \tilde{u} = \begin{bmatrix} u \\ u_p \end{bmatrix}, \quad \tilde{y} = \begin{bmatrix} x \\ p_y \\ p_u \\ p \end{bmatrix}$$

with p, u_p according to (5.16) and where

$$\tilde{A} = \begin{bmatrix} A & 0 & 0 & 0 \\ M_y C & 0 & 0 & 0 \\ 0 & 0 & 0 & 0 \\ 0 & 0 & 0 & 0 \end{bmatrix}, \quad \tilde{B} = \begin{bmatrix} B & 0 \\ 0 & 0 \\ M_u & 0 \\ 0 & I \end{bmatrix}, \quad \tilde{C} = \begin{bmatrix} C & 0 & 0 & 0 \\ 0 & I & 0 & 0 \\ 0 & 0 & I & 0 \\ 0 & 0 & 0 & I \end{bmatrix} \tag{5.26}$$

and the feedback law (5.17):

$$\tilde{u}=\tilde{F}\tilde{y}$$

with the feedback parameters

$$\tilde{F} = \begin{bmatrix} F & F_y & F_u & K \\ G & G_y & G_u & H \end{bmatrix} \tag{5.27}$$

The blockdiagram of the closed–loop system is given in figure 5.3.

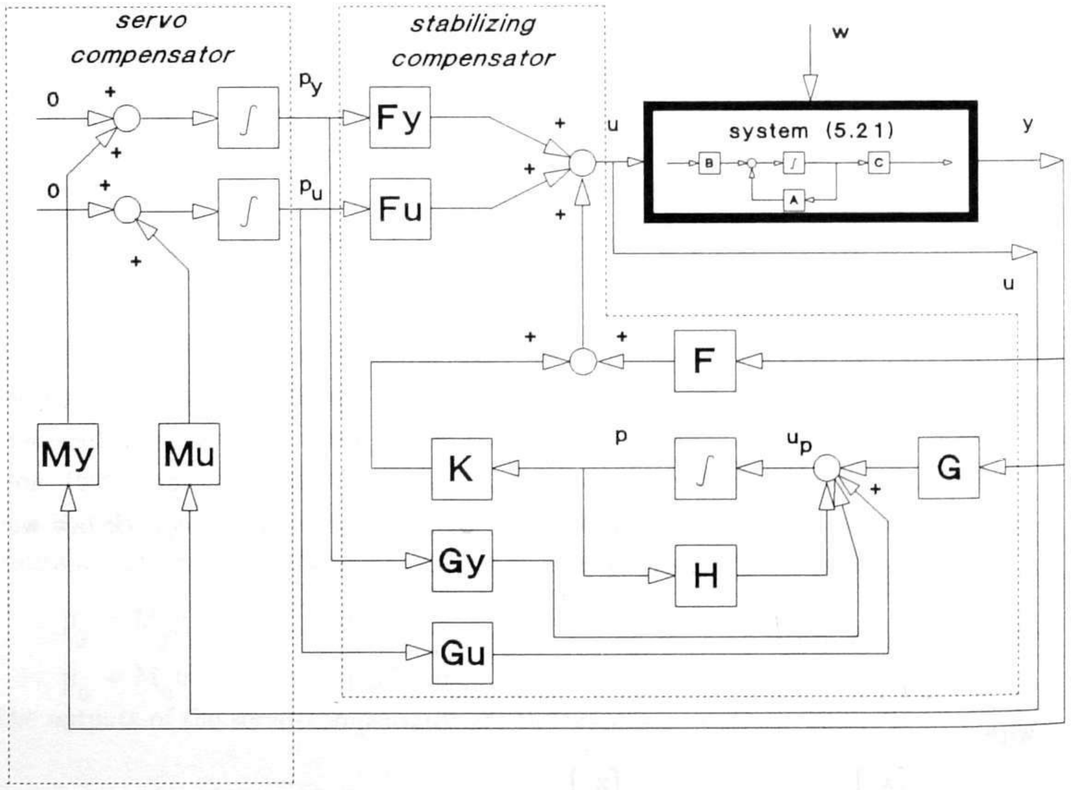

Figure 5.3 Dynamic output feedback for the servo control problem for constant disturbances.

The feedback parameters (5.27) consist of (see also figure 5.3):

F:	the proportional feedback from y to u:	$u=Fy$
F_y:	the integral feedback of the outputs:	$u=F_y\int M_y y$
F_u:	the integral feedback of the inputs:	$u=F_u\int M_u u$
K:	the feedback of the states p:	$u=Kp$
G,G_y,G_u,H:	parameters of the state equation of the stabilizing controller:	$\dot{p}=Hp+Gy+G_y\int M_y y+G_u\int M_u u$

In this way the servo control design problem for LQOF has been reformed to the standard proportional LQOF problem. All results of section 5.2 are therefore applicable in order to design feedback law (5.27).

5.3.2 Cross–product weighting

In the performance criterion (5.4) or (5.19) the variations of the states and inputs are penalized. In some cases such as with model following [Tyler, 1964] or frequency weighting (see section 5.3.3) it is necessary to weight also products of states and inputs: $x^T Nu$. In this section the formulation and necessary conditions of the corresponding LQOF problem will be given.
Define the performance criterion to be minimized as follows.

Definition 5.4. For the system (5.1) the performance criterion with cross–term weighting is defined as

$$J = \int_0^\infty \begin{bmatrix} x \\ u \end{bmatrix}^T \begin{bmatrix} Q & N \\ N^T & R \end{bmatrix} \begin{bmatrix} x \\ u \end{bmatrix} dt, \tag{5.28}$$

with $Q\geq 0$, $Q=Q^T\in\mathbb{R}^{nxn}$, $R>0$, $R=R^T\in\mathbb{R}^{mxm}$, and $N\in\mathbb{R}^{nxm}$ such that $\begin{bmatrix} Q & N \\ N^T & R \end{bmatrix}\geq 0$.

The necessary conditions for Optimization Problem 5.1 with J according to definition 5.4 are given by the following extension of theorem 5.1.

Corollary 5.1.

Define the real nxn matrix $X=x_0x_0^T$ and let $F\in\mathscr{S}_F$, $\mathscr{S}_F\neq\phi$, then in order for F to solve (5.5), with J according to definition 5.4, it is necessary that:

$$F = -R^{-1}(B^TP+N^T)SC^T(CSC^T)^{-1} \tag{5.29}$$

where $P=P^T\geq 0$ is the solution of the Lyapunov equation:

$$P(A+BFC)+(A+BFC)^TP+Q+NFC+C^TF^TN^T+C^TF^TRFC = 0 \tag{5.30}$$

and where $S=S^T\geq 0$ is the solution of the Lyapunov equation:

$$S(A+BFC)^T + (A+BFC)S + X = 0 \tag{5.31}$$

Proof: Substitute u=Fy=FCx in the performance criterion (5.28):

$$J = \int_0^\infty x^T[Q+NFC+C^TF^TN^T+C^TF^TRFC]x\ dt$$

this gives J=tr(PX) with P the solution to (5.30) [Chen, 1984, p.574], see also (5.10). For this criterion J the gradient $\partial J/\partial F$ can be calculated similarly as in theorem 5.1 or by using first order perturbations (see section 5.3.4), with the result:

$$\partial J/\partial f = 2[B^TP+RFC+N^T]SC^T$$

Equating this gradient to zero yields (5.29). □

5.3.3 Frequency weighted Linear Quadratic Output Feedback

For observer based LQ techniques, such as LQG, an extension has been introduced to facilitate the use of frequency weighting on the states (outputs) and inputs [Gupta et al., 1981; Anderson et al., 1983]. The reason of this is to stress certain requirements more at certain frequencies.

A consequence of using frequency weighting in combination with LQ state feedback is that the weighting functions are in fact filters applied to the system. This results in high order controllers.

Here we will present the usage of frequency weighting in combination with the LQOF method. A very important benefit of LQOF is that we still can design low order controllers, despite the dynamics of the weighting filters.

Consider system (5.1). Define as state and input weighting functions the following state space realizations:

$$\begin{aligned} W_x:\ \dot{z}_x &= A_xz_x+B_xx & z_x(0)&=z_{x0} \\ x_w &= C_xz_x+D_xx & & \end{aligned} \tag{5.32}$$
$$\begin{aligned} W_u:\ \dot{z}_u &= A_uz_u+B_uu & z_u(0)&=z_{u0} \\ u_w &= C_uz_u+D_uu & & \end{aligned}$$

with $\dim(z_x)=q_{zx}$, $\dim(x_w)=q_x$, $\dim(z_u)=q_{zu}$, $\dim(u_w)=q_u$.

Assume that the performance criterion (definition 5.2) is extended in the following way.

Definition 5.5. For the system (5.1),(5.32) the performance criterion with frequency weighting is defined as

$$J = \int_0^\infty (x^TQx + x_w^TQ_xx_w + u_w^TQ_uu_w + u^TRu)dt, \tag{5.33}$$

with $Q\geq 0$, $Q=Q^T\in\mathbb{R}^{nxn}$, $Q_x\geq 0$, $Q_x=Q_x^T\in\mathbb{R}^{q_xxq_x}$, $Q_u\geq 0$, $Q_u=Q_u^T\in\mathbb{R}^{q_uxq_u}$ and $R>0$, $R=R^T\in\mathbb{R}^{mxm}$.

In order to state an optimization problem, we first define the extended system for frequency weighting as a combination of (5.1) and (5.32):

$$\begin{aligned} \dot{\tilde{x}} &= \tilde{A}\tilde{x} + \tilde{B}u & \tilde{x}(0)&=\tilde{x}_0 \\ \tilde{y} &= \tilde{C}\tilde{x} & & \end{aligned} \tag{5.34}$$

with

$$\tilde{x} = \begin{bmatrix} x \\ z_x \\ z_u \end{bmatrix} \qquad \tilde{x}_0 = \begin{bmatrix} x_0 \\ z_{x0} \\ z_{u0} \end{bmatrix} \qquad \tilde{y} = \begin{bmatrix} y \\ x_w \\ u_w \end{bmatrix},$$

and where

$$\tilde{A} = \begin{bmatrix} A & 0 & 0 \\ B_x & A_x & 0 \\ 0 & 0 & A_u \end{bmatrix} \quad \tilde{B} = \begin{bmatrix} B \\ 0 \\ B_u \end{bmatrix} \quad \tilde{C} = \begin{bmatrix} C & 0 & 0 \\ 0 & C_x & 0 \\ 0 & 0 & C_u \end{bmatrix} \tag{5.35}$$

and define the feedback law as

$$u=\tilde{F}\tilde{y}$$

with the feedback parameters:

$$\tilde{F} = [F\ G\ H] \tag{5.36}$$

Optimization Problem 5.4

The Linear Quadratic Output Feedback problem for proportional feedback with frequency weighting is stated as:

$$\min_{\tilde{F}\in\mathscr{S}_{\tilde{F}}} \; J \tag{5.37}$$

with $\mathscr{S}_{\tilde{F}}$ according to definition 5.1 applied to the system $(\tilde{A},\tilde{B},\tilde{C})$ and with J as in definition 5.5, under the constraints $\mathscr{S}_{\tilde{F}} \not\in \phi$ and the system (5.34),(5.35),(5.36).

Lemma 5.2

Optimization Problem 5.4 can be solved using the results of corollary 5.1 applied to system (5.34)–(5.36) if the weighting matrices in (5.28) are chosen as

$$\tilde{Q} = \begin{bmatrix} Q+D_x^T Q_x D_x & D_x^T Q_x C_x & 0 \\ C_x^T Q_x D_x & C_x^T Q_x C_x & 0 \\ 0 & 0 & C_u^T Q_u C_u \end{bmatrix}, \quad \tilde{N} = \begin{bmatrix} 0 \\ 0 \\ C_u^T Q_u D_u \end{bmatrix},$$

$$\tilde{R} = R+D_u^T Q_u D_u \qquad \tilde{X} = \begin{bmatrix} X & 0 & 0 \\ 0 & X_x & 0 \\ 0 & 0 & X_u \end{bmatrix} = \begin{bmatrix} x_0 x_0^T & 0 & 0 \\ 0 & z_{x0} z_{x0}^T & 0 \\ 0 & 0 & z_{u0} z_{u0}^T \end{bmatrix} \tag{5.38}$$

Proof: if the weighting matrices (5.38) are substituted into the performance criterion (5.28) we obtain:

$$\begin{aligned} \tilde{x}^T\tilde{Q}\tilde{x} &= x^TQx + z_x^TC_x^TQ_xC_xz_x + 2z_x^TC_x^TQ_xD_xx + x^TD_x^TQ_xD_xx \\ 2\tilde{x}^T\tilde{N}u &= 2z_u^TC_u^TQ_uD_uu \\ u^T\tilde{R}u &= u^TRu + u^TD_u^TQ_uD_uu \end{aligned}$$

and using (5.32) it follows that

$$\begin{aligned} \tilde{x}^T\tilde{Q}\tilde{x} + 2\tilde{x}^T\tilde{N}u + u^T\tilde{R}u &= x^TQx + z_x^TC_x^TQ_xC_xz_x + 2z_x^TC_x^TQ_xD_xx + \\ &\quad x^TD_x^TQ_xD_xx + 2z_u^TC_u^TQ_uD_uu + u^TRu + u^TD_u^TQ_uD_uu \quad = \\ &x^TQx + (C_xz_x+D_xx)^TQ_x(C_xz_x+D_xx) + \\ &\quad (C_uz_u+D_uu)^TQ_u(C_uz_u+D_uu) + u^TRu \quad = \\ &x^TQx + x_w^TQ_xx_w + u_w^TQ_uu_w + u^TRu \end{aligned}$$

which are exactly the arguments of the performance criterion (5.33). This means that the necessary conditions given in corollary 5.1 indeed apply to Optimization Problem 5.4. □

Observe that the feedback parameters (5.36) define a proportional feedback from the outputs y of system (5.1) but also of the filter outputs x_w and u_w (5.32). The consequence is that the dynamics involved in (5.32) must be added to the controller. Besides the fact that in (5.32) the availability of the states x is assumed, it makes the controller at least as complex as the dynamics of the weighting filters. Indeed, for LQ state feedback as well as for observer LQ based designs (LQG) the controller order increases with the order of the dynamics involved in (5.32). A benefit of LQOF is that we can use the results on decentralized feedback structures (§5.2.1) to design simple feedback laws with frequency weighting.

Corollary 5.2

If the parameterization (5.36) of the feedback law is chosen a priori to satisfy

$$\tilde{F} = [F\ 0\ 0] \tag{5.39}$$

so G=0, H=0, and F to be optimized, then the solution to Optimization Problem 5.4, with $\mathscr{S}_{\tilde{F}}$ replaced with $\mathscr{S}_{\tilde{F}C}$ (definition 5.3) yields a proportional feedback law of system (5.1) with a performance criterion (5.33) with frequency weighting.

Proof: the feedback law involved is $u=\tilde{F}\tilde{y}$ and with (5.34) and (5.39) we obtain $u=Fy$, which is similar to (5.2). □

All results mentioned in this section for proportional output feedback also hold if a dynamic feedback law (§5.2.2) is to be designed.

5.3.4 Selection of decentralized control structures

As mentioned before the control design problem as stated in §4.5 requires a simple controller as well as a high closed–loop performance. The question to be answered therefore is how can simple controllers be designed while maintaining a high performance. First the order of a dynamic feedback law should be chosen as low as possible. Secondly, the structure of the feedback (in the sense of definition 5.3) can be selected in order for the controller to be as simple as possible. With respect to the structure selection we will use two approaches. The first consists of choosing feedback structure on the basis on physical considerations. This will become clear in chapter 6. The second approach is to develop a measure for the relevance of entries of a feedback law for the closed–loop performance.

Here we use the sensitivity of the gradient of the performance index to these entries. This means the second derivative of J to F will be used as indicator. First this function is expressed as calculable function and secondly it is shown how a structure selection procedure can be developed. In the sequel definition 5.4 will be used as the performance criterion.

Suppose that for system (5.1) an LQOF controller F with feedback law (5.2) has been found. The necessary conditions (5.29)–(5.31) are thus satisfied. Now we pose the problem which elements of the feedback parameters F are the least important for the performance criterion. These elements might be put to zero resulting in a decentralized feedback law. A solution to this problem is to evaluate the sensitivity of the function J (5.28) with respect to each of the feedback entries, relative to the other elements.
Using variation calculus the formulae for this sensitivity will be derived. Perturb the feedback with a mxl matrix matrix F_e:

$$F := F + \epsilon F_e$$

with

$F_e(i,j) = 1$, for some $(i,j) \notin \mathscr{S}_0$, $\mathscr{S}_0$ is the set of zero entries (definition 5.3)
$F_e(i,j) = 0$, for all other admissible (i,j)
ϵ small compared to $\|F\|$

Because F has been perturbed, the index J and the solution P of (5.30) will be:

$$J(F+\epsilon F_e) = \mathrm{tr}(XP(F+\epsilon F_e)) \tag{5.40}$$

To calculate (5.40) we need an expression for $P(F+\epsilon F_e)$. Perturbing (5.30) we obtain:

$$[A+B[F+\epsilon F_e]C]^T P(F+\epsilon F_e) + P(F+\epsilon F_e)[A+B[F+\epsilon F_e]C] + Q +$$
$$N[F+\epsilon F_e]C + C^T[F+\epsilon F_e]^T N^T + C^T[F+\epsilon F_e]^T R[F+\epsilon F_e]C = 0$$

Write the Taylor expansion (section 3.2.1) of P(.) as:

$$P(F+\epsilon F_e) = P + \epsilon P_\epsilon + \tfrac{1}{2}\epsilon^2 P_{\epsilon\epsilon} + \ldots$$

then the above Lyapunov equation becomes:

$$[A+B[F+\epsilon F_e]C]^T[P+\epsilon P_\epsilon+\tfrac{1}{2}\epsilon^2 P_{\epsilon\epsilon}+\ldots] + [P+\epsilon P_\epsilon+\tfrac{1}{2}\epsilon^2 P_{\epsilon\epsilon}+..][A+B[F+\epsilon F_e]C]$$
$$+ Q + N[F+\epsilon F_e]C + C^T[F+\epsilon F_e]^T N^T + C^T[F+\epsilon F_e]^T R[F+\epsilon F_e]C = 0$$

Taking all terms together for ϵ=0, equation (5.30) is obtained. Taking all terms together proportional to ϵ we get:

$$[A+BFC]P_\epsilon + P_\epsilon[A+BFC] +$$
$$C^T F_e^T[B^T P+N^T+RFC] + [PB+N+C^T F^T R]F_e C = 0 \tag{5.41}$$

and for the second order variations ϵ^2 we obtain:

$$[A+BFC]P_{\epsilon\epsilon} + P_{\epsilon\epsilon}[A+BFC] + C^T F_e^T B^T P_\epsilon + B^T P_\epsilon F_e C + C^T F_e^T R F_e C = 0 \tag{5.42}$$

Now we go back to equation (5.40). Substitute for X the expression (5.31) and expand J in a Taylor series:

$$J(F+\epsilon F_e) = \mathrm{tr}\Big\{[-\bar{A}S-S\bar{A}^T][P+\epsilon P_\epsilon+\tfrac{1}{2}\epsilon^2 P_{\epsilon\epsilon}+\ldots]\Big\} = J(F) + \epsilon J_\epsilon+\tfrac{1}{2}\epsilon^2 J_{\epsilon\epsilon}+\ldots \tag{5.43}$$

with $\bar{A} = A+BFC$.
Equating corresponding powers of ϵ we obtain:

$$\begin{aligned} J(F) &= \mathrm{tr}\Big\{[-\bar{A}S-S\bar{A}^T]P\Big\} \\ J_\epsilon(F_e) &= \mathrm{tr}\Big\{[-\bar{A}S-S\bar{A}^T]P_\epsilon\Big\} \\ J_{\epsilon\epsilon}(F_e) &= \mathrm{tr}\Big\{[-\bar{A}S-S\bar{A}^T]P_{\epsilon\epsilon}\Big\} \end{aligned} \tag{5.44}$$

These equations will be worked out using some properties of the trace (tr) operator for square matrices: tr(A+B)=tr(A)+tr(B), tr(AB)=tr(BA), $\mathrm{tr}(A)=\mathrm{tr}(A^T)$:

$$J_\epsilon(F_e) = \mathrm{tr}\Big\{[-\bar{A}S-S\bar{A}^T]P_\epsilon\Big\} = \mathrm{tr}\Big\{[-\bar{A}^T P_\epsilon - P_\epsilon\bar{A}]S\Big\}$$

and with (5.41) we get:

$$J_\epsilon(F_e) = \mathrm{tr}\Big\{C^T F_e^T[B^T P+N^T+RFC]S + [PB+N+C^T F^T R]F_e CS\Big\}$$

and with the trace relations:

$$J_\epsilon(F_e) = 2\mathrm{tr}\Big\{[B^T P+N^T+RFC]SC^T F_e^T\Big\}$$

Note that for the optimal solution $J_\epsilon(F_e)$=0, resulting in (5.29).
For the second derivative we obtain for (5.44):

$$J_{\epsilon\epsilon}(F_e) = \mathrm{tr}\Big\{[-\bar{A}S-S\bar{A}^T]P_{\epsilon\epsilon}\Big\} = \mathrm{tr}\Big\{[-\bar{A}^T P_{\epsilon\epsilon} - \bar{A}P_{\epsilon\epsilon}]S\Big\}$$

and with (5.42):

$$J_{\epsilon\epsilon}(F_e) = \mathrm{tr}\Big\{[C^T F_e^T B^T P_\epsilon + B^T P_\epsilon F_e C + C^T F_e^T R F_e C]S\Big\}$$

or

$$J_{\epsilon\epsilon}(F_e) = 2\mathrm{tr}\Big\{B^T P_\epsilon S C^T F_e^T\Big\} + \mathrm{tr}\Big\{RF_e CSC^T F_e^T\Big\} \tag{5.45}$$

This last equation gives an expression for the sensitivity of the performance index for variations in the controller parameters F, about the optimal value.

The **procedure to select a decentralized feedback structure** is as follows:

1. Optimize the feedback parameters F, with zero entries $(i,j)\in\mathscr{S}_0$. Then P and S are known.
2. Calculate for all admissible entries $(i,j)\notin\mathscr{S}_0$ the value of $\epsilon^2 J_{\epsilon\epsilon}/2$. The parameter ϵ is chosen equal to $-F(i,j)$. This means that the value of the perturbed feedback law is zero at (i,j). The term $\epsilon^2 J_{\epsilon\epsilon}/2$ is exactly equal to the third term in the Taylor series of the index J (5.43). Calculate P_ϵ with (5.41), and $J_{\epsilon\epsilon}$ with (5.45).
3. Set F(i,j)=0 for (i,j) for which $\epsilon^2 J_{\epsilon\epsilon}$ is the smallest and thus enlarge the set $\mathscr{S}_0$.
4. Go to 1, unless the set $\mathscr{S}_0$ has (ml−1) elements or unless the increase of the performance criterion is to large compared to the previous optimization.

Note that because of step 2 the value of ϵ is not small. Because the performance criterion is a nonlinear function of the feedback law, the quadratic approximation given above will differ substantially from the nonlinear behavior of the performance index with respect to the feedback entries. Nevertheless the procedure might give reasonable results, especially if the value $|F(i,j)|$ is small for some i,j. Note also that the procedure can be also applied for dynamic feedback.
In chapter 6 the procedure will be applied to the wind turbine system.

5.3.5 Optimal multi–model robustness

The LQOF problems described so far address the control design of proportional or dynamic feedback laws for a linear time–invariant system. The robustness of the resulting closed–loop system with respect to perturbations of the model has not been investigated yet. Especially, for the wind turbine system large variations of model parameters occur for instance due to changing aerodynamic operating conditions. The analysis of the closed–loop system under model perturbations will be described in section 5.4. In this section we will consider the **robustness synthesis problem** how to design a feedback law such that a satisfactory performance in multiple operating conditions is obtained.

Suppose we have r linear time–invariant models:

$$\dot{x}_i = A_i x_i + B_i u_i \qquad x_i(0)=x_{i0} \qquad i = 1,\ldots,r \tag{5.46}$$
$$y_i = C_i x_i$$

with $\dim(x_i)=n_i$, $\dim(u_i)=m$, $\dim(y_i)=l$.

The multi–model robustness problem can be formulated as finding <u>one</u> controller F such that by the application of the output feedback law

$$u_i = F y_i \tag{5.47}$$

<u>all</u> r systems (5.46) are stabilized and meet some form of performance requirement.

Several design techniques have been developed which use this concept: based on multi–performance criteria optimization [Kreisselmeier and Steinhauser, 1983] and pole placement techniques [Ackermann, 1983; Hartmann et al., 1986]. Here we will formulate the multi–model LQOF design method [Looze, 1983; Mäkilä and Toivonen, 1987].

Definition 5.6. Define the <u>multi–model performance criterion</u> as :

$$J_{tot} = \sum_{i=1}^{r} w_i J_i \tag{5.48}$$

with w_i weighting scalars, and where J_i is the performance criterion for each model:

$$J_i = \int^{\infty} (x_i^T Q_i x_i + u_i^T R_i u_i)dt, \qquad i=1,\ldots,r \tag{5.49}$$

with $Q_i \geq 0$, $R_i > 0$, i=1,...,r.

<u>Optimization Problem 5.5</u>

The Multi–Model Linear Quadratic Output Feedback problem for proportional feedback is stated as:

$$\min_{F\in\mathscr{S}_F} J_{tot} \tag{5.50}$$

with $\mathscr{S}_F$ and J_{tot} according to definitions 5.1 (applied to all systems i=1,.,r) and 5.6 respectively, under the constraints $\mathscr{S}_F \notin \phi$ and the systems (5.46),(5.47).

A solution for this minimization problem can be found with the same numerical algorithm as used for the standard LQOF problem (§5.2.1, theorem 5.1, remark 1), in the following way. The algorithm is rewritten such that the solutions P_i and S_i of the Lyapunov equations (5.7) and (5.8) are calculated for each system (A_i,B_i,C_i) with the feedback law (5.47). Then the index J_{tot} according to (5.48),(5.49) can be calculated with (5.10) and the gradient $\partial J_{tot}/\partial F = \sum_{i=1}^{r} w_i \partial J_i/\partial F$ can be calculated with (5.12). These values are used in the search algorithm, see also [Mäkilä and Toivonen, 1987].

The LQOF multi–model technique described here offers several advantages:

- all results for single–model LQOF problems (§5.2.1–5.3.4) are applicable also in the multi–model case,
- relative importance of operating conditions can be expressed with the weighting scalars w_i. For instance suppose the system is in point 1 most of the time and only sometimes in point 2. Then we choose $w_1 >> w_2$. The solution we get gives a good performance in 1 and at least guaranteed stability in point 2!
- it is possible to define some of the models as having less sensors or actuators by defining zero rows and columns in C_i and B_i respectively. If (A_i,B_i,C_i) keeps stabilizable for all r models, a solution is found which is robust for sensor or actuator failures (integrity). The definition (5.46) of the systems also allows different orders of the models. This can be used for instance for obtaining robustness against parasitic dynamics.

The method has some consequences:

- for the algorithm an initial stabilizing multi–model feedback is needed. For most problems however a low bandwidth stabilizing design is available and can be used as initial feedback law. The LQOF multi–model design is then used to tune the feedback parameters such that a high performance is achieved,
- the numerical algorithm involved is time–consuming. The multi–model extension gives a factor r more calculation time, compared to the standard LQOF problem of theorem 5.1.

Obviously, the LQOF multi–model approach only gives guaranteed stability and performance for the models contained in the optimization problem. In other words, if the feedback parameters have been optimized for some models there may be a model close to these models which is closed–loop unstable. To be able to detect such situations robustness analysis of the closed–loop systems is necessary.

5.4 PERTURBATION ROBUSTNESS ANALYSIS

Using the results of sections 5.2 and 5.3 it is possible to design stabilizing controllers for one or for multiple systems. However, the models used in the control system design procedure may differ from the real system. In the case of the wind turbine system several model variations, parameter perturbations and other model uncertainties have been considered (§4.3). In order to meet the robustness requirement mentioned in section 4.5 it is necessary to investigate the performance of the closed–loop system under model perturbations. This is called *perturbation robustness analysis*. This analysis can be done in various ways as have been described in section 4.3.1.
In this section the perturbation robustness analysis problem for norm–bounded uncertainty models as used in section 4.3 will be considered. The most relevant property to investigate is whether closed–loop stability is preserved under such model perturbations. To analyze this the Structured Singular Value [Doyle, 1982] will be used as indicator.

Consider the system with uncertainty inputs w and outputs v given by the state space model (4.17), with D=0:

$$\begin{aligned} \dot{x} &= Ax + Bu + W_1 w \\ y &= Cx + W_2 w \\ v &= V_1 x + V_2 u \end{aligned} \tag{5.51}$$

For the wind turbine system D=0 is non–restrictive.
Assume that a stabilizing proportional output feedback law (5.2) has been designed (figure 5.4a):

$$u = Fy$$

Then substitution of (5.2) into (5.51) gives the closed–loop system:

$$\begin{aligned} \dot{x} &= (A+BFC)x + (W_1+BFW_2)w \\ v &= (V_1+V_2FC)x + V_2FW_2 w \end{aligned} \tag{5.52}$$

The transfer function from w to v is called the interconnection matrix M(s):

$$M(s) = (V_1+V_2FC)[sI-(A+BFC)]^{-1}(W_1+BFW_2) + V_2FW_2 \tag{5.53}$$

All uncertainties enter the closed–loop system M(s) via the relation $w=\Delta(s)v$ (4.19), which can be seen as a dynamic feedback of (5.53), see figure 5.4b.

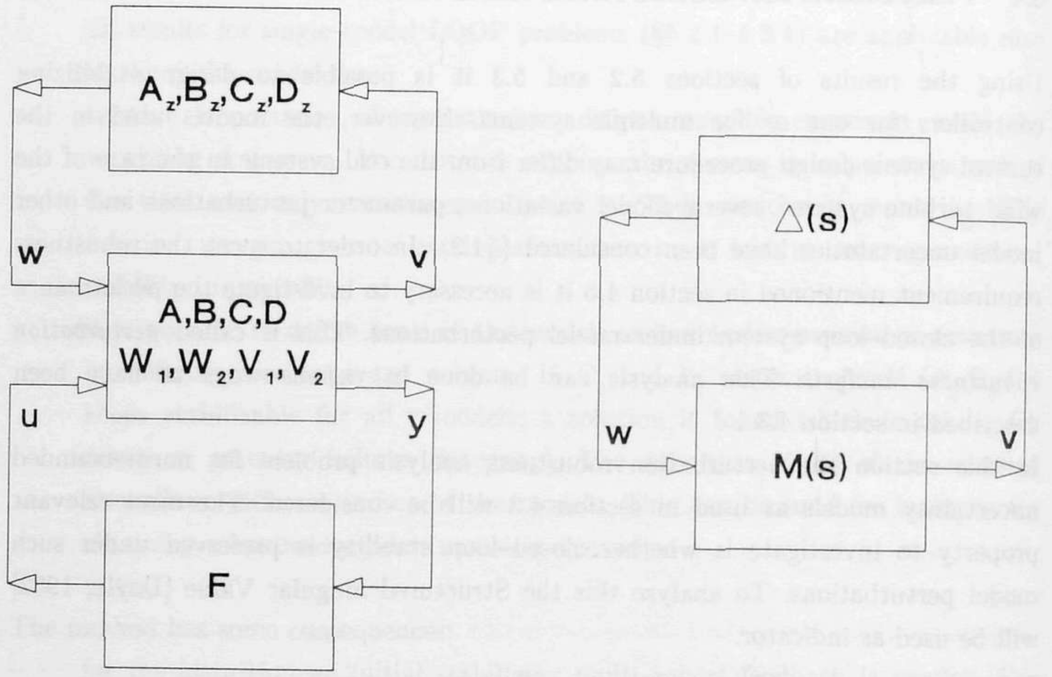

a. state space representation b. transfer function representation

Figure 5.4 General interconnection structure.

The problem of scaling as discussed in section 4.3.6 consists of pre or post multiplying M(s) with appropriate scaling matrices, either as constant matrices or as dynamic systems. In the latter case this is most easily done at each frequency separately (see also §4.3.6). In the sequel it is assumed that $\Delta(s)$ has been scaled (to unity) and that M(s) contains all necessary scalings. We will denote both $\Delta(s)$ and M(s) with s as argument meaning that both functions may be known as transfer functions or as frequency response functions at each frequency $\omega\epsilon[0,\infty)$.
In the general case where F is a dynamic output feedback, the matrices in (5.52) are simply interchanged with their extended versions $(\tilde{A},\tilde{B},\tilde{C},\tilde{F})$ as given in (5.16),(5.17).

The (scaled) uncertainty matrix $\Delta(s)$ is defined as follows.

Definition 5.7. The set $\mathscr{S}_\Delta$ of structured norm–bounded uncertainties is defined as all transfer function matrices $\Delta(s)$ satisfying

$$\Delta(s) = \text{diag}[\Delta_1(s),\Delta_2(s),...,\Delta_k(s)], \qquad \Delta(s)\epsilon\mathbb{C}^{kxk} \tag{5.54}$$

with

$$\bar{\sigma}(\Delta_i(j\omega))\leq 1, \qquad i=1,...,k, \qquad \omega\epsilon[0,\infty) \qquad \Delta_i(s)\epsilon\mathbb{C}^{1x1}$$

with $\bar{\sigma}(.)$ denoting the maximum singular value.

Note that the uncertainty matrix is chosen according to the structure obtained in section 4.3.6. The matrix $\Delta(s)$ contains only 1x1 blocks at the k(=10) diagonal entries. For the notation this is slightly more simple, but the more general case of larger $\Delta_i(s)$'s can be handled also.
Because in the uncertainty description (5.54) the only information of $\Delta(s)$ used is that $\sigma(\Delta_i(j\omega))<1$, phase information of $\Delta_i(s)$ is discarded as well as directionality of $\Delta_i(s)$ if $\Delta_i(s)$ is a matrix function. If phase information is available, as in some of the wind turbine uncertainty models, the analysis using (5.54) might give conservative results. Due to the fact that (5.54) has already some structure (i.e. diagonal) the directionality of the whole kxk $\Delta(s)$ can be taken into account using the structured singular value.

Theorem 5.2: Structured Singular Value Analysis Test
For the interconnection structure given by figure 5.4, the closed–loop system represented by the interconnection matrix M(s) (5.53) remains stable under the structured perturbations defined by (5.54) if and only if

$$\det(I–M(j\omega)\Delta(j\omega)) \neq 0 \qquad \forall\ \Delta\epsilon\mathscr{S}_\Delta,\ 0\leq\omega<\infty \tag{5.55}$$

Furthermore, this condition is equivalent to:

$$\mu(M(j\omega)) < 1, \quad 0\leq\omega<\infty \tag{5.56}$$

where μ is called the Structure Singular Value (SSV).
Proof: for the proof of the general stability result (5.55) see for example [Doyle and Stein, 1981]. See [Doyle, 1982] for the connection with μ. □

From this theorem it follows that the scalar value μ defines a robustness margin for the system M for the structured perturbations Δ. If (5.56) is violated, there exists a $\Delta\epsilon\mathscr{S}_\Delta$ such that the system is unstable.
A similar test can be made for robust performance. However, as mentioned before, here we restrict our attention primarily to stability as the most important robustness feature.

The calculation of the SSV μ is rather comprehensive. Checking condition (5.55) is possible by simulation of all admissible Δ's. Obviously, this would take much computer time. Fortunately, Doyle [1982] proved the following theorem.

Theorem 5.3
For the SSV defined by theorem 5.2 the following holds:

$$\sup_{U \in \mathcal{U}} \rho(MU) \leq \mu(M) \leq \inf_{D \in \mathcal{D}} \overline{\sigma}(DMD^{-1}) \qquad 0 \leq \omega < \infty \qquad (5.57)$$

with ρ the spectral radius of a matrix (max eigenvalue) and $\overline{\sigma}$ the maximum singular value and

$$\mathcal{U} = \{\mathrm{diag}(U_1, U_2, \ldots) \mid U_i^* U_i = I\}$$

$$\mathcal{D} = \{\mathrm{diag}(d_1 I, d_2 I, \ldots) \mid d_i \in \mathbb{R}^+\}$$

Moreover, if $k \leq 3$ the upper bound in (5.57) is satisfied with equality.
Proof: see [Doyle, 1982]. □

Because in our case we have only 1x1 perturbations blocks, we obtain U=I and $D = \mathrm{diag}(d_1, d_2, \ldots)$, $d_i \in \mathbb{R}^+$. It is stated in [Doyle, 1982] that if $k > 3$ the upper bound in (5.57) is close to μ. Theorem 5.3 gives a way to (approximately) compute μ: a gradient search for a diagonal matrix D with k elements, at each frequency. More information about numerical algorithms to compute μ is given in [Fan and Tits, 1986]. The problem is hence reduced to an optimal diagonal scaling problem. Choosing D=I a priori gives the following result.

Corollary 5.3: Singular Value Analysis Test
The closed–loop system represented by the interconnection matrix M(s) remains stable under the structured perturbations given by (5.54) if

$$\overline{\sigma}(M(j\omega)) < 1, \quad 0 \leq \omega < \infty \qquad (5.58)$$

If (5.58) does not hold, there may be uncertainties $\Delta \in \mathcal{S}_\Delta$ for which the system is still stable.
Proof: follows directly from the combination of (5.56) and (5.57). □

Corollary 5.3 gives the well–known singular value robustness analysis test. For structured (multivariable) uncertainties this test gives in general conservative results because the uncertainty set for which the perturbed system is stable (test (5.58) holds) also contains non–diagonal uncertainties $\Delta(s)$ in (5.54). In the case of

the wind turbine system this means that uncertainties modelled for instance in the pitch angle input also are assumed to be present in the other inputs and outputs. Obviously, this would result in a very conservative analysis. Nevertheless, (5.58) is very easy to compute and if the singular value test (5.58) holds for certain perturbations there is no need to compute μ for those perturbations. Moreover, for one perturbation Δ_i test (5.58) is not conservative.

Robustness analysis procedure

Step 1: For the M matrix (5.53) and the associated with the kxk uncertainty matrix defined by (5.54) equation (5.58) is tested. If this test succeeds the system is robustly stable and we can stop the analysis. If (5.58) fails we do not know anything yet about closed–loop stability.

Step 2: Test (5.58) is applied for each individual perturbation Δ_i (k times). This may give information about the 'loop' which has the smallest stability margin. If any test fails we are sure that the complete system can be unstable. A controller redesign is then necessary and the information about the specific Δ_i which is the destabilizing one can be of great help.

Step 3: The structured singular value μ is computed for clusters of perturbations and/or for all Δ_i's simultaneously. The reason to analyze also clusters of Δ_i's is to be able to trace certain small robustness margins.

The application of this perturbation robustness procedure gives insight into the least robust parts of a control system design. This knowledge may be used to reformulate the nominal model or to change the design parameters (i.e. in the case of LQOF: structure, order, Q, R, X). A new feedback law can then be calculated and analyzed again. This iterative process will be applied to the wind turbine system in the next chapter.

6. ROBUST CONTROL DESIGN FOR THE WIND ENERGY CONVERSION SYSTEM

6.1 INTRODUCTION

The application of the robust control system design procedure to the wind energy conversion system should meet the stated requirements (§4.5). Summarizing the requirements: we want to minimize speed and power fluctuations as well as mechanical loads, with a low control effort, taking into consideration disturbances from the wind and from the grid. This must be realized with a simple robust controller.

Compromising control quality (i.e. speed, power and mechanical load variations) and control effort (pitch and delay angle, field voltage) fits very well into the general LQ framework. The LQOF design parameters (Q,R,X, structure and order) can be used to affect the desired closed–loop properties. Because speed and power (current) are states in the nominal design model, the corresponding weighting elements can be used interpretable. This is also the case for the control effort (inputs). More difficult is the question how to address the requirements on the mechanical loads. Because the fatigue loads are primarily of interest, a high damping of the structural dynamics is tried to achieve with the control design. But large instantaneously variations of the torque are not wanted either. With simulations the behaviour of the mechanical torque in the secondary axis will be analyzed during all design stages.

Before a design will be done, the global feedback structure must be chosen first. From the requirements it follows that three integrating actions are necessary: one on the measured speed ω_{gm}, one on the direct current i_{dc} and the third integrator is placed on the input variable α_r (see §4.5). Further a design is made for full load conditions only and all three inputs are used. The resulting global feedback structure is given in figure 6.1.

The state dimension of the model augmented with the integrators is 13 and the system has three inputs (β_r,u_{Fr},α_r) and five outputs (ω_{gm},i_{dc},$\int\omega_{gm}$,$\int i_{dc}$,$\int\alpha_r$). The rest of this chapter is to devoted the design of a stabilizing controller F, such that all requirements are met. The procedure is to design a nominal feedback law for v=16 m/s first (§6.2). Next the multi–model robustification procedure is carried out in section 6.3. Finally, the perturbation robustness is analyzed (§6.4).

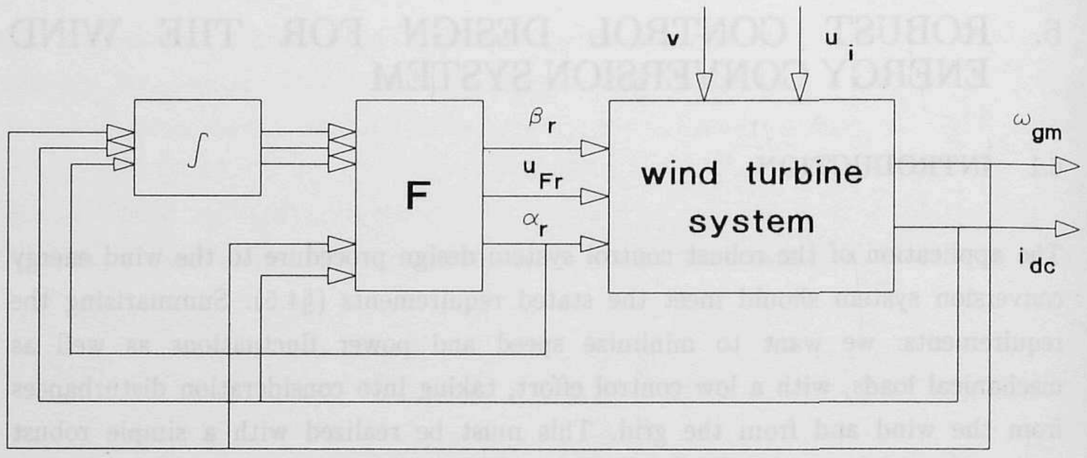

Figure 6.1 Global feedback structure of the system.

6.2 NOMINAL DESIGN

The linear model for the operating point v=16 m/s is given in Appendix A.5. In order to obtain an upper bound for the performance achievable an LQ state feedback (LQR) is designed first (§6.2.1). Based on the development of the performance index (choosing weighting matrices) with state feedback, an LQ Output Feedback (LQOF) design is made, first with a proportional feedback law (§6.2.2). To obtain a better performance a dynamic LQOF is designed subsequently (§6.2.3).

6.2.1 LQ state feedback

For the augmented system with order 13 and 3 inputs an LQ state feedback law can be designed by manipulating matrices Q and R until desirable results are obtained. This is carried out by choosing Q and R and simulation of time and frequency responses. Previous results on LQ state feedback are already published, see [Steinbuch, 1987]. Here we will be very short about this stage.
Note that each diagonal element of matrix Q weights the deviations of the corresponding state. For instance increasing entry Q(5,5) weights deviations of the measured speed ω_{gm} more resulting in a tighter speed control. The final weighting matrices Q and R are given in Appendix A.6. The LQ feedback law obtained has 3x13=39 parameters (see Appendix A.6).

The open–loop and closed–loop eigenvalues are also shown in Appendix A.6. The torsional modes are well damped. The poles introduced by the dynamics of the electrical system are very sensitive to feedback and one pole has become very fast.

Simulations

The step responses of the uncontrolled and LQ controlled wind turbine system are given for two disturbances: wind speed and grid voltage. In figure 6.2 the step responses of the system are given at a unit step increase of the wind speed.

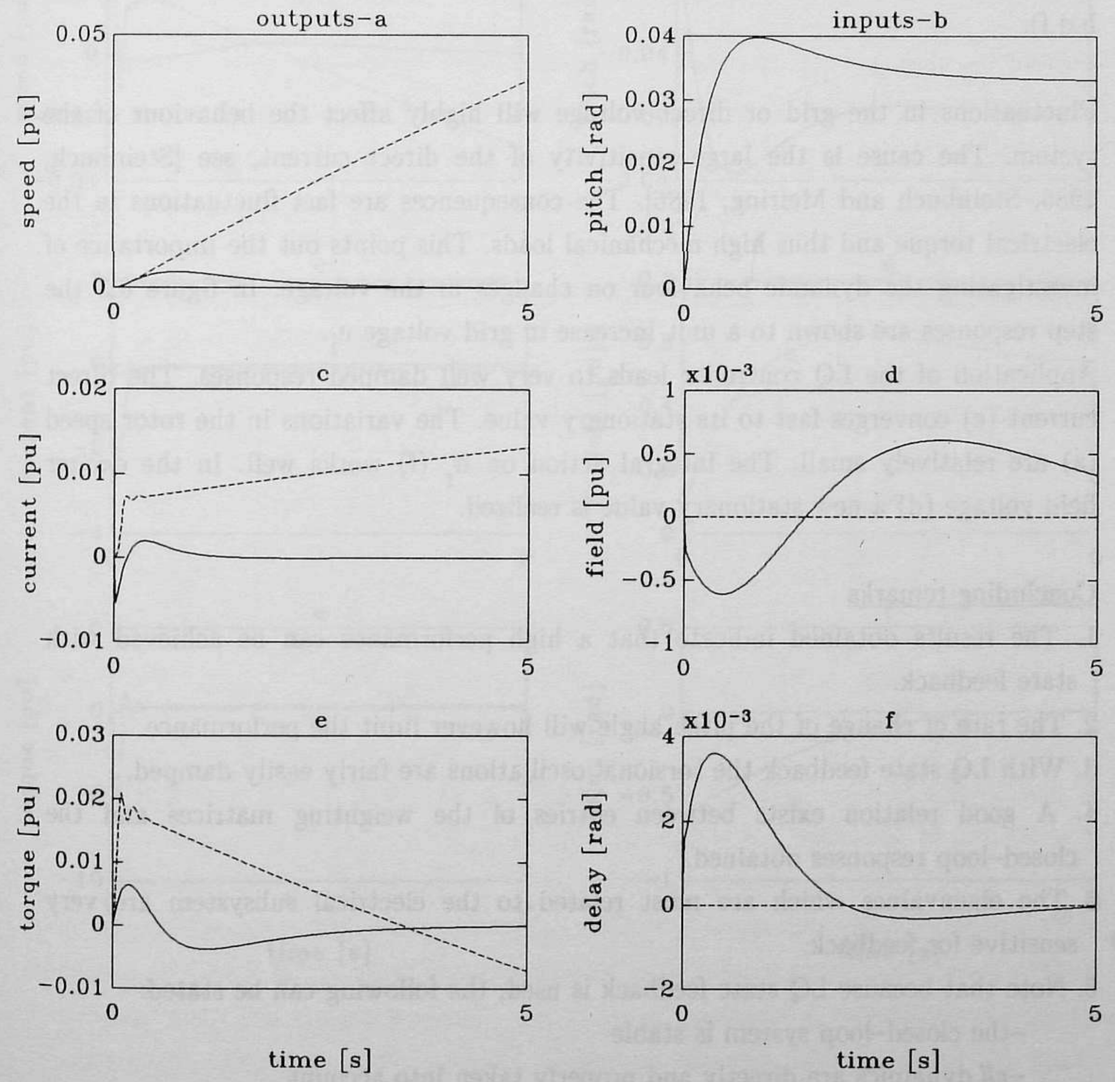

Figure 6.2 Step responses of the wind turbine at a step in wind speed, uncontrolled (– – –) and with LQ state feedback(——).

Although not realistic, a step change in wind speed with small amplitude (1 m/s) is very convenient for an investigation of the dynamic behaviour. In the uncontrolled case (– – –) the system reacts with a relatively slowly increasing measured generator speed (a) and a rather fast reaction of the electrical current (c) and mechanical torque (e). The latter shows the excited torsional oscillations. Application of the LQ controller reduces the variations in the speed considerably. The power (current) fluctuations are kept very small. Note that at the first instant, the current is decreased by the feedback. This is in accordance with the observation that a relation like $i_{dc} \equiv T_e \equiv -d\xi/dt$ gives more damping in the torsional mode, see also equation (4.5). The inputs are plotted also (figure 6.2 b,d,f).

Fluctuations in the grid or direct voltage will highly affect the behaviour of the system. The cause is the large sensitivity of the direct current, see [Steinbuch, 1986, Steinbuch and Meiring, 1986]. The consequences are fast fluctuations in the electrical torque and thus high mechanical loads. This points out the importance of investigating the dynamic behaviour on changes in the voltage. In figure 6.3 the step responses are shown to a unit increase in grid voltage u_i.
Application of the LQ controller leads to very well damped responses. The direct current (c) converges fast to its stationary value. The variations in the rotor speed (a) are relatively small. The integral action on α_r (f) works well. In the exciter field voltage (d) a new stationary value is realized.

<u>Concluding remarks</u>

1. The results obtained indicate that a high performance can be achieved with state feedback.
2. The rate of change of the pitch angle will however limit the performance.
3. With LQ state feedback the torsional oscillations are fairly easily damped.
4. A good relation exists between entries of the weighting matrices and the closed–loop responses obtained.
5 The eigenvalues which are most related to the electrical subsystem are very sensitive for feedback.
6. Note that because LQ state feedback is used, the following can be stated:
   –the closed–loop system is stable
   –*all* dynamics are directly and properly taken into account
   –there exists *no* controller of the same structure which gives the same or better closed–loop performance (in the sense of the performance index), without increasing the control effort.

The last remark indicates that indeed the maximum achievable performance has been obtained. However, serious constraints occur when an output feedback design has to be made.

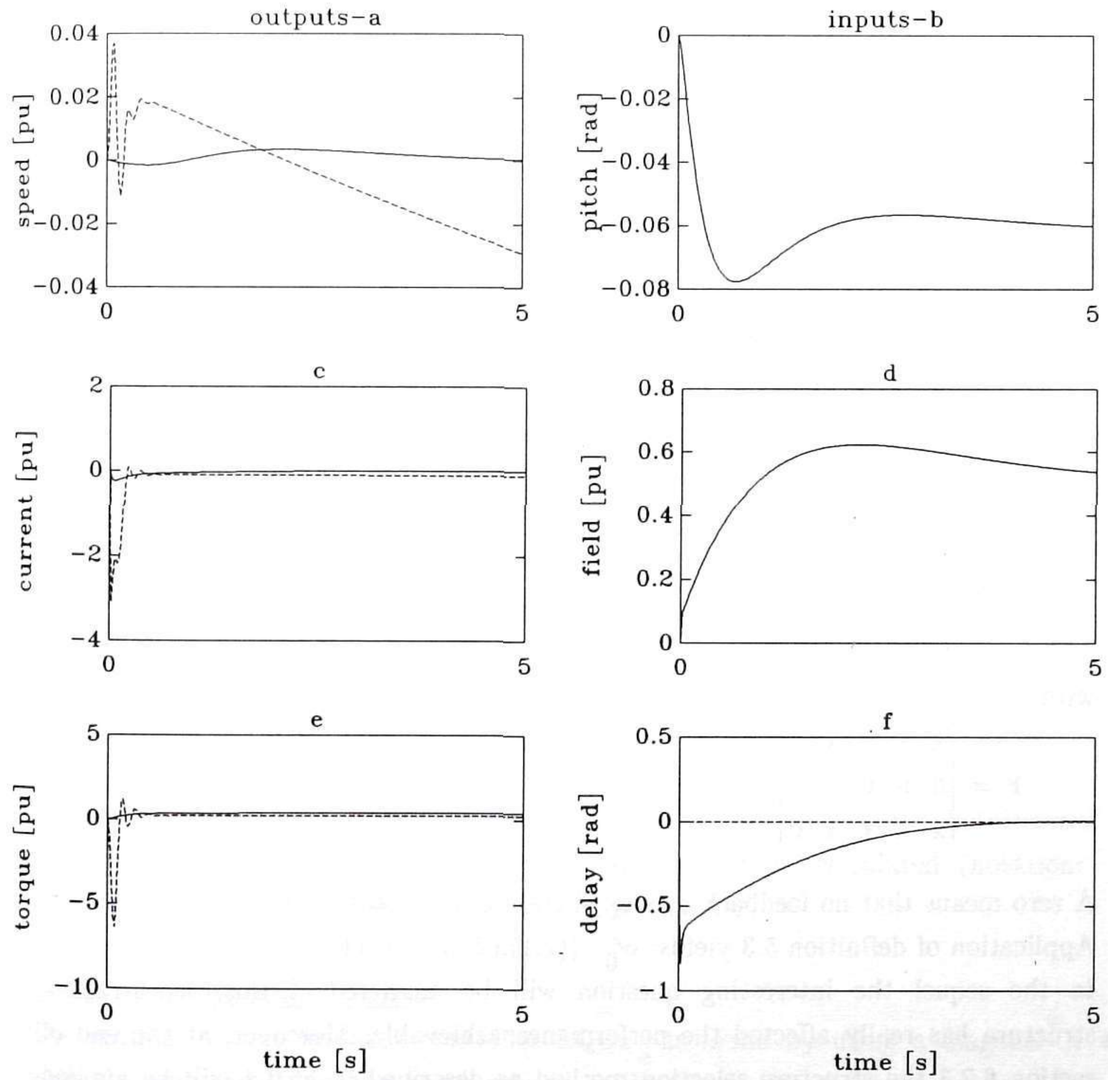

Figure 6.3 Step responses of the wind turbine at a step in grid voltage, uncontrolled (– – –) and with LQ state feedback(——).

6.2.2 LQ output feedback

Stimulated by the good results obtained with LQ state feedback, an LQ output feedback will be designed. In applying LQOF several design parameters are available. Apart from Q and R, the disturbance representation X must be chosen as well as feedback structure and dynamic order. In this section we first try to find the most simple feedback controller for the system augmented with the three integral actions. Hence, an LQOF multivariable PI controller will be designed first.

On the controller's internal structure several remarks can be made. First, both electrical inputs u_{Fr} and α_r are in a way redundant. The input α_r is very fast, but should be zero at low frequencies. On the other hand, the field voltage does consume energy in its usage and is relatively slow. Therefore, at low frequencies the field voltage can be used, while at high frequencies the delay angle is better. A simple solution is to constrain the feedback such that a cascaded structure is obtained: only the integral actions on $\int i_{dc}$ and $\int \alpha_r$ are fed back to u_{Fr}. To obtain a clear steady state situation, the output $\int \alpha_r$ is not fed back to β_r nor to α_r.
The internal controller structure is summarized below.

$$\begin{bmatrix} \beta_r \\ u_{Fr} \\ \alpha_r \end{bmatrix} = F \begin{bmatrix} \omega_{gm} \\ i_{dc} \\ \int \omega_{gm} \\ \int i_{dc} \\ \int \alpha_r \end{bmatrix} \qquad (6.1)$$

with

$$F = \begin{bmatrix} x & x & x & x & 0 \\ 0 & 0 & 0 & x & x \\ x & x & x & x & 0 \end{bmatrix}$$

A zero means that no feedback exists, whereas a 'x' means a path to be optimized. Application of definition 5.3 yields: $\mathscr{S}_0=\{(2,1),(2,2),(2,3),(1,5),(3,5)\}$.
In the sequel the interesting question will be answered if this decentralized structure has really affected the performance achievable. Moreover, at the end of section 6.2.3 the structure selection method as described in §5.3.4 will be applied to investigate further reductions.

The design parameters Q and R are chosen the same as for state feedback. Nevertheless, it might be necessary that due to the output feedback restriction other values of Q and R are necessary.

The choice of the matrix X must be done with care. In fact, entries of X may have a large influence on the resulting feedback. In literature several suggestions are made for this choice, for instance as unity matrix with rank n [Levine and Athans, 1970]. In [Steinbuch and Bosgra, 1988] another choice is made namely X=Q. The experience is that entries in X have similar effects as corresponding entries in Q. Another possibility is to use knowledge about the disturbances affecting the system. For instance choosing $X=EE^T$ with E the disturbance vector from (4.15).

However, in our case it turned out that the idea of using an identity matrix with rank n yielded the best results. To do this the matrix must be scaled, which is done by measurement of the variations of all state variables at representative excitations. In this case the closed–loop step responses of the system with state feedback are chosen, at both a wind speed (figure 6.2) and a grid voltage disturbance (figure 6.3). Because matrix X is a squared measure all maximum variations are squared. The results are collected in table 6.1.

state:	β	ξ	$d\xi/dt$	ω_g	ω_{gm}	u_F	i_{dc}	i_F	i_D	i_Q	$\int\omega_{gm}$	$\int i_{dc}$	$\int\alpha_r$
dist/lqof													
1 : v [*10^{-6}]	2500	1	400	25000	25	100	1	25	0.1	1	100	1	25
2 : u_i [*100]	1	1	100	100	0.01	100	1	25	0.25	4	0.04	1	100
3 : compromise	500	1	200	1000	1	100	1	25	0.2	2	1	1	50

Table 6.1 Squared deviations of the states at wind speed and voltage excitations.

The third row is a compromise disturbance matrix X. For these three disturbance representations X, output feedback controllers have been calculated (notation: $LQOF_1$, $LQOF_2$, $LQOF_3$ respectively, see Appendix A.7).

Comparison with state feedback

The optimal output feedback controller $LQOF_3$ is found by using a diagonal X with the numbers from the third row in table 6.1 on its diagonal entries. As mentioned both the Q and R matrix were chosen the same as with state feedback (design LQR, Appendix A.6). A small difference was the large usage of the field voltage u_F resulting with output feedback. The Q(6,6) entry has been enlarged

from 10 to 100, in order to decrease these variations.
To compare it with state feedback simulations are carried out with $LQOF_3$ and LQR first. For a wind speed variation the time responses are given in figure 6.4.

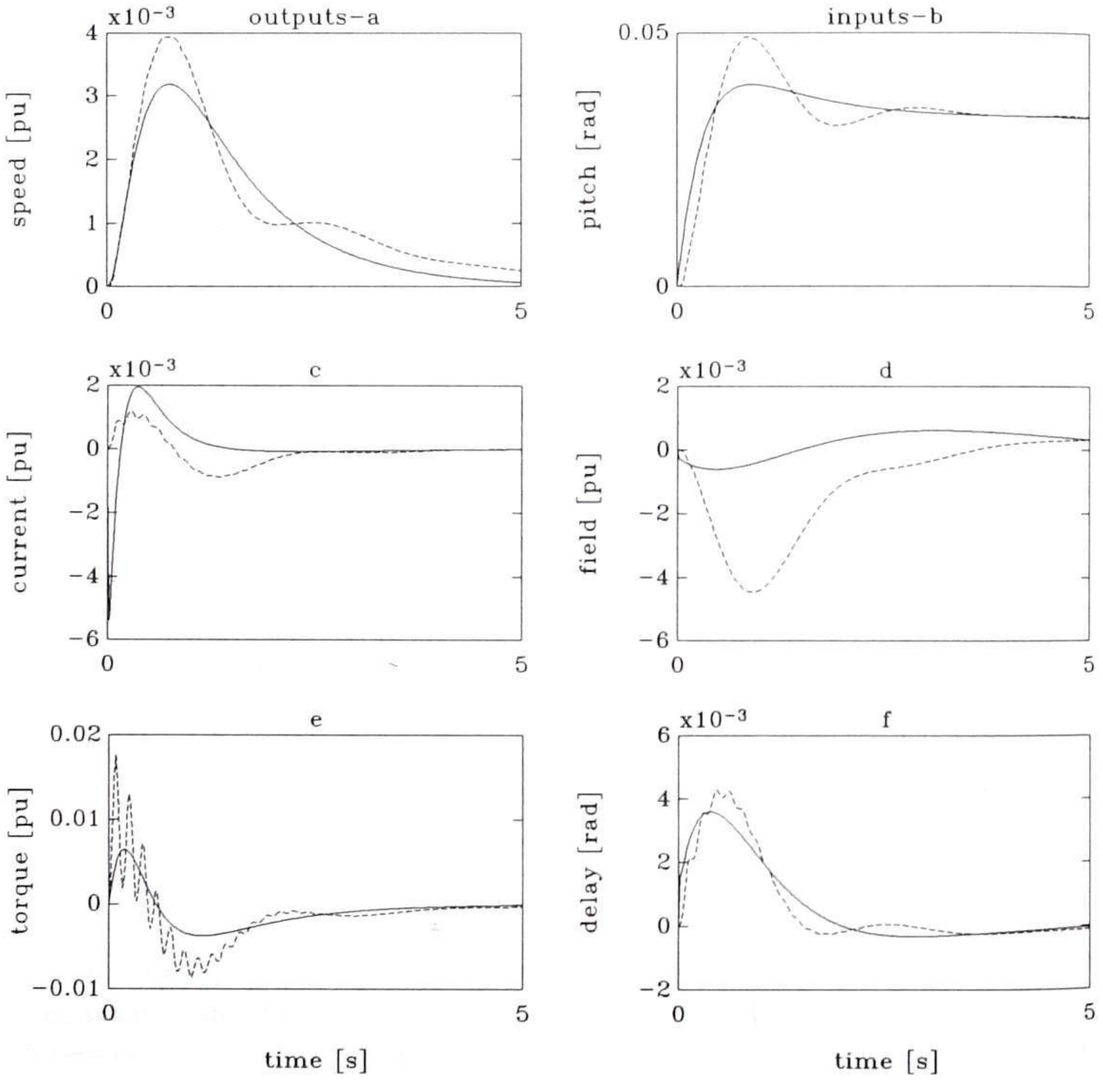

Figure 6.4 Step responses of the wind turbine at a step in wind speed with LQ state feedback(——) and output feedback $LQOF_3$(– – –).

The speed (a) and current (c) variations are comparable for both controllers. With LQOF they are less well–damped. The input energy needed is also nearly the same. However, a major drawback is that the torsional oscillations (e) are much less damped as in the uncontrolled case (compare this result with the CCC method of §4.4.3). Redesigning the controller with incrementing Q(3,3) and/or X(3,3)

corresponding to state $d\xi/dt$ indeed resulted in a better damping, but all other variables were then badly controlled. For this to be solved, more dynamics have to be added to the feedback (§6.2.3).

For the grid voltage disturbance (figure 6.5) similar results are obtained. Only the speed (a) is slightly less well–controlled and the pitch angle (b) is used more.

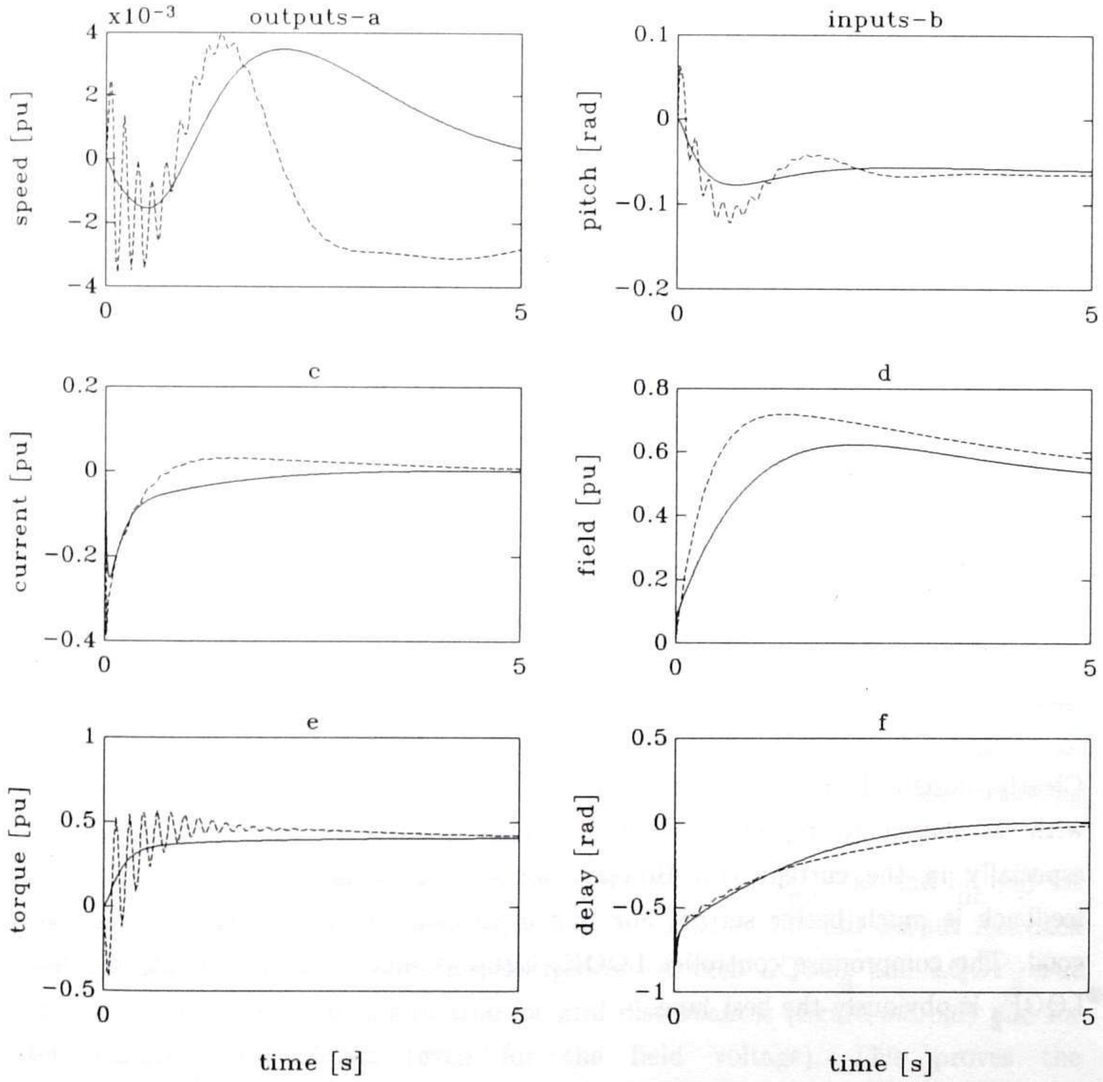

Figure 6.5 Step responses of the wind turbine at a step in grid voltage with LQ state feedback(——) and output feedback $LQOF_3$(– – –).

Design for disturbances

To show the effect of choice of the disturbance representation X, the choices for X from table 6.1 are used for controller design and compared. In figure 6.6 the wind speed step responses of ω_{gm} and i_{dc} are given for the three feedback laws: $LQOF_3$ (compromise between v and u_i), $LQOF_1$ (designed for v) and $LQOF_2$(designed for u_i).

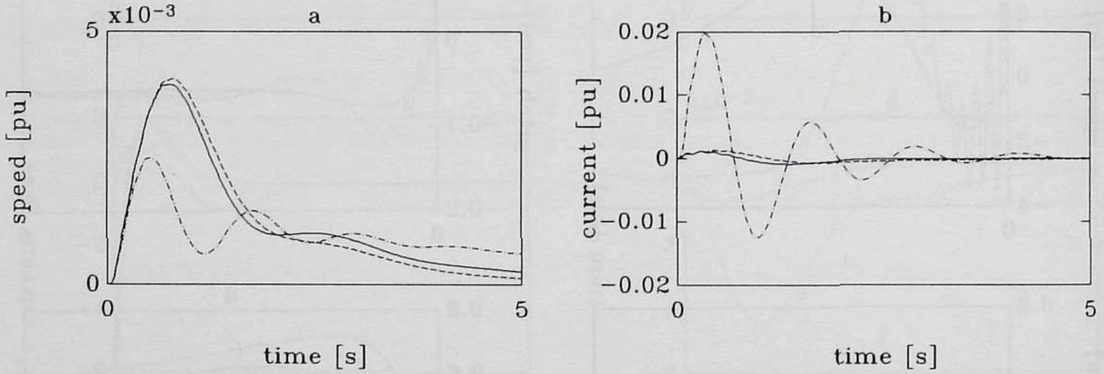

Figure 6.6 Step responses of the wind turbine at a step in wind speed with the output feedback controllers $LQOF_1$ (v,– – –), $LQOF_2$ (u_i,–.–.–) and $LQOF_3$ (v&u_i,——) designed for different disturbances.

Clearly, designs $LQOF_3$(v&u_i) and $LQOF_1$(v) are comparable. Controller $LQOF_2$ with X chosen to represent u_i disturbances gives a much less performance, especially in the current (b). However for a grid disturbance (figure 6.7) this feedback is much better suited. For this disturbance feedback $LQOF_1$(v) is not good. The compromise controller $LQOF_3$(v&u_i) is much better than $LQOF_1$ but $LQOF_2$ is obviously the best here.

The results shown indicate that the feedback can be tuned in such a way that it behaves better for certain disturbances.

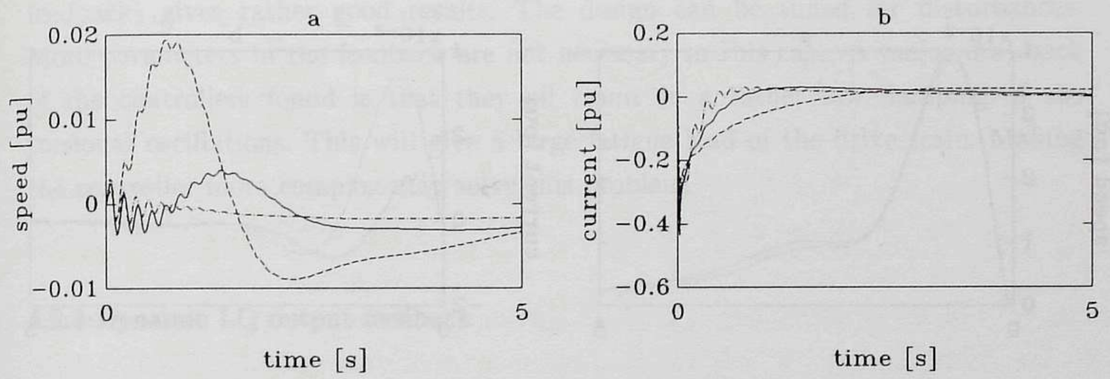

Figure 6.7 Step responses of the wind turbine at a step in grid voltage with the output feedback controllers $LQOF_1$ (v,– – –), $LQOF_2$ (u_i,–.–.–) and $LQOF_3$ (v&u_i,——) designed for different disturbances.

Decentralized versus centralized feedback

The structure selection resulting in the feedback law parameterization (6.1) has been done on the basis of properties of the system. In order to investigate how much the performance criterion (5.4) has increased due to these constraints an optimization was carried out for all feedback entries ($\mathscr{G}_0 \in \phi$). The resulting feedback ($LQOF_4$) is given in Appendix A.7.

In figure 6.8 the wind speed step responses are given for ω_{gm} (a) and i_{dc} (b) for the decentralized output feedback $LQOF_3$ (——) and for the full output feedback $LQOF_4$ (– – –). Clearly, there are differences between $LQOF_3$ and $LQOF_4$ but they are acceptable. This is also true for grid disturbances (figure 6.8 c,d) and for the variables not shown (even for the field voltage). This proves the non–restrictive choice for the decentralized structure in this case.

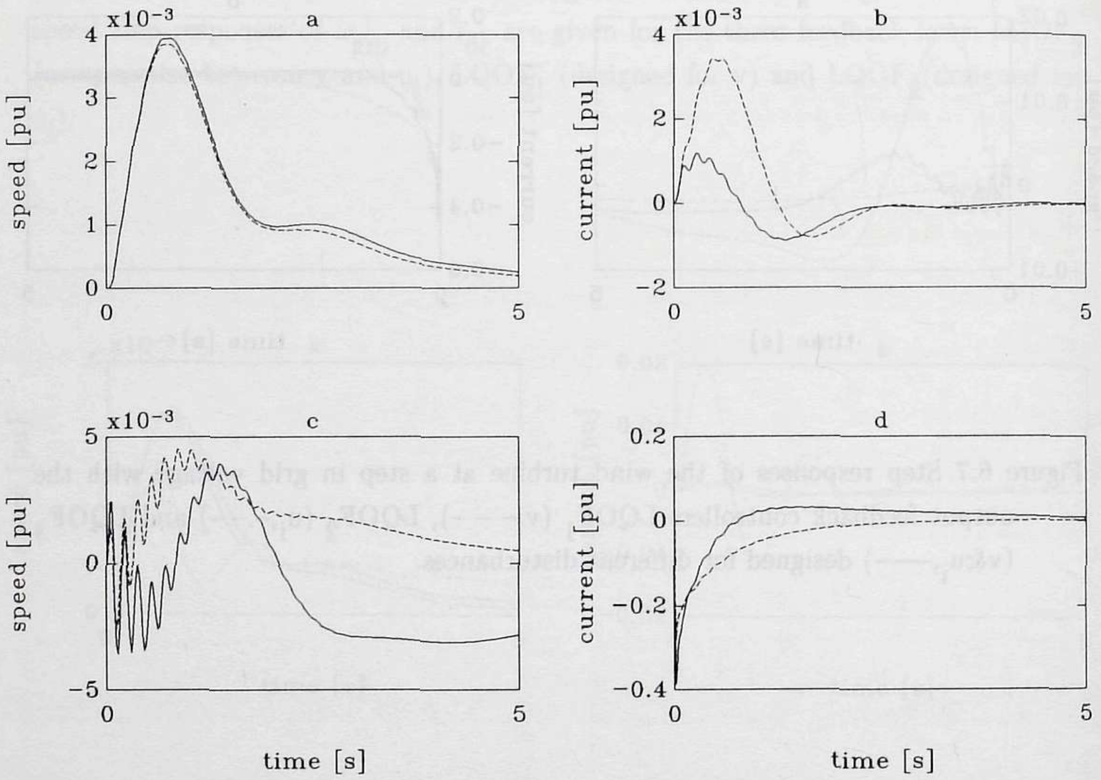

Figure 6.8 Step responses of the speed and current at a step in wind speed (a,b) and at a step in grid voltage (c,d) with the output feedback controller $LQOF_3$ (decentral,——) and $LQOF_4$ (central,– – –).

Summarizing this section, the following remarks can be made.
First, the design procedure is to take the weighting matrices Q and R from state feedback and to define a representative disturbance. The state feedback responses are then used to build up a diagonal matrix X with the squared (maximum) deviations of the state variables. An output feedback is designed using the numerical algorithm. If a large difference occurs between output feedback and state feedback, either the matrices Q, R or the matrix X is retuned. Using time responses this can be done quite systematically. This is also the case for entries of X because variations of X show often similar effects in the resulting closed–loop behaviour as variations of Q.

Second, for the wind energy conversion system, the fairly simple decentralized output feedback controller with only 10 parameters (instead of 39 with state feedback) gives rather good results. The design can be tuned for disturbances. More parameters in the feedback are not necessary in this case. A major drawback of the controllers found is that they all result in a rather low damping of the torsional oscillations. This will give a large fatigue load of the drive train. Making the controller more complex may solve this problem.

6.2.3 Dynamic LQ output feedback

A strong benefit of the LQOF method as described in chapter 5, is the use of controller order as part of the design process. For LQG based controllers, every feedback control law has order equal to the system order n (possibly augmented with integral action orders). In this study we have n=13. Clearly, this results in a *rather large implementation effort eventually. In the former paragraph a PI setup* has been chosen for the output feedback law. In order to obtain better results with respect to the fatigue load (i.e. damping of the mechanical modes), in this section the order of the controller will be enlarged.

In section 5.2.2 a description is given how to deal with optimization of an output feedback law with a predefined dynamic order. Using the extensions of the matrices A,B,C,Q,R,X defined by (5.16) and (5.18) each additional order is then one extra row and one extra column.
In this section this technique is applied to achieve better damping of the oscillations without affecting the performance of the other variables too much. For this to be achieved the corresponding weightings are used: Q(3,3) and X(3,3) of $d\xi/dt$. This directly measures the damping of the mode. If such a state would not exist it is possible to transform the state space model to a real block–diagonal Jordan form and pick out the state related to the damping.
Because there is no need to use integral action filtered by the dynamic feedback (parameters G_y and G_u in (5.27)) the following feedback structure is used (see also eq.(6.1)):

$$\begin{bmatrix} \beta_r \\ u_{Fr} \\ \alpha_r \\ u_1 \\ u_2 \\ \vdots \end{bmatrix} = F \begin{bmatrix} \omega_{gm} \\ i_{dc} \\ \int \omega_{gm} \\ \int i_{dc} \\ \int \alpha_r \\ p_1 \\ p_2 \\ \vdots \end{bmatrix} \qquad (6.2)$$

with

$$F = \begin{bmatrix} x & x & x & x & 0 & x & x & \dots \\ 0 & 0 & 0 & x & x & 0 & 0 & \dots \\ x & x & x & x & 0 & x & x & \dots \\ x & x & 0 & 0 & 0 & x & x & \dots \\ x & x & 0 & 0 & 0 & x & x & \dots \\ \vdots & \vdots & \vdots & \vdots & \vdots & \vdots & \vdots & \vdots \end{bmatrix}$$

Form this structure it follows that the number of feedback parameters in this case increases with $(4q+q^2)$ with q the order of the additional dynamics.

Design procedure

First, Q(3,3) and X(3,3) were enlarged with the same feedback (PI) structure as in the preceding section. This did not result in a better performance as mentioned before.

Then one dynamic order has been added. The oscillations were indeed damped better. A compromise between the behaviour of other variables and the pole location of the torsional mode yielded the results given in row 4 in table 6.2 below.

1.	uncontrolled	–9 ± 39 j
2.	LQ state feedback	real
3.	$LQOF_3$	–2 ± 39 j
4.	one order	–5 ± 39 j
5.	two orders	–6 ± 39 j
6.	two orders, freq weight1 ($LQOF_5$)	–10 ± 38 j
7.	two orders, freq weight2 ($LQOF_6$)	–10 ± 38 j

Table 6.2 Eigenvalues of the torsional mode for various controllers.

Obviously state feedback very easily gives a nice damping. The PI output feedback ($LQOF_3$, §6.2.2) has a much lower damping than for the uncontrolled case.

To obtain better results a second dynamic order has been added. The resulting feedback law yielded slightly better performance. An important drawback of the controller was that increasing Q(3,3) resulted also in serious changes in the way the speed was controlled. This is due to the fact that at non–resonant (high) frequencies $d\xi/dt$ is highly correlated with speed ω_{gm}. However, in this case we would like to optimize only for a certain frequency. As described in section 5.3.3, the use of frequency weighted functions can be applied here. The weighting of $d\xi/dt$ is done at the resonant frequency especially. As weighting filter ($W_x(s)$, eq.(5.24)) we choose a second order transfer function with low damping:

$$W_x(s) = \frac{1}{\frac{s^2}{\omega_0^2} + \frac{2\zeta s}{\omega_0} + 1}$$

with ω_0 chosen as the frequency belonging to the modes depicted in table 6.2. The Bode (amplitude) plot of $W_x(s)$ is given below.

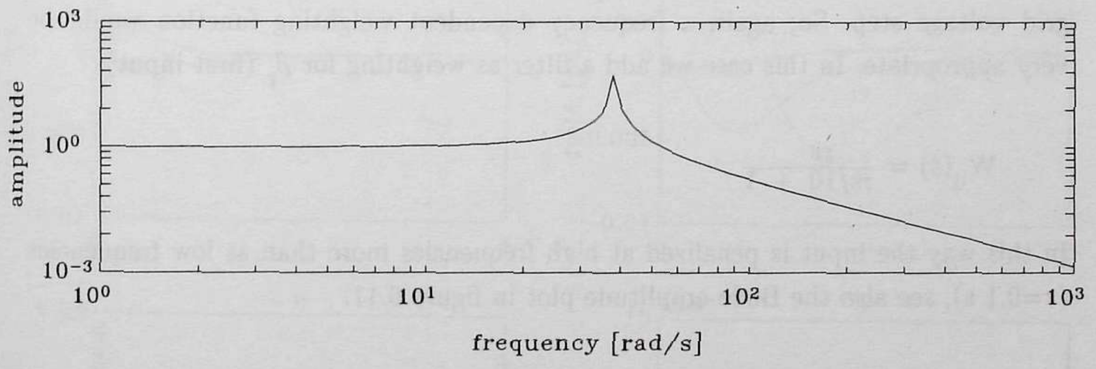

Figure 6.9 Weighting filter for the damping of the torsional oscillations $d\xi/dt$.

By taking a small damping factor ζ (0.001) an output feedback ($LQOF_5$) was found which damps the mode very good (see table 6.2, row 6). This shows the very effective way of using frequency weighting. As mentioned before this is all realized **without increase of controller order despite the use of dynamic weightings**. A comparison of the controllers $LQOF_3$ and $LQOF_5$ using a step response of T_m at a wind speed deviation is shown in figure 6.10a and at a step in grid voltage in figure 6.10b.

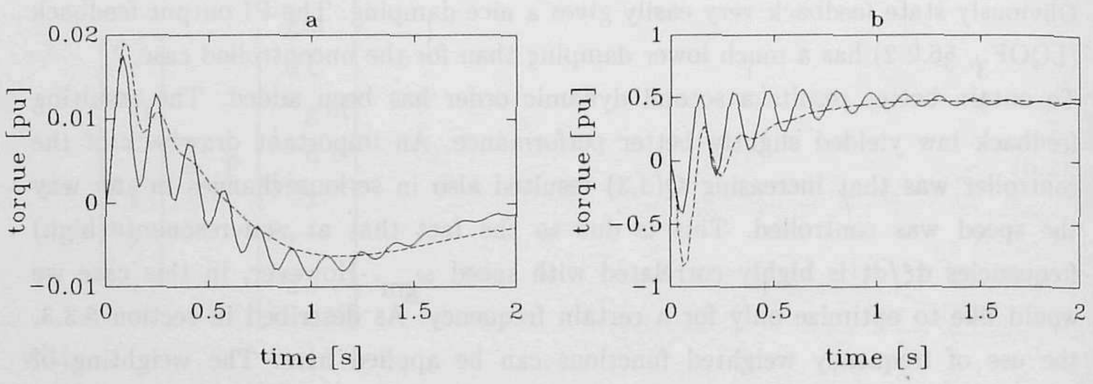

Figure 6.10 Step responses of the torque T_m at a wind speed (a) and voltage deviation (b), for proportional output feedback ($LQOF_3$, ——) and dynamic feedback ($LQOF_5$, – – –).

A trade off appears between damping of the torque ($d\xi/dt$) and excitation level by u_i variations. More damping resulted in stronger excitations of the mode at grid voltage fluctuation, see figure 6.10b. Analysis of the other step responses showed that strong high frequent excitations of the pitch angle occurred at u_j variations. In the time domain the variance of β_r is hardly affected by the small pulses at the grid voltage step. So, again a frequency dependent weighting function would be very appropriate. In this case we add a filter as weighting for β_r (first input):

$$W_u(s) = \frac{\tau s}{\tau s/10 + 1}$$

In this way the input is penalized at high frequencies more than at low frequencies (τ=0.1 s), see also the Bode amplitude plot in figure 6.11.

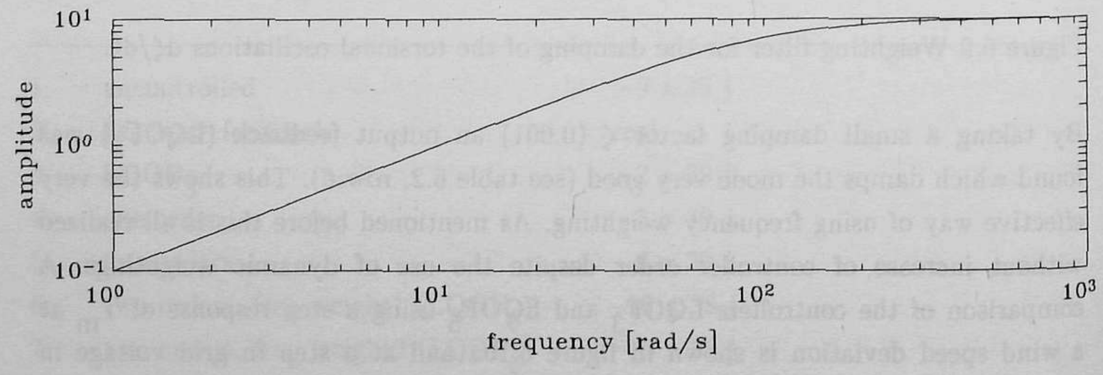

Figure 6.11 Weighting filter for the pitch angle input β_r.

Here, the properness of $W_u(s)$ gives rise to a crossterm in the performance criterion (5.38). The results of section 5.3.2 are necessary to be used in the calculation of the feedback.
The filter $W_u(s)$ is in fact very appropriate to be used in combination with the uncertainty modelling of section 4.3. The filter time constant can be chosen in accordance with the modelled uncertainties in the pitch angle actuator system. However, predefined robustness margins can not be obtained with an LQ criterion only.

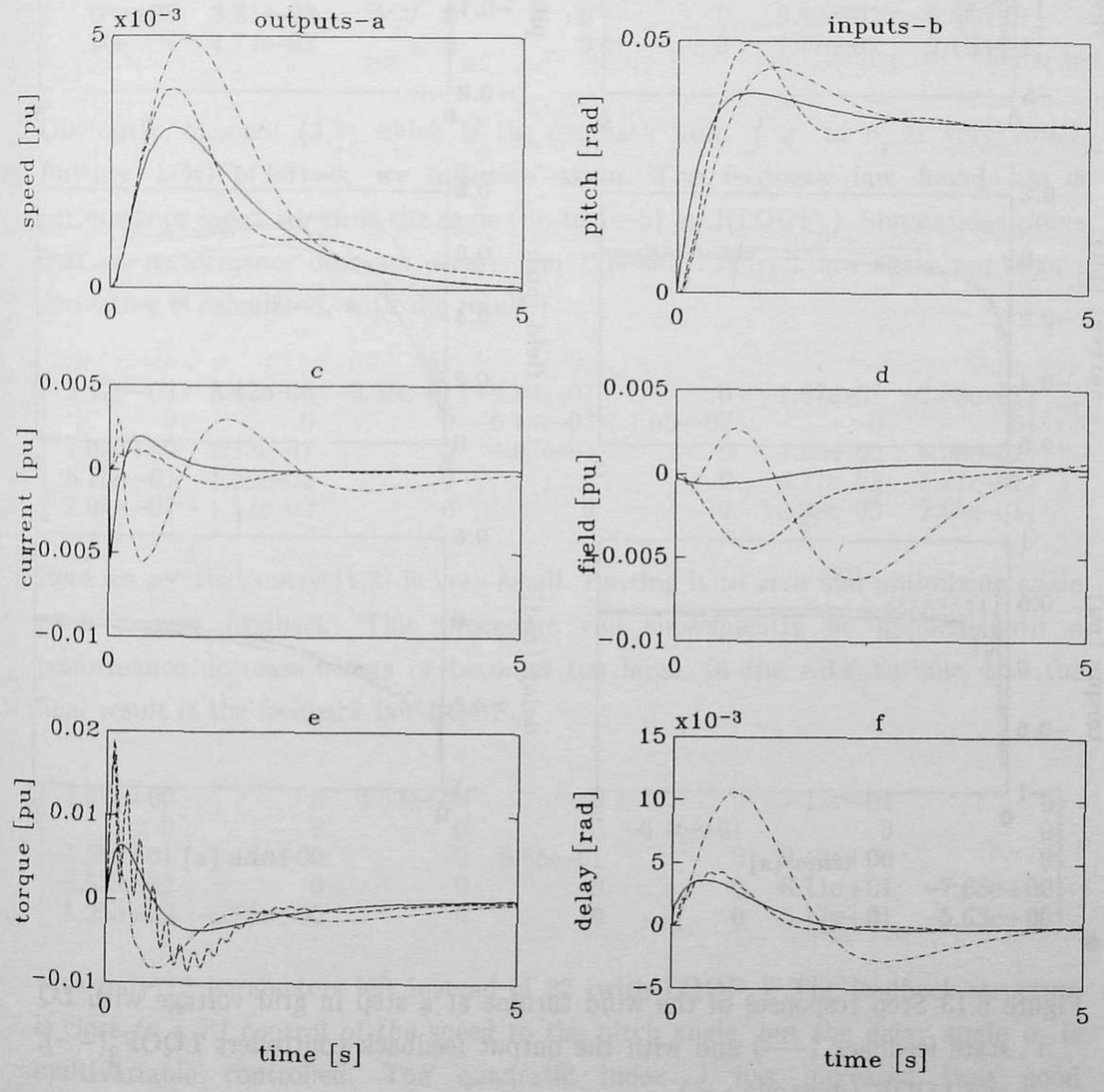

Figure 6.12 Step responses of the wind turbine at a step in wind speed with LQ state feedback (——) and with the output feedback controllers $LQOF_3$(– –), and $LQOF_6$(dynamic,–.–.).

The output feedback controller obtained ($LQOF_6$) is compared with the LQR and $LQOF_3$ controllers. The step responses at a wind speed change are given in figure 6.12 and at a grid voltage change in figure 6.13.

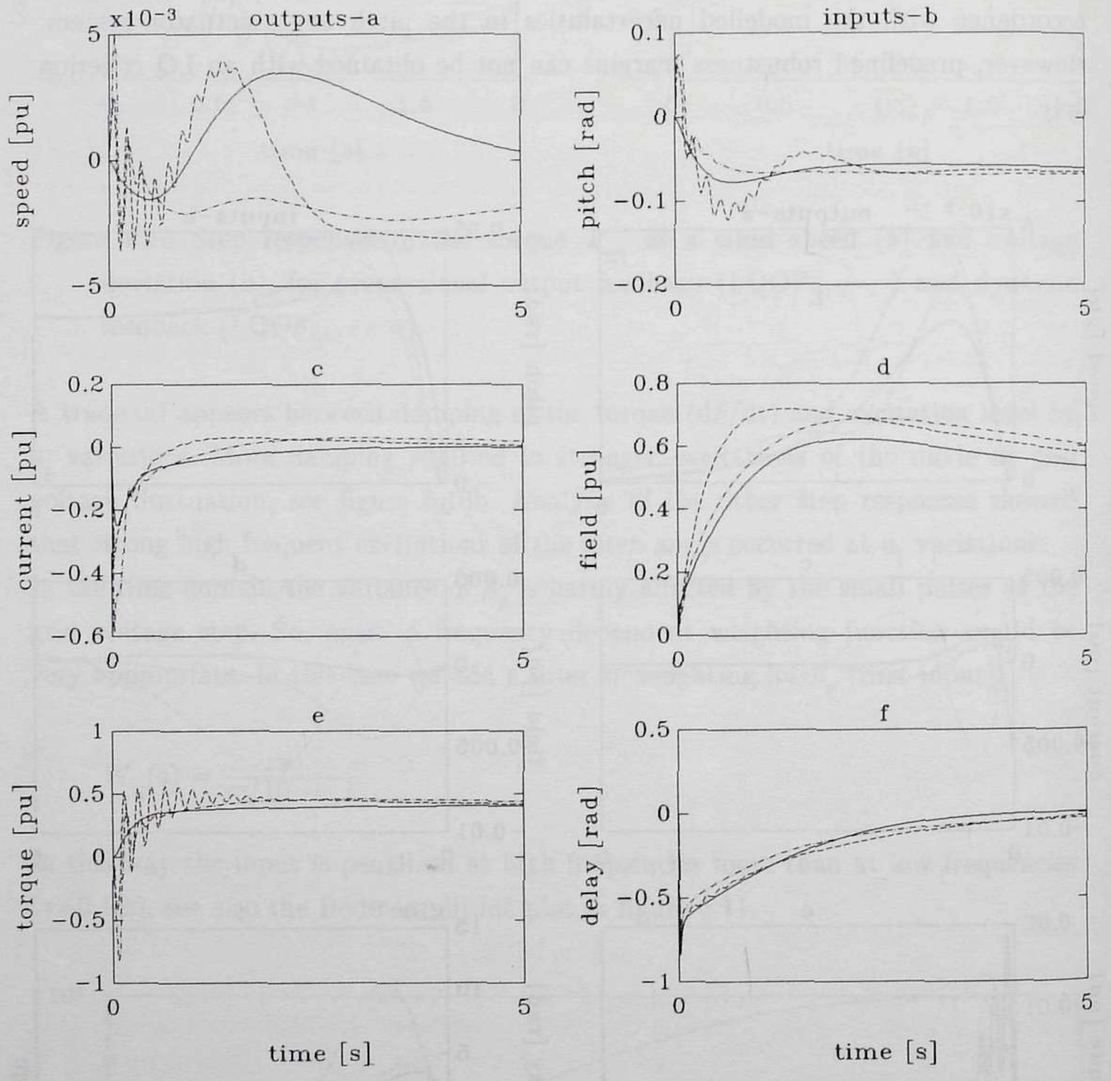

Figure 6.13 Step responses of the wind turbine at a step in grid voltage with LQ state feedback (——) and with the output feedback controllers $LQOF_3$(– –), and $LQOF_6$(dynamic,–.–.).

The simulations indicate that a performance is achieved which is close to the state feedback controller, with a good damping of the mechanical modes.

Selection of decentralized structure

For the final obtained dynamic output feedback law $LQOF_6$ the structure selection procedure described in section 5.3.4 will be applied, in order to reduce the number of feedback parameters. First the second derivative of the performance index with respect to the elements of the feedback is calculated. Multiplied with each entry squared ($\epsilon^2 J_{\epsilon\epsilon}$, eq.(5.43)) we obtain (normed to the largest entry):

$$\begin{bmatrix}
-1.18e{-}01 & 1.06e{-}04 & -1.90e{-}01 & 8.34e{-}04 & 0 & -1.07e{-}02 & -1.60e{-}02 \\
0 & 0 & 0 & 1.65e{-}03 & 3.32e{-}03 & 0 & 0 \\
3.28e{-}01 & 6.75e{-}02 & \mathbf{2.51e{-}05} & 1.04e{-}03 & 0 & 1.51e{-}01 & 1.16e{-}01 \\
1.00e{+}00 & 3.81e{-}03 & 0 & 0 & 0 & 8.40e{-}02 & 6.84e{-}01 \\
4.26e{-}01 & 4.74e{-}03 & 0 & 0 & 0 & 1.77e{-}02 & 3.19e{-}01
\end{bmatrix}$$

Obviously, element (3,3) which is the feedback from $\int \omega$ to α_r is very small. Putting $LQOF_6(3,3)=0$, we optimize again. The feedback law found has a performance index which is the same (up to 1e–5) as $J(LQOF_6)$. Simulations prove that no performance decrease occurs. For this new feedback law again the second derivative is calculated, with the result:

$$\begin{bmatrix}
-2.12e{-}03 & \mathbf{8.42e{-}06} & -3.35e{-}01 & -9.99e{-}03 & 0 & -1.67e{-}01 & -2.89e{-}01 \\
0 & 0 & 0 & 6.44e{-}03 & 1.05e{-}02 & 0 & 0 \\
1.00e{+}00 & 2.13e{-}01 & 0 & 4.05e{-}03 & 0 & 7.80e{-}02 & 8.98e{-}01 \\
6.25e{-}01 & 1.59e{-}02 & 0 & 0 & 0 & 6.71e{-}02 & 5.21e{-}01 \\
2.09e{-}01 & 1.52e{-}02 & 0 & 0 & 0 & 2.98e{-}03 & 2.00e{-}01
\end{bmatrix}$$

Here we see that entry (1,2) is very small. Putting it to zero and optimizing again gives a new feedback. This procedure can subsequently be applied until a performance decrease occurs or becomes too large. In the wind turbine case the final result is the feedback law $LQOF_7$:

$$\begin{bmatrix}
2.67e{+}00 & 0 & 3.53e{+}00 & 0 & 0 & 7.12e{-}01 & 0 \\
0 & 0 & 0 & 0 & -6.46e{-}01 & 0 & 0 \\
-7.58e{+}01 & 1.17e{+}00 & 0 & 6.65e{-}01 & 0 & 9.13e{+}00 & 0 \\
8.53e{+}02 & 0 & 0 & 0 & 0 & -8.71e{+}01 & -7.68e{+}00 \\
5.25e{+}02 & -5.81e{+}00 & 0 & 0 & 0 & -5.17e{+}01 & -5.63e{+}00
\end{bmatrix}$$

with only 15 parameters left instead of 22 (with $LQOF_6$). The feedback structure is close to a PI control of the speed to the pitch angle, but the delay angle α_r is multivariable controlled. The quadratic index J has increased (less good performance) with only 0.01% ! This means that in this case 7 feedback parameters were completely redundant, in the sense of J. With time simulations larger but acceptable differences occur.

More reduction is not feasible. The second derivative of the index for $LQOF_7$ is:

$$\begin{bmatrix} -5.40e{-}02 & 0 & -3.38e{-}02 & 0 & 0 & -3.35e{-}02 & 0 \\ 0 & 0 & 0 & 0 & 1.85e{-}03 & 0 & 0 \\ 1.06e{-}01 & 8.82e{-}03 & 0 & 2.89e{-}04 & 0 & 1.22e{-}01 & 0 \\ 1.00e{+}00 & 0 & 0 & 0 & 0 & 7.30e{-}01 & 3.23e{-}02 \\ 6.38e{-}01 & 5.20e{-}04 & 0 & 0 & 0 & 4.24e{-}01 & 3.28e{-}03 \end{bmatrix}$$

Nearly all entries are quite large. Note that some entries such as (3,4) are relatively small but still very important: it is the only feedback parameter in that column or row. This is an addition to the procedure described in §5.3.3: although entries may be small, if they are the only one in their row or column it should be maintained as feedback path.

Summarizing this section on the nominal design it can be stated that a fairly good output feedback controller is obtained. It has a low order (2, and 3 integral actions) and a rather simple decentralized structure. The performance is close to that of state feedback. The use of frequency weighting functions has shown to be a very effective and strong extension. The structure selection procedure did work very well resulting a much less complicated feedback, without any significant decrease of overall performance.
Due to rather large model variations, the output feedback obtained should also be robustified against these perturbations. In the next section the multi–model design approach will be applied.

6.3 MULTI–MODEL ROBUSTIFICATION

The wind turbine system under investigation has several model variations (§4.3) which are suited to be handled by the multi–model design approach (§5.3.5). From these possibilities only the aerodynamic variations are handled because they are very large (§4.4). Other perturbations are modelled as norm–bounded perturbations and will be analyzed in the next section.

The nominal output feedback design is the one obtained with 2 additional orders and both frequency weighting of $d\xi/dt$ and β_r and has been called $LQOF_7$. The corresponding (extended) state space design model has order 18 and has been derived for v=16 m/s.

As described in §4.4.1 the choice of operating point defines the aerodynamic quantities. The first check is to apply the output feedback $LQOF_7$ to three models: v=12, 16 and 20 m/s. The results are given in figure 6.14 for a wind speed change.

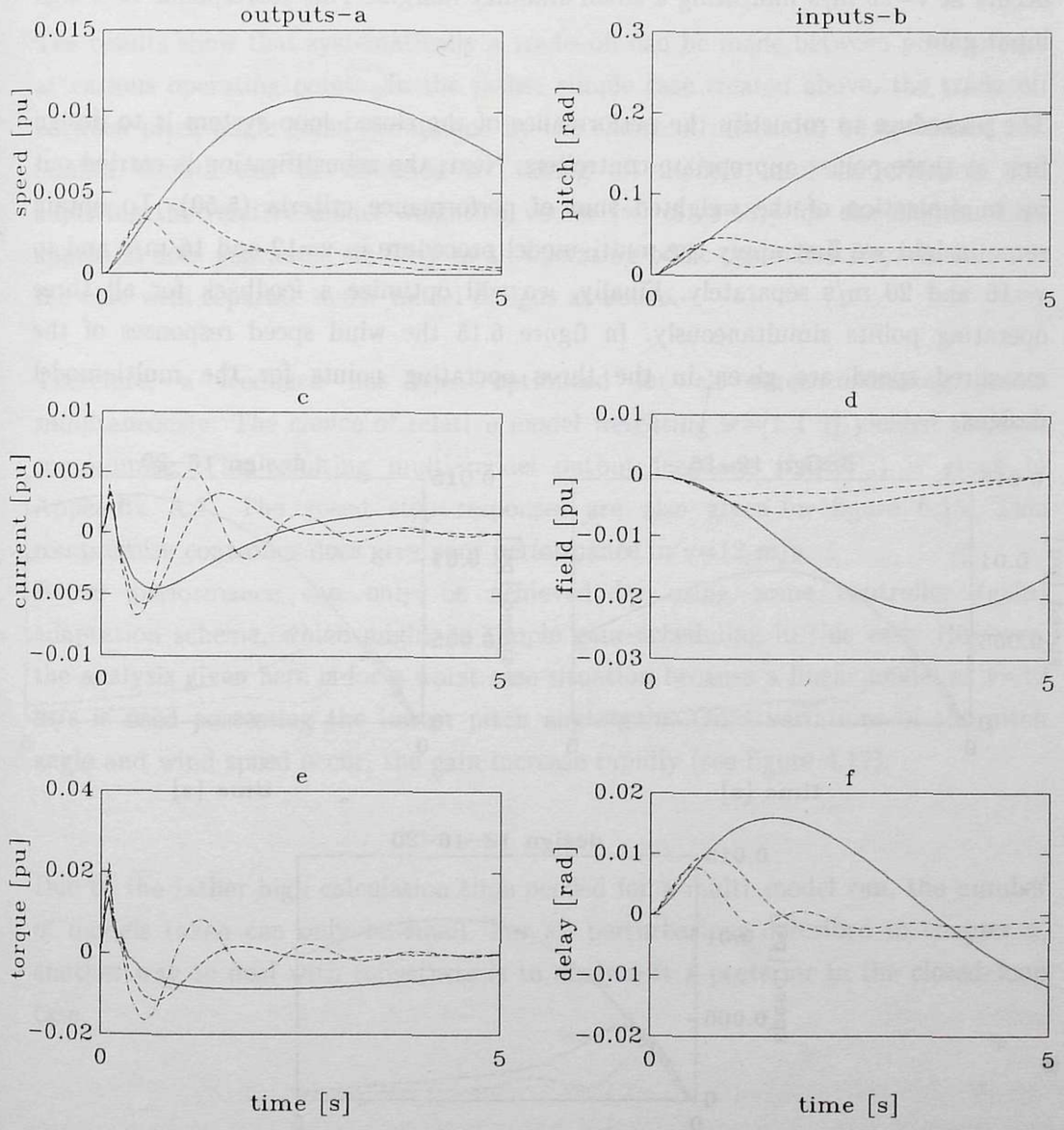

Figure 6.14 Step responses of the wind turbine at a step in wind speed with output feedback $LQOF_7$, in three operating points v=12(——),16(– –) and 20(–.–) m/s.

From the simulations it is clear that at all working points stability is obtained with the output feedback $LQOF_7$. The major problem in this case is the performance. The figure shows variations in the speed which are large at v=12 m/s. This is entirely due to the fact that the pitch angle has only a very small input gain at that wind speed (figure 4.17). On the other hand a low damping occurs at v=20 m/s indicating a small stability margin. This corresponds to a high *input gain*.

The procedure to robustify the performance of the closed–loop system is to design first at three points appropriate controllers. Next, the robustification is carried out by minimization of the weighted sum of performance criteria (5.50). To obtain some insight we first apply the multi–model procedure in v=12 and 16 m/s and to v=16 and 20 m/s separately. Finally, we will optimize a feedback for all three operating points simultaneously. In figure 6.15 the wind speed responses of the measured speed are given in the three operating points for the multi–model designs.

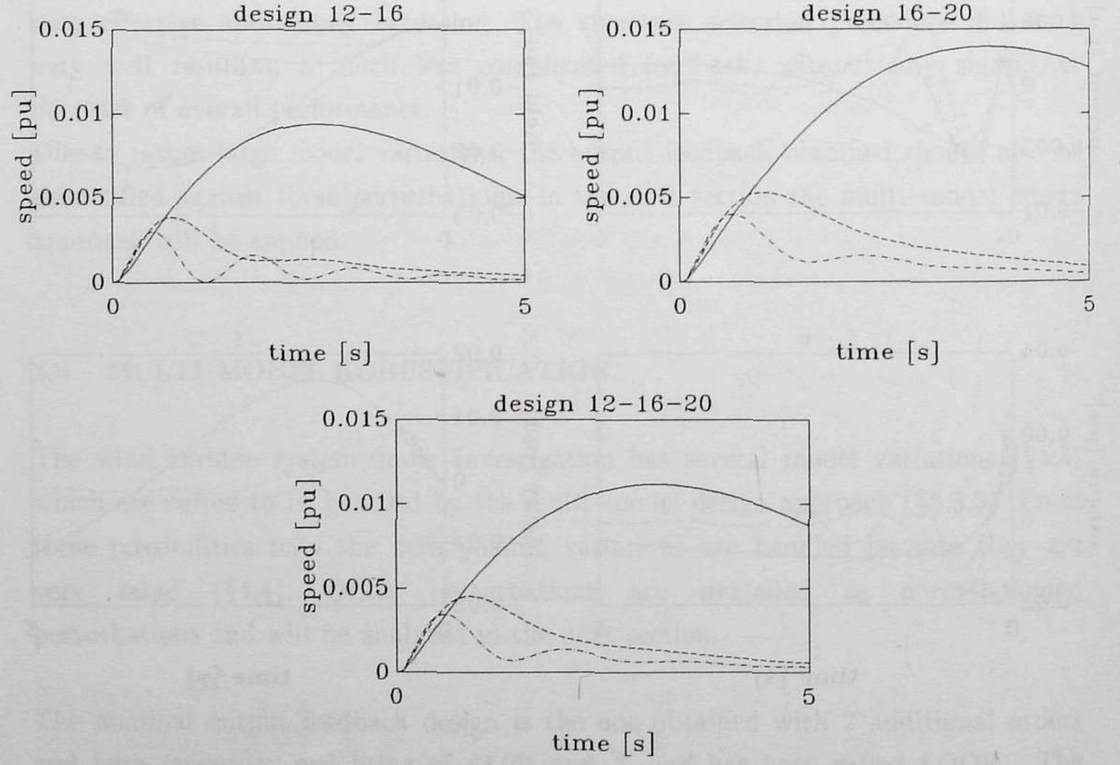

Figure 6.15 Step responses of the wind turbine speed at a step in wind speed, with a multi–model controller designed for v=12,16, for v=16,20 and for v= 12, 16,20 m/s, all applied in the three operating points v=12(——), 16(– –), 20(–.–) m/s.

The step responses with the multi–model controller designed for v=12,16 m/s are better in v=12 m/s, but give a very low damping in v=20 m/s. The multi–model controller designed for v=16,20 m/s results in a good damping in v=20 m/s, but this is realized by a decrease of the gain of the speed control hence resulting in large variations of the speed in v=12 m/s.

The results show that systematically a trade–off can be made between performance at various operating points. In the rather simple case treated above, the trade–off between pitch angle gains is obtained by the choice of models to be optimized for. Similar results can be obtained by taking all models into the criterion and adjusting the relative model weighting vector (w_i of (5.48)) for the models. This approach does guarantee stability in all operating point optimized for, which is not the case with separate multi–model designs as above.

Therefore, a feedback has been optimized for all three operating points simultaneously. The choice of relative model weighting w=[1 1 1] yielded the best compromise. The resulting multi–model output feedback ($LQOF_8$) is given in Appendix A.7. The speed step responses are also given in figure 6.15. This compromise controller does give poor performance in v=12 m/s.
Better performance can only be achieved by using some controller (gain) adaptation scheme, which might be simple gain–scheduling in this case. However, the analysis given here is for a worst case situation because a linear model at v=12 m/s is used possessing the lowest pitch angle gain. Once variations of the pitch angle and wind speed occur, the gain increase rapidly (see figure 4.17).

Due to the rather high calculation time needed for a multi–model run, the number of models taken can only be small. For all perturbations described in chapter 4, another way to deal with robustness is to analyze it a posterior in the closed–loop case.

6.4 ROBUSTNESS ANALYSIS OF THE CONTROLLED WIND TURBINE SYSTEM

In this section the system (4.25) controlled with the optimal controllers designed in the previous section (LQR, $LQOF_8$) will be analyzed on their robustness properties. The construction of the interconnection matrix M(s) or M(jω) has been done according to the formula's of §5.4 and the associated Δ matrix has been scaled to unity.
Both the singular value test (5.58) and the structured singular value test (5.56) will be applied to the system, in accordance to the robustness analysis procedure described in §5.4.
Recall that the uncertainty matrix for the wind turbine system has the following individual uncertainties as elements (§4.3.5):

$\Delta_{\beta t}(j\omega)$	pitch angle input uncertainty
$\Delta_{ut}(j\omega)$	field voltage input uncertainty
$\Delta_{\alpha t}(j\omega)$	delay angle input uncertainty
Δ_{T}	mechanical torque internal uncertainty
Δ_{Cp}	aerodynamic internal uncertainty
Δ_{k}	damping of the torsional mode, internal uncertainty
$\Delta_{Te}(j\omega)$	electrical torque discretization internal uncertainty
$\Delta_{\omega g}(j\omega)$	electrical speed discretization internal uncertainty
$\Delta_{\omega gm}(j\omega)$	speed sensor output uncertainty
$\Delta_{i}(j\omega)$	current output uncertainty

Note that the uncertainties without the argument (jω) are all **real** parameter changes while the tests given above allow complex perturbations.

In figure 6.16 the maximum singular value of M(jω) is shown for all Δ's simultaneously, for multi–model output feedback $LQOF_8$ as well as for the state feedback LQR.

Clearly, $\overline{\sigma}$ is very much larger than one for all frequencies. So test (5.58) does not hold. Because the values are so large it might be expected that the results are very conservative.

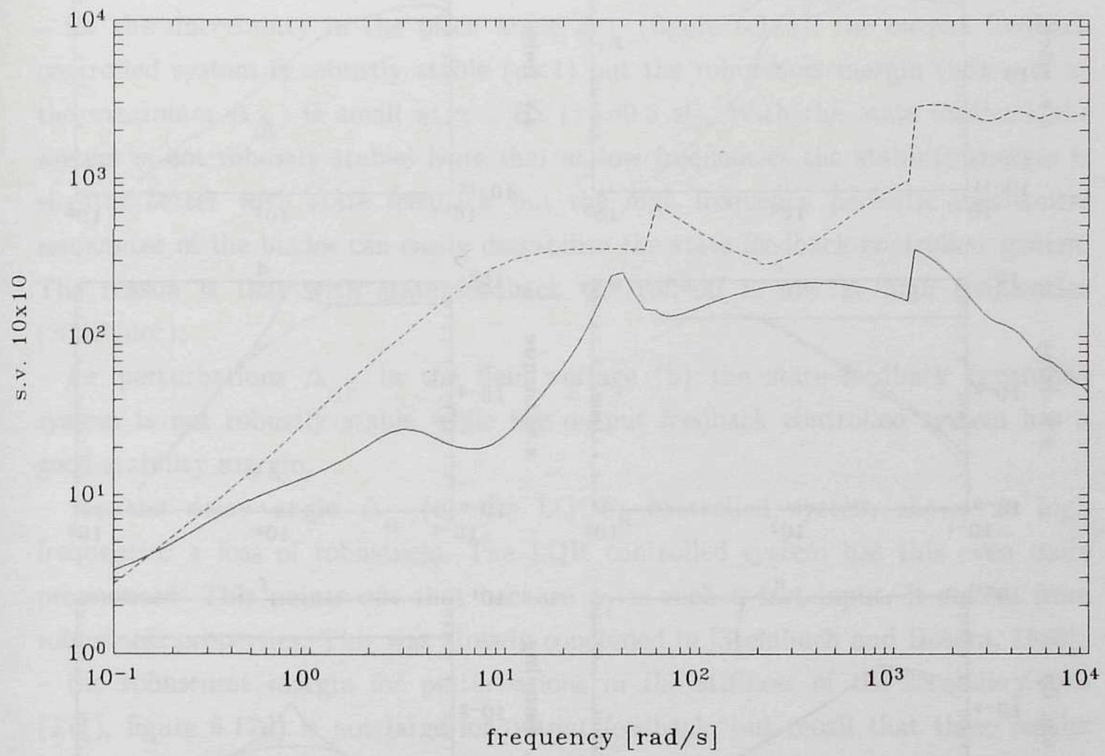

Figure 6.16 Maximum singular value of the wind turbine system controlled with output feedback $LQOF_8$(——) and with state feedback LQR(– –), for all 10 uncertainties.

Before we proceed with the calculation of the structured singular value μ all Δ's are analyzed separately.
For this to be done 10 single–input single–output interconnection matrix transfer functions M(jω) are constructed. This is done for both the multi–model output feedback ($LQOF_8$) and for the state feedback (LQR).

In figure 6.17a–j these singular values are plotted. Recall that for robust stability the curves must be lower than one.

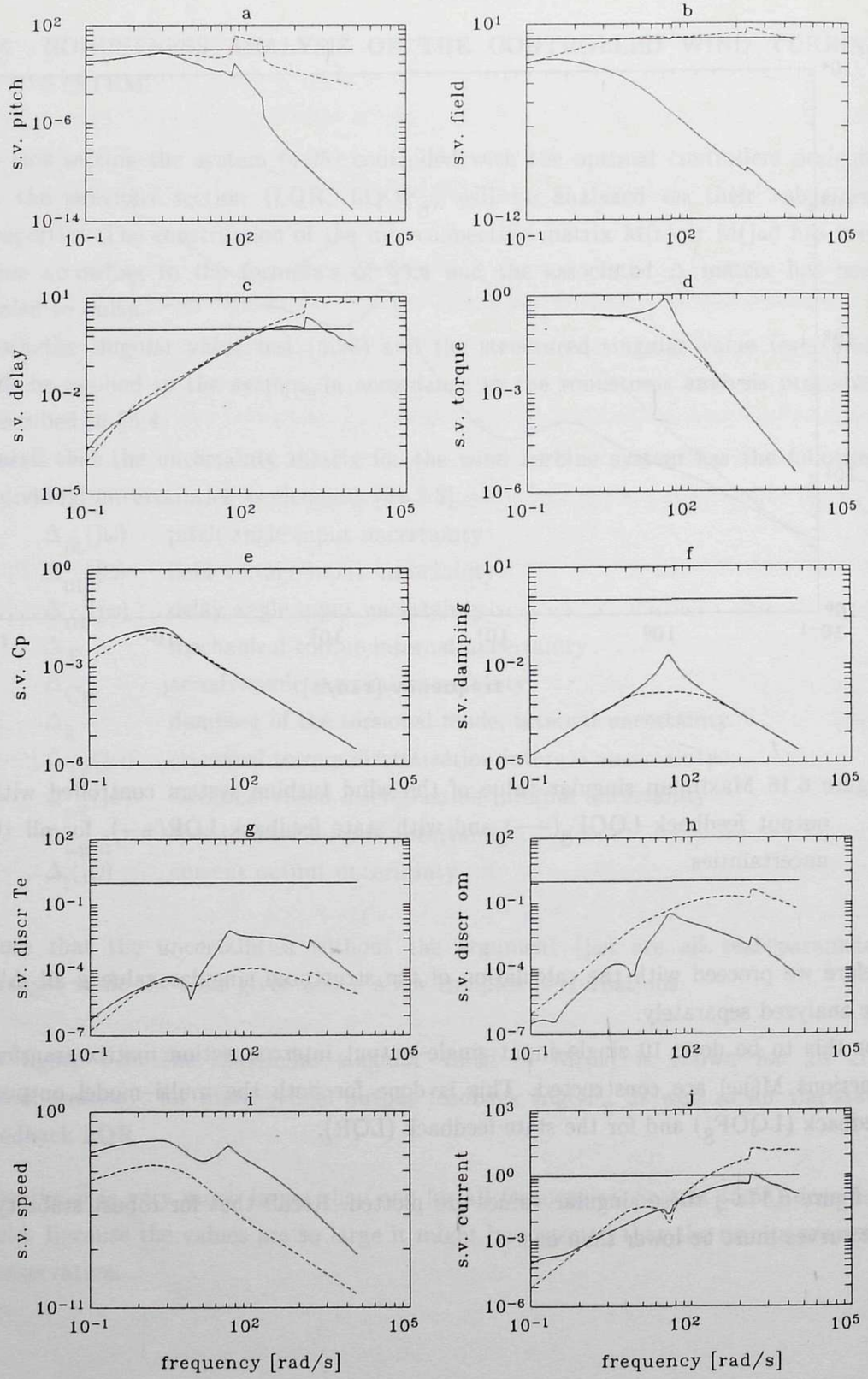

Figure 6.17 Singular values of the wind turbine with output feedback $LQOF_8$ (——) and state feedback LQR(– –) for all 10 uncertainties separately.

From the figure the following observations are made:

– for the uncertainty in the pitch angle $\Delta_{\beta t}$ (figure 6.17a), the output feedback controlled system is robustly stable (σ<1) but the robustness margin (left over at the maximum $\Delta_{\beta t}$) is small at $\simeq$ 2 Hz (τ_β=0.5 s!). With the state feedback the system is **not** robustly stable! Note that at low frequencies the stability margin is slightly better with state feedback but the high frequency parasitic mechanical resonances of the blades can easily destabilize the state feedback controlled system. The reason is that with state feedback the roll–off is low at high frequencies (20dB/dec),

– for perturbations Δ_{uF} in the field voltage (b) the state–feedback controlled system is not robustly stable while the output feedback controlled system has a good stability margin,

– for the delay angle Δ_α (c) the $LQOF_8$–controlled system shows at high frequencies a loss of robustness. The LQR controlled system has this even more pronounced. This points out that because α_r is such a fast input, it suffers from robustness properties. This was already concluded in [Steinbuch and Bosgra, 1988],

– the robustness margin for perturbations in the stiffness of the secondary axis ($T(\xi)$, figure 6.17d) is not large for output feedback, but recall that these results may be conservative because the perturbations are allowed to be complex. Nevertheless, the system is robustly stable. With state feedback the robustness is much better here,

– for the internal uncertainty Δ_{Cp} (e) the output feedback is less robust than the state feedback, this also holds for variations in damping k (f),

– for Δ_{Te} (g), $\Delta_{\omega g}$ (h), $\Delta_{\omega gm}$ (i) both closed–loop systems are robustly stable,

– for the current output Δ_i (j) similar conclusions are valid as for α_r.

Hence, at lower frequencies the state feedback controller is sometimes more robust, but at higher frequencies the output feedback is much better. With output feedback the high roll–off above the bandwidth constitutes higher robustness margins.

Before we proceed with calculations of structured singular value μ, the output feedback controller is redesigned to make it more robust at α_r and i_{dc}. This is done by taking the first order lag of the delay angle into the nominal model. Note that the uncertainty model changes also but still accounts for variations of the time constant. In addition, a first order prefilter (ω_f=2*π*100 rad/s) before α_r has been added. In this way the feedback from i_{dc} to α_r is restricted from having a high frequent coupling between i_{dc} and α_r. The robustness will be increased by

this approach, see also [Steinbuch and Bosgra, 1988]. In addition frequency weighting has been applied for α_r with a filter like figure 6.11. The resulting feedback is called $LQOF_9$ (Appendix A.7). This new controller should be more robust and it maintained a good damping of the torsional mode (eigenvalues $-10\pm37j$). Time responses of this controller are given in Appendix A.8. To show the effect of the adjustments the new output feedback $LQOF_9$ is compared with $LQOF_8$ using singular value plots for the uncertainties Δ_α and Δ_i (figure 6.18).

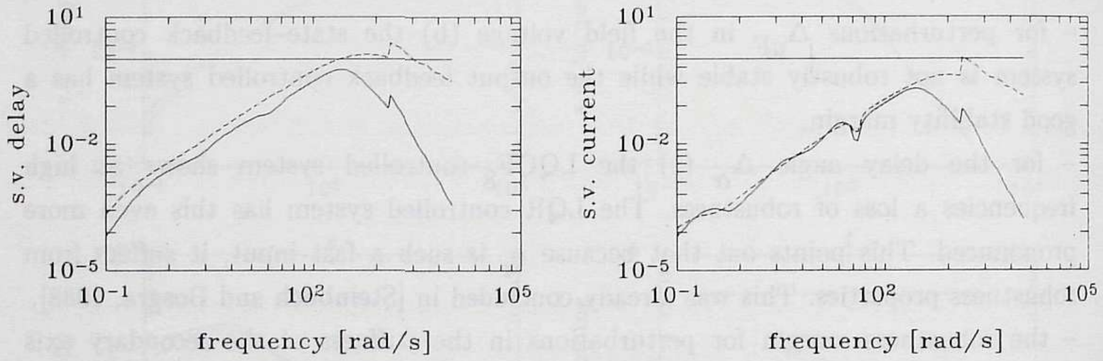

Figure 6.18 Singular values for uncertainties at the delay angle input and current output controlled with the output feedback with filter $LQOF_9$(——) and without filter $LQOF_8$(– –).

From the figure it is clear that the robustness margins at higher frequencies increase both at the delay angle input and the current output. The margin at the 'bandwidth' for Δ_α has increased also, due to the changed uncertainty model. The large perturbations described in chapter 4 are allowed in the new design at both α_r and i_{dc} separately. To obtain results for simultaneous perturbations the structured singular value must be applied.

First the singular value analysis will be completed by applying it in all three operating conditions v=12,16,20 m/s, see figure 6.19. The operating condition only affects Δ_β,Δ_C,Δ_k,Δ_T,$\Delta_{\omega g}$and $\Delta_{\omega gm}$. This is in accordance with the fact that only aerodynamic parameters change. Most important is figure 6.19a showing the robustness with respect to perturbations in the pitch angle input. Clearly, for the low gain situation (——,v=12) the robustness is the largest. For the high gain (v=20) the singular value is slightly more than 1. This means that the robustness margin at v=20 m/s is not as large as at v=12,16 m/s. However, designing a more robust control law at v=20 m/s would inevitably decrease the performance. The feedback law $LQOF_9$ is acceptable as compromise.

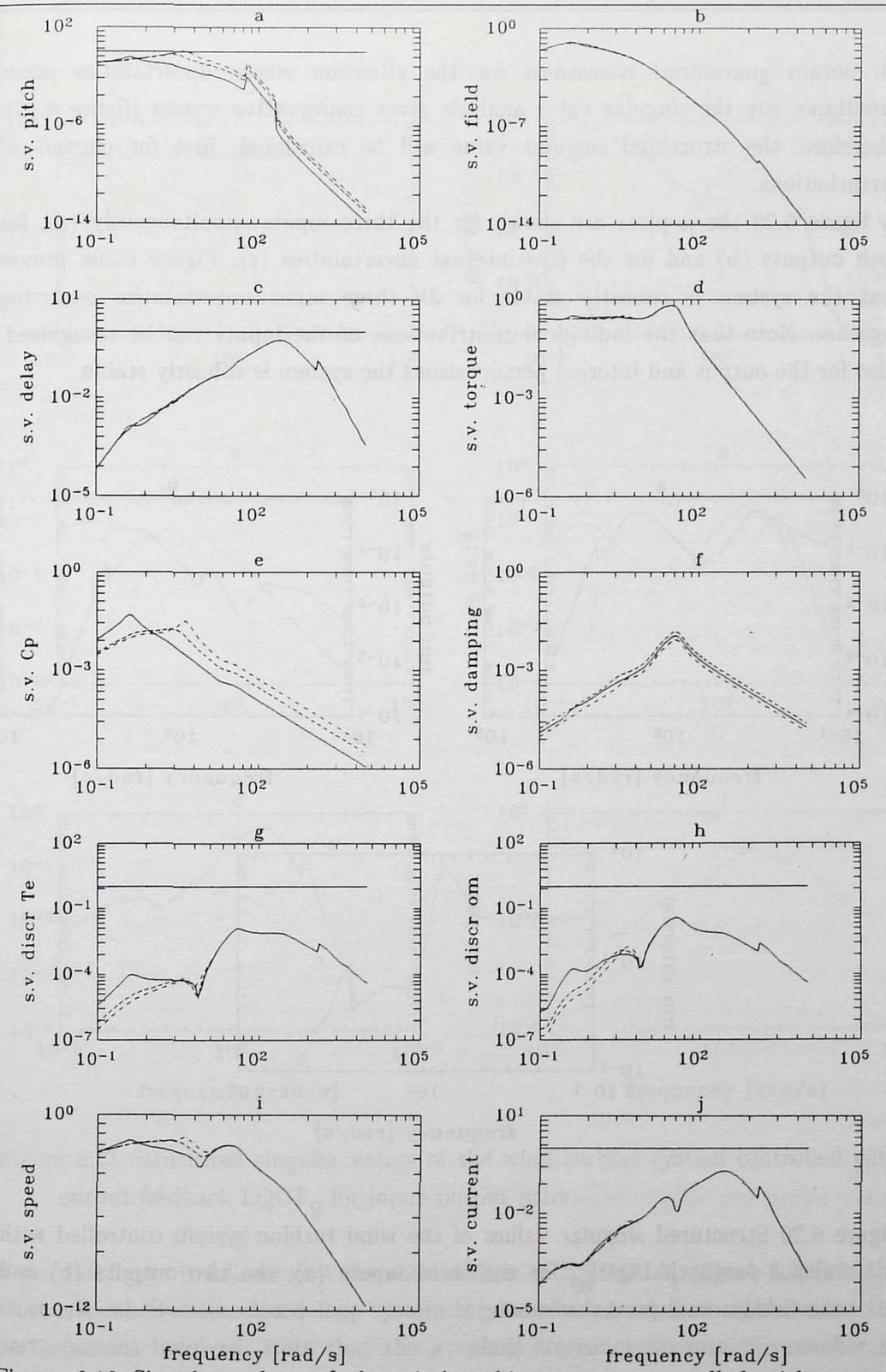

Figure 6.19 Singular values of the wind turbine system controlled with output feedback $LQOF_9$ at three operating conditions: v=12(——), 16(– –) and 20(–.–) m/s, for all perturbations separately.

To obtain guaranteed robustness for the situation where uncertainties occur simultaneously the singular value analysis gives conservative results (figure 6.16). Therefore, the structured singular value will be calculated, first for clusters of perturbations.

In figure 6.20 the μ–plots are shown for the three inputs simultaneously (a), for both outputs (b) and for the five internal uncertainties (c). Figure 6.20a proves that the system is robustly stable for all three input uncertainties occurring together. Note that the individual contributions of the inputs can be recognized. Also for the output and internal perturbations the system is robustly stable.

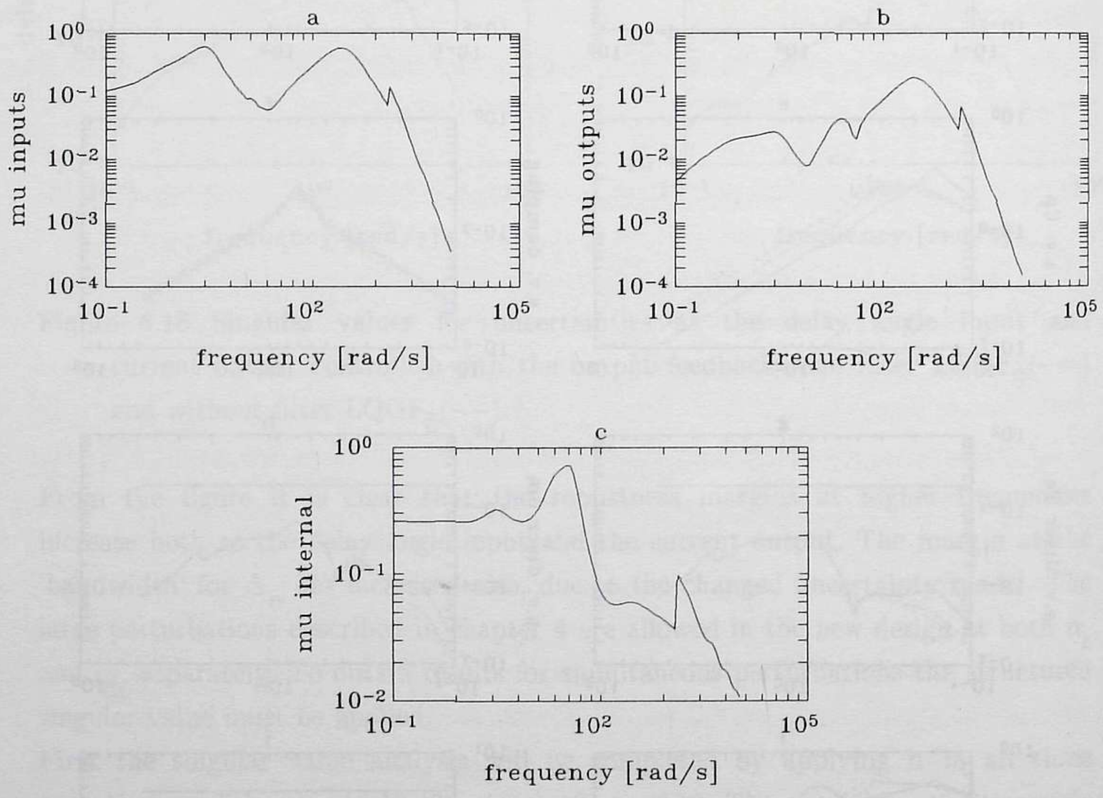

Figure 6.20 Structured singular values of the wind turbine system controlled with output feedback $LQOF_9$ for the three inputs (a), the two outputs (b) and the five internal perturbations (c).

In figure 6.21 μ–plots are given for input/output pairs. In this way we can obtain information about the most critical path in a feedback system.

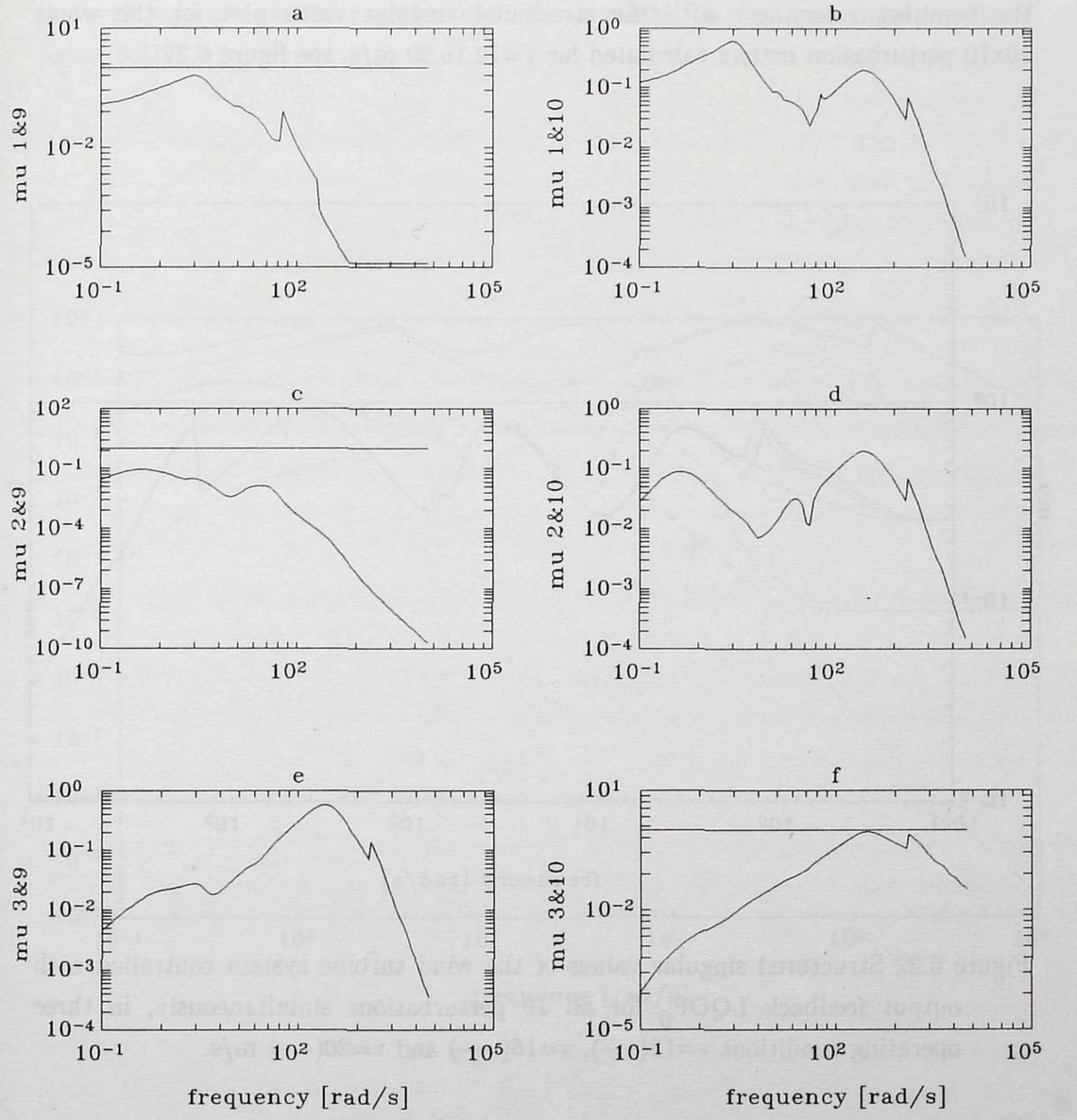

Figure 6.21 Structured singular values of the wind turbine system controlled with output feedback $LQOF_9$ for input–output pairs.

From the figure it follows that the combination of Δ_α and Δ_i (figure 6.21f) is the most critical. But the closed–loop system is guaranteed to remain stable under the perturbations involved. Note that the μ values are exact because the number of

uncertainties in each calculation is less than or equal to 3 (theorem 5.3). We show the resulting robustness with the structured singular value plot for the whole 10x10 perturbation matrix calculated for v=12,16,20 m/s, see figure 6.22.

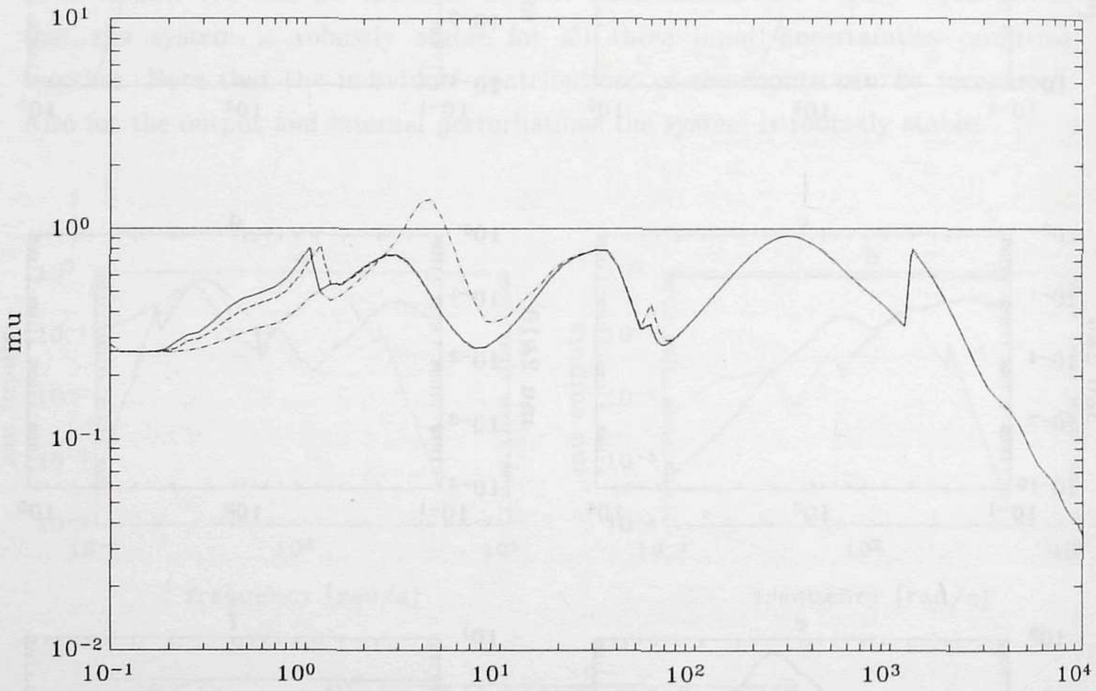

Figure 6.22 Structured singular values of the wind turbine system controlled with output feedback $LQOF_9$ for all 10 perturbations simultaneously, in three operating conditions v=12(– –), v=16(——) and v=20(–.–) m/s.

Obviously, the system is robustly stable for all perturbations occurring simultaneously at v=12 and 16 m/s. As mentioned before at v=20 m/s the robustness is not as good as in the other operating points.

The calculation of μ involved the minimization of a diagonal scaling problem (see §5.4). The upper bound is exact if the number of uncertainty blocks is less than or equal to 3. In our case we have 10 independent blocks. To investigate the tightness

of the upper bound in figure 6.23 the structured singular values for the 10x10 case in v=16 m/s are plotted together with the μ values for the input–output pairs of figure 6.21.

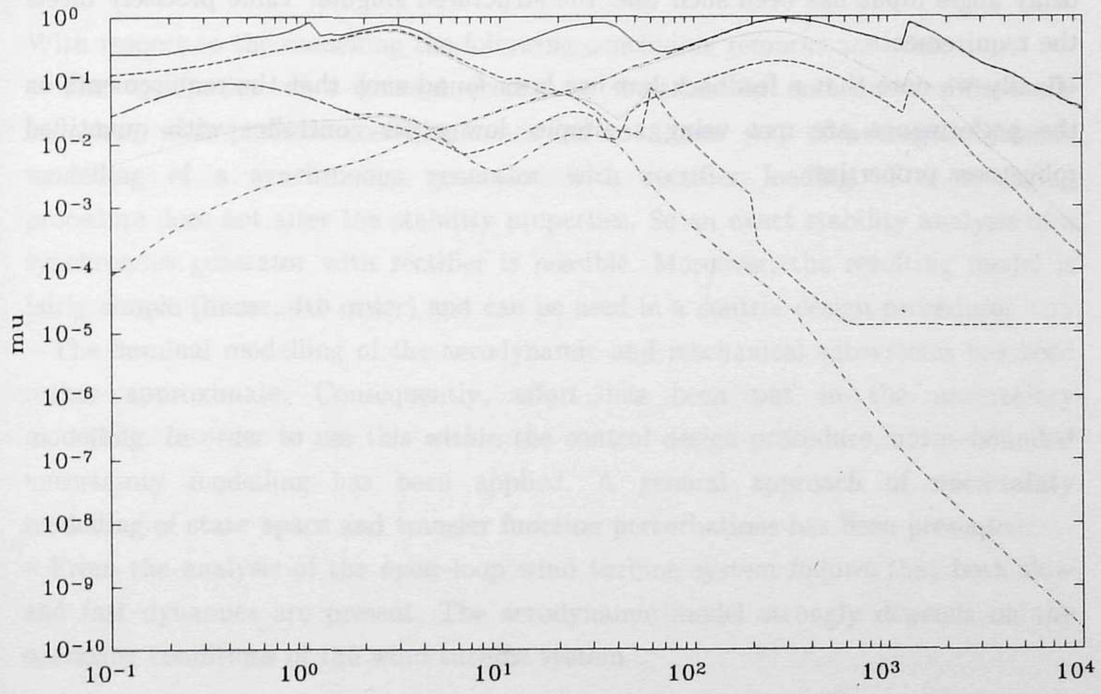

Figure 6.23 Structured singular values of the wind turbine system controlled with output feedback $LQOF_9$ (v=16 m/s) for all 10 perturbations simultaneously and for input–output pairs.

From the figure it may be concluded that the upper bound is very close to the exact value of μ, except between 10–100 rad/s because the internal uncertainties are not contained in the comparison. The tightness of the upper bound of (5.57) is probably due to the fact that the uncertainties all have a different frequency content.

To conclude this section on robustness analysis we **summarize the main results**:
– a feedback law has been found with which stability is preserved under all model uncertainties described in chapter 4. At v=20m/s the robustness margin is smaller but acceptable,
– based on the single and cluster analysis of uncertainties much insight has been gained into the most critical perturbations. Because of this detailed analysis the feedback law has been effectively redesigned,
– the design process itself is iterative. For instance the choice of a prefilter for the delay angle input has been such that the structured singular value precisely meets the requirements,
–finally we note that a feedback law has been found such that the requirements on the performance are met using a simple, low order controller with quantified robustness properties.

7. CONCLUSIONS

In this study the control system design of a variable speed wind turbine system has been investigated. Emphasis was put on obtaining a high performance robust control system using a low order controller.
The modelling and control problem are strongly related. The requirements of high performance and robustness forced the use of both an accurate nominal model as well as uncertainty models.

With respect to the modelling the following concluding remarks are made.
– The application of a general theory on linearization and linear differential equations with periodic coefficients has led to a **new way of averaged dynamic modelling of a synchronous generator with rectifier loading**. The averaging procedure does not alter the stability properties. So an **exact stability analysis** of a synchronous generator with rectifier is possible. Moreover, the resulting model is fairly simple (linear, 4th order) and can be used in a control design procedure.
– The nominal modelling of the aerodynamic and mechanical subsystems has been rather approximate. Consequently, effort has been put in the uncertainty modelling. In order to use this within the control design procedure, norm–bounded uncertainty modelling has been applied. A **general approach of uncertainty modelling of state–space and transfer function perturbations** has been presented.
– From the analysis of the open–loop wind turbine system follows that both slow and fast dynamics are present. The aerodynamic model strongly depends on the operating conditions of the wind turbine system.

The control system design approach involves several analysis and synthesis methods, as well as wind turbine system specific properties. The following observations are made.
– The **Linear Quadratic Output Feedback** method has been successfully applied to the wind turbine system. The LQ framework is very appropriate to address the design problem of wind energy conversion systems. The controller realizes low variations of the speed and power for wind speed and grid voltage disturbances. Using dynamic output feedback the mechanical fatigue loads (damping of the structural mode) are considerably decreased.
– **Frequency weighting** without increase of the controller complexity has been introduced and applied to the wind turbine system. This is a very successful way to put more weighting to certain desired properties, for instance damping of structural modes.

– **Selection of feedback structure** is possible using information on the sensitivity of the performance index with respect to feedback parameters. A selection procedure has been applied to the system and resulted in a rather simple decentralized feedback giving a high performance.

– **Multi–Model LQOF** is a very important tool in the synthesis of robust controllers for highly structured perturbations, as is the case with varying operating conditions of the wind turbine system in full load.

– **Robustness analysis using Structured Singular Values** proved to be successful. Especially, the analysis of single perturbations and clusters gives much insight into the most critical path in a closed–loop system. In the case of the wind turbine system, this knowledge has led to increased robustness by changing the feedback design. The robustness analysis at high frequencies showed the importance of accurate nominal and uncertainty modelling of the synchronous generator with rectifier.

The final conclusion is that a high performance low order controller has be designed successfully for the wind turbine system at full–load. The approach is, in contrast to the wind turbine literature, based on an integrated multivariable design methodology, with the robustness requirements quantitatively assessed.

Several questions however are left open:

– the experimental validation of the models, especially of the model of the synchronous generator with rectifier,

– implementation and evaluation of the controller designed in this work,

– the modelling of the aerodynamics and drive train dynamics has been rather coarse. To investigate the relation between life–time and control system design much more elaborated models are needed,

– in this work an optimal output feedback has been designed for the full load operating conditions. At partial load a tracking problem exists. The electrical system will traverse through several operating conditions. Based on the experiences at full load, it is expected that the LQOF method combined with the Multi–Model synthesis will give good results also at partial load,

– the use of Linear Quadratic Output Feedback has given good results here, partly due to the use of low order, frequency weighting and the Multi–Model robustification. However, a drawback is the unability to synthesize robustness for norm–bounded perturbations directly.

REFERENCES

Ackermann, J. (1983). *Abtastregelung, Band II: Entwurf robuster Systeme.* Springer Verlag, Berlin.

Anderson, P.M. and F.F. Fouad (1982). *Power system control and stability, vol.1.* Iowa State University Press, 3rd ed., Ames.

Anderson, B.D.O., and J.B. Moore (1971). *Linear optimal control.* Prentice–Hall, Englewood Cliffs, N.J.

Anderson, B.D.O., J.B. Moore and D.L. Mingori (1983). Relations between frequency dependent control and state weighting in LQG problems. *Proc. IEEE Conf. on Decision and Control 1983*, San Antonio, TX, pp.612–617, Publ.IEEE New York.

Arrillaga, J., C.P. Arnold and B.J. Harker (1983). *Computer modeling of electrical power systems.* John Wiley and Sons, New York.

Arrillaga, J., J.G. Campos Barros, and H.J. Al–Khashali (1978). Dynamic modelling of single generators connected to HVDC convertors. *IEEE Trans. Power App. and Systems,* PAS–97(4), pp.1018–1026.

Auinger, H., and G. Nagel, (1980). Vom transienten Betriebsverhalten herruehrende Schwingungen bei einem ueber Gleichrichter belasteten Synchrongenerator. *Siemens Forsch.–und Entwickl.–Ber.*,9(1), pp. 1–7, 9(2), pp.85–87

Badawy, E.H. (1984). Performance of a synchronous generator with bridge rectified output. *Electric Power Systems Research*, 8(1), pp.1–7.

Barmish, B.R. (1988). New tools for robustness analysis. *Proc. IEEE Conf. on Decision and Control 1988*, Austin, TX, pp.1–6, Publ.IEEE New York.

Barton, R.S., C.E.J. Bowler, and R.J. Piwko (1979). Control and stabilization of the DOE/NASA MOD–1 two megawatt wind turbine generator. *Proc.14th Intersociety Energy Conversion Engineering Conf.*,Boston, 1979, pp.325–330, Publ.IEEE New York.

Bongers, P.M. and S. Dijkstra (1988). A filter–controller for a flexible wind turbine in partial load. *Proc. 1988 European Community Wind Energy Conference*, Herning, Denmark, 6–10 june 1988.

Bonwick, W.J.,and V.H. Jones (1973). Rectifier–loaded synchronous generators with damper windings. *Proc. IEE*, 120(6), pp.659–666.

Brockett, R.W. (1970). *Finite dimensional linear systems.* John Wiley and Sons, Inc. New York.

Buyse, H., M. Compere, and J.M. Thiry (1985). A simplified analysis of the rectifier bridge fed by a polyphase synchronous machine. In G. Maggetto and Ph.Lataire (Eds.), *Conf. Power Electronics and Applications*, Brussels, 16–18 Oct. 1985, pp 2.167–2.171, Publ. Technologisch Instituut– k.VIV, Antwerpen, Belgium.

Chen, C.T. (1984). *Linear system theory and design.* Holt–Saunders International Editions, New York, 1984, pp.166–167.

Clade, J.J. and H. Perzos (1968). Calculation of dynamic behavior of generators connected to a DC link. *IEEE Trans. Power App. and Systems. PAS–87* (7), pp.1553–1564.

D'Angelo, H. (1970). *Linear time–varying systems: analysis and synthesis.* Allyn and Bacon, Boston.

Davison, E.J. (1972). The output control of linear time–invariant multivariable systems with unmeasurable arbitrary disturbances. *IEEE Trans. on Autom. Control*, AC–17 (10), pp.621–630.

Davison, E.J. (1976). The robust control of servomechanism problem for linear time–invariant multivariable systems. *IEEE Trans. on Autom. Control*, AC–21(2), pp.25–34.

Davison, E.J. and I.J. Ferguson (1981). The design of controllers for the multivariable robust servomechanism problem using parameter optimization methods. *IEEE Trans. on Autom. Control*, AC–26(2), pp.93–110.

Dirkman, R.J. (1983). Generalized state–space averaging. *Proc. 14th IEEE Power Electronics Specialists Conference 1983*, pp.238–294, Publ. IEEE New york.

Doyle, J.C. (1982). Analysis of feedback systems with structured uncertainties. *IEE Proc. –D*, 129(6), pp.242–250.

Doyle, J.C. (1984). *Advances in multivariable control.* Lecture Notes of the ONR/Honeywell Workshop, Honeywell, Minnesota.

Doyle, J.C. (1985). Structured uncertainty in control system design. *Proc. IEEE Conf. on Decision and Control 1985*, pp.260–265, Publ.IEEE, New York.

Doyle, J.C. and G.Stein (1981). multivariable feedback design: concepts for a classical/modern synthesis. *IEEE Trans. on Autom. Control*, AC–26(1) pp.4–16.

Doyle, J.C., J.E. Wall and G.Stein (1982). Performance and robustness analysis for structured uncertainty. *Proc. IEEE Conf. on Decision and Control 1982*, pp.629–639, Publ. IEEE New York.

Elbuluk ,M.E. (1986). *Resonant converters: topologies, dynamic modeling and control.* Ph.D. Thesis, Mass. Inst. Technology, Cambridge, MA., sept. 1986.

Elbuluk, M.E., G.C. Verghese and J.G. Kassakian, (1988). Sampled–data modeling and digital control of resonant converters. *IEEE Trans. on Power Electronics*, PE–3(3), pp. 344–354.

El–Serafi, A.M. and H.S. Khalil (1976). Dynamic stability analysis of parallel AC/DC power systems. *IEEE PES summer meeting*, Portland, OR, july 18–23 1976, paper A 472–1. Publ.IEEE, New York.

Engelen, T.van (1986). Experimental modelling of wind turbines. *International Workshop on the Dynamic Behaviour of Wind Turbines*, 28–30 April 1986, Sophia Antipolis France, Publ. AFME Paris.

Ernst, J. (1984). Control of a variable speed wind energy converter with synchronous generator and a DC link converter. *Proc. European Wind Energy Conference*, 22–26 Oct. 1984, Hamburg, pp. 606–611.

Ernst, J. (1986). *Drehzahlvariable Windenergieanlage mit Gleichstromzwischenkreis –Umrichter und Optimum–suchendem Regler.* Dissertation Tech. University Braunschweig.

Fan, M.K.H. and A.L. Tits (1986). Characterization and efficient computation of the structured singular value. *IEEE Trans. on Autom. Control*, AC–31(8), pp.734–743.

Freudenberg, J.S., and D.P. Looze, (1988). Frequency Domain Properties of Scalar and Multivariable Feedback Systems. *Lecture Notes in Control and Information Sciences*, 104, Springer Vrelag, Berlin.

Glover, K. (1984). All optimal Hankel–norm approximations of linear multivariable systems and their L∞ error bounds. *Int.J.Control*, 39, pp.1115–1193.

Gourieres, D. Le (1982). *Wind power plants, theory and design.* Pergamon Press, Oxford, Paris.

Grötzbach, M., (1981). DC chopper circuits with a structure different in intervals. *Automatica*, 17(2), p.321–334.

Grötzbach, M. and R. von Lutz, (1986). Unified modeling of rectifier–controlled DC power supplies. *IEEE Trans. on Power Electronics*, PE–1(2), pp. 90–100.

Gupta, N.K., M.G. Lyons, J.N. Aubrun and G. Margulies (1981). Frequency–shaping methods in large space structures control. *Proc. AIAA Guidance and Control Conf*, Albuquerque, NM.

Haneda, H. Y. Kuroe and T. Maruhashi (1982). Computer–aided analysis of power–electronic DC–motor drives: Transient and steady–state analysis. Proc. *13th* IEEE *Power Electronics Specialists Conference 1982*, pp.128–139, Publ. IEEE New york.

Harashima, F. and H. Naitoh (1977). Dynamic performance of converter–fed synchronous motors. In W. Leonhard (Ed.), *Proc.* 2nd. *IFAC symposium Control in Power Electronics and Electrical Drives*, Dusseldorf, FRG, 3–5 Oct. 1977,pp.369–378, Pergamon Press, Oxford.

Harrington, R.J. and S.A. Gawish (1985). A digital computer model of three–phase rectifier/inverter systems for transient studies. In G. Maggetto and Ph.Lataire (Eds.), *Conf. Power Electronics and Applications*, Brussels, 16–18 Oct. 1985, pp 2.131–2.136, Publ. Technologisch Instituut– k.VIV, Antwerpen, Belgium.

Hartmann, I., W. Lange, and R. Poltmann (1986). *Robust and insensitive design of multivariable feedback systems– multi model design.* Vieweg, Braunschweig Wiesbaden.

Hashem, A.M. and J.P. Louis (1980). A new method for modelling a synchronous generator associated with a thyristor bridge. *IEEE–Industry Application Society Annual Meeting, Part II*, Cincinatti, OH, sept/oct. 1980, pp.865–870, publ.IEEE New York.

Hinrichsen, E.N. (1984). Control for variable pitch wind turbine generators. *IEEE Trans. Power App. and Systems*, PAS–103(4), pp.886–892.

Hoeijmakers, M.J. (1984). *On the steady–state performance of a synchronous machine with convertor.* Dissertation Eindhoven Univ. of Technology, 1984.

Hoeijmakers, M.J. (1988). A simple model of a synchronous machine with convertor. In Ansaldo (Ed.), *1988 International Conference on Electrical Machines*, Vol.II, September 12–14, 1988, Pisa, Italy, pp.237–241.

Kailath, T. (1980). *Linear Systems.* Prentice Hall, Inc., Englewood Cliffs, N.J., 1980.

Kimbark, E.W. (1971). *Direct current transmission, vol,1.* Wiley–Intersience, New York.

Kovacs, P.K. (1984). *Transient phenomena in electrical machines.* Elsevier, Amsterdam.

Kreisselmeier, G. and R. Steinhauser, (1983). Application of vector performance optimization to a robust control loop design for a fighter aircraft. *Int. J. Control*, 37(2), pp.251–284.

Kwakernaak, H. and R. Sivan (1972). *Linear optimal control systems.* Wiley–Intersience, New York.

Lee, I. (1963). On the theory of linear dynamic system with periodic parameters. *Information and Control*, 6, pp.265–275.

Levine, W.S., and M. Athans (1970). On the determination of the optimal constant output feedback gains for linear multivariable systems, *IEEE Trans. on Autom. Control*, AC–15(1), pp.44–48.

Liebst, B.S. (1983). Pitch control system for large scale wind turbines, *J. Energy,* 7(2), pp.182–192.

Looze, D.P. (1983). A dual optimization procedure for linear Quadratic robust control problems. *Automatica*, 19(3), pp. 299–302.

Louis, J.P. (1983). Non–linear and linearized models for control systems including static converters. Proc. *IFAC Control in Power Electronics and Electrical Drives*, Lausanne, Switzerland, 1983, pp.9–19, Pergamon Press, Oxford.

Lunze, J. (1984). The design of robust feedback controllers in the time domain. *Int.J. Control*, 39(6), pp.1243–1260.

Makila, P.M., and H.T. Toivonen (1987). Computational methods for parametric LQ problems –a survey. *IEEE Trans. on Autom. Control*, AC–32(8), pp.658–671.

Mattsson, S.E. (1984). *Modelling and control of large horizontal axis wind power plants.* Dissertation Lund University, Sweden.

Moore, B.C. (1981). Principal component analysis in linear systems: controllability, observability and model reduction. *IEEE Trans. on Autom. Control,* AC–26(1), pp.17–32.

Moriyasu, S. and C. Uenosono (1986). An analysis on the characteristics of a synchronous machine connected to a d.c.–link. *Archiv. fur Elektrotechnik*, 69, pp.111–120

Mostafa, M.M.F. and C. Iung (1985). A new dynamic model of a self–controlled synchronous motor drive. In G. Maggetto and Ph.Lataire (Eds.), *Conf. Power Electronics and Applications*, Brussels, 16–18 October 1985, pp 3.245–3.250, Publ. Technologisch Instituut– k.VIV, Antwerpen, Belgium.

Murdoch, A., J.R. Winkelman, S.H. Javid and R.S. Barton (1983). Control design and performance analysis of a 6MW wind turbine–generator. *IEEE Trans. on Power App. and Systems*, PAS–102, pp.1340–1347.

Naeije, W.J. (1979). *Optimal output feedback as design method for multivariable control systems.* Dissertation Delft Univ. of technology, (in Dutch).

Naeije, W.J. and O.H. Bosgra (1977). The design of dynamic compensators for linear multivariable systems. In D.P. Atherton (Ed.) *Proc. 4th IFAC Symp. on Multivariable Technological Systems*, Pergamon Press, Oxford, pp.205–213.

Padiyar, K.R., and P.K. Kalra, (1986). Analysis of an HVDC converter with finite smoothing reactor, Part 1: Analysis of a six–pulse converter. *Electric Power Systems Research*, 11, pp. 171–184.

Park, R.H. (1928). Definition of an ideal synchronous machine and formula for the armature flux linkages, *General Electric Review*, 13(6), pp.332–334.

Ploeg, J. (1988). *Servo control of a wind turbine at partial load.* KEMA report APB–88–065, Arnhem, NL. (in Dutch).

Raina, G., and O.P. Malik (1985). Variable speed wind energy conversion using synchronous machine. *IEEE Trans. on Aerosp. Electron. Syst.*, AES–21(1), pp.100–105.

Richards, J.A. (1983). *Analysis of periodically time–varying systems.* Springer Verlag, Berlin.

Rosenbrock, H.H. (1974). Structural properties of linear dynamical systems. *Int. J. of Control*, 20(2), pp.191–202.

Stein, G. (1984). *Advances in multivariable control.* Lecture Notes of the ONR/Honeywell Workshop, Honeywell, Minnesota.

Stein, G. and J.C. Doyle (1978). Singular values and feedback: design examples. *Proc.16th Annual Allerton Conf. on Communication, Control and Computation*, Univ. of Illinois, Oct.1978, pp.460–471.

Steinbuch, M. (1986). Dynamic modelling and analysis of a wind turbine with variable speed. *Journal A*, 27(1), pp. 1–8.

Steinbuch, M. (1987). Optimal multivariable control of a wind turbine with variable speed. *Wind Engineering*, 11(3), pp.153– 163.

Steinbuch, M., W.W. de Boer, O.H. Bosgra, S.A.W.M. Peters and J. Ploeg, (1988). Optimal control of wind power plants. *Journal of Wind Engineering and Industrial Aerodynamics*, 27, pp. 237–246.

Steinbuch, M. and O.H. Bosgra, (1988). Optimal output feedback of a wind energy conversion system. *IFAC symposium on Power Systems, Modelling and Control, Sept.5–8, Brussels, 1988*, pp.11.2.1–11.2.7.

Steinbuch, M. and F. Meiring (1986). Analysis and simulation of a wind turbine with variable speed. *Kema Scientific & Technical Reports*, 4(7), pp. 71–78.

Tahk, M. and J.L. Speyer (1987). Modeling of parameter variations and asymptotic LQG synthesis. *IEEE Trans. on Autom. Control,* AC–32, pp.793–801.

Tarkanyi, M. (1981). Computer simulation of the JET generator–converter set. *GEC Journal of Science and Technology*, 47(1),pp.25–35

Terlouw, J.C. (1989). *Robustness analysis of multivariable control systems.* Report S–469, Delft Univ. of Technology.

Thompson,P.M., R.L. Dailey and J.C. Doyle (1986). New conic sectors for sampled–data feedback systems. *Systems and Control Letters*, 7, pp.395–404.

Tyler, J.S. (1964). The characteristics of model following systems as synthesized by optimal control. *IEEE Trans. on Autom. Control,* 1964, pp.485–499.

Verghese, G.C., M.E. Elbuluk and J.G. Kassakian, (1986). A general approach to sampled–data modeling for power electronic circuits. *IEEE Transactions on Power Electronics*, PE–1(2), pp. 76–89.

Verghese, G.C., M. Ilic–Spong and J.H. Lang, (1986). Modeling and control challenges in power electronics. *Proc. IEEE Conf. on Decision and Control*, pp.39–45., Publ.IEEE New York.

Verghese, G.C., B.C. Levy and T. Kailath (1981). A generalized state–space for singular systems. *IEEE Trans. on Autom. Control,* AC–26(4), pp.811–831.

Vorperian, V. and S. Cuk, (1983). Small signal analysis of resonant converters. Proc. *14th* IEEE *Power Electronics Specialists Conference 1983*, pp.269–282, Publ. IEEE New york.

Willems, J.L. (1970). *Stability theory of dynamical systems.* Nelson, London.

Yakubovich, V.A. and V.M. Starzhinskii (1975). *Linear differential equations with periodic coefficients.* John Wiley and Sons, New York.

Yedavalli, R.K. (1986). Dynamic compensator design for robust stability of linear uncertain systems. *Proc. IEEE Conf. on Decision and Control*, Athens, Greece, Dec.1986, Publ.IEEE, New York.

Yedavalli, R.K. and Z. Liang (1985). Reduced conservatism in the time domain stability robustness bounds by state transformation: application to aircraft control. *Guidance, Navigation and Control Conference*, Publ. AIAA.

Zadeh, L.A. and C.A. Desoer (1963). *Linear system theory.* McGraw–Hill Book Company, Inc. New York.

APPENDICES

A.1 NUMERICAL DATA

Aero–mechanical part.

$J_r = 350000$ kgm^2 $\quad C_1 = 1000$ Nm

$J_g = 32$ kgm^2 $\quad C_2 = 1000$ Nms/rad

$R = 15$ m $\quad C_3 = 100$ Nmrad/s

$\nu = 21.81$ $\quad k = 100$ Nms/rad

$\rho = 1.25$ kg/m^3 $\quad \tau_\beta = 0.2$ s (pitch servo)

$\tau_\omega = 0.1$ s (speed sensor).

Generator & DC link.

$L_d = 2.57$ pu $\quad L_q = 1.69$ pu

$L_{dc} = 0.719$ pu $\quad L_F = 2.53$ pu

$L_Q = 1.68$ pu $\quad L'' = 0.206$ pu

$L_D = 2.51$ pu $\quad L_{mq} = 1.54$ pu

$X_n = 0.0447$ pu $\quad L_{md} = 2.42$ pu

$R_s = 0.0159$ pu $\quad X_{basis} = 2.33\ \Omega$

$R_F = 0.0037$ pu $\quad R_Q = 0.0619$ pu

$R_{dc} = 0.006$ pu $\quad R_D = 0.0345$ pu

$p = 4$

$S_{nom} = 387500$ VA

$\omega_{nom} = 418.88$ rad/s

$\tau_F = 0.5$ s (field excitation system).

A.2 MEAN STEADY–STATE MODEL OF THE SYNCHRONOUS GENERATOR WITH DC LINK

For the analysis of the *mean* steady–state behaviour of synchronous machines with DC link, a lot of literature can be used. Especially, Anderson and Fouad [1982], Kimbark [1971] and Arrillaga et al. [1983] address the modelling of synchronous generators and HVDC transmission respectively. Also in Hoeymakers [1984] and Steinbuch [1986] several equations can be found.

For the synchronous machine, the d,q variables are constants in steady–state. Hence, setting di_k/dt for k=d,q,F,D,Q to zero, equation (3.3) reduces to:

$$u_d = -R_s i_d - \omega L_q i_q \quad (a.1)$$

$$u_q = -R_s i_q + \omega L_d i_d + \omega L_{md} i_F \quad (a.2)$$

$$u_F = R_F i_F \quad (a.3)$$

$$0 = R_D i_D \quad (a.4)$$

$$0 = R_Q i_Q \quad (a.5)$$

From the Park–transformation, the following formulas establish the relations between the d,q and three–phase stator variables:

$$i_d = -\sqrt{3} I_s \sin(\delta+\varphi) \qquad i_q = \sqrt{3} I_s \cos(\delta+\varphi) \quad (a.6)$$

$$u_d = -\sqrt{3} U_s \sin(\delta) \qquad u_q = \sqrt{3} U_s \cos(\delta) \quad (a.7)$$

with I_s and U_s the rms (root mean square) values of the alternating current and voltage of the machine terminals, with φ_s the phase angle between them. The angle δ is the load angle (torque angle [Anderson and Fouad, 1982]) which is the angle between the stator voltage and the induced voltage.

For the DC link the following equations describe the steady–state [Kimbark, 1971]:

$$U_{dc} = \frac{3\sqrt{6}}{\pi} U_s \cos(\alpha_r) - \frac{3}{\pi}\omega L'' I_{dc}, \quad \text{or}$$

$$U_s = \frac{\pi}{3\sqrt{6}} \cdot \frac{U_{dc}}{\cos(\alpha_r)} + \frac{\omega L'' I_{dc}}{\sqrt{6}\cos(\alpha_r)} \quad (a.8)$$

with $3\omega L''/\pi$ the equivalent commutating resistance with $L''=X_d''/\omega_{nom}$ the subtransient inductance of the synchronous generator. The steady–state value for the direct current i_{dc} is denoted with I_{dc}.

The phase relation for the rectifier is:

$$\cos(\varphi_s) = \{\cos(\alpha_r)+\cos(\alpha_r+\mu_r)\}/2 \quad (a.9)$$

with μ_r the commutation angle (in the notations of chapter 3: $\mu_r=t_1-t_0$).

For the current we have approximately:

$$I_s = \frac{\sqrt{6}}{\pi} I_{dc} \quad (a.10)$$

Finally, the DC link equation (3.8) becomes in steady–state:

$$R_{dc} I_{dc} = U_{dc} - u_i \quad (a.11)$$

Now it is possible to derive the set of equations describing the steady–state.

Substitute (a.4) and (a.5) into (3.7):

$$T_e = \{(L_d-L_q) i_d i_q + L_{md} i_q i_F\}/3 \quad (a.12)$$

Manipulating (a.6),(a.7) it is possible to prove that

$$u_d i_d + u_q i_q = 3 U_s I_s \cos(\varphi_s) \quad (a.13)$$

which is in accordance with the power–invariance of the Park–transformation

[Anderson and Fouad, 1982]. For the rectifier the energy balance yields:

$$I_{dc}U_{dc} = 3U_sI_s\cos(\varphi_s) \tag{a.14}$$

and with (a.11),(a.12):

$$u_di_d + u_qi_q = R_{dc}I_{dc}^2 + u_iI_{dc} \tag{a.15}$$

Substitution of (a.1),(a.2), eliminating u_d and u_q, gives:

$$R_{dc}I_{dc}^2 + u_iI_{dc} = -R_s(i_d^2+i_q^2) + \omega(L_d-L_q)i_di_q + \omega L_{md}i_Fi_q \tag{a.16}$$

and with (a.12):

$$R_{dc}I_{dc}^2 + u_iI_{dc} = -R_s(i_d^2+i_q^2) + 3\omega T_e \tag{a.17}$$

Squaring (a.6) gives $3I_s^2 = i_d^2+i_q^2$, and with (a.10) we get:

$$(R_{dc}+\frac{18}{\pi}R_s)I_{dc}^2 + u_iI_{dc} = 3\omega T_e \tag{a.18}$$

Using the necessary condition $I_{dc}\geq 0$, the following solution is obtained:

$$I_{dc} = \frac{-u_i}{2(R_{dc}+\frac{18}{\pi}R_s)} + \sqrt{\frac{\frac{1}{4}u_i^2R_{dc}+\frac{9}{2\pi}u_i^2R_s+3\omega T_e}{(R_{dc}+\frac{18}{\pi}R_s)}} \tag{a.19}$$

Given ω, T_e and u_i the current I_{dc} can thus be calculated. With (a.11) also U_{dc} is known and with (a.8) and (a.10) we get U_s and I_s. Then using (a.14) we get φ_s and with (a.9) we obtain μ_r.

Substitution of (a.6) and (a.7) into (a.1) yields:

$$-U_s\sin(\delta) = R_sI_s\sin(\delta+\varphi_s)-\omega L_qI_s\cos(\delta+\varphi_s) \quad \Leftrightarrow$$

$$\tan(\delta) = \frac{\omega L_q - R_s\tan(\varphi_s)}{R_s+\omega L_q\tan(\varphi_s)+U_s/(I_s\cos(\varphi_s))} \tag{a.20}$$

And using the calculated U_s,I_s,φ_s we obtain a value for the load angle δ of the machine. Then with (a.10),(a.6),(a.7) we get i_d,i_q,u_d,i_q. With (a.2) we obtain i_F using:

$$i_F = \frac{u_q+R_si_q-\omega L_di_d}{\omega L_{md}} \tag{a.21}$$

Finally, with (a.3) the field voltage u_F can be calculated.

For the angle θ as defined in figure 3.2 we have the relation [Anderson and Fouad, 1982]:

$$\theta = \delta + \alpha_r + \pi/6 \tag{a.22}$$

with which $\theta_0=\theta$ can be calculated.

This completes the derivation of the mean steady–state model for the synchronous machine with rectifier load.

A.3 LINEARIZATION OF THE AERO–MECHANICAL MODEL

First let us recall that the inputs of the aero–mechanical subsystem are v, β_r and T_e, and the outputs are ω_{gm}, ω_r and T_m. We start the linearization with the differential equation (4.5), which is almost linear (in the sequel we denote the variations of the original value x with δx). First order Taylor expansion of (4.5) and subtracting the static values yields:

$$\delta\ddot{\xi} = \frac{\nu}{J_r}\delta T_r - \frac{\nu}{J_r}\delta T_D + \frac{1}{J_g}\delta T_e - \frac{k}{J_v}\delta\dot{\xi} - \frac{1}{J_v}\delta T_\xi, \tag{a.23}$$

and we must calculate δT_r, δT_D, and δT_ξ. The variable δT_e follows from the electrical model.

For the rotor torque we have with (4.1) and (4.4):

$$T_r = P_r/\omega_r = C_p(\lambda,\beta)\cdot\tfrac{1}{2}\rho\pi R^2\cdot v^3/\omega_r \tag{a.24}$$

Linearization gives:

$$\delta T_r = \frac{\partial T_r}{\partial\omega_r}\delta\omega_r + \frac{\partial T_r}{\partial\beta}\delta\beta + \frac{\partial T_r}{\partial v}\delta v \tag{a.25}$$

and for the partial derivatives we find

$$\frac{\partial T_r}{\partial\omega_r} = -C_p\cdot\frac{\pi\rho R^2v^3}{2\omega_r^2} + \frac{\partial C_p}{\partial\lambda}\cdot\frac{\partial\lambda}{\partial\omega_r}\cdot\frac{\pi\rho R^2v^3}{2\omega_r}$$

with (4.2):

$$\frac{\partial\lambda}{\partial\omega_r} = \frac{R}{v} \tag{a.26}$$

we get

$$\frac{\partial T_r}{\partial\omega_r} = -C_p\cdot\frac{\pi\rho R^2v^3}{2\omega_r^2} + \frac{\partial C_p}{\partial\lambda}\cdot\frac{\pi\rho R^3v^2}{2\omega_r} \tag{a.27}$$

also

$$\frac{\partial T_r}{\partial\beta} = \frac{\partial C_p}{\partial\beta}\cdot\frac{\pi\rho R^2v^3}{2\omega_r} \tag{a.28}$$

and

$$\frac{\partial T_r}{\partial v} = C_p\cdot\frac{3\pi\rho R^2v^2}{2\omega_r} + \frac{\partial C_p}{\partial\lambda}\cdot\frac{\partial\lambda}{\partial v}\cdot\frac{\pi\rho R^2v^3}{2\omega_r}$$

and with

$$\frac{\partial\lambda}{\partial v} = -\frac{\omega_rR}{v^2} \tag{a.29}$$

we find

$$\frac{\partial T_r}{\partial v} = C_p\cdot\frac{3\pi\rho R^2v^2}{2\omega_r} - \frac{\partial C_p}{\partial\lambda}\cdot\frac{\pi\rho R^3v}{2} \tag{a.30}$$

For the friction torque T_D the linear form of (4.7) is

$$\delta T_D = \frac{\partial T_D}{\partial \omega_r}\delta\omega_r = (-C_2/\omega_r^2 + C_3)\delta\omega_r \qquad (a.31)$$

And finally for the drive train stiffness T_ξ we get with (4.6):

$$\delta T_\xi = \frac{\partial T_\xi}{\partial \xi}\delta\xi = (300\xi^2 - 40\xi + 2)10^4 \cdot \delta\xi \qquad (a.32)$$

Substituting the expressions (a.25),(a.31) and (a.32) into (a.23) we obtain

$$\begin{aligned}\ddot{\delta\xi} = &-\frac{1}{J_v}(300\xi^2 - 40\xi + 2)10^4 \cdot \delta\xi - \frac{k}{J_v}\dot{\delta\xi} + \\ &\frac{\nu}{J_r}\left\{-C_p\frac{\pi\rho R^2 v^3}{2\omega_r^2} + \frac{\partial C_p}{\partial\lambda}\cdot\frac{\pi\rho R^3 v^2}{2\omega_r} + C_2/\omega_r^2 - C_3\right\}\delta\omega_r + \\ &\frac{\partial C_p}{\partial\beta}\cdot\frac{\nu\pi\rho R^2 v^3}{2J_r\omega_r}\delta\beta + \frac{\nu}{J_r}\left\{C_p\frac{3\pi\rho R^2 v^2}{2\omega_r} - \frac{\partial C_p}{\partial\lambda}\cdot\frac{\pi\rho R^3 v}{2}\right\}\delta v + \frac{1}{J_g}\delta T_e \qquad (a.33)\end{aligned}$$

Next we take the variational version of (4.10):

$$\delta\omega_r = (\dot{\delta\xi} + \delta\omega_g)/\nu \qquad (a.34)$$

Substitution of this relation into (a.33) gives an equation which can be recognized in the state space model (4.15); see coefficients a_{31}–a_{34},a_{37}–a_{30} and e_{31}.

For the other mechanical differential equation (4.8) the linear model is:

$$J_g\dot{\delta\omega}_g = \frac{\partial T_\xi}{\partial\xi}\delta\xi + k\dot{\delta\xi} - \delta T_e, \qquad (a.35)$$

with $\partial T_\xi/\partial\xi$ from (a.32). See coefficients a_{42},a_{43},a_{47}–a_{40} in (4.15).

Finally, the output equation (4.11) for the mechanical torque is in its linearized form:

$$\delta T_m = k\dot{\delta\xi} + \frac{\partial T_\xi}{\partial\xi}\delta\xi \qquad (a.36)$$

see coefficients c_{42},c_{43}.

The other relations (4.3),(a.34),(4.12)–(4.14) can directly be used in the state space model (4.15). For convenience, in the model (4.15) and further, the steady state values of variables (x) are denoted with a bar ($\bar{x}$) and the variations with their original symbol (x).

A.4 LINEAR MODEL OF THE WIND TURBINE SYSTEM

Dimensions of the variables:

β_r,β	rad
u_{Fr},u_F	1000*pu (rotor units)
α_r	rad
v	m/s
u_i	pu = 577 V
ξ	rad
$\dot{\xi}$	rad/s
ω_g	rad/s
ω_{gm}	pu = 418.88 rad/s
i_{dc}	pu = 228 A
i_F,i_D,i_Q	pu (rotor units)
ω_r	rad/s
T_m	pu = 3600 Nm

The linear state space model (4.15) has the following parameters:

$$a_{11} = -1/\tau_\beta$$

$$a_{31} = \frac{\partial C_p}{\partial\beta}\cdot\frac{\nu\pi\rho R^2 v^3}{2J_r\omega_r}$$

$$a_{32} = (-300\xi^2 + 40\xi - 2)10^4/Jv$$

$$a_{33} = \frac{-k}{J_v} + \frac{\partial C_p}{\partial\lambda}\cdot\frac{\pi\rho R^3 v^2}{2J_r\omega_r} - C_p\cdot\frac{\pi\rho R^2 v^3}{2J_r\omega_r^2} + \frac{C_2}{J_r\omega_r^2} - \frac{C_3}{J_r}$$

$$a_{34} = \frac{\partial C_p}{\partial\lambda}\cdot\frac{\pi\rho R^3 v^2}{2J_r\omega_r} - C_p\cdot\frac{\pi\rho R^2 v^3}{2J_r\omega_r^2} + \frac{C_2}{J_r\omega_r^2} - \frac{C_3}{J_r}$$

$$[a_{37}\ a_{38}\ a_{39}\ a_{30}] = \frac{T_B}{J_g}\cdot C^e_{T_e}$$

$$a_{42} = (300\xi^2 - 40\xi + 2)10^4/J_g$$

$$a_{43} = k/J_g$$

$$[a_{47}\ a_{48}\ a_{49}\ a_{40}] = -\frac{T_B}{J_g}\cdot C^e_{T_e}$$

$$a_{54} = p/(\tau_\omega\omega_{nom})$$

$$a_{55} = -1/\tau_\omega$$

$$a_{66} = -1/\tau_F$$

$$[a_{74}\ a_{84}\ a_{94}\ a_{04}]^T = \frac{p}{\omega_{nom}}B^e_\omega$$

$$[a_{76}\ a_{86}\ a_{96}\ a_{06}]^T = B^e_{u_F}/1000$$

$$\begin{bmatrix} a_{77} & \cdots & a_{70} \\ a_{87} & \cdots & a_{80} \\ \vdots & \ddots & \vdots \\ a_{07} & \cdots & a_{00} \end{bmatrix} = A^e$$

$$b_{11} = 1/\tau_\beta$$

$$b_{62} = 1/\tau_F$$

$$[b_{73}\ b_{83}\ b_{93}\ b_{03}]^T = B^e_{\alpha_r}$$

$$c_{33} = 1/\nu$$

$$c_{34} = 1/\nu$$

$$c_{42} = (300\xi^2 - 40\xi + 2)10^4/T_B$$

$$c_{43} = k/T_B$$

$$e_{31} = C_p \cdot \frac{3\nu\pi\rho R^2 v^2}{2J_r\omega_r} - \frac{\partial C_p}{\partial\lambda} \cdot \frac{\nu\pi\rho R^3 v}{2J_r}$$

$$[e_{72}\ e_{82}\ e_{92}\ e_{02}]^T = B^e_{u_i}$$

with A^e the continuous–time approximate linear model according to section 3.6.3, and with $B^e_\omega, B^e_{u_F}, B^e_{\alpha_r}, B^e_{u_i}$ the appropriate columns of the related input matrix, and with $C^e_{T_e}$ the output matrix for the electrical torque.

A.5 LINEAR MODELS IN THREE OPERATING POINTS

v=12 m/s:

$$A = \begin{bmatrix}
-5.0000e{+}00 & 0 & 0 & 0 & 0 \\
0 & 0 & 1.0000e{+}00 & 0 & 0 \\
-5.5005e{+}00 & -1.4791e{+}03 & -3.2812e{+}00 & -1.7889e{-}02 & 0 \\
0 & 1.4164e{+}03 & 3.1250e{+}00 & 0 & 0 \\
0 & 0 & 0 & 9.5493e{-}02 & -1.0000e{+}01 \\
0 & 0 & 0 & 0 & 0 \\
0 & 0 & 0 & 7.8416e{+}00 & 0 \\
0 & 0 & 0 & 4.6042e{+}00 & 0 \\
0 & 0 & 0 & 5.7968e{+}00 & 0 \\
0 & 0 & 0 & -2.8663e{+}00 & 0
\end{bmatrix}$$

$$\begin{bmatrix}
0 & 0 & 0 & 0 & 0 \\
0 & 0 & 0 & 0 & 0 \\
0 & 1.6968e{+}02 & 3.6137e{+}01 & 3.6137e{+}01 & 1.4483e{+}02 \\
0 & -1.6968e{+}02 & -3.6137e{+}01 & -3.6137e{+}01 & -1.4483e{+}02 \\
0 & 0 & 0 & 0 & 0 \\
-1.0000e{+}01 & 0 & 0 & 0 & 0 \\
1.1552e{-}01 & -1.2571e{+}03 & 1.0151e{+}03 & 1.0111e{+}03 & 4.9909e{+}02 \\
2.0960e{+}00 & -6.9313e{+}02 & 5.5933e{+}02 & 6.3131e{+}02 & 3.0618e{+}02 \\
-1.8671e{+}00 & -9.7681e{+}02 & 7.8851e{+}02 & 7.0825e{+}02 & 3.5508e{+}02 \\
-4.7856e{-}02 & 4.1358e{+}02 & -3.4335e{+}02 & -3.4163e{+}02 & -2.1245e{+}02
\end{bmatrix}$$

$$B = \begin{bmatrix}
5.0000e{+}00 & 0 & 0 \\
0 & 0 & 0 \\
0 & 0 & 0 \\
0 & 0 & 0 \\
0 & 0 & 0 \\
0 & 1.0000e{+}01 & 0 \\
0 & 0 & -3.0565e{+}02 \\
0 & 0 & -1.6627e{+}02 \\
0 & 0 & -2.3988e{+}02 \\
0 & 0 & 9.6020e{+}01
\end{bmatrix}$$

$$C = \begin{bmatrix}
0 & 0 & 0 & 0 & 1 & 0 & 0 & 0 & 0 & 0 \\
0 & 0 & 0 & 0 & 0 & 0 & 1 & 0 & 0 & 0 \\
0 & 0 & 4.5455e{-}02 & 4.5455e{-}02 & 0 & 0 & 0 & 0 & 0 & 0 \\
0 & 1.2249e{+}01 & 2.7025e{-}02 & 0 & 0 & 0 & 0 & 0 & 0 & 0
\end{bmatrix}$$

$$E = \begin{bmatrix}
0 & 0 \\
0 & 0 \\
8.1083e{-}01 & 0 \\
0 & 0 \\
0 & 0 \\
0 & 0 \\
0 & -4.0820e{+}02 \\
0 & -2.3953e{+}02 \\
0 & -3.0191e{+}02 \\
0 & 1.4907e{+}02
\end{bmatrix}$$

v=16 m/s:

$$A(3:4,1:4) = \begin{bmatrix} -3.3690e+01 & -1.4791e+03 & -3.3531e+00 & -8.9802e-02 \\ 0 & 1.4164e+03 & 3.1250e+00 & 0 \end{bmatrix}$$

Rest of A as for v=12 m/s.
B,C as for v=12 m/s.

$$E(3,1) = [1.1127]$$

Rest of E as for v=12 m/s.

v=20 m/s:

$$A(3:4,1:4) = \begin{bmatrix} -7.0878e+01 & -1.4791e+03 & -3.4321e+00 & -1.6877e-01 \\ 0 & 1.4164e+03 & 3.1250e+00 & 0 \end{bmatrix}$$

Rest of A as for v=12 m/s.
B,C as for v=12 m/s.

$$E(3,1) = [1.3043]$$

Rest of E as for v=12 m/s.

A.6 LQ STATE FEEDBACK PARAMETERS

Weighting parameters:
States:

β: 1 ξ: 0 $d\xi/dt$: 10 ω_g: 0.1 ω_{gm}: 0
u_{Fr}: 10 i_{dc}: 10 i_F: 0.1 i_D: 0 i_Q: 0 $\int\omega_{gm}$: 1000
$\int i_{dc}$: 500 $\int\alpha_r$: 1000

Inputs:

β_r: 10 u_F: 0.001 α_r: 0.0004

uncontrolled	LQR
–7.7583e+01+ 3.2414e+01j	–4.8400e+04
–7.7583e+01– 3.2414e+01j	–1.0000e+03
–9.2608e+00+ 3.8899e+01j	–1.6381e+02
–9.2608e+00– 3.8899e+01j	–7.5876e+01
–1.5789e+01+ 1.0922e+01j	–6.0320e+01
–1.5789e+01– 1.0922e+01j	–6.8837e+00+ 3.6748e+00j
–5.8998e–02	–6.8837e+00– 3.6748e+00j
–5.0000e+00	–3.7465e+00+ 9.1757e–01j
–1.0000e+01	–3.7465e+00– 9.1757e–01j
–1.0000e+01	–9.9963e+00
0	–7.2687e–01+ 4.7566e–01j
0	–7.2687e–01– 4.7566e–01j
0	–1.0571e+00

Table A.1 Eigenvalues uncontrolled and with LQ state feedback.

LQR=

$$\begin{bmatrix} 7.2369e-01 & 7.5047e-01 & -1.3888e-01 & -1.3932e-01 & -9.8803e-01 & -4.6561e-05 \\ -9.3123e-01 & -1.8777e+01 & 2.1135e-01 & 1.4358e-01 & -1.2860e+01 & 9.9078e+01 \\ 2.7721e+00 & -7.6823e+02 & -1.5526e+02 & -5.9213e-01 & -1.6968e+00 & 3.1395e-02 \end{bmatrix}$$

$$\begin{matrix} 4.0537e-01 & -3.1477e-01 & -3.0307e-01 & -9.4377e-03 \\ -6.3168e+02 & 4.8685e+02 & 4.6840e+02 & 6.1562e-01 \\ -4.2866e+02 & 1.8987e+02 & 1.8242e+02 & -7.6508e+01 \end{matrix}$$

$$\begin{bmatrix} -9.9165e+00 & -4.1513e-01 & -2.2959e-01 \\ -1.2867e+02 & 3.5941e+02 & 1.7031e+02 \\ -1.3213e+01 & -9.6061e+02 & 1.6178e+02 \end{bmatrix}$$

A.7 LQOF PARAMETERS

$$\mathrm{LQOF}_1=\begin{bmatrix} 8.7571e{+}00 & 1.1612e{+}00 & 5.1452e{+}00 & 5.0058e{-}01 & 0 \\ 0 & 0 & 0 & -2.0380e{+}00 & -5.0284e{-}01 \\ 1.6995e{-}02 & 2.7198e{+}00 & 6.6130e{-}02 & 1.1096e{+}00 & 0 \end{bmatrix}$$

$$\mathrm{LQOF}_2=\begin{bmatrix} 1.9287e{+}01 & 2.4764e{-}02 & 3.2197e{+}00 & 1.0305e{+}00 & 0 \\ 0 & 0 & 0 & -8.7807e{+}00 & -5.8699e{-}01 \\ -3.2156e{+}01 & 1.5738e{+}00 & -4.2927e{+}00 & 7.3407e{+}00 & 0 \end{bmatrix}$$

$$\mathrm{LQOF}_3=\begin{bmatrix} 9.9117e{+}00 & -1.6342e{-}01 & 4.8788e{+}00 & 1.1338e{+}00 & 0 \\ 0 & 0 & 0 & -5.2720e{+}00 & -5.6782e{-}01 \\ 1.2443e{-}01 & 1.9859e{+}00 & 2.4729e{-}01 & 4.4029e{+}00 & 0 \end{bmatrix}$$

$$\mathrm{LQOF}_4=\begin{bmatrix} 9.6753e{+}00 & 2.8514e{-}01 & 5.1169e{+}00 & 4.1462e{-}01 & 6.9450e{-}02 \\ 3.2004e{+}00 & -2.5161e{+}00 & 1.1369e{+}00 & -4.2989e{+}00 & 2.3438e{-}01 \\ -2.9156e{+}00 & 2.9360e{+}00 & -1.0926e{+}00 & 4.0550e{+}00 & -9.8798e{-}01 \end{bmatrix}$$

$$\mathrm{LQOF}_5=\begin{bmatrix} 9.6452e{+}01 & -1.2992e{+}00 & 4.6673e{+}00 & 7.2193e{-}01 & 0 \\ 0 & 0 & 0 & -2.8844e{+}00 & -5.6732e{-}01 \\ -6.9902e{+}01 & 1.9416e{+}00 & -3.9539e{-}02 & 1.5191e{+}00 & 0 \\ 8.0604e{+}02 & -8.6821e{+}00 & 0 & 0 & 0 \\ 5.4041e{+}02 & -7.7175e{+}00 & 0 & 0 & 0 \end{bmatrix}$$

$$\begin{bmatrix} -1.7795e{+}00 & -7.4431e{+}00 & 0 & 0 \\ 0 & 0 & 0 & 0 \\ 2.5918e{+}00 & 5.8080e{+}00 & 0 & 0 \\ -4.0090e{+}01 & -6.6476e{+}01 & 0 & 0 \\ 1.4325e{+}01 & -4.8641e{+}01 & 0 & 0 \end{bmatrix}$$

$$\mathrm{LQOF}_6=\begin{bmatrix} 2.4299e{+}00 & -7.2715e{-}02 & 4.1445e{+}00 & 3.0989e{-}01 & 0 \\ 0 & 0 & 0 & -2.4298e{+}00 & -5.5227e{-}01 \\ -7.3454e{+}01 & 1.9166e{+}00 & 3.9949e{-}01 & 1.2283e{+}00 & 0 \\ 8.0545e{+}02 & -6.9321e{+}00 & 0 & 0 & 0 \\ 5.4016e{+}02 & -7.9252e{+}00 & 0 & 0 & 0 \end{bmatrix}$$

$$\begin{bmatrix} 4.3544e{-}01 & 2.7349e{-}01 & 0 & 0 \\ 0 & 0 & 0 & 0 \\ 6.4678e{+}00 & 5.4440e{+}00 & 0 & 0 \\ -5.6282e{+}01 & -6.1294e{+}01 & 0 & 0 \\ -3.3025e{+}01 & -4.1773e{+}01 & 0 & 0 \end{bmatrix}$$

$$\mathrm{LQOF}_7=\begin{bmatrix} 2.6700e{+}00 & 0 & 3.5274e{+}00 & 0 & 0 \\ 0 & 0 & 0 & 0 & -6.4628e{-}01 \\ -7.5824e{+}01 & 1.1720e{+}00 & 0 & 6.6487e{-}01 & 0 \\ 8.5254e{+}02 & 0 & 0 & 0 & 0 \\ 5.2492e{+}02 & -5.8107e{+}00 & 0 & 0 & 0 \end{bmatrix}$$

$$\begin{bmatrix} 7.1156e{-}01 & 0 & 0 & 0 \\ 0 & 0 & 0 & 0 \\ 9.1279e{+}01 & 0 & 0 & 0 \\ -8.7135e{+}01 & -7.6812e{+}00 & 0 & 0 \\ -5.1703e{+}01 & -5.6342e{+}00 & 0 & 0 \end{bmatrix}$$

$$\mathrm{LQOF}_8=\begin{bmatrix} 9.6452e{+}00 & 0 & 4.6673e{+}00 & 0 & 0 \\ 0 & 0 & 0 & 0 & -5.6732e{-}01 \\ -6.9902e{+}01 & 1.9416e{+}00 & 0 & 1.5191e{+}00 & 0 \\ 8.0604e{+}02 & 0 & 0 & 0 & 0 \\ 5.4041e{+}02 & -7.7175e{+}00 & 0 & 0 & 0 \end{bmatrix}$$

$$\begin{bmatrix} 1.7795e{+}00 & 0 & 0 & 0 \\ 0 & 0 & 0 & 0 \\ 2.5918e{+}00 & 0 & 0 & 0 \\ -4.0090e{+}01 & -6.6476e{+}01 & 0 & 0 \\ 1.4325e{+}01 & -4.8641e{+}01 & 0 & 0 \end{bmatrix}$$

$$\mathrm{LQOF}_9=\begin{bmatrix} 5.2488e{+}00 & 0 & 2.6605e{+}00 & 0 & 0 \\ 0 & 0 & 0 & 0 & -9.7487e{-}01 \\ 0 & 0 & 0 & 0 & 0 \\ 4.4921e{+}02 & 0 & 0 & 0 & 0 \\ -1.4064e{+}01 & -2.7250e{+}00 & 0 & 0 & 0 \\ -6.7232e{+}00 & 5.2783e{-}01 & 0 & 4.2026e{-}01 & 0 \\ 0 & 0 & 0 & 0 & 0 \end{bmatrix}$$

$$\begin{bmatrix} 2.1367e{-}01 & 0 & 0 & 0 & 0 & 0 \\ 0 & 0 & 0 & 0 & 0 & 0 \\ 0 & 0 & 0 & 0 & 0 & 5.0000e{+}02 \\ -2.6456e{+}01 & -2.3383e{+}01 & 0 & 0 & 0 & 0 \\ 2.8745e{+}00 & 2.4480e{-}01 & 0 & 0 & 0 & 0 \\ 1.6872e{+}00 & 0 & 0 & 0 & -6.2832e{+}02 & 0 \\ 0 & 0 & 0 & 0 & 6.2832e{+}02 & -5.0000e{+}02 \end{bmatrix}$$

A.8 STEP RESPONSES FOR $LQOF_9$

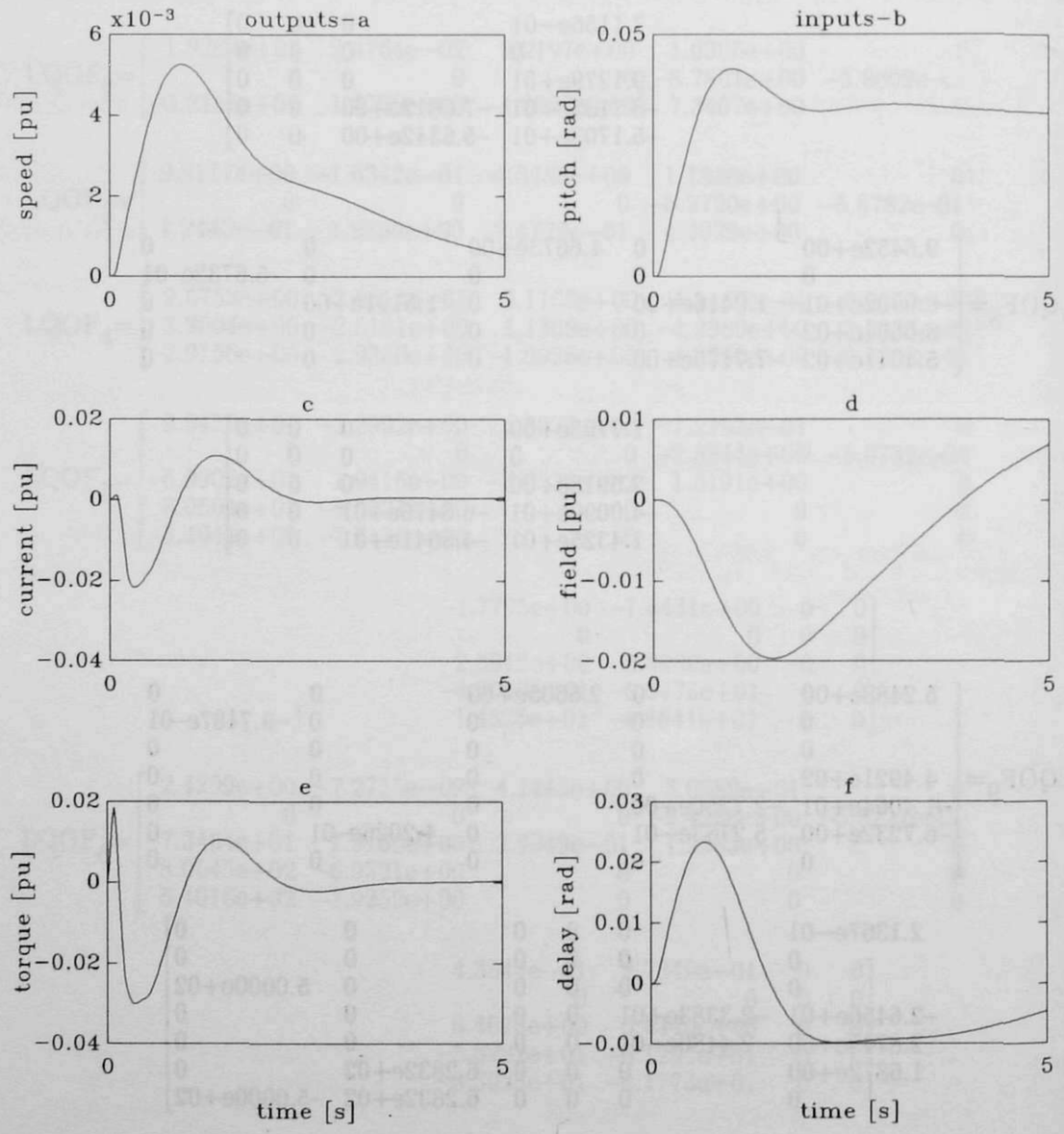

Figure A.1 Step responses of the wind turbine at a step in wind speed with the dynamic output feedback $LQOF_9$.

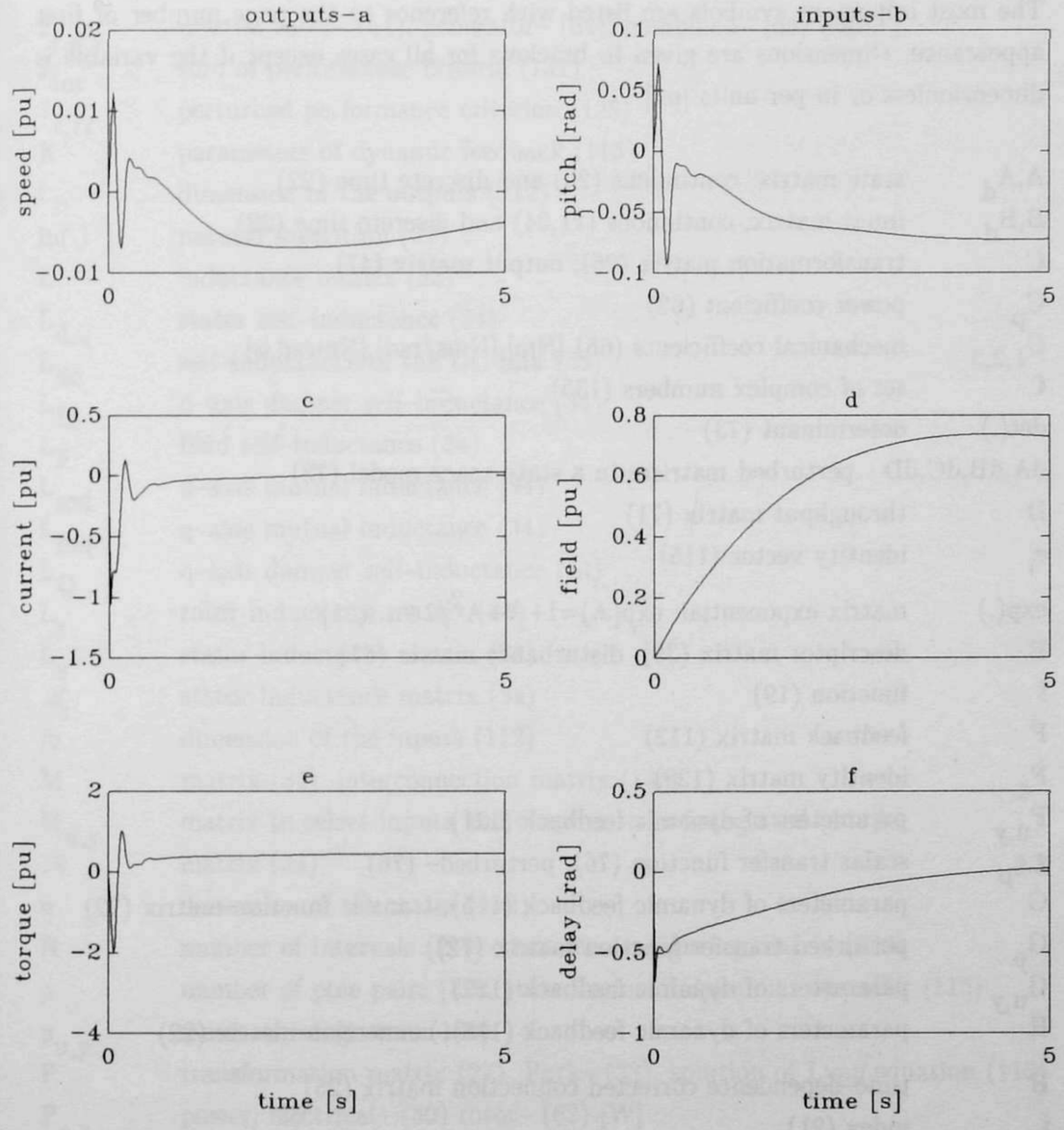

Figure A.2 Step responses of the wind turbine at a step in grid voltage with the dynamic output feedback $LQOF_9$.

LIST OF SYMBOLS

The most important symbols are listed with reference to the page number of first appearance. Dimensions are given in brackets for all cases except if the variable is dimensionless or in per units [pu].

A, A_d	state matrix, continuous (20) and discrete time (22)
B, B_d	input matrix, continuous (21,34) and discrete time (22)
C	transformation matrix (26), output matrix (47)
C_p	power coefficient (62)
$C_{1,2,3}$	mechanical coefficients (65) [Nm],[Nms/rad],[Nmrad/s]
$\mathbb{C}$	set of complex numbers (135)
det(.)	determinant (73)
dA,dB,dC,dD	perturbed matrices in a state space model (73)
D	throughput matrix (71)
e_i	identity vector (115)
exp(.)	matrix exponential: $\exp(A)=I+A+A^2/2+...$ (21)
E	descriptor matrix (39), disturbance matrix (67)
f	function (19)
F	feedback matrix (112)
F_e	identity matrix (128)
$F_{u,y}$	parameters of dynamic feedback (121)
g, g_p	scalar transfer function (76), perturbed– (76)
G	parameters of dynamic feedback (115), transfer function matrix (72)
G_p	perturbed transfer function matrix (72)
$G_{u,y}$	parameters of dynamic feedback (122)
H	parameters of dynamic feedback (115), connection matrix (22)
$\hat{H}$	time–dependence corrected connection matrix (25)
i	index (21)
$i_{a,b,c}$	phase currents (33)
$i_{d,q}$	stator currents in rotor coordinates (33)
i_{dc}	direct current (35)
i_D	d–axis damper current (32)
i_F	field current (15), reference (67)
i_Q	q–axis damper current (32)
i_ϵ	commutation current (37)
I	identity matrix (20)

j	index (21), imaginary value (53)
J	performance criterion (112)
$J_{r,g,v}$	inertia, rotor– (64), generator– (64), combined– (65) [kgm^2]
J_{tot}	sum of performance criteria (131)
$J_{\epsilon,\epsilon\epsilon}$	perturbed performance criterion (128)
K	parameters of dynamic feedback (115)
l	dimension of the outputs (112)
ln(.)	natural logarithm (27)
L	inductance matrix (33)
$L_{d,q}$	stator self–inductance (34)
L_{dc}	self–inductance of the DC link (35)
L_D	d–axis damper self–inductance (34)
L_F	field self–inductance (34)
L_{md}	d–axis mutual inductance (34)
L_{mq}	q–axis mutual inductance (34)
L_Q	q–axis damper self–inductance (34)
L_r	rotor inductance matrix (34)
L_s	stator inductance matrix (34)
$\mathscr{L}_s$	stator inductance matrix (34)
m	dimension of the inputs (112)
M	matrix (34), interconnection matrix (135)
$M_{u,y}$	matrix to select inputs and outputs to be integrated (119)
$\mathscr{M}$	matrix (34)
n	dimension of the states (112)
N	number of intervals (21), cross–term weighting matrix (123)
p	number of pole pairs (32), state vector of dynamic controller (115)
$p_{u,y}$	states of integrators (120)
P	transformation matrix (27), Park– (33), solution of Lyap.equation (113)
$P_{e,r}$	power, electrical– (50) rotor– (62) [W]
$P_{\epsilon,\epsilon\epsilon}$	perturbed solution of Lyap.equation (128)
$q, q_{x,u}$	dimension of the controller states (115), order weighting filters (125)
Q	matrix (22), weighting matrix (112)
$Q_{x,u}$	weighting matrices of filtered states and inputs (130)
r	number of models (130)
R	matrix (27), resistance– (34), radius (62) [m], weighting matrix (112)
$R_{d,q}$	stator resistance (34)
R_{dc}	resistance of the DC link (35)

R_D	d–axis damper resistance (34)
$Re(.)$	real part (112)
R_F	field resistance (34)
R_Q	q–axis damper resistance (34)
R_r	rotor resistance matrix (34)
R_s	stator resistance matrix (34)
$\mathbb{R}$	set of real numbers (77)
s	Laplace variable (72)
S	switching matrix (38), solution of Lyapunov equation (113)
S_{nom}	nominal electrical power (67) [VA]
$S_{1,2}$	scaling matrices (89)
$\mathscr{S}$	derivative of switching matrix (39)
$\mathscr{S}_{F,Fc}, \mathscr{S}_0$	set of stabilizing feedback matrices (112,116), set of zero entries (116)
t,t_0	time (19) [s, pu], initial time (20)
tr(.)	trace operator (114)
T	period (25), switching matrix (37)
T_B	basis torque (67) [Nm]
T_D	damping torque (66) [Nm]
T_m	mechanical torque in the secondary shaft (66) [Nm, pu]
T_e	electro–mechanical torque (16,35)
T_r	rotor torque (61) [Nm]
T_ξ	static axis torque (66) [Nm]
$T_{1,2.}$	thyristor number (35)
u	input vector (20)
$u_{a,b,c}$	phase voltages (33)
$u_{d,q}$	stator voltages in rotor co–ordinates (33)
u_{dc}	direct voltage (35)
u_F, u_{Fr}	field voltage (15), reference (67)
u_i	inverter voltage (16), inputs to be integrated (119)
u_p	inputs of the dynamics of the compensator (116)
u_w	filtered inputs (125)
v	wind speed (61) [m/s], uncertainty outputs (71)
V	matrix (42,71)
w	uncertainty inputs (71)
w_i	weighting scalars of performance criteria (131)
W	matrix (42,71)
x,x_0	state vector (19), initial values (19)

x_w	filtered states (125)
X	matrix of initial states (113)
y	averaged solution (28), output vector (67)
z	state vector of uncertainty model (71)
$z_{x,u}$	state vector of weighting filters (124,125)

Greek

α_r	delay angle of the rectifier (16) [rad]
β,β_r	pitch angle (61) , reference– (64) [rad]
δ	scalar value (91)
Δ	uncertainty matrix or scalar (72–84)
$\Delta.$	variation (20)
ΔT	time interval (21) [s]
ϵ	element of (112), (128)
θ	rotor angle (32), [rad]
λ	eigenvalue (28,51) [1/s], speed ratio (63)
μ	structured singular value (135)
μ_r	commutation angle (35) [rad]
ν	gear ratio (64)
ξ	angular torsion of the secondary shaft (65) [rad]
ρ	air density (62) [kg/m^3]
σ,σ_H	singular value (73), Hankel– (106)
τ_F,τ_{Fp}	field exciter time constant (67), perturbed– (80) [1/s]
τ_α	delay angle time constant (81) [1/s]
$\tau_\beta,\tau_{\beta p}$	pitch angle servo time constant (64), perturbed– (76) [1/s]
τ_ω	speed sensor time constant (66) [1/s]
ϕ	state transition matrix (20,27), empty set (112)
ω	electrical normalized speed (32), frequency (77) [rad/s]
ω_g,ω_{gm}	generator speed (32) [rad/s], measured– (66)
ω_{nom}	nominal generator frequency (32) [rad/s]
ω_r	rotor speed (61) [rad/s]
$\partial.$	differential (19)

Abbreviations

CCC	constant current control (106)
det	determinant (73)
diag	diagonal matrix
DC	direct current (15)
inf	infimum (136)
LQ	linear quadratic (111)
LQG	linear quadratic gaussian (108)
LQOF	linear quadratic output feedback (111)
re	real part (112)
sup	supremum (136)
tr	trace (114)
ZOH	zero order hold (85)

SAMENVATTING

De toepassing van windenergie conversie systemen voor de produktie van elektrische energie vereist een betrouwbare en goedkope bedrijfsvoering. Vooral bij hoge windsnelheden zijn de mechanische belastingen van windturbine installaties groot als gevolg van verstoringen vanuit het windveld. Ook fluctuaties van de netspanning kunnen hoge dynamische belastingen tot gevolg hebben. Teneinde een lange levensduur en een grote betrouwbaarheid te garanderen is het noodzakelijk hoogwaardige regelsystemen toe te passen.
Het doel van de in dit proefschrift beschreven studie is om voor een windturbine met variabel toerental een aanpak te ontwikkelen voor het ontwerp van dergelijke hoogwaardige en betrouwbare regelsystemen.

Het onderhavige windturbine systeem bestaat uit een drie–bladige rotor welke via een overbrenging is verbonden met de generator. Het elektrische conversie systeem bestaat uit een synchrone generator met gelijkstroomtussenkring. Op het systeem kan worden ingegrepen via de bladhoek, de veldspanning van de generator en via de ontsteekhoek van de gelijkrichter. Zowel het generator toerental als de gelijkstroom worden gemeten.
Het regelprobleem bij vollast is geformuleerd als het minimaliseren van fluctuaties in toerental en gelijkstroom, waarbij de (vermoeiings–) belasting dient te worden beperkt. De regeling moet dit realiseren zonder al te grote variaties in de ingangssignalen, en dient bovendien eenvoudig implementeerbaar te zijn.

Ten behoeve van het ontwerp van een hoogwaardige regeling is de modelvorming van groot belang. Hierbij gaat de aandacht vooral uit naar het elektrische conversie systeem. De schakelende thyristoren van de gelijkrichterbrug veroorzaken een hoogfrequent periodiek gedrag. Ten behoeve van het regelaar ontwerp is hiervan een middelend model afgeleid, en wel door toepassing van de Floquet theorie voor periodieke systemen.
De eigenschappen van de aerodynamische overdracht en van de aandrijving zijn zeer benaderend gemodelleerd. De mogelijke verschillen tussen de nominale modellen en het werkelijke systeemgedrag zijn beschreven door middel van norm–begrensde onzekerheidsmodellen. Op basis van het nominale model en de onzekerheidsmodellen is de regeling ontworpen.

Het regelprobleem leent zich zeer goed voor toepassing van de Lineair Quadratische ontwerpmethode. Echter in plaats van de gebruikelijke toepassing van waarnemers, is de optimaliseringstheorie toegepast binnen een voorgeschreven regelaarstruktuur. Hierdoor kan de keuze van orde en structuur van de terugkoppeling worden ondergebracht in de probleemstelling. De toepassing op het windturbine probleem toont aan dat een hoogwaardige regeling mogelijk is met behulp van relatief eenvoudige lage orde multivariabele regelaars. Het gebruik van frequentie–afhankelijke weegfuncties geeft een effectieve reductie van de rol van mechanische parasitaire effecten. Door toepassing van het multi–model principe in combinatie met de LQ optimaliseringstheorie is de regelaar zodanig ontworpen dat in alle (aerodynamisch verschillende) werkpunten een goed regelgedrag ontstaat. Uit een uitgebreide robuustheidsanalyse met behulp van gestructureerde singuliere waarden blijkt dat de robuustheid sterk verbeterd kan worden door aanpassing van de ontwerpparameters.

De gevolgde aanpak, te weten een grondige modelvorming gecombineerd met onzekerheidsmodellering, en met gebruik van optimaliseringstheorie en robuustheidsanalyse, is gebleken succesvol te zijn. Kenmerkend is dat het regelconcept een integrale aanpak van het regelprobleem behelst, waarbij gecombineerd wordt ingegrepen via de mechanica en via het elektrische conversie systeem. Het verdient aanbeveling een dergelijke integrale aanpak van het regelprobleem ook bij andere typen windturbines toe te passen.

CURRICULUM VITAE

14 mei 1960	Geboren te Zeist
1972–1975	Scholengemeenschap De Breul te Zeist
1975–1979	Zeister Vrije School te Zeist
1979	VWO diploma
1979–1984	Technische Universiteit Delft Afdeling der Werktuigbouwkunde Vakgroep Werktuigkundige Meet– en Regeltechniek Afstudeeronderwerp: "Modelvorming en systeemgedrag van een windturbine met synchrone generator en gelijkstroom–tussenkring", uitgevoerd bij KEMA, te Arnhem. Voor dit afstudeerwerk is de KIvI Regeltechniekprijs 1984 toegekend.
1984	Diploma Werktuigkundig Ingenieur (met lof)
1984–1986	Wetenschappelijk medewerker aan de Technische Universiteit Delft, vakgroep Werktuigkundige Meet– en Regeltechniek, gedetacheerd bij KEMA, Automatiserings Projecten Bureau, te Arnhem. Onderzoek: Modelvorming en regeling van windturbines bij grootschalige toepassing in parkopstelling.
1986–1987	Medewerker Automatiserings Projecten Bureau KEMA, te Arnhem
1987–heden	Wetenschappelijk medewerker Philips Natuurkundig Laboratorium, te Eindhoven, groep Mechanica en Systeem– en Regeltechniek.

Address of the author:

Philips Research Laboratories Eindhoven
P.O.Box 80000
5600 JA Eindhoven
The Netherlands
Tel:+31 40 743597

4. Het ontwerp van regelingen voor windenergie conversiesystemen dient te worden gebaseerd op een model waarin zowel de aerodynamica, de mechanica als de elektrotechniek/elektronica gerepresenteerd worden. Hierdoor kunnen de onderlinge interacties tussen de deelsystemen op een systematische wijze worden betrokken bij het ontwerp van regelsystemen. In de tot nu toe gepubliceerde onderzoeksresultaten betreffende de regeling van dergelijke systemen wordt dit onvoldoende onderkend. Dezelfde integrale aanpak is gewenst bij andere elektro–mechanische systemen.

5. Windturbines en Compact Disc spelers hebben regeltechnisch gezien meer overeenkomsten dan hun maatschappelijke doelstellingen doen vermoeden.

6. Het Integraal Programma Windenergie dient niet alleen een hoger jaarlijks budget te verkrijgen, doch dient mede gericht te worden op de middellange termijn.

7. De discipline Werktuigkundige Regeltechniek biedt een goed uitgangspunt voor de concrete invulling van het begrip 'Mechatronica'.

8. Het feit dat artsen een onvoldoende bedrijfmatige aanpak wordt verweten dient niet te worden gecompenseerd door binnen de gezondheidszorg niet–geneeskundig geschoolde managers aan te nemen, doch zou moeten leiden tot meer aandacht voor management in het curriculum van de opleidingen geneeskunde.

9. Indien U besluit dit proefschrift weg te gooien, is het vanuit milieukundig oogpunt gewenst dit te doen via het oud–papier circuit.

Delft, november 1989

Address of the author:

Philips Research Laboratories Eindhoven
P.O.Box 80000
5600 JA Eindhoven
The Netherlands
Tel:+31 40 743597

STELLINGEN
behorende bij het proefschrift

DYNAMIC MODELLING AND ROBUST CONTROL OF A WIND ENERGY CONVERSION SYSTEM

van
Maarten Steinbuch

1. Modelvorming van het dynamische gedrag van industriële producten en processen vormt een integraal onderdeel van het ontwerp van regelingen voor dergelijke systemen. De toepassing van methoden voor robuust regelen wordt met name zinvol indien de modelvorming wordt uitgebreid met een quantitatieve beschrijving van de modelonzekerheden. Dit geldt zowel voor theoretische als voor experimentele modelvorming (systeemidentificatie).

2. De toepassing van de H^∞ ontwerpmethode voor robuuste regelingen leidt met name tot goede resultaten bij systemen waarbij het aantal gemodelleerde onzekerheden zeer klein is. Voor het in dit proefschrift beschreven regelprobleem zouden daarentegen met de H^∞ methode onbruikbare regelaars zijn verkregen. De μ–synthese [Doyle, 1984] biedt hiervoor wel een oplossing.

   Doyle, J.C. (1984). *Advances in multivariable control.* Lecture Notes of the ONR/Honeywell Workshop, Honeywell, Minnesota.

3. Bij multivariabele systemen met significante interactie is het (benaderend) ontkoppelen en met klassieke regelschema's terugkoppelen [Hung and MacFarlane, 1982] niet noodzakelijkerwijs gunstig ten aanzien van de robuustheidseigenschappen van de totale regelkring.

   Hung, Y.S. and A.G.J. MacFarlane (1982). Multivariable feedback: A quasi–classical approach. *Lecture Notes in Control and Information Sciences*, 44, Springer Verlag, Berlin.